Universitat Politècnica de Catalunya

Optical Communications Group

Characterization, design and re-optimization on multi-layer optical networks

Marc Ruiz Ramírez

A thesis presented in partial fulfillment of the requirements for the degree of

Philosophy Doctor

Advisor:

Luis Velasco Esteban

September 2012

Agraïments

Vull mostrar el meu principal agraïment i dedicar aquesta tesi al meu director Luis Velasco. Amb la seva impecable direcció, inestimable dedicació, i constant recolzament aquest projecte ha pogut ser completat. Així doncs, aquesta tesi ha de ser considerada com un mèrit tant meu com seu.

Vull donar les gràcies a tots els companys del Grup de Comunicacions Òptiques de la UPC que m'han ajudat en tots aquests anys a superar els petits i grans obstacles d'aquest camí i que m'han ensenyat tot allò que m'ha fet falta aprendre.

Finalment, a la família i amics els hi vull agrair el seu recolzament i comprensió. Especialment, vull agrair a la Montse la generositat i altruisme que m'ha demostrat cada dia i que espero poder-li recompensar merescudament.

Abstract

The explosion of IP traffic due to the increase of IP-based multimedia services such as HDTV, video conferencing, or Internet telephony poses new challenges to network operators to provide a cost-effective data transmission. Although Dense Wavelength Division Multiplexing (DWDM) meshed transport networks support high-speed optical connections, these networks lack the flexibility to support sub-wavelength traffic leading to poor bandwidth usage. To cope with the transport of that huge and heterogeneous amount of traffic, multilayer networks represent the most accepted architectural solution.

Multilayer optical networks allow optimizing network capacity by means of packing several low-speed traffic streams into higher-speed optical connections (lightpaths). During this operation, a dynamic virtual topology is created and modified the whole time. Because new connections are dynamically allocated in the network, and connection holding times are typically random, a suboptimal allocation of resources may exist at any time. In this context, a periodically resource reallocation could be deployed in the network, thus improving network resource utilization.

This dynamic connection capability in multilayer optical networks has been enhanced with the advent of the Automatically Switched Optical Network (ASON) architecture. To accomplish such dynamicity, a control plane responsible for the establishment, maintenance, and release of connections is deployed over the optical transport plane. In this regard, Generalized Multiprotocol Label Switching (GMPLS) protocols are commonly used to implement a common control plane, able to manage several switching regions in an integrated way.

This thesis is devoted to the characterization, planning, and re-optimization of next-generation multilayer networks from an integral perspective including physical layer, optical layer, virtual layer, and control plane optimization. To this aim, statistical models, mathematical programming models and meta-heuristics are developed. More specifically, this main objective has been attained by developing five goals covering different open issues.

First, we provide a statistical methodology to compute the Q-factor for impairment-aware routing and wavelength assignment problems (IA-RWA). Aiming at reducing the Q-factor computation time, we present a polynomial-based model to compute

the Cross-Phase Modulation (XPM) variance (which represents the bottleneck in terms of computation time) in on-line IA-RWA problems. Compared with analytical XPM computation procedures, our polynomial model provides negligible Q-factor computation times without losing accuracy. Additionally, we present a linear method that can be used in mixed-integer linear programming (MILP) formulations of off-line IA-RWA problems instead of the polynomial model. Moreover, this linear model allows directly embedding the Q-factor computation in a MILP formulation. We prove that both models provide accurate Q-factor values in real traffic scenarios.

Second and moving to the optical layer, we present a new wavelength partitioning scheme that allows maximizing the amount of extra traffic provided in shared path protected environments compared with current solutions. To evaluate these current and new schemes, we define several statistical models to estimate the traffic intensity that a network can support without unleashing a target blocking probability. Using those statistical models, we define different network planning problems aiming at maximizing the expected revenues and net present value (NPV). Solving these problems for real backbone networks, we conclude that our proposed scheme maximizes both revenues and NPV.

Third, we tackle the design of survivable multilayer networks against single failures at the IP/MPLS layer (i.e.: IP/MPLS node and OE port), as well as single failures at WSON links. To efficiently solve this problem, we propose a new approach based on over-dimensioning IP/MPLS devices and lightpath connectivity and recovery and we compare it against the conventional solution based on duplicating backbone IP/MPLS nodes. After evaluating both approaches by means of MILP models and heuristic algorithms, we conclude that our proposed approach leads to significant CAPEX savings as well as OPEX and energy savings.

Fourth, we introduce an adaptive mechanism to reduce the usage of opto-electronic (O/E) ports of IP/MPLS-over-WSON multilayer networks in dynamic scenarios. A MILP formulation and several heuristics are developed to solve this problem. After an exhaustive evaluation of heuristics, the best one in terms of quality of the solution and computational time is implemented in a real test-bed, obtaining a reduction in the usage of O/E ports nearby 50%.

Finally, we address the design of resilient control plane topologies in GMPLS-enabled transport networks. After proposing a novel analytical model to quantify the resilience in mesh control plane topologies, we take advantage of that model and propose a problem to design the control plane topology subject to some given resilience requirements. To solve this problem, an iterative linear procedure and a heuristic are proposed and used to solve real instances, concluding that a significant reduction in the number of control plane links can be performed without affecting the quality of service of the network.

It shall be mentioned that part of the work reported in this thesis has been done within the framework of several European and National projects, namely

STRONGEST (FP7-247674), DICONET (FP7-216338), and BONE (FP7-216863) founded by the European Commission, and ENGINE (TEC2008-02634) founded by the Spanish Science Ministry.

Resum

L'augment de volum de trafic IP provocat per l'increment de serveis multimèdia com HDTV, vídeo conferencia o telefonia IP planteja nous reptes als operadors de xarxa per tal de proveir transmissió de dades eficient. Tot i que les xarxes mallades amb multiplexació densa per divisió de longitud d'ona (DWDM) suporten connexions òptiques de gran velocitat, aquestes xarxes manquen de flexibilitat per suportar trafic amb granularitat inferior a la longitud d'ona, fet que provoca un ús pobre de l'ample de banda. Per tal de fer front al transport d'aquesta gran quantitat de trafic heterogeni, les xarxes multicapa representen la millor solució arquitectònica.

Les xarxes òptiques multicapa permeten optimitzar la capacitat mitjançant l'empaquetament de connexions de baixa velocitat dins de connexions òptiques de gran velocitat. Durant aquesta operació, es crea i modifica constantment un topologia virtual dinàmica. Donat que les noves connexions són dinàmicament establertes a la xarxa i que els temps de connexió son típicament aleatoris, un ús sub-òptim de recursos pot existir a la xarxa en un moment donat. En aquest context, una re-optimització periòdica dels recursos utilitzats pot ser aplicada, millorant així l'ús de recursos.

Aquesta capacitat de connexió dinàmica en xarxes òptiques multicapa ha sigut millorada gràcies a l'arquitectura de xarxa òptica commutada automàticament (ASON). Per acomplir tal comportament dinàmic, un pla de control responsable de l'establiment, manteniment, i alliberament de connexions és desplegat per sobre del pla de transport. En aquest sentit, el conjunt de protocols GMPLS s'usa habitualment per implementar un pla de control comú, capaç de gestionar diferents regions dins d'una mateixa xarxa d'una manera integrada.

Aquesta tesi està dedicada a la caracterització, planificació, i re-optimització de xarxes òptiques multicapa de nova generació des d'un punt de vista unificat incloent optimització als nivells de capa física, capa òptica, capa virtual i pla de control. Per tal d'aconseguir aquest objectiu, s'han desenvolupat models estadístics i de programació matemàtica i meta-heurístiques. En més detall, aquest objectiu principal s'ha assolit mitjançant el desenvolupament de cinc objectius concrets cobrint diversos temes oberts de recerca.

En primer lloc, proposem una metodologia estadística per calcular el factor Q en problemes d'assignació de ruta i longitud d'ona considerant interaccions físiques entre connexions òptiques (IA-RWA). Amb l'objectiu de reduir el temps de computació del factor Q, presentem un model polinòmic per computar l'efecte XPM (que suposa el coll d'ampolla en termes de computació) per problemes IA-RWA resolts durant el funcionament de la xarxa (*on-line*). Comparat amb altres metodologies exactes, el nostre model polinòmic proporciona temps de computació negligibles sense pèrdua de precisió en el càlcul. Adicionalment, presentem un model lineal que es pot fer servir en formulacions de programació lineal entera mixta (MILP) per planificar l'enrutament i assignació abans de l'operació de la xarxa (*off-line*). Aquest model lineal permet inserir directament el càlcul del factor Q dins del cos de restriccions d'un model MILP. Finalment provem que ambdós models proporcionen un precís calcul del factor Q en escenaris reals de trafic.

En segon lloc i fixant-nos a la capa òptica, presentem un nou particionament del conjunt de longituds d'ona que permet maximitzar, respecte el particionament habitual, la quantitat de trafic extra proveït en entorns de protecció compartida. Per tal d'avaluar ambdues estratègies, definim diversos models estadístics per estimar la quantitat de tràfic que una xarxa pot suportar sense sobrepassar una determinada probabilitat de bloqueig objectiu. Usant aquests models estadístics, definim diferents models de planificació de xarxa amb l'objectiu de maximitzar els ingressos previstos i el valor actual net de la xarxa. Després de resoldre aquests problemes per xarxes reals, concloem que l'esquema que proposem maximitza tant els ingressos com el valor actual net respecte la solució actual.

En tercer lloc, afrontem el disseny de xarxes multicapa robustes davant de fallida simple tant a la capa IP/MPLS (als nodes i ports) com als enllaços de fibra. Per resoldre aquest problema eficientment, proposem un enfocament basat en sobre-dimensionar l'equipament de la capa IP/MPLS i recuperar la connectivitat i el comparem amb la solució convencional basada en duplicar els elements de la capa IP/MPLS. Després d'avaluar ambdues solucions mitjançant models MILP i algoritmes heurístics, concloem que la nostra solució permet obtenir un estalvi significatiu en termes de costos de desplegament i també d'operació i energètics.

Com a quart objectiu, introduïm un mecanisme adaptatiu per reduir l'ús de ports opto-electrònics (O/E) en xarxes multicapa sota escenaris de tràfic dinàmic. Una formulació ILP i diverses heurístiques són desenvolupades per resoldre aquest problema. Després d'una exhaustiva avaluació de les heurístiques, la millor en termes de qualitat de la solució i temps de computació s'implementa en una xarxa de proves real, obtenint una reducció en l'ús de ports O/E propera al 50%.

Finalment, adrecem el problema de disseny resilient del pla de control GMPLS. Després de proposar un nou model analític per quantificar la resiliència en topologies mallades de pla de control, aprofitem aquest model per proposar un problema de disseny de pla de control subjecte a uns determinats requisits de resiliència. Per resoldre aquest problema, proposem un procediment iteratiu lineal

i una heurística i els usem per resoldre instàncies reals, arribant a la conclusió que es pot reduïr significativament la quantitat d'enllaços del pla de control sense afectar la qualitat de servei a la xarxa.

Finalment mencionar que part del treball presentat en aquesta tesi ha estat realitzat dins del marc de diferents projectes europeus i nacionals: STRONGEST (FP7-247674), DICONET (FP7-216338), and BONE (FP7-216863) subvencionats per la Comissió Europea, i ENGINE (TEC2008-02634) subvencionats pel Ministeri de Ciència espanyol.

Table of Contents

List of Figures

List of Tables

Chapter 1

Introduction

1.1 Motivation

The role of IP as a convergent technology has triggered the development of a wide range of IP-based multimedia services, like HDTV, video conferencing, telemedicine applications, or Internet telephony, each having different bandwidth or quality of service (QoS) requirements. This huge, heterogeneous, and predominantly bursty-generated amount of traffic poses new challenges to network operators to provide a cost-effective data transmission. Because the bandwidth granularity of wavelength-routed optical networks is very coarse, typically a whole wavelength supporting 10 or even 40 Gbps Ethernet or Optical Transport Networks (OTN) signals, these networks lack the flexibility to support sub-wavelength traffic demands, which leads to poor bandwidth usage.

In this context, the term traffic grooming identifies the process of packing several low-speed traffic streams into higher-speed optical connections (lightpaths), maximizing optical channel bandwidth usage in general Dense Wavelength Division Multiplexing (DWDM) meshed transport networks. During this operation, a dynamic virtual topology is created and modified the whole time. Because new connections are dynamically allocated in the network, and connection holding times are typically random, a suboptimal allocation of resources may exist at any time. In this context, a periodically resource reallocation could be deployed in the network, thus improving network resource utilization.

In addition to the use of dynamic virtual topologies, DWDM networks capacity can also be further improved by increasing the spectral efficiency using narrower channel spacing and higher bit-rates. Since the signal is transmitted from source to destination through lightpaths in the absence of optical-to-electrical-to-optical (O/E/O) conversions at intermediate nodes, the optical signal might be degraded due to physical layer impairments induced by transmission through optical fibers

and components. For this reason, recently network planning and operation include those physical effects with the aim to find solutions ensuring a certain desired QoS degree at the optical network.

With the advent of the Automatically Switched Optical Network (ASON) architecture, the International Telecommunication Union - Telecommunication Standardization Sector (ITU-T) has enhanced wavelength-routed optical networks with dynamic connection capability. This capability is accomplished by means of a control plane entity, responsible for the establishment, maintenance, and release of connections over the optical transport plane. The Internet Engineering Task Force (IETF) has standardized Generalized Multiprotocol Label Switching (GMPLS) as a set of protocols to implement a common control plane, able to manage several switching regions in an integrated way. In fact, not only can packet-switched-capable interfaces be managed by the different GMPLS protocols, but they can also manage time-division multiplexing, lambda, and even fiber switched-capable interfaces. This makes GMPLS the most accepted solution for implementing the control plane functionalities in the ASON architecture.

In light of the described above, the characterization and planning of next-generation multilayer networks should be attained within an integral framework including optical, virtual and control topology design. Moreover, the assumption of dynamic traffic opens the need to develop reconfiguration procedures for keeping the optimality of current networks.

The work here presented is being developed as a part of the research inside the Advanced Broadband Communications Center (CCABA). This center integrates researchers from several Departments which have interests on complementary communications research fields: Integrated Broadband Communications, Optical Communications, and Radio and Mobile Communications. Currently the CCABA is a Specific Research Center of the UPC.

This thesis continues in part the work developed during the PhD thesises of Luis Velasco [Lu09] and Jordi Perelló [Pe09].

1.2 Thesis goals

The main objective of this thesis is the creation of analytical models for GMPLS-controlled multilayer networks to allow characterize, design, and perform periodical re-optimizations. To this aim, statistical models, integer and mixed integer linear programming (ILP, MILP) models and meta-heuristics are developed. With this objective in mind, we deeply reviewed the current literature and we detected several open issues allowing us to specify five goals to develop this thesis; these are:

G.1 – Statistical Q-factor computation for IA-RWA problems

This goal consists in the development of a statistical Q-factor computation model used in impairment-aware network planning problems with the aim to improve the current methodology. Since the exact computation of the Chross-phase Modulation (XPM) effect is the bottleneck of the Q-factor computation, we propose two statistical models to compute XPM aiming at overcoming analitical computation drawbacks. On the one hand, we propose a polynomial-based model that allows significantly reducing the computational time of exact XPM computation in on-line network problems. On the other hand, we present a linear-based model that allows directly including Q-factor computation as part of the linear constraints of an off-line network planning using an ILP formulation.

G.2 – Service and resource-differentiated network design

This work is separated in two sub-goals:

- **G.2.1**: Develop pseudo-analytical expressions to accurately estimate the intensity of a certain traffic class that can be carried over a network without violating some grade of service requirements (e.g., a maximum blocking probability). To this end, we will consider different resource partitioning schemes.
- **G.2.2**: Define mathematical models to design optical networks that maximize the expected network operator's revenues and the net present value of those networks. The output of the model will be the best network topology and the best resource partitioning scheme. These mathematical models will use the intensity expressions obtained in G.2.1.

G.3 – Survivable Hierarchical IP/MPLS-over-DWDM network design

ILPs formulation and several meta-heuristics will be developed to obtain the optimal logical topology of a large-scale IP/MPLS-over-DWDM network. The objective is to reduce network costs satisfying that the network is survivable against any single failure. Considered failures are at the IP/MPLS network e.g., a port in a router, a router (software failure), and also any link of the optical network.

G.4 – On-line resource re-allocation in dynamic traffic scenarios

The main focus is in developing a resource re-allocation module to be implemented in the network management system (NMS) of an ASON/GMPLS test-bed. This module should reconfigure the logical layer aiming to release as much as opto-electronic ports as possible, reducing thus the cost of the network. The first step will be the formulation of the problem as a MILP. The second step will be the

development of a meta-heuristic to solve the problem in real-time for real size instances. Finally, the third step will be the implementation and performance of the model in the experimental ASON/GMPLS CARISMA test-bed.

G.5 – Analysis and design of GMPLS control plane with resilience guarantees

This work is separated in two sub-goals:

- **G.5.1**: Develop an analytical expression to accurately estimate the resilience at the control plane for mesh networks. The work presented in [Pe07] for ring networks will be our starting point.
- **G.5.2**: Develop an optimization procedure to design control plane topologies, aiming to reduce network costs without violating some given resilience requirements.

A summary of the goals of the thesis is presented in Table 1-1.

Table 1-1: Thesis goals

		Characterization	**Design**	**Re-optimization**
Physical Layer		**G.1** Statistical Q-factor model for IA-RWA problems		
Data Plane	Optical Layer	**G.2.1** Intensity models for service and resource-differentiated networks	**G.2.2** Service and resource-differentiated networks.	
	Client Aggregation Layer		**G.3** Survivable hierarchical IP/MPLS-over-DWDM networks.	**G.4** Centralized resource re-allocation in dynamic traffic scenarios.
Control Plane		**G.5.1** Resilience model in GMPLS-enabled mesh networks.	**G.5.2** GMPLS control plane with resilience guarantees.	

1.3 Thesis Outline

The remainder of this thesis is as follows:

Chapter 2 introduces some background on the graph teory, intelligent multilayer optical networks, operational research and statistics needed for a better understanding of the contributions in this thesis.

Chapter 3 provides state-of-the-art of characterization, design and re-optimization in optical networks, highlighting those open issues that become the goals presented above.

Chapter 4 presents the work made on statistical Q-factor computation and XPM models (goal G.1). This chapter is based on already published material ([JOCN12], [ICC12]).

Chapter 5 presents the work made on the characterization of the maximum intensity that can be carried over a network without violating some grade of service requirements (goal G.2.1). This chapter is based on already published material ([JOCN11.2]).

Chapter 6 introduces both the problem of designing optical networks that maximize the expected network operator's revenues and the problem of designing optical networks maximizing the network net present value (goal G.2.2). This chapter is based on already published material ([JOCN11.2], [ICTON11.1], [DRCN11]).

Chapter 7 presents the contributions made on the design of survivable hierarchichal multilayer IP/MPLS-over-DWDM networks (goal G.3). This chapter is based on already published material ([JOCN11.1], [COR11])

Chapter 8 is devoted to the contributions made on resource re-optimization under dynamic traffic scenarios (goal G.4). This chapter is based on already published material ([JOCN09], [NOC09]).

Chapter 9 presents the work made on the characterization of the resilience and on the design of control plane with resilience guarantees (goals G.5.1 and G.5.2). This work is based on already published material ([CL09], [JLT11], [ICTON11.2]).

Finally, Chapter 10 presentes the main conclusions of the thesis and proposes new issues to continue the research pathway explored in this thesis.

Chapter 2

Background

In the last years, core transport networks have evolved from Synchronous Optical Networking (SONET) / Synchronous Digital Hierarchy (SDH) over static point-to-point dense wavelength division multiplexing (DWDM) links towards wavelength-switched optical networks (WSONs) introducing dynamic reconfiguration, i.e. automatic optical connection (lightpath) set-up and tear-down and recovery mechanisms such as protection and restoration. Moreover, benefits achieved are significantly increased by applying an intelligent interworking strategy between IP/Multi-Protocol Label Switching (MPLS) networks and WSON based on a multilayer optimization process capable of efficiently aggregating the various bandwidth granularities.

This chapter introduces basic concepts and terminology that are relevant to the work presented in this thesis. We start by introducing some general concepts regarding the graph theory and static and dynamic traffic scenarios. Then, the main features of WSON networks are presented focusing on three aspects: quality of service at the optical layer, the basic multilayer architecture, and network control and management.

In addition, since the work presented in this thesis is based on developing optimization and statistical models, some concepts regarding operational research and statistical modeling are afterwards presented. Finally, some economic concepts are introduced for evaluating the approaches presented in the rest of the chapters.

2.1 General concepts

2.1.1 Graph theory

A *graph* or *topology* $G(V,E)$ consists of a set V of nodes or vertices and a set E of edges or links, being the degree of a node defined as the number of edges incident

with that node [Ha94]. As a measure of the mesh degree, the *average nodal degree* (δ) is defined as follows:

$$\delta = \frac{2 \cdot |E|}{|V|} \tag{2.1}$$

where $|V|$ and $|E|$ represent the number nodes and links, respectively.

Given a graph, a *path* can be defined as of a sequence of nodes that can be sequentially visited without repetitions from a source to a destination following a connected set of links. Several relations can be defined between two different paths with the same source and destination. Thus, two paths are *distinct* if exist at least one link different between them. When all the links are different, the paths are *link-disjoint*, whereas if all the intermediate visited nodes are different the paths are *node-disjoint*.

Regarding paths distance, we can define the *shortest path* between each pair of nodes as the minimum number of visited links needed to connect both ends. Thus, the *average shortest path* (*h*) computes the mean value of all these shortest paths. In addition to this, the *diameter* is the longest shortest path and the *radius* is the minimum eccentricity in a node, which can be computed as the maximum distance between this node and any other in the network.

Among different characteristics which allow classifying graphs, we focus on the definition of *planarity* and *connectivity*. A graph is *planar* if and only if it can be drawn on the plane in such a way that no edges cross each other. A graph is *connected* if exists, at least, one path between each pair of nodes. More generally, a topology is *k*-connected if exists, at least, *k* link-disjoint paths between every pair of nodes. In this thesis we consider 2-connected graphs as the minimal connected topology.

Finally, Fig. 2-1 shows the *homeomorphic graph* of the depicted source topology. This graph is built by removing the nodes with degree equal to two from the original topology [Gr03].

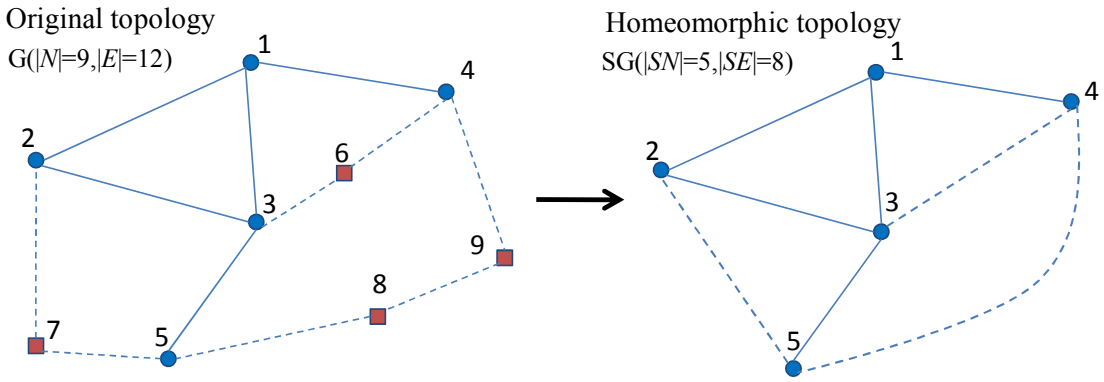

Fig. 2-1 Homeomorphic topology construction

2.1.2 Static and dynamic traffic

Two different approaches can be considered for planning and operating communications networks: static and dynamic traffic scenarios [Gu04]. In static traffic scenarios, no changes are considered in the connections established during the working period of the network. Thus, the information about *client demands* to be served, i.e. the source and destination nodes and the required bandwidth, is known in advance. Since the routing of those demands can be done before the network begins to operate and no changes are allowed during the working time, the optimality of the network planning is always kept. When the network resources are limited and some demands cannot be established, we can define the *blocking rate* as the proportion of those refused demands over the total.

On the contrary, in dynamic traffic scenarios demands are not known in advance and connections are continuosly set up and torn-down. We assume that *client requests* arrive to the network following a certain probability distribution function. Moreover, connections remain active during a certain period of time, i.e. the service time, which can be also modeled by another probability function. For the sake of clarity, we will use client request instead of client demand in the case of dynamic traffic scenarios.

The most common model for dynamic traffic is the Erlang model [ITU05], where arrivals are modeled following a Poisson probability function identified by the mean time between two consecutive arrivals, namely *inter-arrival time* (*iat*). When Poisson arrivals are assumed, the service time follows an exponential probability function identified by the mean *holding time* (*ht*). The inverses of *iat* and *ht* are called *inter-arrival rate* (λ) and *service rate* (μ), respectively. The *traffic intensity* (or *offered load*) can be computed as *ht*/*iat* or, alternatively, λ/μ and its unit is the *erlang*. The traffic intensity represents the mean number of established connections in a network at a random time. The source and destination of the demands are also random variables and they can follow several models, e.g. uniformly distributed, proportional to the distance between nodes, etc.

When a connection request arrives to its source node, some routing procedure is executed to find an available route over the network. If routes are precomputed and remain invariable independently of the load and the availability of resources of the network, the procedure is called *static routing*. On the contrary, when the route is found by means of some routing algorithm executed upon the request arrives, thus considering the current status of the network, the procedure is called *dynamic routing* [Za02]. In both cases, when the network does not contain enough free resources to establish the connection request, that connection is blocked. Then, we can define the *blocking probability* as the probability to refuse (block) a connection request at a random time. To compute the blocking probability of a network during a period of time, the amount of blocked connections is divided into the amount of

connections requested. The blocking probability of a network is used to define and quantify the *Grade of Service (GoS)* of a network.

2.2 Optical networks

In this thesis, the study of the Quality of Service (QoS) at the optical network has been addressed from two different points of view: the physical layer impairments affecting optical connections and the network recovery capability after a failure. This section provides some concepts regarding optical networks.

2.2.1 WDM technology

The Wavelength Division Multiplexing (WDM) technology allows transmitting different data flows on different optical wavelengths within one single optical fiber. Most WDM systems currently use the frequency region around 1550 nm, since this is one of the frequency regions where the signal attenuation reaches a local minimum. Fig. 2-2 shows an example of the WDM technology.

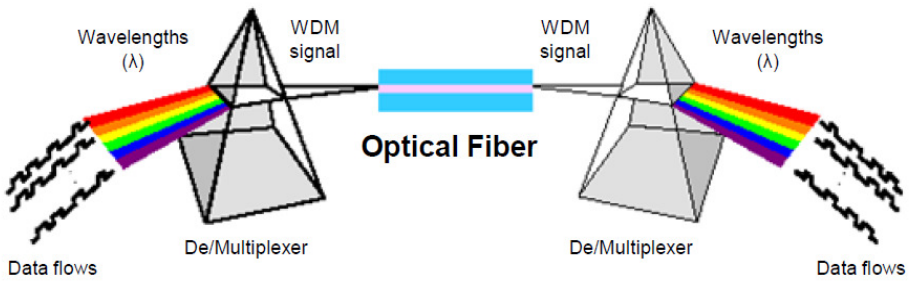

Fig. 2-2 WDM technology (reproduced from [Lu09])

Using the WDM technology, the number of optical wavelength channels being multiplexed onto a single fiber can be up to 400. When such a large amount of channels can be transported by the WDM system, the term Dense Wavelength Division Multiplexing (DWDM) is used, in contrast with Coarse Wavelength Division Multiplexing (CWDM), which is considered for the metropolitan network and multiplexes a limited number of wavelengths onto a single fiber.

2.2.2 Physical layer impairments

Physical layer *impairments* (PLI) are those effects that can affect or degrade the optical information on lightpaths and can be classified into linear and non-linear [Az09]. Linear impairments such as fiber attenuation, amplifier spontaneous emission (ASE) noise, chromatic dispersion (CD) (or group velocity dispersion (GVD)), and polarization mode dispersion (PMD) are independent of the signal

power and affect each of the wavelengths individually. On the other hand, nonlinear impairments affect not only each optical channel individually but they also cause disturbance and interference between them. The most important nonlinear effects are: self-phase modulation (SPM), cross-phase modulation (XPM), and four-wave mixing (FWM) [Sa09].

The effect of both linear and nonlinear PLI can be quantified by using the quality factor Q [Ji10], which includes PMD, ASE noise, the combined SPM/GVD and optical filtering effects, XPM, and FWM. Without going into the details, ASE, FWM, and XPM can be calculated assuming that they follow a Gaussian distribution. For the combined SPM/GVD and optical filtering effects, they can be quantified through an *eye closure metric* calculated on the most degraded bit-pattern. Furthermore, the power penalty due to PMD can be calculated basing on the length of the lightpath, bit rate, and lightpath PMD parameter. Thus, the Q-factor of a lightpath is given according to:

$$Q = \frac{pen_{eye} \cdot P_{transmitte\,r}}{pen_{PMD} \cdot \sqrt{\sigma^2_{ASE} + \sigma^2_{XPM} + \sigma^2_{FWM}}} \tag{2.2}$$

where $P_{transmitter}$, pen_{eye}, pen_{PMD}, σ^2_{ASE}, σ^2_{XPM}, and σ^2_{FWM}, are the power of the transmitted signal, the relative eye closure attributed to SPM/GVD and optical filtering effects, the power penalty due to PMD, the electrical variance of ASE noise, and the electrical variance of XPM and FWM induced degradation, respectively.

Among non-linear impairments, XPM is the dominant effect being the value of the σ^2_{XPM} several times greater than the one of σ^2_{FWM} [Te99]. Without going into details about σ^2_{XPM} computation, the σ^2_{XPM} of a fiber link can be obtained by solving an integral function as follows:

$$\sigma^2_{XPM} = P^2 \sum_{1}^{N} \frac{1}{2\pi} \int_{-\infty}^{\infty} \left[|f(\omega)|^2 \cdot |g(\omega)|^2 \cdot h(\omega) \right] \tag{2.3}$$

where P is the average channel power, N is the total number of link amplifiers, and $f(\omega)$, $g(\omega)$, and $h(\omega)$ are functions dependent on several physical factors such as the XPM-induced intensity modulation, optical filter transfer, and power spectral density. For a detailed explanation of XPM analytical computation, we refer the reader to [Ji10, Pa03, Ca99].

2.2.3 Network recovery

In general, a *recovery mechanism* is a set of actions to return a network to its normal condition after a failure occurs, e.g.: a fiber cut. To quantify the quality of a recovery mechanism, two parameters can be defined and computed: *resilience* and *availability*. Resilience is generally defined as the capability of the network to continue into operation even when a failure occurs. The way to compute the

resilience of a network is not strictly defined and can consider the interactions between different network planes, for example, the probability that a failure in the control plane affects to the data plane operation [Pe07]. On the contrary, the *availability* is strictly defined as the probability that a network will be found in the operating state at a random time in the future [Gr03]. Note that a value equal to 1 represents that the network is always available.

Two types of recovery mechanisms can be implemented to increase the resilience and the availability of the network: *restoration* and *protection*. When restoration is implemented, the data flow affected by a failure is re-routed after the failure is detected, using network spare capacity. Since some affected path could not be rerouted due to the lack of capacity, the availability could be lower than one.

Aiming at increasing the availability, protection can be implemented; it consists in replacing the failed working connection with a pre-assigned backup path. If each backup path is dedicated to protect only one working connection, the scheme is called *Dedicated-Path Protection* (DPP). On the contrary, when a wavelength channel can be used to protect more than one working connection, the scheme is called *Shared-Path Protection* (SPP). Note that the availability of DPP networks is equal to 1 for single fiber link failures.

Although SPP networks are typically more complex to implement and manage than DPP schemes, SPP provides significantly lower resource consumption than DPP. For this reason, SPP have received lot of research attention due to its good trade-off between resilience, recovery time, and capacity consumption [Ou04.2, Mu08].

In DPP networks, backup paths can convey the same data that the working flows (1+1 scheme) or can be used to convey low priority traffic (1:1 scheme). In the 1:1 case every low priority data flow using a certain backup path is torn down when a failure affecting some working path protected by this path occurs.

2.3 WSON multilayer networks

2.3.1 Two-layered architecture

As shown in Fig. 2-3, the basic multi-layer model consists of two-layers: the *optical layer* and the *aggregation layer*, in a client-server relationship [Pi04]. In constrast to this multilayer architecture, a *single layer* network consists of only one layer, i.e. the afore-mentioned optical layer.

The optical layer, the lower layer, consists of optical cross connects (OXC) and DWDM links. Aiming at serving client layer demands, optical connections, also known as lightpaths, are established between two optical nodes. A lightpath is a concatenated set of wavelength channels (one in each fiber), being each wavelength

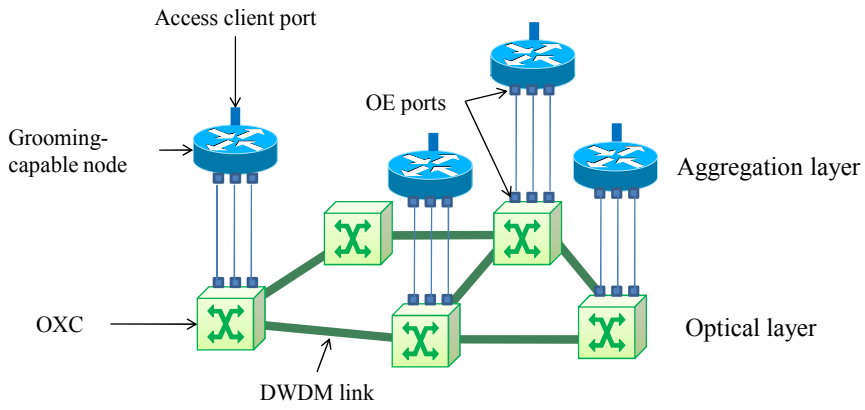

Fig. 2-3 Two-layered network

channel used for one lightpath at most. Lightpaths can use different wavelengths in each link along its route, in which case wavelength conversion capacity must be installed in the OXCs. In contrast, they can be restricted to use the same wavelength (*wavelength continuity constraint*). Thus, two extreme cases are defined [To07]: a *Virtual Wavelength Path* (VWP) network, where all the OXCs of the network have full wavelength conversion capacity, and a *Wavelength Path* (WP) network, where no OXC of the network has wavelength conversion capacity.

On top, the aggregation layer allows grooming client traffic to be transported over the optical layer, thus optimizing the overall network capacity usage. In contrast with a single layer network where each client demand is routed using one lightpath, in a multilayer network various client flows can be grouped and carried into the same lightpath. For this reason, the nodes in this layer provide electrical packet switching, flow aggregation, and other features by means of some of the available technologies, such as SONET/SDH, IP/MPLS, Gigabit Ethernet, etc. The links in this layer represent lightpaths of the optical layer, being known as *virtual links*. In fact, the topology of this layer is known as *virtual topology* (VT) since there are no physical links connecting IP/MPLS nodes.

Finally, aggregation nodes are connected to the underlying OXCs by means of *opto-electronic* (OE) ports. Although different architectures are allowed, in the basic one every node in the aggregation layer is collocated with one OXC in the optical layer.

As introduced in a Section 2.1, in dynamic traffic scenarios the connections are set up and torn down continuosly depending on the client requests. Aiming at illustrating those client requests establishing in a multilayer network, Fig. 2-4 represents a segment of a multilayer network where traffic is currently being transported.

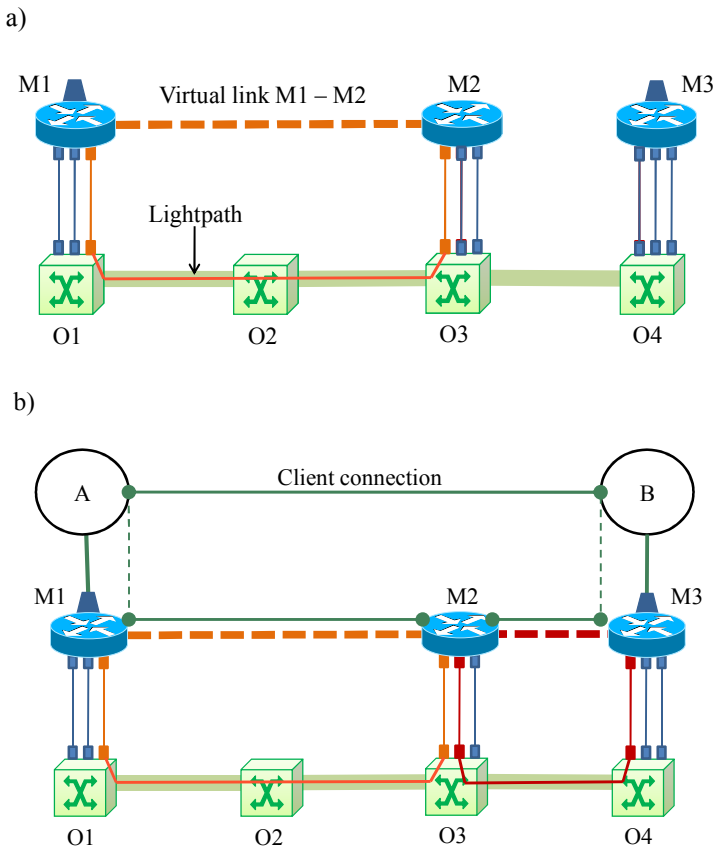

Fig. 2-4 Client connection set up

In Fig. 2-4a a virtual link between nodes M1 and M2 in the aggregation layer supported by a lightpath in the optical layer has been created. Let us assume that virtual link M1-M2 carries few client flows and its remaining capacity is equal to 2 bandwidth units. Then, a new connection request between clients M1 and M3, directly connected to nodes O1 and O4, respectively, arrives to the network requesting for 1 bandwidth unit. The connection request can be set up by using the remaining capacity of virtual link M1-M2 and by establishing a new virtual link between nodes M2 and M3 (Fig. 2-4b).

While in static traffic environments the optimal topology for both optical and aggregation layers can be computed beforehand during the planning phase, the optimal use of resources is a challenging problem when dynamic traffic scenarios are considered. Subsequently to the network design, some strategies of resources re-optimization should be applied to periodically adapt the network to traffic fluctuations. In this regard, two re-optimization problems have been widely studied in literature, namely *Lightpath Rerouting* (LR) and *Virtual Topology Reconfiguration* (VTR).

LR consists of rerouting an existing lightpath from its original route to a different one, without changing neither the source nor the destination [Mo99, Xi05, Ch07]. This rerouting can improve the performance of the network, e.g. reducing the blocking probability. In fact, since wavelength conversion is one technique to alleviate the inefficiency caused by wavelength continuity constraints, works like [Le96] show that LR also helps to increase the overall resource utilization efficiency in VP networks.

More sophisticated than LR, VTR [La94, Ra00, Ge03] consists of two steps: first, the virtual topology under new traffic conditions is re-designed; second, an ordered sequence of changes to migrate from a non-optimal to the optimal topology for the current conditions is applied.

2.4 Network control and management

The MPLS technology [RFC3013] was designed with a set of protocols for routing and signalling Label Switched Paths (LSP). In contrast, optical networks have evolved from point-to-point WDM systems to complex OXCs that can perform optical switching. In this scenario, Automatically Switched Optical Network (ASON) [G.8080] was specified to introduce dynamic connection capability to optical networks. As depicted in Fig. 2-5, the ASON architecture defines three different planes which exchange information through a set of defined interfaces.

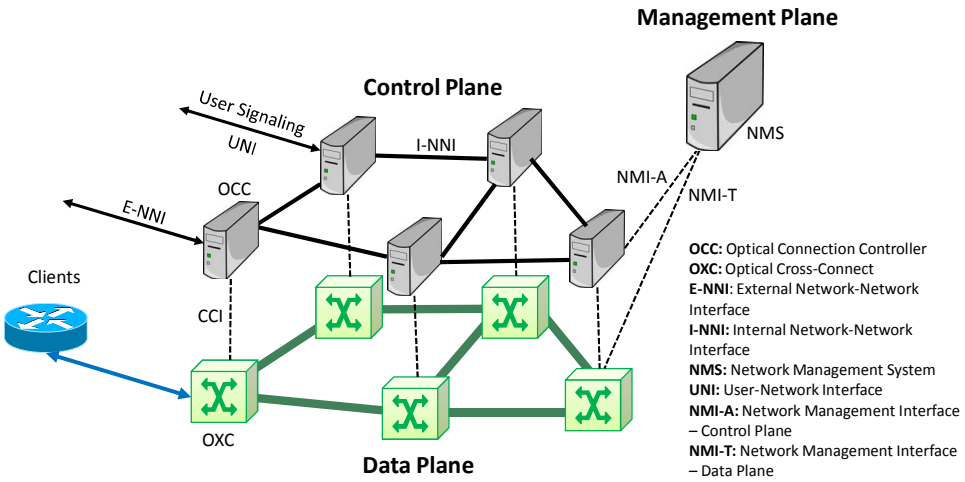

Fig. 2-5 The ASON architecture

The data plane represents the functional resources of the optical network which convey user information between locations. It includes OXCs and optical fibers, and is able to measure parameters to characterize the connections state, detecting failures, etc.

The control plane is in charge of the resource management, routing and connection signaling. The objective is to define an intelligent control plane able to create, modify and release connections automatically.

The management plane provides the network management functions (FCAPS): Failure management, Configuration management, Accounting, Performance management, and Security. It is also referred as network management system (NMS)

Generalized Multiprotocol Label Switching (GMPLS) has been identified as the enabling technology to provide ASON with the required functionalities [RFC3945]. GMPLS is a set of IP protocols defined by the IETF, an extension of the existing ones in MPLS, allowing the management of different switching capabilities in an integrated way. Not only Packet Switched Capable (PSC) interfaces as in MPLS can be managed, but also Time-Division Multiplexing Capable (TDMC), Lambda Switched Capable (LSC) or even Fiber Switched Capable (FSC) ones. This creates a LSP hierarchy spanning different switching domains.

From an architectural point of view, the control plane in multi-layer networks can follow three differentiated models namely overlay, *augmented* and *peer* [RFC3717]. In the traditional overlay model different control plane instances run on each layer. Thus, layers are independently controlled. Alternatively, in the *augmented* approach, although different control plane instances run on each layer, some information is exchanged amongst them aiming at bandwidth allocation improvement in the network. Finally, in the *peer* approach all layers are controlled by a unified control plane and decisions are taken considering the whole network information.

There are two possible control plane configurations; control channels can be established either *in-fiber*, so that control and data planes share the same transmission medium, or *out-of-fiber* thus introducing a physical separation in between [OIF01]. In the former, two sub-configurations could be also differentiated depending on whether control channels are transmitted *out-of-band*, over a separated wavelength, or *in-band* along with the end-user traffic.

As discussed in [Jj06], where the out-of-band configuration is selected, the control plane can be deployed congruent with the corresponding data plane, thus following a *symmetrical* topology or, on the contrary, it can be deployed following an *asymmetrical* topology, describing control and data planes different topologies (Fig. 2-6). Note, that the *in-fiber* configuration typically represents a *symmetrical* topology, as control channels are constrained to the same path as data channels. Contrarily, the freedom introduced with the *out-of-fiber* configuration fosters the deployment of *asymmetrical* topologies.

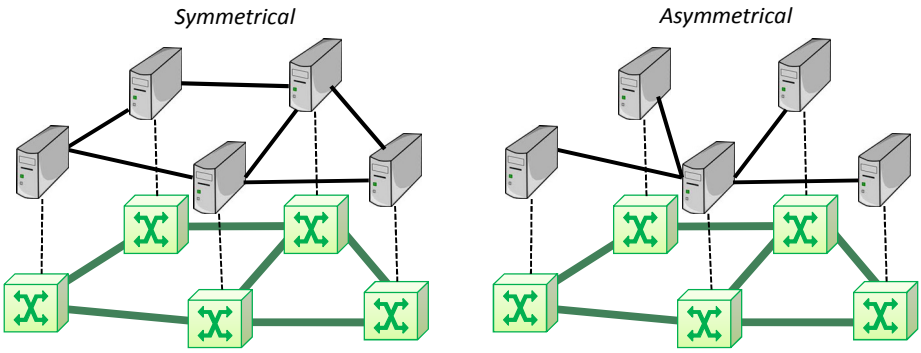

Fig. 2-6 Out-of-band control plane topologies

2.5 Mathematical Programming

A *Mathematical Programming* (MP) is a mathematical method to find an optimum point x^* of a function where satisfying a set of constraints [Ch83]. More formally, a minimization mathematical programming can be defined as follows:

$$Z^* = \min\ f(x) \tag{2.4}$$

subject to:

$$g_i(x) \geq b_i, \quad \forall i \in R \tag{2.5}$$

where x represents a vector of variables, $f(x)$ represents the objective function and R represents the set of constraints. A constraint is an equality or inequality defined by a function $g_i(x)$ and a constant b_i.

Let us define X as the set of all possible x vectors. Then, we can define the set S of feasible solutions of the problem as follows:

$$S = \{x' \in X \mid g_i(x') \geq b_i, \forall i \in R\} \tag{2.6}$$

Thus, S contains all elements in X satisfying the whole set of constraints. From the set S we can define an optimal solution x^*as follows:

$$x^* = \{x' \in S \mid f(x') \leq f(x''), \forall x'' \in S\} \tag{2.7}$$

Note that a problem could have alternative optimal solutions, i.e. different x^* with the same Z^* value. In that case, we define X^* as the set of optimal solutions. The problem, however, could have no feasible solution. In that case, where $S = \emptyset$ the problem is called unfeasible. Finally, when $f(x^*) = -\infty$ the problem is called unbounded.

A *Linear Programming* (LP) problem is a special case of MP, where $f(x)$ and $g_i(x)$ are linear functions with real variables. When variables are restricted to be

integer, the problem is called *Integer Linear Programming* (ILP), whereas if the problem combines integer and real variables, the problem is defined as *Mixed Integer Linear Programming* (MILP). Finally, a *Non-Linear Programming* (NLP) contains, at least, one non-linear function [Ch83].

Regarding complexity, a problem is said to be Non-deterministically Polynomial (NP) if its solution comes from a finite set of possibilities, and it takes polynomial time to verify the correctness of a candidate solution, being easier and faster to grade a solution than to find a solution from scratch. Among NP problems, NP-complete are the hardest computational problems.

Several exact procedures have been developed to solve MP problems. For example, the *simplex algorithm* is used for solving LPs, whereas *Branch&Bound* and *Branch&Cut* algorithms are used for ILPs [Ch83]. When the problem is large-scaled, i.e. the size in number of variables and constraints makes impractical to solve it with the previous described algorithms, decomposition methods such as basic *LP-based decomposition* and *column and row generation* can be applied to reduce the computational effort [De05]. In the case of NLPs the use of interior methods such as the *Newton barrier method* has been exploited for non-linear constrained problems [Fo02]. Although the output of these exact methods is the optimal solution, the required computation time tends to be too high for practical purposes when real-life instances need to be solved, even in the case of using good solver engines such as CPLEX [CPLEX] or Gurobi [Gur].

When the achievement of the optimal solution is not required, some relaxation methods such as *Lagrangian relaxation* [Ah93] or *randomized rounding* [Ra87] provide good-quality solutions by relaxing some integer constraints, thus decreasing the problem's complexity. Alternatively to these relaxation methods, meta-heuristic methods have been also deeply studied to provide near-optimal feasible solutions [Bl03]. Next section provides the basic concepts of meta-heuristics, as well as the details of the meta-heuristics used in this thesis.

2.6 Heuristic methods

A heuristic is a method to provide near-optimal solutions in practical times. Although the optimality of the solution cannot be guaranteed, heuristics solutions can be compared to that of exacts methods obtaining the optimality gap. Among heuristics, *constructive* algorithms and *local search* methods can be distinguished. Constructive algorithms generate solutions from scratch by adding components to an initially empty partial solution, until a solution is complete. Local search algorithms start from some initial solution and iteratively try to replace the current solution by a better solution in an appropriately defined neighborhood of the current solution.

A meta-heuristic can be defined as an iterative master process that guides and modifies the operations of subordinate heuristics to efficiently produce high-quality solutions. The subordinate heuristics are simple constructive and local search methods, or just a *constructive* method. Thus, meta-heuristics are generic algorithm frameworks which can be applied to different optimization problems with relatively few modifications. Examples of common meta-heuristics are *Simulated Annealing*, *Path Relinking*, *Tabu Search*, *Ant Colony* and *Genetic Algorithms* [Gl03]. In the next section the details of the *Greedy Randomized Adaptative Search Procedure* (GRASP) [Fe95] and the *Biased Random Key Genetic Algorithm* (BRKGA) [Go10] meta-heuristics are presented for better understanding of next chapters.

2.6.1 GRASP meta-heuristic

The GRASP meta-heuristic is an iterative procedure consisting of a two-phase main algorithm which finds a good-quality solution at each iteration [Fe95]. Within the first phase of the algorithm (*constructive* phase) one feasible solution is built by means of an *ad-hoc* randomized greedy algorithm. The degree of randomness is determined by the parameter α. Next, the *local search* phase, designed to explore the neighborhood of the solution, is applied aiming at improving the current solution. The procedure finish when some criterion is met, e.g.: a number of iterations without improving the best solution or a maximum execution time. Table 2-1 shows the main algorithm of the GRASP meta-heuristic for minimization.

Table 2-1: GRASP Main Algorithm

```
Procedure GRASP main Algorithm
begin
   x* = ∞.
   while stop criteria is not attained do
   x = constructivePhase(GCF(.), α);
   x = localSearch(f(.), x);
   if f(x)<f(x*) then
      x* = x;
   return x*
end
```

The *constructive phase* (Table 2-2) is characterized by a greedy cost function (*GCF*) that allows ordering the elements to be included in the solution. At each *constructive* phase iteration, a candidate list (*CL*) containing all elements suitable to be included in the solution is created. Then, the restricted candidate list (*RCL*) is defined as a subset of *CL* containing the best elements given a certain *GCF*. The size of the *RCL* is determined by the α parameter. When α=0, *RCL* is equal to the best element, whereas when α=1, then *RCL*=*CL*.

The following equation is used to create the *RCL*:

$$RCL(CL, GCF) = \left\{ l \in CL : GCF(l) \leq GCF^{\min} + \alpha \cdot \left(GCF^{\max} - GCF^{\min} \right) \right\} \qquad (2.8)$$

where:

$$GCF^{\min} = \min_{l \in CL} GCF(l) \tag{2.9}$$

$$GCF^{\max} = \max_{l \in CL} GCF(l) \tag{2.10}$$

Table 2-2: GRASP Constructive Phase

```
Procedure constructive Phase(GCF(.),α)
begin
   x = ∅;
   Initialize CL;
   while CL ≠∅ do
     Build RCL(CL,GCF);
     Select s randomly from RCL;
     x = x ∪ {s};
     Update CL;
  return x
end
```

Regarding the *local search* algorithm (Table 2-3), a neighborhood H of the solution x is built from a certain algorithm or function, for example, a simple exchange between one element in x and other not in x. Thus, depending on the improving strategy we can distinguish two cases: the *best-improving* and the *first-improving* strategies. While in the former all neighbors are investigated and the current solution is replaced by the best, in the latter the current solution moves to the first neighbor whose cost function value is smaller than that of the current solution.

Table 2-3: GRASP local search

```
Procedure local Search(f(.),NB(.),x)
begin
   Compute H(NB,x)
   while H≠∅ do
     Select x from H.
     Compute H(NB,x)
  return x
end
```

2.6.2 BRKGA meta-heuristic

BRKGA, recently presented by Resende in [Go10], belongs to the genetic algorithms (GA) family and it has been proposed to effectively solve optimization problems. In particular, it can be used to network related problems such as routing in IP networks and RWA in optical networks. Compared with other meta-heuristics, BRKGA has provided better solutions in shorter running times [Go10]. Fig. 2-7 illustrates the general framework of BRKGA.

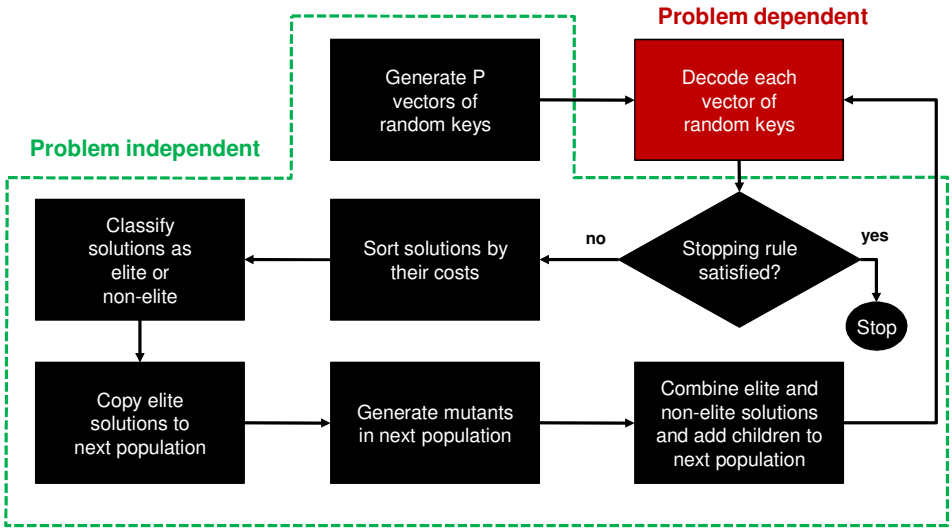

Fig. 2-7 BRKGA framework (reproduced from [Go10])

As in GAs, each individual solution is represented by an array of n genes (chromosome), and each gene can take any value in the real interval [0, 1]. Each chromosome encodes a solution of the problem and a fitness value, e.g., the value of the objective function. A set of individuals, called a population, evolves over a number of generations. At each generation, individuals of the current generation are selected to mate and produce offspring, making up the next generation. In BRKGA, individuals of the population are classified into two sets: the elite set containing those individuals with the best fitness values, and non-elite set. Elite individuals are copied unchanged from one generation to the next, thus keeping track of good solutions. The majority of new individuals are generated by crossover combining two elements, one elite and another non-elite, selected at random. An inheritance probability is defined as the probability that an offspring inherits the gene of its elite parent. Finally, to escape from local optima a small number of mutant individuals (randomly-generated) to complete a population are introduced at each generation. A deterministic algorithm, named *decoder*, transforms any input chromosome into a feasible solution of the optimization problem and computes its fitness value

In the BRKGA framework, the only problem-dependent parts are the chromosome internal structure and the decoder, and thus, one only needs to define them to completely specify a BRKGA heuristic.

2.7 Statistics

2.7.1 Multiple linear regression

A *linear model* (LM) is a statistical expression to predict a scalar *response* variable y from a vector $x=(x_1, x_2,\ldots, x_n)$ of *independent variables*. More formally, a LM can be defined as follows:

$$y = \beta x + \varepsilon \tag{2.11}$$

In this expression, βx represents the *linear predictor* and ε represents the error inherent to any statistical model. A β coefficient vector is computed from a set of observations characterized by a matrix X of *independent values* and a vector Y of *response values*. The most common method to compute β is by least squares minimization, solving the following formula:

$$\beta = (X' \cdot X)^{-1} \cdot X' \cdot Y \tag{2.12}$$

where X' represent the transposed X matrix.

The generalized linear model (GLM) [Ha07] is a generalization of the basic LM. In a GLM a *link function* $g(\cdot)$ is used to transform the linear predictor. Thus, the expression of a GLM is:

$$y = g(\beta x) + \varepsilon \tag{2.13}$$

The link function provides the relationship between the linear predictor and the response variable. In LM the link function is the identity and for GLM the most common link functions are the inverse, the logarithmic and the *logit* transformation.

Note that some transformation can also be done to the response variable. In order to validate a GLM, the probability distribution of the response variable should belong to one of the exponential family of distributions, i.e. Gaussian, Poisson, exponential, binomial, etc.. Thus, any transformation keeping the properties of exponential functions can be done, and then, the general form of a GLM can be finally stated as follows:

$$f(y) = g(\beta x) + \varepsilon \tag{2.14}$$

Although GLM fitting is a powerful method to model complex relations between response and independent variables, this methodology lacks of accuracy in some cases, e.g. when only one independent variable is used and its relation with the response variable is clearly non-linear. In this case, two special techniques of multiple linear regression can be applied, these are, *polynomial regression* and *segmented regression* [Sn80].

Polynomial regression consists in finding the γ-th degree polynomial in x whose coefficients (b) minimize the distance between predicted and observed values by using least squares minimization. More formally, a polynomial model can be expressed as follows:

$$y = \sum_{i \in [0,\gamma]} b_i x^i + \varepsilon \tag{2.15}$$

Segmented regression consists in finding a set of linear segments each one of them fitting a part of the response variable range. To apply this methodology, the first step is to find the set of *break points* that allow partitioning the variable range into a finite set of segments (S). Then and for each segment, a classical linear regression is applied, being thus the segmented model formulated as follows:

$$y = \{\beta_k x + \varepsilon_k, \quad s_k \le x < s_{k+1}, \quad \forall s \in S\} \tag{2.16}$$

In all models described above, the error ε identifies the information that the model cannot predict (i.e.: the lost information). The accuracy of the model can be quantified by estimating this error and/or by computing some *goodness-of-fit* statistic as described below.

2.7.2 Goodness-of-fit statistics

The goodness-of-fit of a statistical model is a measure that describes how well the model fits a set of observations. More specifically, a goodness-of-fit statistic evaluates the discrepancy between observed (i.e.: real) values and the values predicted (i.e.: expected) by a certain model.

Among different statistics, the *Mean Squared Error* (MSE) and the *Pearson determination coefficient* (R^2) are commonly used to validate linear models. Let $N=\{1, 2,\ldots, n\}$ be a set of individuals, $Y=(y_1, y_2,\ldots, y_n)$ a vector of observed values and $F=(f_1, f_2, \ldots, f_n)$ a vector of predicted values. Then, MSE and R^2 are computed as follows:

$$MSE=\sqrt{\frac{\sum_{i \in N} (y_i - f_i)^2}{N}} \tag{2.17}$$

$$R^2=1-\frac{\sum_{i \in N} (y_i - f_i)^2}{\sum_{i \in N} (y_i - \bar{y})^2} \tag{2.18}$$

A low value of MSE (which is the objective function minimized in the least squares minimization problem) indicates a model with high level of accuracy. However, since MSE is an absolute value which lacks of any comparison against a reference benchmark, it is difficult to take conclusions regarding the model accuracy only using MSE. For this reason the R^2 coefficient is more powerful for deciding if a

model is enough good, since its value is in the range [0, 1]. Thus, a R^2 value equal to 1 indicates the perfect linear correlation between model and observations, whereas a value equal to 0 denotes a completely random relation and, thus, a useless model. R^2 can be also represented as a percentage, so that when the number of parameters of a model is equal to the number of observations, the obtained R^2 is 100%. In that case (called *overfitting*), the model fits perfectly the observations but lacks from degrees of freedom, which are necessary to validate the model for predicting out from the set of observations.

Aiming at avoiding that overfitting, the *Akaike Information Criterion* (AIC) allows selecting the most useful model given a set of models with similar goodness-of-fit measures. Specifically, AIC not only computes goodness of fit, but also includes an increasing penalty function with respect to the number of model parameters. AIC can be computed for linear models as follows:

$$AIC = \log(V) - \frac{2|\beta|}{|N|} \tag{2.19}$$

In this expression V represent a loss function that computes the amount of information lost by the model. The quotient between the number of model parameters ($|\beta|$) and the number of observations ($|N|$) represents the penalty function. Given a set of candidate models, the preferred model is the one with the minimum AIC.

2.8 Economic evaluation

Aiming at evaluating optical networks from an economic point of view, three different components are defined: the *capital expenditures* (CAPEX), the *operational expenditures* (OPEX), and the *revenues*.

CAPEX can be defined as those costs related with purchasing and installing fixed structures such as cables, buildings, equipments, etc. Complementary to CAPEX, OPEX are those costs related with keeping the company operational, and includes personnel cost, rented infrastructures, external services, etc. In the opposite side, the revenues are the incomes that the network operator receives from its normal business activities, i.e. connectivity services to the clients.

In the decision making process, a network operator can evaluate a network investment project from the viewpoint of costs or revenues. Nevertheless, although costs can be used for comparing among alternatives, it is important to consider also the expected revenues. In this regard, the Net Present Value (NPV) is the most extended criteria to compare among investments taking in account costs and revenues [Ro02]. The NPV can be computed as follows:

$$NPV = \sum_{t=1}^{Y} \left[\frac{REVENUES_t - OPEX_t}{(1+r)^t} \right] - CAPEX \quad (2.20)$$

where Y is the total time period considered (in years), and r is the annual discount rate. In light of the NPV expression, it is worth mentioning that the operator will choose, among several options, the investment with higher NPV.

2.9 Summary

In this chapter, the most important concepts and terminology used in this thesis are presented. After introducing general concepts regarding graph theory and traffic engineering, the main features of WSON are highlighted. Then, a review of mathematical programming techniques and meta-heuristic methods are introduced. Finally, basic economic evaluation concepts are briefly defined.

After introducing these concepts, next section reviews the related work regarding the goals described in Chapter 1 with the aim to find open niches to cover with our contributions.

Chapter 3

Related work

This chapter reviews some previous works in the literature regarding characterization, planning and re-optimization of single layer and multilayer networks. Specifically, the differences between previous works and the goals proposed in this thesis are highlighted.

3.1 Network characterization

This section reviews some previous works on traffic estimation models and control plane resilience characterization.

3.1.1 Traffic estimation models

Several works provide estimation models for different network variables, among them, [Ko04] presents several models used to quantify some key network variables. These exact and semi-empirical expressions can be used as tools to provide quick approximate results for preliminary evaluation and design of mesh networks. Especially interesting is the expression of the average shortest path length (h) for planar networks:

$$h \cong \sqrt{\frac{|N|-2}{\delta-1}} \tag{3.1}$$

where $|N|$ represents the number of nodes and δ is the average nodal degree of the network. Alternative expressions to estimate h can be found in [La05].

Since blocking probability is considered the most important parameter to evaluate the GoS of a network, several works have faced the problem to analytically evaluate it [Bi96, Ba96.3, Li00, Al05, Ca07]. Basic blocking probability models for WP and VWP networks are presented in [Ba96.3]. Although the authors analyze the effect of some variables such as the average path length and the node size on

blocking probability over a wide range of networks, the proposed models do not accurately predict the blocking probability under dynamic traffic, e.g. Poisson arrivals and exponential holding times. Improving the previous work, authors in [Al05] proposed a decomposition method based on recursive computations to accurately estimate blocking probability in WP mesh networks for dynamic traffic scenarios. Nevertheless, author's assumption of static routing prevents from its application to our work.

Authors in [Bi96] propose an analytical model to calculate the blocking probability using random wavelength assignment over small and simple mesh networks. Although the model can be applied under static and dynamic routing, the accuracy obtained under dynamic routing is far from the fitness of the models when static routing is considered. Being accurate for dynamic routing but restricted to ring topologies, the study in [Ca07] presents recursive models to estimate the blocking probability when the first-fit algorithm is used for wavelength assignment.

In the case of multiple fibers in each link, the method proposed in [Li00] can be used to estimate the blocking probability for both ring and mesh topologies. The analytical results, however, only fit accurately the simulations when low traffic intensity and several fibers per link are considered.

Table 3-1 summarizes the related work presented above. Note that it contains those works that provide high-quality results for each feature.

Table 3-1: Survey of blocking probability models

Feature	References
Real mesh networks	[Ba96.3, Li00, Ca07]
Dynamic traffic	[Bi96, Li00, Al05, Ca07]
Dynamic routing	[Ba96.3, Li00, Ca07]
One fiber per link	[Bi96, Ba96.3, Al05, Ca07]
Single analitycal expression (w/o recursive computations)	[Ba96.3, Li00]

As shown, to the best of our knowledge, no work in the literature has addressed single analytical expressions to relate blocking probability and traffic intensity considering mesh networks with one single fiber per link, dynamic traffic and dynamic routing.

3.1.2 Control plane resilience quantification

Looking at the literature, some works have addressed the resilience of the GMPLS-enabled control plane. Amongst them, [Li02] and [Jj06] highlighted the reasons of a decoupled control plane in all-optical networks and addressed the resilience

requirements that this would impose. In addition, [Ko08] and [Pe07] concluded that the most severe GMPLS protocol disruptions due to message losses were found in RSVP-TE, the protocol used for path signaling.

Especially interesting is the contribution in [Pe07], where the new parameter P_d is introduced to quantify the resilience of the GMPLS control plane. P_d stands for the probability that any connection request or tear-down is dropped during the failure recovery time Δt (i.e., forwarded onto the failed control link). Both situations would affect the network GoS, by either blocking/delaying a connection request, or keeping allocated but not used data plane resources. Moreover, they present an analytical formulation to accurately estimate P_d given some traffic intensity parameters, the required Δt and a factor called P_L, that stores the probability that a connection request or tear-down is signaled on a certain control plane link. Finally, they present an analitycal formulation to accurately estimate P_L for ring topologies.

Although the analitycal P_d expression defined in [Pe07] could be used for our work, the estimation of P_L does not work properly for asymmetrical mesh control planes, which is one of our goals.

3.2 Optical network design

In this section, the main contributions found in the literature regarding single layer network problems are firstly reviewed. Secondly, several works on multilayer networks design are analyzed, emphasizing the design of survivable networks. Finally, the state-of-the-art regarding control plane design is reviewed.

3.2.1 Single layer networks

A good survey on single layer network design can be found in [To07], where the authors define the WDM network design problem as follows: given a static traffic demand matrix, the aim is to find the optimal values of a set of network variables that minimize a given cost function under a set of constraints. At this point, problems can be separated into two main groups: single fiber network design and multi-fiber network design. The former group consists in optimal routing and wavelength assignment of the lightpaths, also known as the RWA problem [Ra98]. The latter consists in routing and fiber and wavelength assignment (the RFWA problem) and extends the RWA problem with the inclusion of fiber link allocation constraints. Note that the RWA problem can be solved not only under static traffic scenarios (called *off-line* RWA) but also under dynamic traffic assumption (i.e. *on-line* RWA). It is worth mentioning that the complexity of the RFWA problem is higher than the complexity of the RWA one. In fact, achieving an optimal solution

for the RFWA problem is quite challenging even for small networks [Ca98], and thus some works explored the complexity of both RWA and RFWA problems.

Among the contributions analyzing the complexity of the above problems, authors in [Ch92] demonstrated that the RWA problem is NP-complete. Since the addition of link allocation increases the complexity of RWA, the RWFA problem is also NP-complete. Moreover, the complexity of RFWA increases hardly in case of dynamic traffic [Xu00], complex node and link cost functions [Ca98], and in the case of non-linear functions [Le98] where non-linear programming is required. For this reason, the reduction of the complexity in single layer network design problems has been widely studied from three different points of view.

First, the use of the most appropriate mathematical formulation for each specific problem leads into a significant complexity reduction. In this regard, two main formulations can be found in literature: the flow formulation (FF) and the route formulation (RF) [To07]. While the variables in FF are the flows on each link relative to each source-destination OXC pair, the variables in RF are the paths connecting each source-destination demand pair. Note that a set of pre-computed routes for each demand pair is required in RF. These formulations are exhaustively compared in [Wa96], for VWP and WP networks. Alternatively to FF, authors in [To07] proposed a novel formulation called source formulation (SF). More specifically, they present models for WP and VWP networks providing better performance results than FF. However, the main drawback of SF with respect to FF is that it cannot be extended to optimize path-protected WDM networks, which is one of our objectives.

Second, several methods to reduce the complexity of the well-known RWA and RWFA formulations have been presented. For instance, authors in [Ra95] improved the performance of RWA by means of bounds derived from the relaxation of integer constraints for RF and FF formulations. In [Oz03], authors present new ILP formulations that tend to provide integer solutions even when the integrality constraints are relaxed. This method provides feasible and optimal solutions faster than classical ILP formulations. In the case of RWFA, RF scales better than FF when the size of instances makes RFWA impractical to solve. Reducing the number of considered routes to the first k shortest paths reduces the number of variables and constraints of ILP, making its exact solving more affordable. This method is called constrained routing and it has been studied in [Wa96, Ba00]. Although methods proposed there allow reducing the complexity, solving real-life instances could be still being unaffordable in terms of computational effort.

Third and aiming at obtaining solutions within practical computational effort, several works propose solving methods to control the problem complexity. In this regard, authors in [Ca98] introduced the possibility of stopping the branch-and-bound algorithm after finding a certain number of feasible solutions or after running for a certain time period. A simplification of the RWFA problem, where the main problem is decomposed into a sequence of separated and simpler problems

was proposed in [Po99]. Other research works illustrate how optimization techniques and tools become useful to solve RWFA efficiently; applications of Lagrangian relaxation [Sa02], integer constraints relaxation [Ba00], randomized rounding [Ba96.1], or column generation [Se09] are some examples. The use of heuristic methods, such as the one in [Xu00] or genetic algorithms [Sa99, Mo11], were investigated to solve large instances or complex problems.

In addition to the basic problems presented above, some extensions of the RWA and the RWFA problems have been studied in the literature. As an example, authors in [Al00] include routed signal degradation to the RWA formulation obtaining the RWA-P version. However, the most common extension to RW(F)A problem is the inclusion recovery. In this context, a new ILP formulation based on protection structures called *p-trees* is presented in [Se09] providing fault tolerant networks. Authors in [Mo11] faced the problem of designing a single layer optical network to be survivable against any single link failure.

Since several classes of protected and unprotected paths co-exist in real networks, differentiated traffic environments have been deeply studied [Gr03, Ko05, Gu06]. In this regard, authors in [Gr03] and [Ko05] suggest four service levels based on different recovery mechanisms in a mesh network. These works, however, do not consider any separation of the network resources. Aiming at providing a better overall network performance in traffic differentiated environments, resource differentiation could also be applied. To this end, authors in [Gu06] define a new protection scheme and three resource types: 1) primary resources that can be used by primary paths; 2) spare resources that can be shared by backup paths; and 3) mixed resources that can be shared by both primary and backup paths. Although this strategy outperforms other protection schemes such as classical SPP environment, the requirement of VWP networks, i.e. with full wavelength conversion capability, is needed.

Another extension of the basic RWA receiving recent research attention is the impairment-aware (IA) RWA. IA-RWA problems include the computation of Q-factor of lightpaths as constraints for the RWA decisions [Az09]. However, the inclusion of Q-factor computation in the RWA problem presents some drawbacks, mainly due to the computation of non-linear impairments. Since XPM presents the main drawbacks in computational effort, some works study ways to reduce the impact of XPM computation time in on-line IA-RWA. Authors in [Sa11] present an approach where lightpath set-up times are minimized by means of guard bands, i.e., leaving unused wavelength channels between lightpaths to reduce the effect of XPM. In [Ca99] a generalized model of the XPM degradation in fiber links consisting of multiple fiber segments with different characteristics and optical amplifiers is presented. Although this original model was subsequently simplified in other works (e.g. [Pa03]), Q-factor computation times were still in the order of seconds and thus impractical when used in the control plane, even using ad-hoc hardware-accelerated computation [Qi11].

In the case of off-line IA-RWA, the inclusion of non-linear impairments prevents from using ILP formulations. For this reason, many works addressed the IA-RWA problem considering only linear impairments which can be pre-computed beforehand when using pre-computed routes in arc-path formulations. Other works propose the use of a *worst-case approach* for non-linear impairments such as FWM [Pa08], assuming links fully loaded. This approach, however, is not valid for XPM since its effect is several times higher than the one of FWM and, thus, the expected error provided by that worst-case assumption would be too high to obtain meaningful results [Te99].

Few works have considered non-linear impairments in a more precise way, e.g. authors in [Ma09] propose an ILP formulation designed for reducing interference among lightpaths as much as possible. They propose to compute the Q values of the lightpaths to evaluate its quality in a post-optimization process. However, that method does not take advantage of the Q values to improve the solution. Some other works propose ILP formulations with similar constraints combined with iterative methods to compute the *Q-factor* during the optimization process. Among them, authors in [Pa09] propose a sophisticated iterative algorithm composed by four simple ILP formulations. The results obtained by these ILPs are afterwards evaluated in terms of *Q-factor* and some tuning parameters are modified for the next iteration, until the convergence is reached. In spite of the good quality and performance of this method, the impossibility to embed the *Q-factor* computation in the ILP (mainly due to the non-linearity of the XPM mathematical expressions) prevents from reducing the IA-RWA problem with Q constraints to a single ILP formulation.

Finally and regarding the objective function, the most used are the minimization of the blocking rate [Ra95, Kr01], the number of used wavelengths [Wa96], and the total number of used WDM channels in the network [Ba96.1]. In the case of RFWA, the cost of fiber links and other equipment is usually added to the minimization. From an economic perspective, authors in [Xi09] addressed the maximization of revenues from the perspective of SLA penalties, as SLA breaches represent large revenues losses for network operators. This work lacks from a fair comparison between costs and revenues, which are especially interesting for network operators. In the opposite, investment evaluation functions, such as the NPV are commonly used in techno-economic studies over optical networks [Ve07]. Nevertheless, and to the best of our knowledge, any work addressed the design of a single layer optical network minimizing the NPV.

3.2.2 Multi-layer networks

Looking at the literature, two main problems can be distinguished: the virtual topology design problem and the virtual and optical topology design. First, the virtual topology design (VTD) problem contains different versions with different degree of complexity. The most basic problem is the grooming, routing, and

wavelength assignment, also known as the GRWA problem [Hu04.1]. The GRWA problem focuses on the optimization of flow aggregation and on the routing and wavelength assignment of the lightpaths associated to virtual links, given an optical topology. Several works can be found in the literature studying the GRWA problem (e.g., see [Sa99, Gr01, Ra04, Ja06]). In addition, extensions of the GRWA including dimensioning were presented in [Mu96, Or07, Be08]. Note that the complexity of these versions is higher than that of the basic GRWA problem.

Second, the virtual and optical topology design (VOTD) problem jointly optimizes both aggregation and optical layer and it has been considered in [Xi03, Ka05, Ku05.1]. It is worth mentioning that the complexity of VOTD problems is significantly higher than that of the VTD. In fact, the most basic GRWA problem is NP-complete, as proven in [Hu04.1] and, consequently, every other multilayer network design problem derived from GRWA is NP-complete. For this reason, the development of methods to obtain good (near-optimal) solutions in practical execution times represent a key topic in multilayer networks research.

Several works exploiting the way to reduce the complexity and the computational effort for both types of multilayer networks have been proposed. On the one hand, optimization methods and tools have been extensively exploited in the literature, such as column and row generation [Kn07], Lagrangian Relaxation [Zh10], branch&cut with cut-set inequalities [Or07], and LP-based decomposition [Ku05.2]. On the other hand, in order to solve large instances, several heuristics methods have been developed adapting well-known meta-heuristic algorithms. As an example, adaptations of genetic algorithms are presented in [Sa99, Xi03], whereas tabu search is used in [Gr01]. Authors in [Mu96] combine simulated annealing for topology design and flow deviation, a specific network design algorithm presented in [Fr73], for traffic routing. The references presented here not only introduce different optimization methods but also solve different variants of multilayer network design problem.

Among different extensions to the GRWA problem, the inclusion of dynamic traffic patterns has been proposed in few works. Statistical multiplexing in GRWA is considered in [Be08], whereas stochasticity is considered in [Gr01] by means of probability density functions instead of static traffic demands.

Several works consider hierarchical flow aggregation as a way to increase the capacity of the network. Authors in [Ch08] consider the nodes grouped in clusters with a central hub. Hub nodes are responsible for grooming traffic before leaving the cluster. In [Ch10.1], authors develop an algorithm to find optimal clusters. However, the main weak aspect of those works is the limitation of the virtual topology, restricted to be a star. Other extensions, as QoS-related constraints have been studied such as a maximum bit error rate in the logical topology design [Ra04].

Nevertheless, the most important extension is the design of survivable multilayer networks considering some kind of recovery scheme [Pi06, Ch01, Ch03, Ch10.2,

Ou04.1, Ja06]. In survivable multilayer networks, protection and restoration schemes at different layers can be jointly applied. In this regard, authors in [Ja06] and [Ou04.1] propose a survivable logical topology design able to recover all the traffic after any single link failure. Since IP/MPLS nodes are not always as reliable as traditional telecom equipments, authors in [Ch01] propose a joint IP/optical layer restoration after a router failure. Applying redundancy, backbone nodes are duplicated and, consequently, the network CAPEX highly increases.

Notwithstanding, other recovery schemes different than redundancy can be specifically designed for multilayer networks, e.g., authors in [Ch10.2] present a tutorial of several multilayer recovery schemes, evaluating the quality of them based on some parameters such as availability, recovery time and affected traffic. Another example of recovery scheme without node duplication is presented in [Ch03], where authors proposed and evaluated a coordinated link restoration scheme to be used in packet-over-optical networks. Although the proposed scheme is cost-effective compared with duplicating nodes, they require the IP/MPLS and the optical topologies to be symmetrical, i.e. every node has both aggregation and optical switching capacities.

Finally, regarding the objective function, several mathematical formulations with different objective functions have been developed to solve the above design problems. Authors in [Mu96] propose a basic ILP formulation with two different objective functions: minimize the average delay of traffic demands and minimize the maximum flow in a link. Other authors propose the minimization of the number of transponders [Hu04.1] and the minimization of traffic congestion [Ra04] for the GRWA problem. In [Be08] a MILP model for the problem of optimizing the number and the location of the nodes and the link capacities of a MPLS-over-DWDM multi-layer network is presented. From an economic perspective, authors in [Zh10] present an ILP formulation to maximize a utility function for the network operator, i.e. the difference between revenues and costs.

Table 3-2 summarizes the works surveyed above regarding multilayer network design.

3.2.3 Control plane design

As mentioned in Chapter 2, the separation introduced in GMPLS between control and data planes provides several benefits to the network operators, such as an enhanced flexibility in the control plane deployment or the possibility to run control-plane-driven data plane recovery mechanisms (e.g.: [Gr03], [Ve08]) especially in the *out-of-fiber* configuration where the control plane remains alive upon data plane failures. However, it also poses new challenges for efficiently designing the control plane efficiently as well as providing it with resilience to fulfill the necessities of emerging services.

Table 3-2: Survey of multilayer network design

Feature	References
GRWA	[Gr01, Hu04.1, Ou04.1, Ra04, Ja06, Ch08, Ch10.1, Zh10]
GRWA + Dimensioning	[Mu96, Or07, Be08]
Non-Symmetrical Layers	[Hu04.1, Be08, Ch08, Ch10.1]
Hierarchical Grooming	[Ch08, Ch10.1]
Survivability against failures	[Ch03, Ja06] (link failures), [Ou04.1] (link and port failures), [Ch01, Ch10.2] (node failures)

In next-generation optical networks, every control plane link counts for two full-duplex control interfaces i.e. two light transmitter-receiver pairs in the *in-fiber* control plane configuration that must be equipped, configured, and managed, thus increasing both CAPEX and OPEX. Hence, significant cost savings can be expected from reducing the number of control plane links. Notice, however, that a reduction of control plane links increases the amount of control information in the remaining ones, which accentuates the negative effects of control plane link failures. Moreover, the resulting control plane paths become also longer, and so the data plane failure recovery times if control-plane-driven restoration is implemented in the network.

To the best of our knowledge, the problem of design an optimal GMPLS control plane topology has not been faced since no works can be found in the literature.

3.3 Resources re-optimization

As stated in Chapter 2, two re-optimization problems are considered: the lightpath rerouting problem and the virtual topology reconfiguration problem. This section reviews the related work on both problems.

3.3.1 Lightpath rerouting

Although rerouting was originally introduced in the design of circuit-switched telephone networks [Gi83], it has been also recently applied to optical WDM networks [Ya04]. Rerouting algorithms may generally be categorized following two different criteria: the mechanism that triggers the rerouting procedure and the rerouting granularity.

Regarding the trigger mechanism, algorithms can be classified into passive and active. In passive rerouting, when the normal routing procedure fails, the rerouting procedure tries to accommodate the new connection request by migrating some existing lightpaths/connections [Mo99, Ya04]. On the contrary, an active rerouting procedure is typically controlled by a timer, and it periodically migrates existing lightpaths/connections to minimize the use of network resources [Xi05].

With respect to the granularity of the rerouting, algorithms can be divided into lightpath level and connection level. In lightpath level algorithms all the flows transported in a lightpath are rerouted as a single connection [Mo99, Xi05], whereas in connection level rerouting algorithms the flows transported in a lightpath can be separately rerouted [Ya04].

In general, the aim of rerouting is to minimize the inefficiency caused in dynamic traffic scenarios. In this regard, authors in [Le96] proposed a move-to-vacant wavelength retuning (MTV-WR) rerouting scheme with the aim to alleviate the effects of wavelength continuity constraint. This algorithm was improved with faster, simpler and more efficient versions in [Mo99, Ch07]. Although the results of all these works show a considerable reduction in the blocking probability, the performance was still far away from the performance when wavelength conversion is available in the network.

Recent works have proposed new algorithms with better performance results. Among them, three contributions can be highlighted. Authors in [Ra07] proposed two wavelength reassignment heuristics, namely the Minimum Overlap wavelength to Least Congested wavelength (MOLC) heuristic and the Random heuristic. Their performance on some standard backbone optical networks shows that the proposed algorithms can mostly remove the blocking due to the wavelength continuity constraint and can achieve the wavelength conversion performance.

Authors in [Wa10.1] introduce the shortest path wavelength rerouting (SPWRR), a rerouting algorithm for dynamic provisioning of lightpaths. Although the SPWRR rerouting algorithm offers very small blocking probability when the length of the lightpaths is short, the usefulness of the algorithm decreases for large networks with longer routes. The same authors present an extension of this work in [Wa10.2], where the Lightpath Rerouting Algorithm (LRRA) was proposed for larger networks. The behavior of LRRA is complementary to that of SPWRR, since it gives better results for large networks than for small ones. Note that in the best situation for each algorithm the negative effects of wavelength continuity constraint are significantly reduced. Thus, the selection of the algorithm can be done depending on the size of the network, being both algorithms part of the same rerouting method.

3.3.2 Virtual topology reconfiguration

The problem of on-line virtual topology reconfiguration (VTR) in WDM mesh networks under dynamic traffic has been widely studied in the literature [La94, Ba01, Ba96.2, Ba00, Ra00]. The problem is generally faced as a two-phase operation: first, the virtual topology is redesigned for the new traffic conditions and, second, some operations are executed to migrate from the old to the new topology. While the complexity of the redesign problem is comparable with that of the design problems presented in the previous section, the migration problem has proven to be NP-complete [Di07].

In view of the VTR procedure, two main problems are detected: the prediction of future traffic conditions and the impact of the migration phase over the current working traffic. Regarding future traffic patterns, authors in [Ba00, Sr01] assume future traffic demand known in advance. With this information in hand, considerable effort can be dedicated to the design of the new virtual topology, thus reducing the amount of changes during the transition phase. However, the assumption on future traffic being known in advance may decrease the value of the newly designed virtual topology if the traffic changes are inaccurately predicted. Authors in [Ge03] improve the results of previous works proposing a VTR version where the ongoing traffic, instead of being estimated in advance, is systematically monitored changing the virtual topology accordingly. There configuration process is seen as a continuous measurement-adaptation system where small adjustments are made, instead of waiting for a noticeable system efficiency drop to change the entire topology.

Regarding the impact of the migration phase, note that lightpaths involved in the transition cannot be used for the ongoing traffic. This fact could lead into temporary traffic disruption during lightpaths reconfiguration. For this reason, earlier studies developed techniques to minimize the disruption of the ongoing traffic [La94, Ro95, Na00]. These studies dealt with this problem either by performing the reconfiguration on all network elements in parallel [Ro95] or by applying step-by-step changes until the new virtual topology is settled upon [La94, Na00]. The consideration of traffic grooming capability provides better performance than that of the classical VTR problem in terms of network disruption and resource utilization, as demonstrated in [Ak06]. Moreover, the use of meta-heuristics has been proposed in works such as [Di07], where authors proposed a genetic algorithm for solving the migration phase of the VTR problem. Nevertheless, all the methods proposed in these works cannot completely eliminate the traffic disruption.

In order to provide a hitless reconfiguration method, i.e. without traffic disruption, authors in [Ba96.2] propose a methodology to perform it without any loss of data, where the transition between topologies is achieved by first establishing all new virtual links without removing any existing virtual link. Then, the virtual links of

the old topology are removed after the traffic is rerouted through the virtual links of the new topology.

Although traffic disruption represents a key aspect to evaluate the quality of a VTR method, other objective functions can be found in literature. To minimize the traffic disruption, some works propose MILP formulations where objective functions such as network capacity or network cost are minimized [Ak06, Hu04.2]. In this regard, examples of objective functions are the minimization of the maximum link load [Na00], the minimization of reconfiguration duration [La94], and the minimization of disrupted transceivers [Ta02]. Multiple comparisons are proposed in [Ra00], where authors compared the performance of three different cost functions: the average hop count, the total number of lightpaths, and the total number of used physical link channels. Finally, authors in [Ak06] proposed a single objective function that merges the traffic load, the traffic grooming ratio, and the route length of lightpaths.

An algorithm to solve the VTR problem when a link failure occurs in a IP-over-WDM network is presented in [Sr06]. This algorithm, which limits the number of steps of the reconfiguration process, achieves better performance in larger networks than in smaller ones.

Table 3-3 summarizes the related work regarding VTR problems. Note that the amount of changes in the migration phase and the traffic disruption are minimized in the vast majority of works. Nevertheless, hitless VTR problem versions are barely present in literature.

Table 3-3: Survey of virtual topology reconfiguration

Feature	References
Minimize O/E port cost	[Ra00, Ma04]
Minimize reconfiguration costs (number of changes, disrupted lightpaths)	[La94, Ro95, Ba00, Na00, Ra00, Sr01, Ma04, Ak06, Sr06]
Minimize used network capacity	[Ba96.2, Ra00, Ak06, Sr06]
Hitless reconfiguration (No traffic disruption)	[Ba96.2]
Reconfiguration strategy	[La94, Ba96.2, Ba00, Sr01] (static traffic pattern), [Ra00, Ge03, Ma04, Ak06] (dynamic adaptation), [Sr06] (after link failure)

3.4 Summary

In this chapter, the most relevant contributions related with the objectives defined in Chapter 1 are reviewed.

Regarding characterization, from the perspective of blocking probability estimation, several analytical models were developed, even for mesh networks, based on some recursive algorithms. Nevertheless, no single analytical or empirical formula for predicting blocking probability given a certain topology and traffic intensity is currently available. Additionally, the estimation of control plane resilience for mesh networks has not been addressed yet.

Optical network planning has been widely studied for single layer and multilayer scenarios. Although some key works study planning problems considering traffic and resource differentiation, our aim is to minimize the revenues of differentiated resource and traffic WP networks, which differs from the previous work. Moreover, when impairments are considered, the current models for computing XPM in on-line IA-RWA and off-line IA-RWA could be improved in terms of computational time and easiness for being included in ILP formulations, respectively.

Regarding survivable multilayer network design, several works faced the survivability against different types of single failures. Notwithstanding, and to the best of our knowledge, the design of a multilayer network considering simultaneously survivability against single OE port, optical link and IP/MPLS node failures, and considering hierarchichal grooming has not been addressed.

Finally, many contributions about LR and VTR problems have been found in literature. To minimize the impact of traffic migration, the reduction of the traffic disruption has been a hot topic. However, the hitless VTR problem, which represents one of our main goals, has not been covered in the literature.

Several open issues have thus been detected. Next chapters will focus on occupy the revealed niches studying them and providing our contributions.

Chapter 4

Statistical Q-factor computation for impairment-aware RWA problems

Impairment-aware RWA (IA-RWA) algorithms include the Q-factor evaluation in their decisions on whether to establish or block new optical connections. Nevertheless, Q-factor computation presents some drawbacks that make difficult its use in both on-line (dynamic) and off-line (static) IA-RWA algorithms. In the case of dynamic scenarios, the long computation times inherent to calculate Q values drastically increases lightpath set-up times. On the other hand, the use of Q-factor analytical expressions in mathematical programming formulations for static off-line IA-RWA involves those problems to be non-linear, which make them complex and prevents from solving them in practical times. Both, long computation times and non-linearities are mainly as a consequence of non-linear impairments computation. In view of that, this chapter presents a statistical Q model which includes two models to compute XPM noise variance, the dominant non-linear impairment, fitting on-line and off-line IA-RWA scenarios. Exhaustive evaluation reveals that the proposed models provide fast and accurate methods to estimate PLI in terms of Q-factor that can be easily used to solve IA-RWA problems. Finally and aiming at illustrating the uselfulness of statistical Q-factor computation, two on-line and off-line IA-RWA examples are presented, focusing on the benefits of applying statistical Q models.

4.1 XPM Noise Variance Computation

In this section, some properties of XPM noise variance are analized with the aim to present a deterministic approach which represents the basis of next statistical models.

4.1.1 XPM noise variance analysis

Let $G(N, E, W)$ be a graph describing an optical network, where N is the set of nodes, E be the set of fiber links, and W be the ascending frequency ordered set of wavelengths. Every wavelength is associated with an optical channel labeled from 1 to $|W|$. Note that each label uniquely identifies one specific frequency in the spectrum. Additionally, let $a(e)$ be the number of amplifiers in the link $e \in E$.

Since the XPM of a lightpath depends on the physical route and the assigned wavelength, $\sigma^2_{XPM}(r,\lambda)$ stores the XPM of a lightpath using the route r and the wavelength λ. Besides, let $\sigma^2_{XPM}(e,\lambda)$ be the XPM noise variance on the reference channel λ in the link e. $\sigma^2_{XPM}(e,\lambda)$ represents the interference of every used optical channel in the link e over the reference channel λ. Equation (4.1) illustrates the relation between $\sigma^2_{XPM}(r,\lambda)$ and $\sigma^2_{XPM}(e,\lambda)$, where φ_{re} is equal to one if link e in route r.

$$\sigma^2_{XPM}(r,\lambda) = \sum_{e \in E} \varphi_{re} \cdot \sigma^2_{XPM}(e,\lambda) \tag{4.1}$$

Additionally, let $\sigma^2_{XPM}(e,\lambda,i)$ be the XPM noise variance on the reference channel λ as a consequence of the channel I, in link e. Aiming at empirically finding some relation between $\sigma^2_{XPM}(e,\lambda)$ and $\sigma^2_{XPM}(e,\lambda,i)$, we developed a classical factorial experiment [Mo04] consisting of thousands of XPM variance computations using the analytical model in [Pa03]. Each computation has been defined by a unique combination of experimental variables, being those the number of link amplifiers, the number of wavelengths, the reference channel, and the state of the other channels (i.e., busy or free). Note that when the number of busy channels is equal to one, the obtained $\sigma^2_{XPM}(e,\lambda)$ value matches with a specific case of $\sigma^2_{XPM}(e,\lambda,i)$. After analyzing the obtained values using statistical correlation tools, the following can be stated without error, where δ_{ei} is equal to 1if the channel I is busy in the link e. This is in perfect accordance with similar expressions deduced in [Ca99] and [Pa03].

$$\sigma^2_{XPM}(e,\lambda) = \sum_{\substack{i \in W \\ i \neq \lambda}} \delta_{ei} \cdot \sigma^2_{XPM}(e,\lambda,i) \tag{4.2}$$

As conclusion, each channel being used by an active lightpath adds some interference to the XPM variance of the reference channel independently of the state of the rest of the channels. This additive behavior paves the way to consider an alternative model to calculate $\sigma^2_{XPM}(e,\lambda)$ based on modeling $\sigma^2_{XPM}(e,\lambda,i)$.

For illustrave purposes, Fig. 4-1 plots the $\sigma^2_{XPM}(e,\lambda,i)$ values for $i=\lambda+1$ (i.e., interference of the adjacent wavelength channel) and $i=\lambda+2$ (i.e., interference of the wavelength channel at a distance of two with respect to the reference one) with λ=1 to 79, for links different values of $a(e)$. Illustrated $\sigma^2_{XPM}(e,\lambda,i)$ values have been computed from the parameter values specified in [Ji10] with a channel spacing of 50 GHz and a channel bit rate equal to 10 Gb/s. As shown, $\sigma^2_{XPM}(e,\lambda,i)$, λ, and $a(e)$

are clearly nonlinearly related. This fact increases the required complexity of the models, since considering simple linear relations between variables leads to models with unacceptable goodness-of-fit.

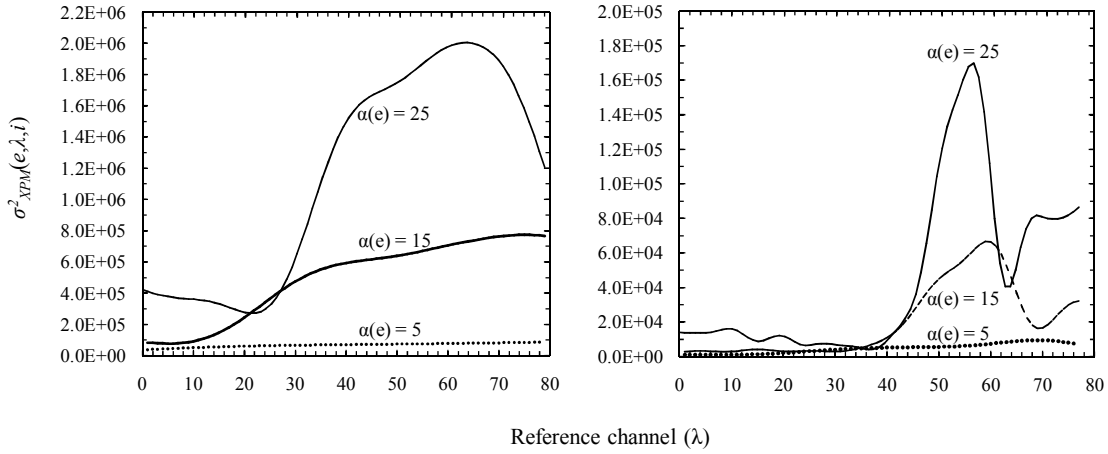

Fig. 4-1 $\sigma^2_{XPM}(e,\lambda,i)$ plots for i= λ+1 (left) and i= λ+2 (right) for links with 5, 15, and 25 amplifiers.

4.1.2 Deterministic XPM models

In view of the additive behavior of XPM variance shown above, a very basic approach for modeling $\sigma^2_{XPM}(e,\lambda,i)$ consists of pre-computing and storing the whole set of possible $\sigma^2_{XPM}(e,\lambda,i)$ values (hereafter referred to as *full-deterministic* model). $\Sigma^2_{XPM}(e,\lambda,i)$ depends on three discrete variables (i.e. $\alpha(e)$, λ, and i) and then, the set of $\sigma^2_{XPM}(e,\lambda,i)$ values is finite and countable, being its size equal to $|W|*(|W|-1)*maxAmp$, where $maxAmp=max\{\alpha(e),\ e\in E\}$. Thus, the application of the full-deterministic approach provides an alternative valid method to obtain exact values for the XPM variance. Nevertheless, the weak aspect of this approach is the size of the set of XPM noise variance values to store in real networks. For instance, consider fiber links with a number of amplifiers up to 25 (2,000 km) then the size of the whole set raises to the impractical value of 39,000 for 40, or even to 158,000 for 80 wavelengths.

The size of the set of values to be stored can be decreased at the expense of adding some error. In this regard, recall that although each busy wavelength channel adds some interference to the XPM variance of a certain wavelength reference channel, this interference decreases with the distance between wavelength channels until the gap is too large to produce any significant effect. Then, the first step for reducing the size of the *full-deterministic* model is to determine the range of wavelength channels significantly 43ortioning43 the reference one. At this point, we define the *channel-interference negligible distance* (η) as the parameter defining the half-size of that range. Thus, those wavelength channels at a distance greater that η from the reference wavelength channel are assumed to have a negligible

XPM interference over the reference one. This model is hereafter called *restricted deterministic*

Equation (4.3) shows the general expression of the restricted deterministic model, where ε_{link} represents the error as a consequence of reducing information, i.e. dismissing every wavelength channels at a distance longer than η. Note that when $\eta=(|W|-1)/2$ all wavelengths in the optical spectrum are considered, being the obtained model equal to the full deterministic one (i.e., $\varepsilon_{link}=0$).

$$\sigma^2_{XPM}(e,\lambda) = \sum_{\substack{i=\max(1,\lambda-\eta) \\ i\neq\lambda}}^{\min(\lambda+\eta,|W|)} \delta_i(e)\cdot\sigma^2_{XPM}(e,\lambda,i) + \varepsilon_{link} \tag{4.3}$$

It is worth noting how, after this first step, the number of $\sigma^2_{XPM}(e,\lambda,i)$ values to be computed in the worst case is reduced to $2\eta*|W|*maxAmp$ (from $\lambda-\eta$ to $\lambda+\eta$).

Although the size of the restricted deterministic model can be significantly smaller than the one of the full deterministic, it is still too high. For instance, assuming $\eta=4$, 16,000 XPM variance values need to be stored when links with 80 wavelengths are considered. Then, aiming at reducing the size of the deterministic models without a significant loss of information, statistical models to accurately compute XPM are proposed in the following section. These models are based on the restricted deterministic one defined in eq. (4.3).

4.2 XPM statistical models

In this section, we propose two different statistical models to predict $\sigma^2_{XPM}(e,\lambda,i)$ with the aim to reduce the size of the full deterministic model without introducing significant error.

4.2.1 The restricted polynomial model

The *restricted polynomial* model consists of finding a polynomial to estimate each $\sigma^2_{XPM}(e,\lambda,i)$ value for those channels in the range $[\lambda-\eta, \lambda+\eta]$. We denote that approximate model as $s^2_{XPM}(e,\lambda,i)$, and then $\sigma^2_{XPM}(e,\lambda,i) \approx s^2_{XPM}(e,\lambda,i)$. The mathematical formulation of the polynomial is as follows:

$$s^2_{XPM}(e,\lambda,i) = \sum_{j\in[1,\gamma]} u_{ij}\cdot\lambda^j + \sum_{k\in[1,\gamma]} v_{ik}\cdot\alpha(e)^k + \sum_{j\in[1,\gamma]}\sum_{k\in[1,\gamma]} w_{ijk}\cdot\lambda^j\cdot\alpha(e)^k + b_i \pm \varepsilon_{pair} \tag{4.4}$$

where u, v, w, and b are the polynomial coefficients. Note that the superscripts on variables indicate the corresponding powers of the polynomial. From eq. (4.5), the number of coefficients of each $s^2_{XPM}(e,\lambda,i)$ model is $(\gamma^2+2\gamma+1)$. Note, however, that some of these coefficients could be zero. Then, the total number of coefficients for the restricted polynomial model (eq.(4.3) and eq. (4.4)) is bounded to $2\eta*(\gamma^2+2\gamma+1)$.

For the sake of simplicity, we have modeled every $s^2_{XPM}(e,\lambda,i)$ with the same parameter γ. The optimal value of γ and the respective polynomial coefficients can be obtained by adapting a classical problem of least squares minimization [Mo04] as follows:

Given:

- a set of σ^2_{XPM} values,
- a η value,
- a target error.

Output:

- the degree of the polynomials γ,
- the set of coefficients u, v, w, and b.

Objective: Minimize the degree of the polynomials γ that fits the target error.

The restricted polynomial model opens the possibility to compute XPM values from solving a simple mathematical operation. Since the time needed to execute this operation is negligible, the use of this statistical model in on-line IA-RWA algorithms provides a better performance than the use of recursive XPM computation. Nonetheless, the presence of exponents over λ avoids using this model in ILP formulations, since the wavelength assignment of each path, i.e. the value of λ, becomes part of the unknowns of the problem. To overcome this drawback, the next section provides a linear XPM model specially designed to be used in ILP formulations.

4.2.2 The restricted linear model

The restricted linear model for estimating $s^2_{XPM}(e,\lambda,i)$ is a continuous function in λ consisting of a number C of connected linear segments, each represented by a slope and a range of wavelengths. Equation (4.5) formally states the restricted linear model where f_{eic} and g_{eic} represent the slope and the first wavelength of each segment (*break point*), respectively. Note that the first and last breakpoint are the first and last wavelength in the spectrum, respectively (i.e. $g_{ei1} = 1$ and $g_{eiC+1} = |W| - i$).

$$s^2_{XPM}(e,\lambda,i) = \left\{ f_{eic} \cdot \lambda, \quad \forall g_{eic} \le \lambda \le g_{ei(c+1)} \quad \forall c = 1..C \right\} \tag{4.5}$$

The coefficients of the restricted linear model are the values of the slopes (f_{eic}) and the break points (g_{eic}). Aiming at reducing the number of coefficients to store, every f_{eic} and g_{eic} can be modeled by means of mathematical expressions such as polynomials, exponential forms, etc. However, λ cannot be part of those expressions to produce a linear function. Therefore, we model f_{eic} following a polynomial of degree ρ using the number of amplifiers in the link as unique variable. Equation

(4.6) illustrates the model to estimate f_{eic}, where t_{icj} represents the j-th coefficient of the polynomial:

$$f_{eic} = \sum_{j\in[0,\rho]} t_{icj} \cdot \alpha(e)^j \tag{4.6}$$

Regarding g_{eic}, note that it represents an integer in the range $1..|W|$. In order to avoid rounding operations and to provide a linear expression, eq (4.7) defines a linear function that predicts an integer g_{eic} value:

$$g_{eic} = b_{ic} \cdot \alpha(e) + a_{ic} \mid a_{ic}, b_{ic}, g_{eic} \in \mathbb{Z}^+ \tag{4.7}$$

Note that for each segment we need (ρ+1) coefficients to predict f_{eic} and 2 to predict g_{eic}, being the total size of the restricted linear model $2\eta*(C*(3+\rho))$.

To find the coefficients so to obtain the best goodness-of-fit we face an optimization problem similar to that of the restricted polynomial model. In this case, however, there are two variables to optimize: the number of segments C and the polynomial degree ρ, which can be jointly minimized to reduce the whole size of the model at the expense of increasing the complexity of the optimization problem. For this reason, we divide this problem into two parts: the problem to obtain the optimal value of C; and the problem of fit the optimal value of ρ for the optimal C. For the former, we solve the following optimization problem:

Given:

- A set of σ^2_{XPM} values,
- a η value,
- a target error.

Output

- a number C of segments,
- a set of real coefficients f_{eic}, and integer g_{eic}, a_{ic}, and b_{ic}.

Objective: Minimize C that fits the target error with a set of break points guaranteeing the equation (4.7).

Once the number of segments is obtained, to problem of finding the minimum size of ρ and its associated t_{icj} values that fit the target error is solved. Since t_{icj} can be fitted with high accuracy by polynomials with relative low degree, the key factor of this restricted linear model is to solve the problem of finding the optimal set of segments with the integrality constraint of the break points estimation.

4.3 Performance evaluation

This section first analyzes and compares the performance of each of the XPM models presented above in terms of error and size of the model. The exact $\sigma^2_{XPM}(e,\lambda,i)$ values used for fitting were obtained according to the analytical model in [Pa03]. XPM noise variance values were computed for links with $|W|$=80 and a number of amplifiers ranging from 1 to 25, obtaining 158,000 different values. Next, aiming at providing a final validation of both XPM statistical models, a comparison of the models in terms of the Q value of lightpaths is provided.

The models were evaluated in terms of two goodness-of-fit statistics: the Pearson determination coefficient (R^2) and a normalized mean squared error (MSE) [Mo04]. The normalized MSE was obtained by comparing the MSE of a given model against the MSE of the *null model* which contains only one value representing the average of all the $\sigma^2_{XPM}(e,\lambda,i)$. Thus, we compare the error of the models against the error of the more basic (and worst) statistical model where every wavelength of every link produces the same XPM noise regardless of the number of link amplifiers and the frequency in the spectrum. Since the best R^2 possible is 1 (or 100%) and the optimal normalized MSE is 0, we used 1-MSE instead of MSE as goodness-of-fit measure so both statistics can be read in the same way. A normalized 1-MSE value near 90% provides enough precision when the model is used for Q statistical computation, whereas R^2 greater or equal than 95% is enough to validate a model.

4.3.1 Restricted Deterministic model

Fig. 4-2 illustrates the impact of the size of η over the amount of information that the restricted deterministic model incorporates. This information, defined as $1-\varepsilon_{link}$, allows measuring the relative effect of the $2*\eta$ neighbor wavelength channels over the XPM value of a certain reference one. Using eq. (4.3), the amount of information in $\sigma^2_{XPM}(e,\lambda)$ against η is plotted. As shown, the restricted deterministic model with η=4 contains about 97% of information of the full deterministic one, which, as will be proved, is enough for our purposes.

The restricted deterministic with η=4 contains 16,000 coefficients, which $\varepsilon\approx10\%$ of the full deterministic size. Since η=4 has been proved to provide a good trade-off between model accuracy and model size, we use that value for the ongoing analysis.

4.3.2 Restricted Polynomial model

Aiming at obtaining each $s^2_{XPM}(e,\lambda,i)$ in the range of $i=[\lambda-\eta,\ \lambda+\eta]$, we applied polynomial interpolation to the set of exact $\sigma^2_{XPM}(e,\lambda,i)$ values described in the previous section. As a result of each fit, we obtained a set of polynomial coefficients and the values of the two goodness-of-fit statistics which were used to obtain an overall goodness-of-fit measure of the $\sigma^2_{XPM}(e,\lambda)$ model described in equation (4.3).

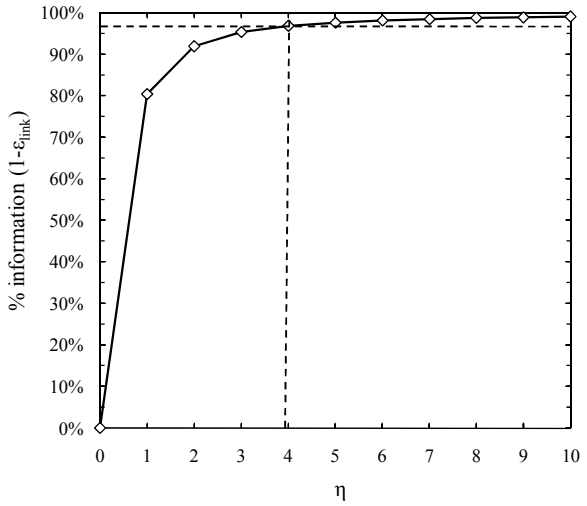

Fig. 4-2 Amount of information against η

Since each wavelength channel in the range defined by η produces a different effect over the reference wavelength channel, the evaluation of the overall goodness-of-fit cannot be done considering a simple summation among the wavelength channels. For this reason, we weighted the goodness of fit of each channel by a measure of the effect that that wavelength channel provides to the XPM of the reference one (obtained from the values depicted in Fig. 4-2). To this end, we define the weights 0.83, 0.12, 0.03, and 0.02 for i=λ±1, λ±2, λ±3, and λ±4, respectively.

Fig. 4-3 illustrates the weighted R^2 and normalized 1-MSE for different values of γ. As shown, values close to 95% for R^2 and 90% for 1-MSE are obtained when degree 5 polynomials are fitted.

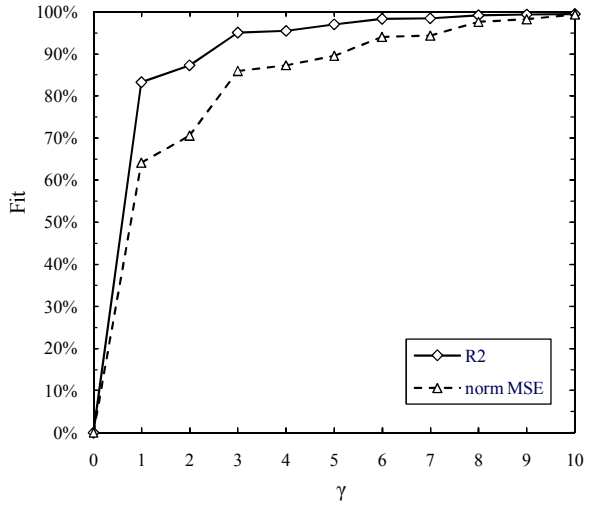

Fig. 4-3 Fit against γ

Aiming at providing comparison between the restricted polynomial the full-deterministic models with γ=5, we computed $s^2_{XPM}(e,\lambda,i)$ for a set of selected cases. Fig. 4-4 provides both $\sigma^2_{XPM}(e,\lambda,i)$ exact values (dotted lines) and $s^2_{XPM}(e,\lambda,i)$ fitted ones (solid lines) for $i=\lambda+1$ and $i=\lambda+2$. For the sake of broad comparison we depict three different link sizes in terms of $\alpha(e)$ ranging from 3 to 23. As illustrated, the closer the interference wavelength channel to the reference one, the better is the fitted value. In fact the effect of the first neighboring wavelength channel provides 80% of the total XPM interference over a given reference channel. In light of these results, we conclude that the restricted polynomial model tights the analytical.

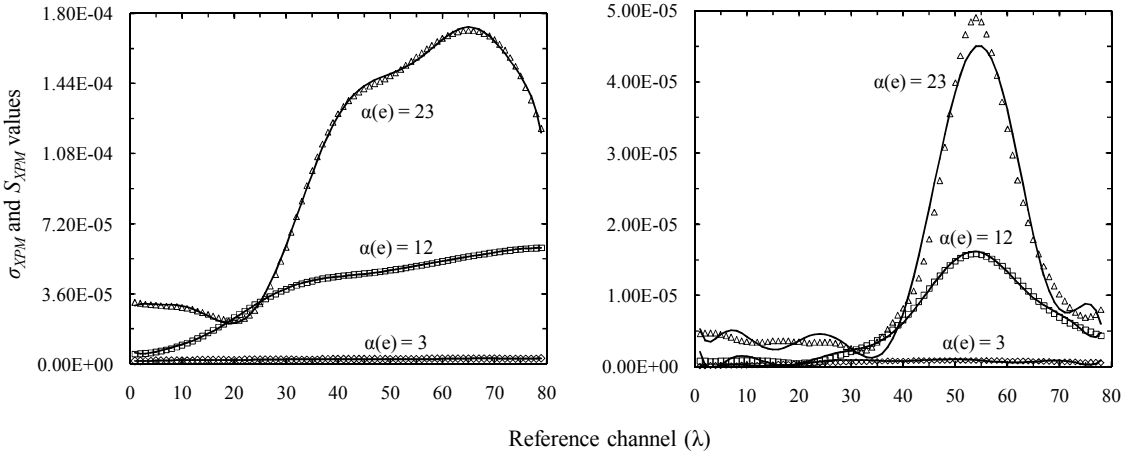

Fig. 4-4 $\sigma^2_{XPM}(e,\lambda,i)$ and $s^2_{XPM}(e,\lambda,i)$ for i= λ+1 (left) and i= λ+2 (right)

To really appreciate the low error introduced by the model, Fig. 4-5 presents that error as a function of the value of σ^2_{XPM}. A vast majority of values are obtained with an error lower than ±5%. Few of them are computed with higher error but most of those correspond to low σ^2_{XPM} values which add low or negligible total error to the final Q value of a lightpath, as will be proved in the next section. In contrast, error is within ±2.5% for higher σ^2_{XPM} values, those with higher contribution to the final XPM noise variance and Q value of a lightpath.

Finally, regarding the size of the restricted polynomial model, it is worth mentioning that the number of coefficients to be stored falls to 288, in contrast with 39,000 or 158,000 of the deterministic models. Note that this number does not even depend on the considered number of wavelengths in the case of this model. Recall that our model allows predicting the XPM noise variance for links with 80 wavelengths covering a wide range of frequencies.

4.3.3 Restricted linear model

Similarly to the methodology applied to the restricted polynomial model, we use the weighted R^2 and normalized 1-MSE metrics to compare among different linear

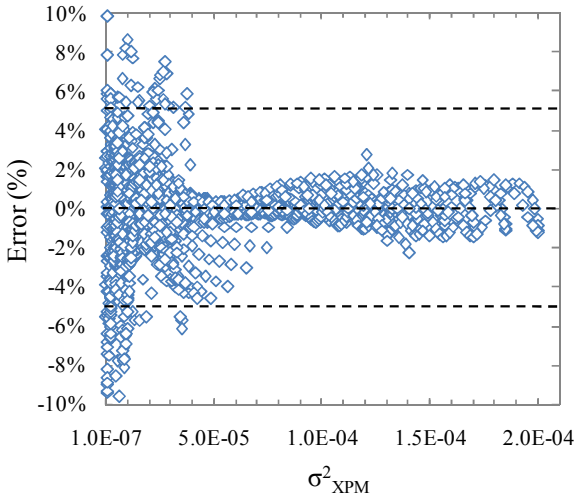

Fig. 4-5 Restricted polynomial model error

models. To solve the problem of finding the optimal number of segments, different sets of break points were generated to ensure the integrality condition in eq. (4.7) for a given number of segments ranging from 2 to 5. Fig. 4-6 shows the best obtained value of the goodness-of-fit statistics for each value of C. As shown an good fit is obtained when the number of segments is set to 4. Next, every slope f_{eic} of the optimal set of segments was fitted using the polynomial form described in eq. (4.6). After testing different values of ρ, we obtain a R^2 greater than 99% for all the slopes when ρ=4.

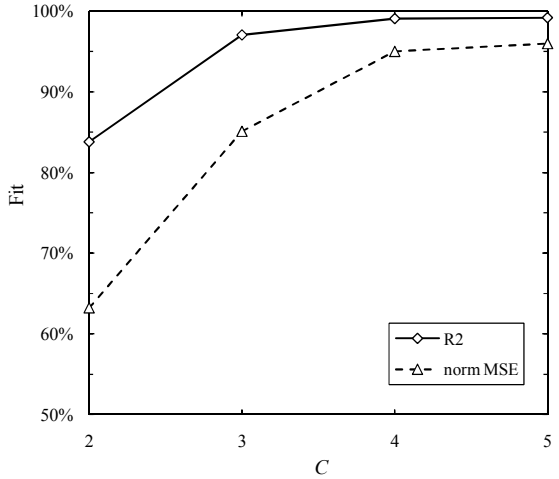

Fig. 4-6 Fit against the number of segments

Next, prediction of the model using C=4 and ρ=4 was compared against exact values. Similarly to Fig. 4-4, Fig. 4-7 shows the predicted $s^2_{XPM}(e,\lambda,i)$ and the exact $\sigma^2_{XPM}(e,\lambda,i)$ values for the same examples used to validate the restricted polynomial

model. As observed, the curves of real and fitted values are very close, even when the integrality constraint of the break points restricts the goodness-of-fit of the model. In fact, this condition causes a sub-estimation of the XPM variance when $\sigma^2_{XPM}(e,\lambda,i)$ is high. Similar conclusions can be stated after reviewing the relative error of the restricted linear model shown in Fig. 4-8. As shown, an error higher than that of the restricted polynomial model can be appreciated clearly trending towards $s^2_{XPM}(e,\lambda,i)$ sub-estimation when the value of $\sigma^2_{XPM}(e,\lambda,i)$ increases. Nevertheless, as proved in the next section, this error does not lead to significant errors in the Q computation.

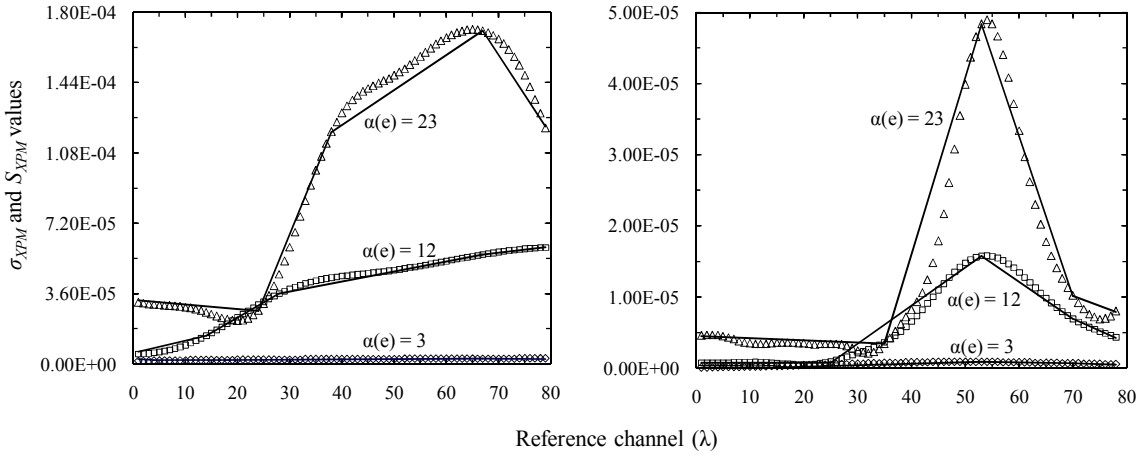

Fig. 4-7 $\sigma^2_{XPM}(e,\lambda,i)$ and $s^2_{XPM}(e,\lambda,i)$ for i= λ+1 (left) and i= λ+2 (right)

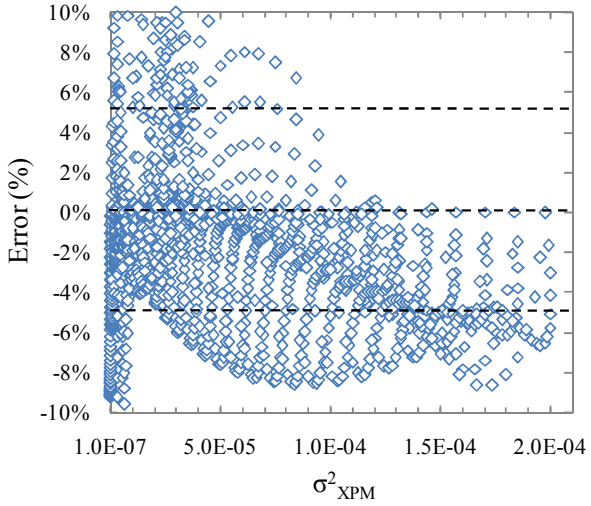

Fig. 4-8 Restricted linear model error

Regarding the model size, the restricted linear model used in the previous results contains 224 coefficients, which is similar to the size of the restricted polynomial model reducing in 99.8% the size of the full deterministic model.

Table 4-1 summarizes the number of coefficients and the goodness-of-fit of the described XPM models. The greatest difference among the models is the size of the set of coefficients. On the one hand, the full deterministic model stores the whole set of possible $\sigma^2_{XPM}(e,\lambda,i)$ values (which depends on the number of considered wavelengths per link) and the restricted deterministic reduces that size reducing the amount of information to consider. On the other hand, the size of both the restricted polynomial and the restricted linear model is lower than 1% of the size of the full deterministic model. Regarding the goodness-of-fit, the R^2 of the statistical models is higher than 96%, which represents a tight fit.

Table 4-1: XPM Models Summary

	$\|W\|$=40	$\|W\|$=80	% Information	R^2(%)	1-ECM (100%)
Full deterministic	39,000	158,000	100%	100%	-
Restricted deterministic (η=4)	8,000	16,000	96.85%	100%	-
Restricted polynomial (η=4 γ=5)	288		96.85%	96.93%	89.48%
Restricted linear (η=4, C=4, ρ=4)	224		96.85%	96.14%	92.16%

4.3.4 Q-factor statistical computation

In this subsection we compare the Q value obtained using one of our two statistical approaches to compute σ^2_{XPM} against the value obtained using the analytical model in [Pa03]. To this end, we randomly generated a set of 15,000 lightpaths each characterized by the number of hops, the length of the links in its route, the assigned wavelength, and the state (busy or free) of the wavelengths channels in each link. We generated each lightpath as a concatenated sequence of links where each link has a random length and load. For each lightpath, we obtained the values of $P_{transmitter}$, pen_{eye}, pen_{PMD}, σ^2_{ASE}, and σ^2_{FWM} from the analytical expressions and reference values detailed in [Ji10]. Besides, three different values for σ^2_{XPM}, one for each model were computed thus obtaining 3 different Q values per lightpath.

Fig. 4-9 compares the Q value obtained by the restricted polynomial model against the full deterministic one. Dotted lines represent an error of the 5%, which we considered as the maximum error allowed for statistical Q computations. As observed, the Q value obtained by the restricted polynomial model tightly fits the exact Q.

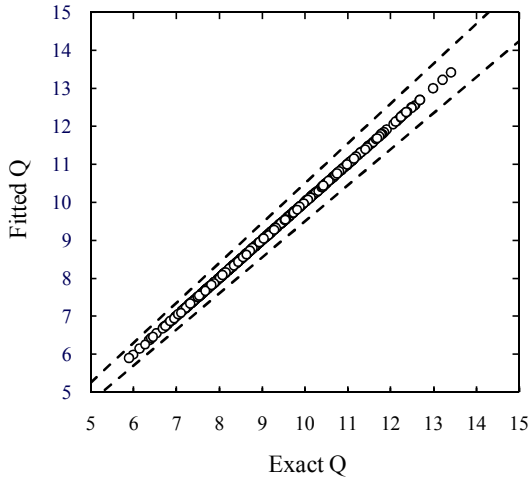

Fig. 4-9 Exact Q against statistical Q using the restricted polynomial XPM model

Similarly, Fig. 4-10 illustrates the goodness-of-fit of the statistical Q model when the restricted linear model is used. Although the accuracy of this model is lower than that of the restricted polynomial one, errors are also within the range of 5%. In a deeper analysis, not shown in the figures, we observed than the restricted linear model provides Q values slightly higher than the restricted polynomial model. These differences are in line with the relative errors depicted in Fig. 4-8, where it can be observed that the restricted linear model trends to sub-estimate XPM, thus leading in an over-estimation of Q (as can be easily deduced from eq. (2.2)).

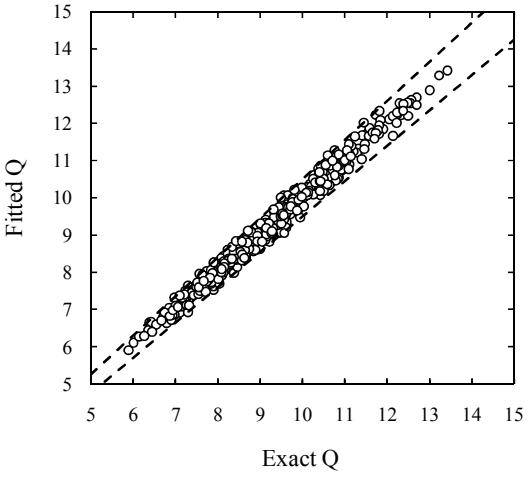

Fig. 4-10 Exact Q against statistical Q using the restricted linear XPM model

To weight the impact of the error in the statistical Q computation the models were evaluated in terms of wrong decisions to be taken regarding whether the Q value of a lightpath is better than a given Q threshold. To this end, six different Q

thresholds (ranging from 7 to 12) were fixed and the amount of lightpaths ensuring each threshold when the Q value was computed using the analytical and each statistical model were counted. We define a decision as wrong when the decision taken on a given lightpath using the analytical and a statistical model is different. This is the kind of decisions to be taken when the models are used within IA-RWA algorithms.

Table 4-2 details the amount of wrong decisions (total and percentage) taken for each model as a function of the Q threshold, with respect to the set of 15,000 lightpaths generated. Although the percentage of wrong decisions made by the restricted linear model is significantly higher than the percentage of the restricted polynomial one, the highest error is only 2%, which represents a negligible error in the operation of an IA-RWA algorithm. Note that the quality of service is involved in the case when the connection is accepted by the statistical model being the exact Q worse than the threshold. In contrast, the grade of service is involved when the connection is blocked by the statistical model being the exact Q better than the threshold. In light of these results, we can conclude that both the restricted polynomial and the restricted linear XPM model provide an accurate statistical Q estimation really close to the exact Q values.

To illustrate the usefulness of the Q statistical estimation, the next section presents two different application cases in IA-RWA problems, highlighting the advantages of using the proposed models.

Table 4-2: Statistical Q Model Validation

	Q	**7**	**8**	**9**	**10**	**11**	**12**
	# paths	15,000	15,000	15,000	15,000	15,000	15,000
Restricted Polynomial	**Wrong**	13	32	28	20	14	7
	%	0.09%	0.21%	0.19%	0.13%	0.09%	0.05%
Restricted Linear	**Wrong**	137	314	295	257	131	65
	%	0.91%	2.09%	1.97%	1.71%	0.87%	0.43%

4.4 IA-RWA examples

In this section we firstly present a classical on-line IA-RWA algorithm that takes advantage of the Q statistical computation using the restricted polynomial model for estimating the XPM noise variance. Secondly, we define a single ILP formulation for an off-line IA-RWA problem that incorporates an accurate Q computation by means of the restricted linear XPM model.

4.4.1 On-line IA-RWA algorithm

In dynamic traffic scenarios the problem of finding a feasible route must be solved each time a connection request arrives. For a route and wavelength assignment to be feasible for an incoming connection request, three conditions must be satisfied: first the involved network resources need to be unused, second, the Q-factor of the route and wavelength is better than a given threshold, and third, the Q-factor of all the established lightpaths in the network will remain being higher than the threshold after the new lightpath is established through that route and wavelength. Among different feasible routes and wavelength assignments for a connection request, the one with minimum Q value is chosen, i.e. Q minimization is the objective function [Az09]. Then, the on-line IA-RWA problem can be generically stated as follows:

Given:

- an optical topology G(*N*, *E*) where *N* represents the set of nodes and *E* the set of fiber links,
- a set of currently established lightpaths *L* in the optical network,
- a demand *d* characterized by the source and destination nodes and the required Q threshold.

Output:

- a new lightpath *l'* for the demand *d*.

Objective: Minimize the Q of lightpath *l'*.

Subject to: the Q-factor of all the established lightpaths must be higher or equal than the required Q threshold.

Table 4-3 shows an algorithm to solve the problem stated above. First of all, a set of routes is pre-computed over the topology *G* for the end nodes of the new demand. After finding an available wavelength to establish a route, the Q-factor is computed for that route. If the route provides a Q higher than the threshold, the Q-factor is re-computed for all the established lightpaths in order to ensure that the Q threshold is still being accomplished. If the demand could be assigned to a route and a wavelength without violating any Q threshold, then that route and that wavelength is selected as possible lightpath with a certain Q value. Once all the routes and wavelengths are explored and all the possible lightpaths to serve the demand are founded, the one with the highest Q value is established. Note that a demand cannot be served when no lightpaths can be established due to lack of resources or Q threshold violation.

As mentioned in the introduction, Q-factor computation time can strongly impacts the lightpaths set-up time. This computation time varies depending on the method to compute the XPM noise variance. In this regard, we computed the value of σ^2_{XPM}

Table 4-3: On-line IA-RWA algorithm

```
Procedure IA-RWA
Input: Node s, d , Lighpath[] lightpaths
Output: Route r
begin
    Route[] routes = compute k-ShortestPath (s, d, k)
    Route candidateRoute
    w=0
    bestQ=0
    for each route r_i in routes do
     for each wavelength w_i in W do
      if w is end-to-end available in r_i then
         thisQ = compute Q-factor using the XPM restricted
                    polynomial model for r_i and w
       if (thisQ > bestQ) then
        threshold='true'
        for each lightpath l in lightpaths do
          newQ= compute Q-factor using the XPM restricted
                  polynomial model for lightpath l.
          if newQ<Q_threshold then
           threshold='false'
           break for
        if threshold=='true' then
         candidateRoute = r_i
         w = w_i
         bestQ = thisQ
    if no candidateRoute found then
     return no route, lack of resources
    if bestQ < Q_threshold then
     return no route, Q reasons
    if threshold=='false'then
     return no route, Q reasons
    return candidateRoute in wavelength w
end
```

according to the expressions in [Pa03] for several link distances and wavelength scenarios on a dual-core-based computer with 4 Gbytes of RAM and the computation time was 50ms on average. On the other hand, the time to compute σ^2_{XPM} using the restricted polynomial model is lower than 1 ms, which represents a negligible time. This difference becomes higher when we compare Q-factor computation times, which would be in the order of seconds when the exact computation of σ^2_{XPM} is performed (which is in line with [Qi10]), in contrast with few miliseconds needed when the statistical σ^2_{XPM} computation is used.

4.4.2 Off-line IA-RWA problem

Contrarily to the on-line IA-RWA problem, in the off-line case all the routes of the demands needed to satisfy the traffic matrix are simultaneously founded over the empty network. Since this problem is an extension of a classical RWA problem, the minimization of the capacity used by the lightpaths can be adopted as the objective function Thus, we define the off-line IA-RWA problem as follows:

Given:

- an optical topology G(*N*, *E*) where *N* represents the set of nodes and *E* the set of fiber links,
- a set of demands, characterized by the source and destination nodes and the required Q threshold.

Output: a route and wavelength assignment for each of the demands.

Objective: Minimize the used capacity subject to each demand is routed through a lightpath with a Q higher than the threshold.

As already mentioned, the Q expression in eq. (2.2) cannot be directly used in an ILP formulation due to its non-linearity. Nevertheless, the elements that only depend on the length of the route, i.e. the linear impairments, can be previously pre-computed if an arc-path [Pi04] formulation is used to define the ILP. This is the case of pen_{PMD} and σ^2_{ASE} that become constant elements, thus being only σ^2_{XPM} and σ^2_{FWM} dependent on the route and wavelength assignment. Since σ^2_{FWM} is several times lower than σ^2_{XPM}, we can assume a worst case for the FWM noise variance ($\sigma^2_{FWM}(WC)$, similarly to [Pa08]), being that a constant value for our problem. At this point, equations (4.8), (4.9), and (4.10) represent a reformulated version of the Q expression in eq. (2.2) where AI and BI contain those terms that can be generated as input data of the ILP problem.

$$Q = \frac{A(r)}{\sqrt{B(r) + \sigma^2_{XPM}(r,\lambda)}} \tag{4.8}$$

$$A(r) = \frac{pen_{eye} \cdot P_{transmitter}}{pen_{PMD}(r)} \tag{4.9}$$

$$B(r) = \sigma^2_{ASE}(r) + \sigma^2_{FWM}(WC) \tag{4.10}$$

From equation (4.8) and given a Q threshold (Q^{thres}), we define the corresponding XPM threshold (XPM^{thres}). More specifically, given a certain route r the maximum amount of XPM noise variance that the lightpath could admit without violating the Q threshold can be defined as follows:

$$XPM^{thres}(r) = \left(\frac{A(r)}{Q^{thres}}\right)^2 - B(r) \tag{4.11}$$

Therefore, a constraint is added in the RWA ILP that ensures a minimum Q for each lightpath by ensuring a maximum XPM threshold. Using an arc-path formulation and pre-computing the linear impairments and constants, the required Q threshold can be converted into a XPM threshold for each alternative route. Note that the XPM threshold of a demand varies depending on the route due to the linear impairments associated to it. When a route and a wavelength assignment is founded ensuring the required XPM threshold, the required Q threshold is also

guaranteed without needing any post-processing computation. Finally, it is worth mentioning that the XPM of each lightpath is computed using the restricted linear model presented in section 4.2.2.

The ILP formulation presented below takes advantage from the XPM restricted linear model and the XPM threshold defined in equation (4.11). For the sake of clarity, we extend the notation of some expressions with the new index d, which represents a specific demand. Then, the following notation is used for sets and parameters:

N	Set of nodes of the network, index n.
E	Set of links of the network, index e.
W	Set of wavelengths, index w.
D	Set of demands, index d.
$R(d)$	Set of routes of demand d, index r.
t_{dre}	Equal to 1 if the route r of the demand d contains the link e.
Q_d^{thres}	Required Q of demand d.
$A(d,r)$, $B(d,r)$	Linear impairments and constants associated to the route r of the demand d.
M	Large positive constant.

The following notation is used for variables:

x_{drw}	Binary, equal to 1 if the demand d is routed following the route r and the wavelength w.
y_{ew}	Binary, equal to 1 if the wavelength channel w is used in the link e.
s_d	Real positive, with the statistical XPM variance assigned to demand d.

Finally, the ILP formulation is as follows:

$$\min \sum_{e \in E} \sum_{w \in W} y_{ew} \tag{4.12}$$

subject to:

$$\sum_{r \in R(d)} \sum_{w \in W} x_{drw} = 1, \quad \forall d \in D \tag{4.13}$$

$$\sum_{d \in D} \sum_{r \in R(d)} t_{dre} \cdot x_{drw} = y_{ew}, \quad \forall e \in E, w \in W \tag{4.14}$$

$$\sum_{e\in E} t_{dre} \cdot \sum_{\substack{w'=w-\eta \\ w'\neq w}}^{w+\eta} y_{ew'} \cdot s^2_{XPM}(e,w,w') - (1-x_{drw}) \cdot M \leq s_d, \quad \forall d \in D, r \in R(d), w \in W \tag{4.15}$$

$$s_d \leq \sum_{r\in R(d)} \sum_{w\in W} x_{drw} \cdot \left[\left(\frac{A(d,r)}{Q_d^{thres}} \right)^2 - B(d,r) \right], \quad \forall d \in D \tag{4.16}$$

The objective function (4.12) minimizes the total amount of used wavelength channels and, thus, the total used capacity. Constraint (4.13) guarantees that each route is assigned to only one route and wavelength, whereas constraint (4.14) makes sure that each wavelength channel contains only one lightpath. Constraint (4.15) computes the XPM noise of each demand according to its route and the occupation of the network using the restricted linear model for $s^2_{XPM}(e,\lambda,i)$ specified in equations (4.6), (4.7), and (4.8). The XPM noise is compared with the threshold permitted by the used route in (4.16) in order to ensure that all the assigned lightpaths have an XPM noise lower than the threshold and, thus, a Q-factor higher that the Q threshold.

4.5 Summary

In this chapter, two statistical models to accurately compute the XPM noise variance of lightpaths under both static and dynamic scenarios have been presented. Aiming at reducing the lightpath set-up delay in dynamic scenarios, a polynomial model has been proposed. Although this model allows significantly reducing the Q-factor computation time, it cannot be used in classical ILP formulations of the static IA-RWA problem due to its non-linearity. Thus, a linear model has been presented to provide linear expressions to estimate XPM.

Both XPM statistical models were validated against a wide set of values (full deterministic model) obtained from analytical models. The results showed that our models provide a goodness-of-fit greater than 96% in terms of R^2, which represents a high accuracy level. Moreover, the size of both the polynomial and the restricted model remains lower than 288 parameters, thus reducing in more than 99% that of the full deterministic model. Since the main objective of this work is to provide models to estimate lightpaths' Q-factor, a final comparison between exact and approximated Q values was performed. As proved, the error in terms of Q remains lower than the commonly accepted error for statistical models of 5%. Finally, when the Q statistical model is used to decide whether or not a path can be established the percentage of wrong decisions remains lower than 2.1%, thus validating the usefulness of the models.

In light of these results, we conclude that the presented statistical models provide a fast and accurate method to estimate the XPM noise variance and, consequently, the Q-factor of lightpaths in IA-RWA problems.

Chapter 5

Service and resource differentiation to maximize network operator revenues

In this chapter, we firstly analyze the provisioning of differentiated services in current SPP environments over WSON single layer networks. This analysis concludes that, with current resource assignment policies, only a very poor grade of service can be provided to the carried best effort traffic. Hence, we propose *diff-WS*, a resource partitioning scheme that differentiates those wavelengths supporting each class of service in the network.

The benefits of diff-WS in front of current resource assignment policies are afterwards evaluated from an economic perspective. To this goal, we define the NORMA problem as a revenue maximization problem. To solve NORMA, we introduce statistical models to obtain, for a given grade of service, the highest traffic intensity for each supported class of service and resource assignment scheme.

Finally, the performance of NORMA is evaluated for real backbone topologies. From the numerical results, we show that diff-WS maximizes resource utilization in the network and, thus, network operator's profit.

5.1 Wavelength partitioning schemes

5.1.1 Best effort traffic and SPP

The topology of an optical network can be represented by a graph $G(N, E, WL)$, where N represents the set of nodes, E the set of links and WL the set of available wavelengths in each link, with size W. Assuming that wavelength conversion is not possible in the network, forcing the connections to satisfy the wavelength

continuity constraint, we can split the graph G into W independent subgraphs $G^i(N, E, i)$, one per wavelength. Each subgraph G^i represents the network connectivity through wavelength I, that is, $G(N, E, WL) = \{G^i \mid i \in WL\}$.

As mentioned in Chapter 2, SPP achieves high resource efficiency by sharing the backup resources where possible. This resource sharing is attained by reserving the backup resources but postponing their allocation until the working path fails. SP connection requests are routed on subgraphs G^i. Therefore, in order to assign a wavelength to both working and backup paths, enough resources must exist for them. As a result, working and backup paths might interfere between them, since they might compete for the same resources. To illustrate this, Fig. 5-1a shows a number of SP connections established on two subgraphs, G^1 and G^2, where the same wavelength has been assigned to the working and backup paths for simplicity. In this example, a new connection 3-9 cannot be established.

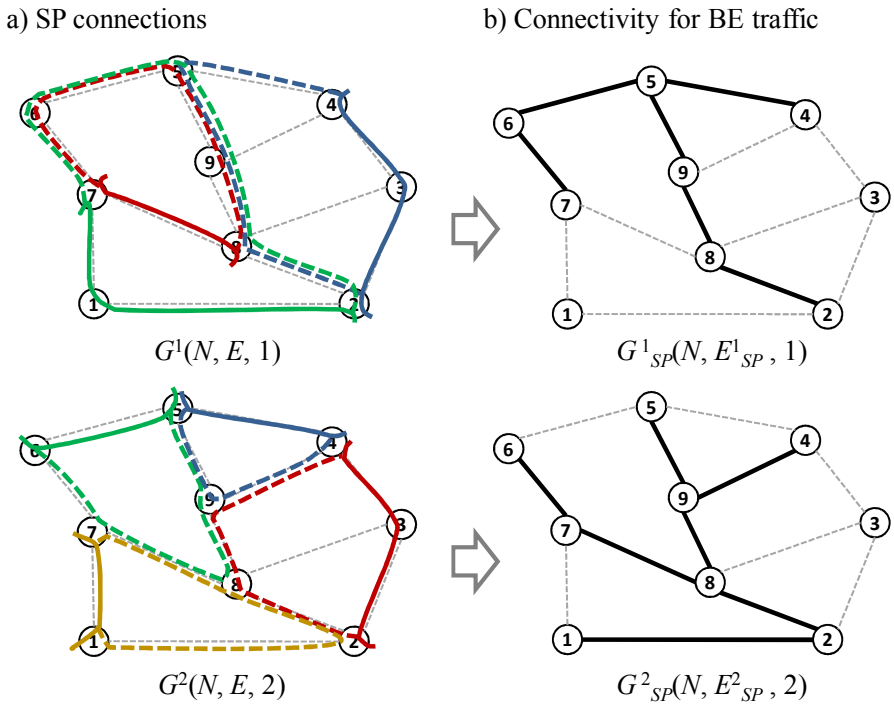

Fig. 5-1 Resource availability for BE traffic

Conversely, BE connections are established using only resources reserved for the backup paths that are currently idle. Therefore, BE traffic is subordinated to the SP traffic. In other words, while the SP traffic blocking probability (Pb_{SP}) depends on the network topology G and the offered load, that of the BE traffic (Pb_{BE}) also depends on the amount of resources loaned by the currently established SP connections. Furthermore, as BE connections are borne on reserved backup resources, they are torn down abruptly when the resources supporting them are unallocated, even if their requested holding time (ht) has not expired yet. In order

to show this, we will assume in Fig. 5-1a that SP connection 1-7 is torn down. This would lead to the release of link 1-2 in G^2, forcing the tear down of any BE connection supported on such resource. In this context, we define the billable time (bt) of a connection as the total time being operative. Thus, $bt=\rho \cdot ht$, where ρ is the proportion of consumed ht over the total. Note that $\rho_{BE} \leq 1$ as a consequence of the anticipated connection releases, whereas $\rho_{SP} = 1$.

Aiming to quantify Pb_{BE}, let us consider that a certain number of SP connections are established in the network. In this scenario, we denote G^i_{SP} (N, E^i_{SP}, i) as the subgraph representing the resources available for BE traffic at wavelength i. Hence, $G_{SP}(N, E_{SP,}WL) = \{G^i_{SP} \mid i \in WL\}$, as shown in Fig. 5-1b.

In fact, Pb_{BE} can be described as the contribution of two different factors: the connectivity of the graph where the routes are computed (note that in the case of BE connections, subgraphs G^i_{SP} could be not connected) and the offered load to the network. For the ongoing analysis, let R_{BE} be the set of BE connection requests and $R^i_{BE}(G^i_{SP})$ the subset of R_{BE} having a connected path over G^i_{SP}. Then, the complete set of BE connection requests with a feasible route on G_{SP} (R^*_{BE}) is given by:

$$R^*_{BE} = \bigcup_{\forall i \in WL} R^i_{BE}\left(G^i_{SP}\right) \tag{5.1}$$

Moreover, we define $P(R_{BE}, G_{SP})$ as the probability thata BE connection request can be established subject to the current G_{SP} connectivity, which can be expressed as:

$$P\left(R_{BE}, G_{SP}\right) = \frac{\left|R^*_{BE}\right|}{\left|R_{BE}\right|} \tag{5.2}$$

Therefore, we can formulate Pb_{BE} as the sum of two terms. The first one, capturing the graph's unconnectivity, is the number of BE connection requests without feasible route on G_{SP} over the size of R_{BE}. The second one, capturing the lack of resources, is the number of BE connection requests with feasible route on G_{SP} weighted by a probability function that depends on G and the offered loads of SP (I_{SP}) and BE (I_{BE}) traffic, also over the size of R_{BE}. This is expressed in equation (5.3). As shown, $P(R_{BE}, G_{SP})$ leads to a lower bound for Pb_{BE}:

$$Pb_{BE} = \frac{\left|R_{BE}\right| - \left|R^*_{BE}\right|}{\left|R_{BE}\right|} + f(G, I_{SP}, I_{BE}) \cdot \frac{\left|R^*_{BE}\right|}{\left|R_{BE}\right|} \geq 1 - P\left(R_{BE}, G_{SP}\right) \tag{5.3}$$

Aiming at illustrating such a lower bound for Pb_{BE}, let us assume that R_{BE} contains all possible node pairs (i.e., uniform traffic distribution). For each node pair, we investigate if a feasible route exists on G_{SP}. For example, node pairs 7-5 and 4-1 in Fig. 5-1 can be connected through feasible routes (e.g. 7-6-5 in G_{SP}^1 and 4-9-8-2-1 in G_{SP}^2), whereas pair 7-3 not. Applying now eq. (5.2), $P(R_{BE}, G_{SP})$ equals 0.78, having Pb_{BE} a lower bound equal to 0.22, that is, as a result of the G_{SP} unconnectivity. In conclusion, the BE traffic GoS will generally be very poor due to its dependence on the SP traffic, thus leading to very low BE traffic revenues.

5.1.2 Proposed wavelength partitioning scheme

In view of the above, we propose a novel wavelength partitioning scheme for provisioning differentiated traffic in DWDM transport networks. Our main objective is to improve the BE traffic performance and, as a result, the expected network revenues.

To this end, we split the complete set of wavelengths into two different subsets of size *W*/2, namely, WL_{SP} and WL_{BE}, dedicated to SP working and backup path reservations, respectively. The wavelengths in both sets are rigidly related as follows. Being an SP working path assigned to wavelength *I*, its backup path is assigned to wavelength *W-i*. Fig. 5-2 shows an example with four wavelengths per link, carrying the same traffic as in Fig. 5-1. We call this wavelength partitioning scheme as differentiated wavelength set (diff-WS), in contrast to the traditional unpartitioned wavelength set where all resources are shared by working and backup paths (*sh-WS*) [Ou04.2, Mu08], as detailed in the previous section.

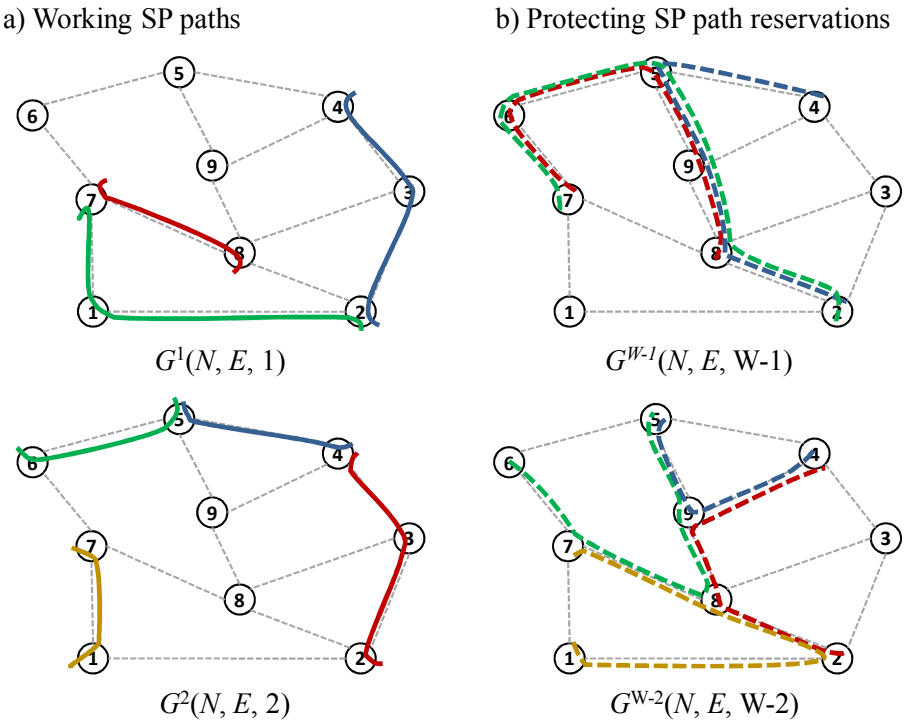

Fig. 5-2 Example of SPP and BE paths under *diff-WS* scheme

In particular, backup resource sharing in diff-WS is restricted to those connections whose working paths are assigned the same wavelength. For this purpose, an algorithm that computes two link-disjoint paths jointly, considering those wavelengths in WL_{BE} as unused, would be required. As an example, Table 5-1 describes an algorithm adapted from [Ve09.1], where G^0 is the graph describing the

network physical topology. The algorithm finds the shortest route for the working path, assigns a wavelength within WL_{SP}, and finds a link-disjoint path.

Table 5-1: RWA Algorithm for SP connections

```
Procedure RWA-SP
Input: Node, s, d
Output: working, backup

begin
   Route working, backup
   Route w = ShortestRoute (s, d, working)
   if length(working) == 0 then
      No route found
      exit
   Look for route backup link-disjoint with working in G^0
   Move backup to wavelength W-wavelength(working)+1
end


Procedure ShortestRoute
Input: Node s, d
Output Route r

begin
  distance = get distance from s to d in G^0
  minDistance = INFINITE
  minWL = 0
  for each wavelength I in WL_SP do
     distanceWL = get distance from s to d in G^i
     if (distanceWL<minDistance) then
        minDistance = distanceWL
        minWL = i
     if (minDistance==distance) then
         break loop
  if minWL>0 then
     Create the route r from s to d in G^minWL
end
```

It shall be also highlighted that the whole WL_{BE}set in diff-WS is dedicated to backup path reservations. Hence, it can be entirely used to support BE traffic. This makes diff-WS more beneficial than sh-WS, where only those resources already reserved for backup SP paths can be used for carrying BE traffic. As will be shown in section 5.3, this new approach provides optimum GoS for BE traffic. In fact, this is achieved in certain network topologies at expenses of slightly lowering the amount of SP traffic served. Nonetheless, the total network revenues from both kinds of services are drastically leveraged when diff-WS is applied.

Furthermore, the diff-WS partitioning scheme can be used under a wide set of traffic scenarios by appropriately tuning the size of WL_{SP} and WL_{BE} sets. Fig. 5-3 shows a conceptual representation of a DWDM link. A symmetrical diff-WS partitioning such as the represented in Fig. 5-3a becomes suitable when $I_{SP} \geq I_{BE}$,

whereas the asymmetrical diff-WS partitioning shown in Fig. 5-3b fits better when $I_{SP}<I_{BE}$. Note that $|WL_{BE}| \geq |WL_{SP}|$ is necessary to provide protection to SP connections. Moreover, the size of the wavelength sets can be dynamically managed adapting the network to traffic fluctuations. Finally, a third class of service, e.g., the unprotected class (UP), has been defined in Fig. 5-3c and thus a new set WL_{UP} has been created. In particular, this work focuses on the symmetrical configuration with two classes of traffic depicted in Fig. 5-3a.

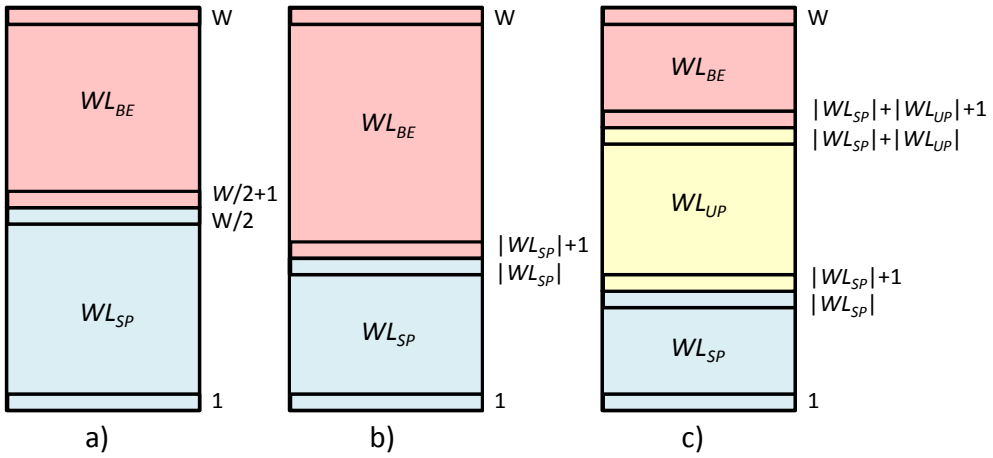

Fig. 5-3 Conceptual representation of a diff-WS-based DWDM link

Aiming at evaluating both schemes from an economic point of view, the Network Operator Revenues Maximization (NORMA) problem is next introduced. Given an optical topology, the problem chooses the wavelength partitioning scheme which maximizes the expected revenues from provisioning SP and BE traffic.

5.2 Network operator revenues maximization

In this section, the Network Operator Revenues Maximization (NORMA) problem is stated, whose objective is to maximize the revenues from serving as much differentiated traffic as possible, while meeting certain GoS levels specified in terms of network blocking probability. Being the network traffic intensity the key of the problem, accurate statistical models to compute it for SP and BE traffic classes under current sh-WS and new diff-WS schemes are provided.

5.2.1 Problem statement

The NORMA problem can be formally stated as follows:

Given:

a) the physical network topology represented by a graph *G(N, E, WL)*, with *N* the set of nodes, *E* the set of links and *WL* the set of wavelengths in each optical link;

b) a set *S* of classes of service to be provided, index *j*;

c) the network operator's pricing structure, specified by a fixed fee C_j charged to the customers per time unit of class of service *j*;

d) the blocking probability threshold Pb_j^{max} allowed for each class of service *j*;

e) a set *K* of wavelength partitioning schemes, index *k*. In this work we assume *K*={sh-WS, diff-WS}.

Output:

a) a wavelength partitioning scheme *k*;

b) the maximum traffic intensity for the given classes of service unleashing Pb_j^{max} thresholds.

Objective: Maximize the expected revenues from serving the maximum amount of traffic belonging to the defined classes. Therefore, the NORMA objective function can be expressed as:

$$\text{(NORMA)} \quad \underset{\forall k \in K}{Maximize} \quad REVENUES^k \tag{5.4}$$

The revenues from selling these services can be computed knowing the billable time. We define bt_j^k as the billable time of service class *j* during a certain time interval Δt (e.g., one year) using wavelength partitioning scheme *k*. Note that such a time can be computed as the amount of expected arrivals during Δt multiplied by the average connection *ht*. Therefore, defining iat_j^k as the average inter-arrival time, bt_j^k can be formulated as:

$$bt_j^k = |N| \cdot \frac{\Delta t}{iat_j^k} \cdot \left(1 - Pb_j\right) \cdot \left(ht_j^k \cdot \rho_j^k\right) = |N| \cdot I_j^k \cdot \rho_j^k \cdot \left(1 - Pb_j\right) \cdot \Delta t \tag{5.5}$$

where $I_j^k = ht_j^k \,/\, iat_j^k$ represents the offered load per node belonging to class of service *j* when wavelength partitioning scheme *k* is used. Then, the revenues obtained from serving the two classes of service over an optical network using wavelength partitioning scheme *k* can be computed as

$$REVENUES^k = \sum_{\forall j \in S} bt_j^k \cdot C_j = \sum_{\forall j \in S} \left(|N| \cdot I_j^k \cdot \rho_j^k \cdot \left(1 - Pb_j\right) \cdot \Delta t \cdot C_j\right) \tag{5.6}$$

By inspection of equation (5.6), two unknowns can be identified: the offered load I_j^k and the actual proportion ρ_j^k of provided *ht*. To the best of our knowledge, no models for predicting these variables can be found in the literature. As consequence, in the next section we focus on modeling these *response* variables from a statistical point of view.

5.2.2 Traffic statistical models

Aiming at obtaining likely values for the response variables, we have studied their behavior over a meaningful set of networks. These network scenarios were chosen from the set of real backbone optical transport networks presented in [Pa10]. From the complete set, a subset of 13 bi-connected and planar networks was selected, covering in this way a wide range of distinct topologies. Each network was identified by means of 11 *topology-dependent characteristics* (*independent variables*) candidates to be part of the model. These topology-dependent characteristics are:

$\|N\|$	Number of nodes
$\|E\|$	Number of links
δ	Average nodal degree
δ^{max}	Maximum nodal degree
δ^{med}	Median nodal degree
h	Average path length
dia	Diameter
rad	Radius
$\|sN\|$	Number of nodes of the homeomorphic graph
$\|sE\|$	Number of links of the homeomorphic graph
$s\delta$	Average nodal degree of the homeomorphic graph

We conducted a large amount of simulations over the networks under study for every traffic class and wavelength partitioning scheme. In such experiments, each DWDM link was equipped with 16 wavelengths and no wavelength conversion capabilities were provided to the optical nodes. For sh-WS, the CAFES algorithm in [Ou04.2] was adapted to compute feasible routes for the SP connections while satisfying the wavelength continuity constraint, whereas algorithm in Table 5-1 was used for diff-WS. In this regard, $Pb_{SP}{}^{max}$ = 1% was assumed for the SP class, avalue largely used in the literature. In contrast, a significantly higher $Pb_{BE}{}^{max}$ = 5% was assumed for the BE class.

Table 5-2 shows the values of the topology-dependent variables for the 13 topologies used for estimation.

Every simulation for a specific traffic class and wavelength partitioning scheme resulted in a tuple containing the offered load to the network, the blocking probability, and the proportion of *ht* served. We chose those tuples with *Pb* equal to $Pb_j{}^{max}$. Then, together with the candidate set of independent variables, we applied a

multiple linear regression to obtain statistical models for the response variables. Aiming at avoiding over-fitting, which could be a drawback in further predictions, we limit the number of independent variables in the models to be two.

Table 5-2: Characteristics of the analyzed networks

ID	$\|N\|$	$\|E\|$	δ	δ^{max}	δ^{med}	h	dia	rad	$\|sN\|$	$\|sE\|$	$s\delta$
1	9	11	2.44	4	2	2.06	4	2	3	5	3.33
2	9	13	2.89	5	3	1.86	3	2	5	9	3.60
3	11	18	3.27	6	3	2.00	4	2	10	17	3.40
4	14	23	3.29	6	3	2.34	5	3	11	20	3.64
5	17	26	3.06	6	3	2.70	6	3	10	19	3.80
6	19	24	2.53	4	2	3.05	7	4	8	13	3.25
7	19	28	2.95	4	3	2.92	6	4	14	23	3.29
8	19	32	3.37	6	3	2.61	6	3	15	28	3.73
9	21	25	2.38	4	2	3.46	7	4	6	10	3.33
10	28	35	2.50	5	2.5	4.07	9	6	14	23	3.29
11	28	39	2.79	5	3	3.95	9	5	18	29	3.22
12	28	41	2.93	5	3	3.56	8	4	19	32	3.37
13	28	44	3.14	5	3	3.47	7	5	22	38	3.45

An additive linear model without interactions was firstly attempted. For all combinations of two independent variables, the best fitting was obtained with the following model:

$$I_j^k \cong a(k,j) + b(k,j) \cdot h + c(k,j) \cdot \delta \tag{5.7}$$

which coefficients and goodness-of-fit for k=diff-WS and j=SP are:

- a=1.956, b=-0.741, c=0.581.
- R^2: 95.29%
- AIC: -8.9269.

Although a R^2 close to 95% denotes a high correlation between real and predicted values, we observed that the intensity estimation error leads into an unacceptable variability in the blocking probability. Thus, a higher goodness-of-fit is required. This requirement is, however, unreachable when only two variables in a linear model are considered.

Aiming at increasing the goodness-of-fit of the model without increasing the number of coefficients, we used a logarithmic transformation for the response and

independent variables. This transformation allows using linear regression techniques with logarithmic variables and, at the same time, considering non-linear relations among original variables [Ch97]. Equation (5.8) shows the best logarithmic model for all intensity models:

$$\log\left(I_j^k\right) \cong \alpha(k,j)\cdot\log(10)+\beta(k,j)\cdot\log(h)+\gamma(k,j)\cdot\log\left(|E|\right) \tag{5.8}$$

For k=diff-WS and j=SP traffic, coefficients and goodness-of-fit values are:

- α=0.334, β=-2.720, γ=0.724.
- R^2: 99.51%
- AIC: -68.38.

This model provides a correlation coefficient higher than 99% and an AIC significantly lower than the obtained with the linear model. The high correlation between real and fitted values is plotted in Fig. 5-4, graphically illustrating the goodness-of-fit of the model. As can be observed, all real values are included into the centered confidence interval (dotted lines) of the fitted ones.

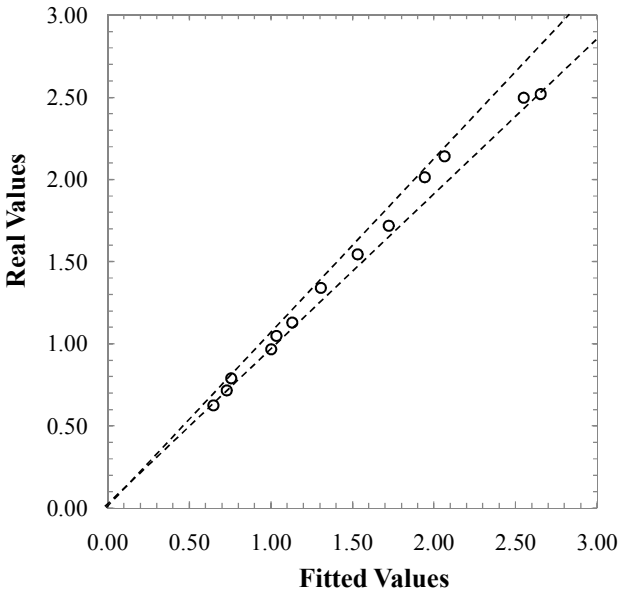

Fig. 5-4 Observed vs Fitted values for SP traffic and diff-WS

Thus, we obtained the best fit using $|E|$ and h as independent variables. The former provides the amount of network resources (i.e., the network capacity), whereas the latter gives information about the amount of resources per connection. We also concluded that a general parametrical formula with those independent variables can be used with specific linear coefficient values for each I_j^k model. Equation (5.9) shows the prediction model where the logarithmic transformation has been reversed, so that the linear coefficients become exponents.

$$I_j^k = \frac{10^{\alpha(k,j)} \cdot |E|^{\beta(k,j)}}{h^{\gamma(k,j)}} \pm \varepsilon(k,j) \quad (5.9)$$

Table 5-3 shows the values of the exponents for each I_j^k model. In order to provide a confidence interval to the statistical models, the parameter $\varepsilon(k,j)$ collecting the relative error has been also included. As shown, these errors are close to 5%, except for the BE traffic class with sh-WS, where fewer networks were available for the model (a discussion about this case is given below). Moreover, the values of the R^2 are higher than 95% as shown in Table 5-3, thus giving a tight fit for the offered load models.

Table 5-3: Parameters and Observed Adjust for the Intensity Models

Scheme (*k*)	Class (*j*)	α	β	γ	ε (%)	R^2(%)
sh-WS	**SP**	0.222	0.931	3.07	5.62	99.2
	BE	1.522	0	6.40	9.94	95.1
diff-WS	**SP**	0.334	0.724	2.72	5.44	99.5
	BE	0.548	0.603	2.56	5.48	99.1

At this point, we take up again the blocking probability bound (1-$P(R_{BE}, G_{SP})$) defined in equation (5.3); if that bound is higher than Pb_j^{max}, the traffic intensity must be set to zero since any traffic load would not satisfy the requested GoS.

However, there is only one case where this may happen, namely, the case of the BE traffic under sh-WS as a consequence of its subordination to the SP traffic. In view of this, the $I_{BE}^{sh\text{-}WS}$ model needs to be completed with an expression to predict whether (1-$P(R_{BE}, G_{SP})$) >Pb_{BE}^{max}. We have computed $P(R_{BE}, G_{SP})$ for every network under study, finding a tight relation between $P(R_{BE}, G_{SP})$ and h. We observed (1-$P(R_{BE}, G_{SP})$) >Pb_{BE}^{max} in every network with h> 2.5. Therefore, the $I_{BE}^{sh\text{-}WS}$ model becomes a discontinuous function, where equation (5.9) models $I_{BE}^{sh\text{-}WS}$ provided that $h \leq 2.5$, otherwise $I_{BE}^{sh\text{-}WS} = 0$.

Regarding the proportion of provided ht, only the model for the particular case of BE traffic under sh-WS is finally needed. By simple inspection of the simulation results, we concluded that $\rho_{BE}^{\text{sh-WS}} \approx 0.6$. For the rest of the models $\rho_j^k = 1$, thus reflecting the independence between traffic classes.

Once we have the statistical models for the response variables and its goodness of fit have been assessed, we use them to solve the NORMA problem for real backbone topologies.

5.3 Illustrative numerical results

Two backbone optical networks have been used: the moderately meshed DT_14n_23e topology and the quite sparse NSFNET_28n_37e topology (see Appendix A). In this chapter, we refer them as DT and NSFNET topologies, respectively. These networks did not belong to the set of networks used to obtain the statistical models and thus they can be used for evaluation.

Aiming at comparing the offered loads obtained under the two wavelength structure schemes, let us define the intensity ratio $I_j^{sh\text{-}WS}$:$I_j^{diff\text{-}WS}$. An intensity ratio of one depicts a network that can carry the same amount of traffic under both wavelength structure schemes; a value greater (lower) than one means more traffic being carried under the sh-WS (diff-WS) scheme. Fig. 5-5 shows the intensity ratio for SP and BE traffics. Each plot represents the values of the ratio for networks grouped by the number of links (within the range of our study). Additionally, the test topologies DT and NSFNET are also positioned.

Fig. 5-5a shows that the sh-WS scheme supports more traffic intensity when it is applied to moderately or highly meshed networks (low average path lengths). This is the case for the DT network that can transport 10% of additional traffic under the sh-WS scheme with respect to the diff-WS one. On the contrary, the diff-WS scheme supports more traffic when it is applied to sparsely meshed networks. In this context, the NSFNET topology provides approximately the same amount of traffic under both schemes since its ratio is nearby 1.

A similar study can be done for the BE traffic (Fig. 5-5b). In this case, the diff-WS scheme provides more traffic than the sh-WS one regardless of the network mesh degree. The latter scheme can carry, in the best case, only 40% of the traffic carried by the former. As an example, the sh-WS scheme can carry only 5% of the traffic carried under the diff-WS scheme over the DT network. In fact, since the great majority of the networks under study have h> 2.5 hops, the BE traffic intensity becomes zero under the sh-WS scheme. This is the case also of the NSFNET network.

Similarly to the intensity ratio, we define the revenues ratio $Z^{sh\text{-}WS}$:$Z^{diff\text{-}WS}$. In this case, a ratio of one means both schemes obtaining the same revenues, whereas a ratio greater (lower) than one means more revenues being obtained under the sh-WS (diff-WS) scheme. Additionally, to compare the prices of the SP and BE services we define the price ratio c_{SP}:c_{BE}. Note that a fair price ratio could be in the order of 5:1, reflecting the amount of resources used by each service, as suggested in [Xi09].

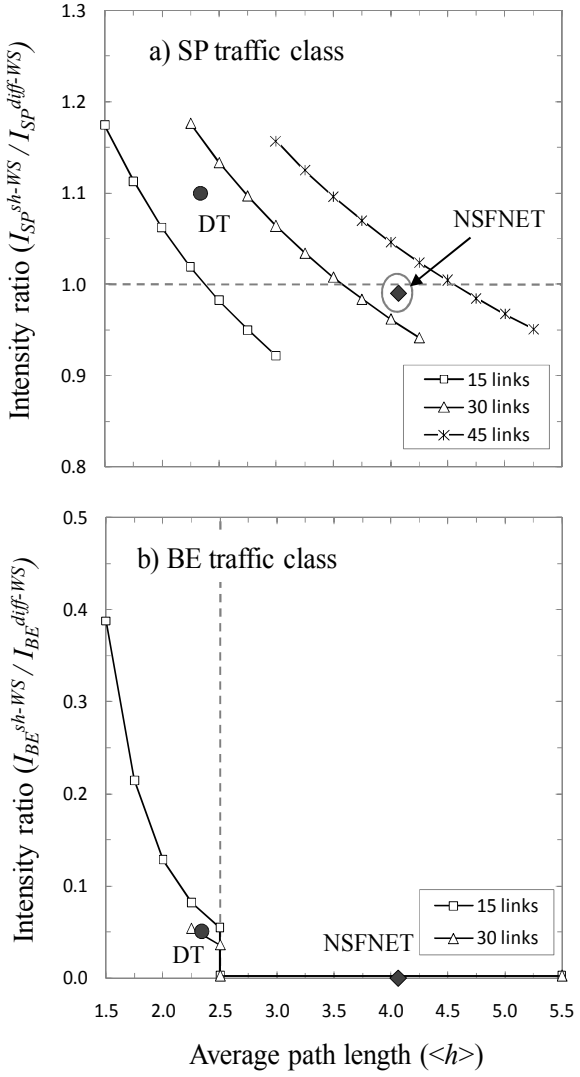

Fig. 5-5 Intensity ratio for (a) SP and (b) BE traffics

Fig. 5-6 plots the revenue ratio as well as the total revenues obtained by each wavelength scheme as a function of the price ratio for the test networks. In the case of the DT network we observed the break-even price ratio being near to 12:1. In the case where the price ratio 5:1 was applied, the diff-WS scheme would obtain 11.25% of additional revenues with respect to that of the diff-WS one. Applying a more aggressive price rate of 8:1 the diff-WS scheme would still obtain more revenues (~4.5%). Note that although more SP traffic intensity can be carried with the sh-WS scheme higher revenues are obtained with the diff-WS one.

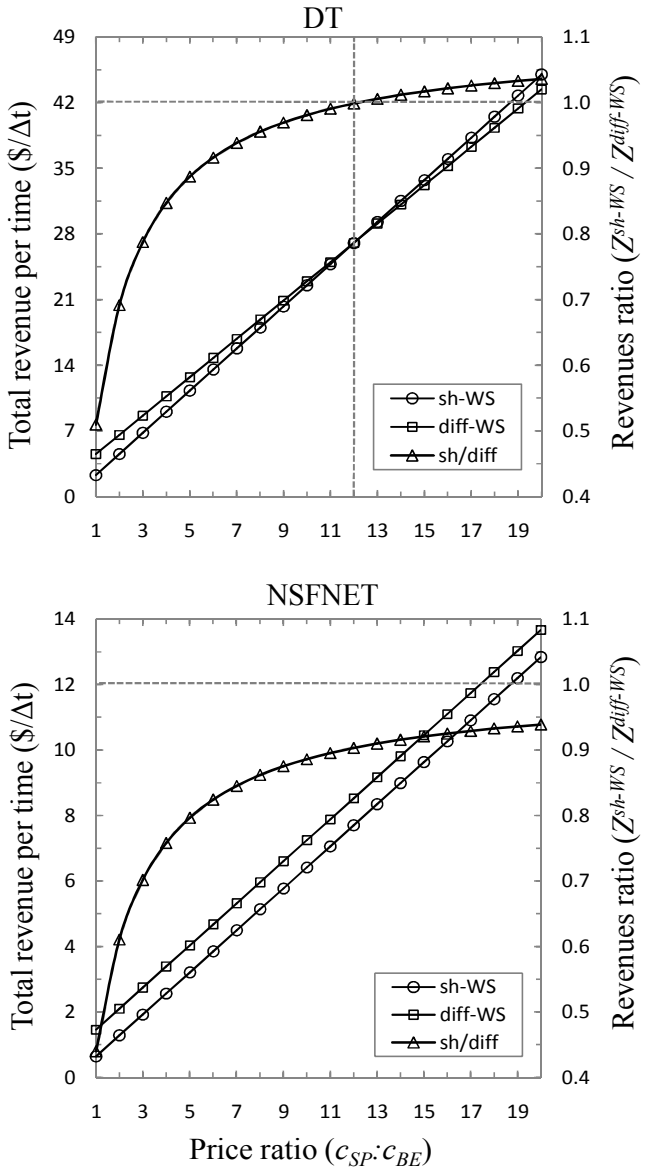

Fig. 5-6 Total revenues and revenues ratio against the price ratio

Then, the revenues from operating the DT network would be higher in a wide range of price ratios when the diff-WS scheme is chosen. A similar analysis can be done on the NSFNET network. In this case, there is not break-even price ratio since the diff-WS scheme already carries more SP traffic on this network. Then, the revenues from operating this network are always higher with the diff-WS scheme (20.36% higher with the price ratio 5:1).

5.4 Summary

In this chapter a study about the way differentiated services are currently provisioned was presented, concluding that only very poor GoS can be expected from the BE class. Aiming at improving the amount of BE service provided without deteriorate the SP one, thus maximizing the network operator revenues, the diff-WS scheme defining differentiated sets of resources to provide each class of service was proposed.

Next, to evaluate sh-WS and diff-WS schemes in terms of expected revenues from selling SP and BE traffic, the NORMA problem was introduced. The NORMA problem departs from a deployed topology and returns the partitioning scheme which maximizes revenues. To solve the problem, statistical models to compute traffic intensity for the objective GoS were derived. In light of the results we can conclude that diff-WS maximizes the revenues from operating a great range of backbone networks.

The following chapter extends NORMA in two ways: first, network design is also included in the problem, and second to compare not only revenues but also CAPEX and OPEX, the net present value formula is selected as the objective function to be minimized.

Chapter 6

Network and partitioning scheme planning

In this chapter, the NORMA problem is extended to include network planning (NORMA++). Using the statistical traffic models developed in the previous chapter, NORMA++ designs the network topology to provide as much revenues as possible to the network operator. From an extensive performance analysis, we conclude that diff-WS maximizes resource utilization in the network and, thus, network operator's profit.

This problem, however, does not take into account costs. Then, with the aim to provide a fair trade-off between costs and revenues, we define the OVALO problem as a network net present value maximization problem. We present an iterative method based on an integer linear programming, where a linear approximation of the net present value is used. From the obtained performance analysis, we conclude that the net present value is maximized when diff-WS is applied.

6.1 Network planning to maximize network operator revenues

6.1.1 The NORMA++ problem statement

The Network Operator Revenues Maximization planning problem (NORMA++), allows finding the optimal network topology that maximizes the expected revenues under a certain resource partitioning scheme, such as sh-WS or diff-WS. It is worth noting that real backbone optical transport network topologies (e.g. [Pa10]) share planarity as a common characteristic. Moreover, to provide protection, two-connectivity is another requirement for feasible topologies.

The NORMA++ problem can be stated as follows:

Given:

a) the physical network topology represented by a graph *G(N, E, WL)*, with *N* the set of locations where a node must be placed, *E* the set of already deployed optical fibers and *WL* the set of wavelengths in each optical link,

b) a set *S* of classes of service to be provided, index *j*,

c) the network operator's pricing structure, specified by a fixed fee C_j charged to the customers per time unit of class of service *j*,

d) the blocking probability threshold Pb_j^{max} allowed for each class of service *j*,

e) a set *K* of wavelength partitioning schemes, index *k*. In this work we assume *K*={sh-WS, diff-WS}.

Output:

a) a wavelength partitioning scheme *k*,

b) the set of links *E*(*k*) in the network designed for the partitioning scheme *k* ensuring that the resulting topology is planar and, at least, 2-connected.

c) the maximum traffic intensity for the given classes of service unleashing Pb_j^{max} thresholds.

Objective: Maximize the expected revenues for the designed network coming from serving the maximum amount of traffic belonging to the defined classes. Therefore, the NORMA++ objective function can be expressed as:

$$(\text{NORMA++}) \quad \underset{\forall k \in K}{Maximize} \quad REVENUES^k \tag{6.1}$$

In light of equations (5.6) and (5.9), the maximization of revenues is equivalent to maximize the offered load while still meeting the blocking probability threshold. In view of the intensity model in equation (5.9) and the revenues expression in equation (5.6), we can reformulate the NORMA++ objective function (i.e., removing constants, grouping terms, etc.) as:

$$Maximize\ REVENUES^k \equiv Maximize \sum_{\forall j \in S} \frac{\theta_j^k \cdot |E|^{\beta(k,j)}}{h^{\gamma(k,j)}} \tag{6.2}$$

for a given partitioning scheme *k*, where θ_j^k is a positive constant. Looking at equation (6.2), we are facing to a non-linear problem. Next subchapter provides an iterative linear method based on some mathematical properties.

6.1.2 NORMA++ ILP model and iterative method

In equation (6.2) the topology-dependent variable $|E|$ is divided by the topology-dependent variable *h*. This fact avoids using equation (6.2) as the objective function of an ILP. Proposition 1 allows us to introduce an iterative method where a linear problem is solved at each iteration.

Proposition 1: Let $G_1(N, E_1)$ and $G_2(N, E_2)$ be two graphs with $|E_1|$ and $|E_2|$ links and with minimum h_1 and h_2, respectively (G_1 and G_2 are optimal with respect to h). If $|E_2| = |E_1|+1$, then for a given scheme k:

$$\sum_{\forall j \in S} \frac{\theta_j^k \cdot |E_2|^{\beta(k,j)}}{h_2^{\gamma(k,j)}} > \sum_{\forall j \in S} \frac{\theta_j^k \cdot |E_1|^{\beta(k,j)}}{h_1^{\gamma(k,j)}} \quad \begin{matrix} \forall \beta(k,j) > 1 \\ \forall \gamma(k,j) > 1 \end{matrix} \tag{6.3}$$

where $\beta(k, j)$ and $\gamma(k, j)$ become parameters greater than 1 for each scheme and class of service.

Proof: If h_1 is the minimum for every network with $|E_1|$ links, optimizing for $|E_2|=|E_1|+1$ links will result in a graph $G_2(N, E_2)$ with average path length $h_2 \leq h_1$, provided that a feasible solution exists. □

As a consequence of Proposition 1, the NORMA++ problem can be solved iteratively by fixing the number of links a at each iteration. In this way, a linear problem is solved, since $|E|$ remains constant and the objective function to minimize is h.

It is worth mentioning that each linear problem finds the 2-connected and planar topology with a number of links that minimizes h. Therefore, the optimal solution of the NORMA++ problem is obtained with the maximum number of links and the minimum h.

To solve NORMA++ the following sets and parameters are defined:

N	set of nodes, index n
E	set of links, index e
$\Omega(n)$	set of incident links on node n
K	set of partitioning schemes, index k
D	set of suitable source-destination pairs $\{s_d, t_d\}$, index d.
X	set of exclusions to ensure planarity, index x
φ_e^x	1 if link e is in the exclusion x, 0 otherwise
δ_{max}	maximum nodal degree
a	desired number of links
M	a large positive constant

Additionally, the following variables are defined:

ζ_e	binary, 1 if link e is in the designed network, 0 otherwise
ω_e^d	binary, 1 if the source-destination pair d uses link e for the shortest path, 0 otherwise

κ_e^d binary, 1 if source-destination pair d uses link e for the alternative path, 0 otherwise

We use the set D to ensure that two link-disjoint routes can be found in the designed network topology (2-connectivity condition). Note that if D does not contain all node pairs, one (or more) 2-connected subgraph(s), containing the source/destination nodes, will be obtained instead.

The iterative method starts fixing the parameter a to the maximum number of links, reducing this number until a feasible solution is found. Table 6-1 shows the NORMA++ iterative method to obtain the optimal solution for a given partitioning scheme.

Finally, the NORMA++ ILP model for a fixed number of links a can be formulated as follows:

$$(\text{NORMA++}) \text{ minimize} \quad h = \frac{1}{|D|} \sum_{\forall d \in D} \sum_{\forall e \in E} \omega_e^d \tag{6.4}$$

subject to:

$$\sum_{\forall e \in \Omega(n)} \omega_e^d = 1 \quad \forall d \in D \quad \forall n \in \{s_d, t_d\} \tag{6.5}$$

$$\sum_{\forall e \in \Omega(n)} \omega_e^d \leq 2 \quad \forall d \in D \quad \forall n \in N - \{s_d, t_d\} \tag{6.6}$$

$$\sum_{\substack{\forall e' \in \Omega(n) \\ e' \neq e}} \omega_{e'}^d \geq \omega_e^d \quad \forall d \in D \quad \forall n \in N - \{s_d, t_d\} \quad \forall e \in \Omega(n) \tag{6.7}$$

$$\sum_{\forall e \in \Omega(n)} \kappa_e^d = 1 \quad \forall d \in D \quad \forall n \in \{s_d, t_d\} \tag{6.8}$$

$$\sum_{\forall e \in \Omega(n)} \kappa_e^d \leq 2 \quad \forall d \in D \quad \forall n \in N - \{s_d, t_d\} \tag{6.9}$$

$$\sum_{\substack{\forall e' \in \Omega(n) \\ e' \neq e}} \kappa_{e'}^d \geq \kappa_e^d \quad \forall d \in D \quad \forall n \in N - \{s_d, t_d\} \quad \forall e \in \Omega(n) \tag{6.10}$$

$$\omega_e^d + \kappa_e^d \leq 1 \quad \forall d \in D \quad \forall e \in E \tag{6.11}$$

$$\sum_{\forall d \in D} \left(\omega_e^d + \kappa_e^d \right) \leq M \cdot \zeta_e \quad \forall e \in E \tag{6.12}$$

$$\sum_{\forall e \in E} \zeta_e = a \tag{6.13}$$

$$\sum_{\forall e \in E} \zeta_e \cdot \varphi_e^x \leq 1 \quad \forall x \in X \tag{6.14}$$

$$\sum_{\forall e \in \Omega(n)} \zeta_e \leq \delta_{max} \quad \forall n \in N \tag{6.15}$$

Table 6-1: NORMA++ Iterative Method

```
Procedure
Input: G(N, E, WL), X, Cj, δmax, α(k,j), β(k,j), γ(k,j),
       ε(k,j)
Output: E(k), I^k_SP, I^k_BE, REVENUES^k
begin
  Compute D
  Set initial point a = |E|
  Initialize BestSolution
  while (a ≥ |N|) do
    Solve NORMA ILP model with a links
    if feasible solution found then
      BestSolution.E = {e∈E, ζe=1}
      BestSolution.I_BE = Compute I_BE using eq.(5.11)
      BestSolution.I_SP = Compute I_SP using eq.(5.11)
      BestSolution.Rev = Compute Revenues using eq.(5.6)
      break
    a = a- 1
end
```

In the model, the objective function (6.4) indirectly maximizes revenues for the given number of links. Constraints (6.5)-(6.11) ensure that the designed topology is at least 2-connected, that is, a pair of link-disjoint routes must exist in the network for every source-destination pair. Constraint (6.12) stores the use of every link. Constraint (6.13) guarantees that the desired number of links a is provided. Constraint (6.14) ensures that the topology is planar. Finally, constraint (6.15) limits nodal degrees.

The NORMA++ method and model were implemented in iLog-OPL and solved by the CPLEX v.11.0 optimizer [CPLEX] on a 2.4 GHz Quad-Core machine with 8 GB RAM memory. Next section discusses the obtained results.

6.1.3 Illustrative numerical results

For evaluation, three backbone optical network series were created, starting from three well-known base topologies and adding extra connectivity. To this end, we used the moderately meshed DT_14n_23e and EON_16n_23e topologies, in addition to a quite sparse NSFNET_20n_38e topology. From these base topologies (in this chapter referred as DT, EON and NSFNET, respectively), DT series, EON series and NSFNET series have been created (see Appendix A).

Aiming to compare the traffic intensities under sh-WS and diff-WS schemes, Fig. 6-1 plots their absolute values as a function of the number of links for every optimal network in each topology series. Focusing on the SP traffic class, the traffic intensity under diff-WS is higher than under sh-WS for quite sparsely meshed networks, but lower for moderately meshed ones.

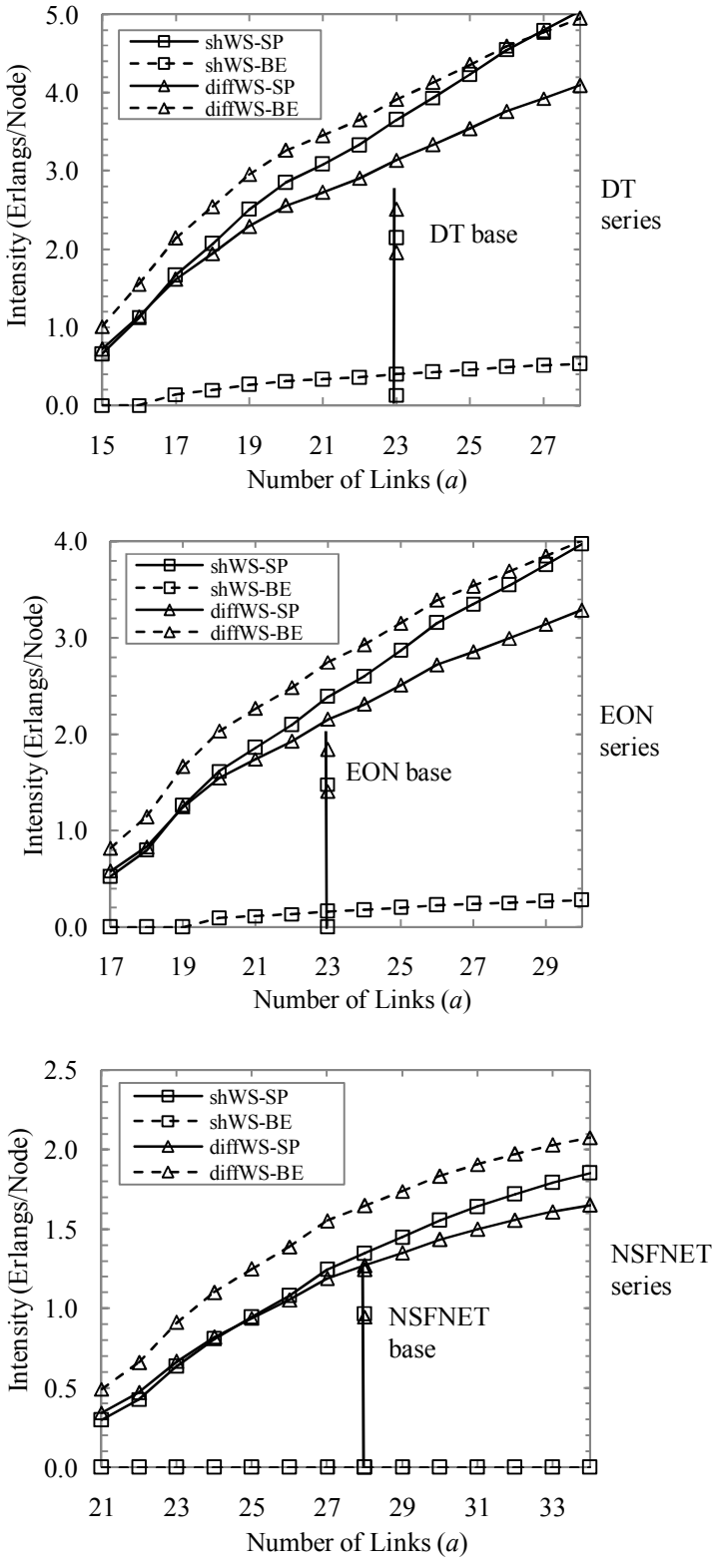

Fig. 6-1 Traffic intensities against number of links

It is worth noting that the number of SP connections being established under the sh-WS scheme depends on the shareability degree of the protection resources, i.e., the number of protection paths sharing each resource. The higher this degree the more resources are kept available for working paths. The shareability degree depends on the existence of multiple disjoint working paths in the network, by definition of the SPP scheme, and thus on the network's mesh degree. Then, the available resources will be increased by increasing δ. In contrast, the number of resources available for working paths under the diff-WS scheme is given by the fixed size of WL_{SP}, since differentiated resources are used for working and for protection paths.

For the BE traffic class, the obtained intensity is much higher under diff-WS as a consequence of resource differentiation. Note that the intensity becomes zero for those sparsely and moderately meshed networks with $h > 2.5$. In fact, the BE traffic intensity is zero for each topology belonging to the NSFNET series.

Besides, the corresponding base topology is also positioned in each graph in Fig. 6-1. As seen, the traffic intensity values are clearly worse than those of the optimal network with the same number of links.

In order to compare the relative values of traffic intensity obtained under sh-WS and diff-WS, let us define their intensity ratio as $I_j^{\text{diff-WS}}:I_j^{\text{sh-WS}}$. An intensity ratio equal to one describes a network that can carry the same amount of traffic under both wavelength partitioning schemes; a value greater (lower) than one means more traffic being carried under diff-WS (sh-WS). Fig. 6-2 shows this intensity ratio for SP and BE traffics as a function of h. Each plot represents the ratio values in the networks under study. Additionally, the base test topologies are also positioned.

Fig. 6-2a shows that the sh-WS scheme supports more SP traffic intensity when applied to moderately and highly meshed networks (short average path lengths). Note that δ and h are closely related. This is also the case for the DT, EON, and NSFNET base networks, only supporting 91%, 95% and 98% of traffic under diff-WS with respect to sh-WS, respectively. In contrast, diff-WS supports more SP traffic when applied to sparsely meshed networks.

A similar study can be done for the BE traffic (Fig. 6-2b). In this case, diff-WS allows more traffic than sh-WS regardless of the average nodal degree value. As observed, diff-WS can carry at least 10 times more traffic than diff-WS. For instance, the diff-WS scheme allows carrying about 19.3 times more traffic than sh-WS over the DT base network. In fact, since most of the networks under study present $h > 2.5$ hops, the BE traffic intensity becomes zero under sh-WS, resulting in infinite intensity ratios. This also happens in the EON and NSFNET base networks.

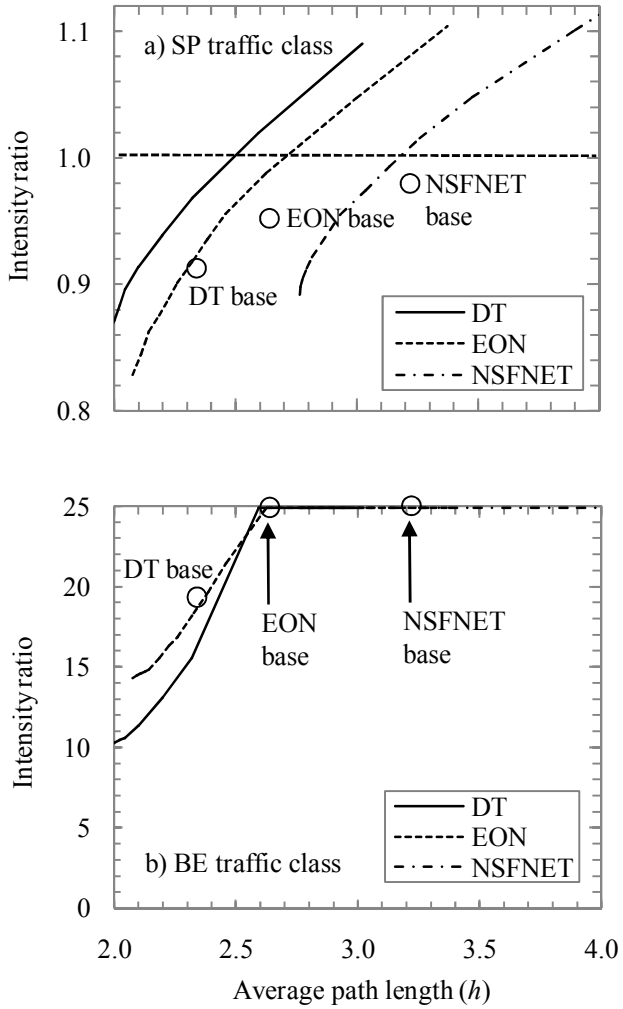

Fig. 6-2 Intensity ratio against average path length

With aims to compare the revenues obtained under each partitioning scheme, Fig. 6-3 illustrates the evolution of the revenues increment percentage with diff-WS with respect to sh-WS as a function of the average nodal degree. As shown, although SP traffic intensity is lower under diff-WS, the finally obtained revenues are higher even in highly meshed network topologies. As shown, only those optimal topologies in the DT series with $\delta > 3.7$ lead to increased revenues with sh-WS.

In addition, the corresponding base topologies are also positioned in Fig. 6-3. Interestingly, the obtained percentages are much higher than those of the optimal network with the same number of links. Therefore, any non-optimal network topology increases the revenues increment percentage with diff-WS against sh-WS, thus being the former more beneficial.

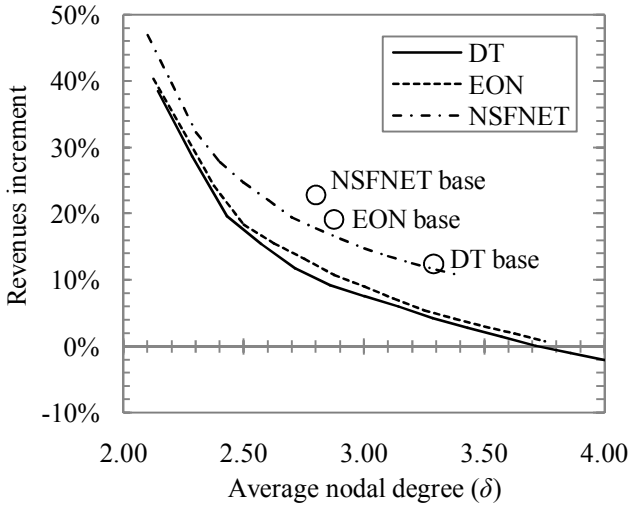

Fig. 6-3 Revenue increment against average nodal degree

Fig. 6-4 plots the total revenues obtained with each wavelength partitioning scheme as a function of the price ratio for the base topologies. In the case of the DT network we observed the break-even price ratio at 12:1. In case that a fair 5:1 price ratio (as considered in Chapter 5) would be applied, diff-WS would obtain 12.4% additional revenues than sh-WS. Applying a more aggressive price rate of 8:1 diff-WS would still obtain more revenues (4.5%). As a result, the revenues from operating the DT network would still be higher in a wide range of price ratios if the diff-WS scheme is applied. A similar analysis can be done for the EON and NSFNET networks. In these cases, the break-even price ratio is higher than 20:1, being the revenues from operating this network higher with the diff-WS scheme (19.1% and 22.7% higher with 5:1 price ratio for the EON and NSFNET, respectively).

In light of these results, we can conclude that the expected benefits in terms of revenues from applying diff-WS are higher than the provided from sh-WS. Nevertheless, the costs from deploying and operating networks are not considered in the NORMA++ problem.

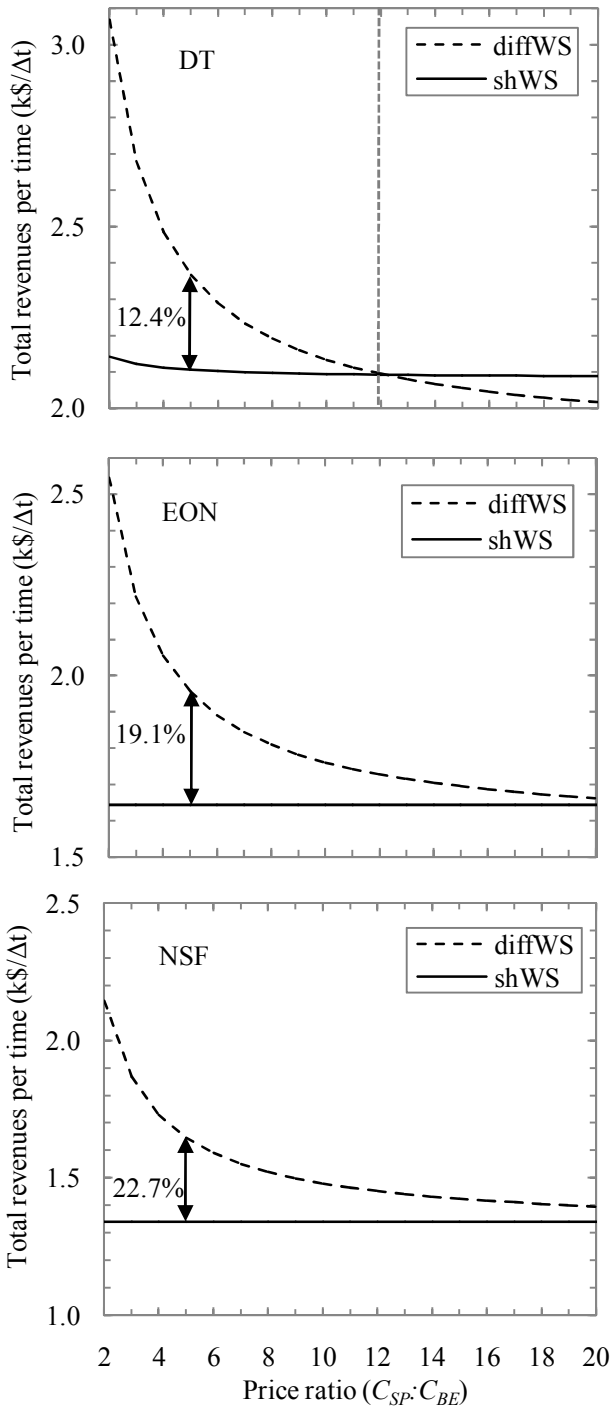

Fig. 6-4 Total revenues against price ratio

6.2 Optical network net present value optimization

This subchapter presents OVALO, an extension of the NORMA++ problem to include also CAPEX and OPEX to the objective function.

6.2.1 The OVALO problem statement

Recall that the NPV was introduced in Chapter 2. By inspection of equation (2.20), the NPV of a network depends on three factors, i.e., revenues, OPEX, and CAPEX.

Regarding CAPEX costs, they can be computed as the sum of the cost of the nodes plus the sum of the cost of the links. To model the cost of the optical nodes we assume that they are based on the design presented in [Ro08] for colorless nodes, were the cost of increasing the nodal degree is lineal up to a maximum of 8 when 1x9 wavelength selective switches (WSS) are used. Then, the cost of an optical node can be modeled as the summation of three factors: firstly, C_{BASE} which includes the cost of common equipment (e.g., sub-rack, power cards, control card, etc.) and the installation cost; secondly, the cost of the WDM interfaces, which is proportional to the nodal degree (δ) and to the cost of one WDW interface, C_{Trunk}; finally, the cost of the access to the optical network, which is proportional to the cost of every optical transponder, $C_{Transponder}$, and depends on the traffic intensity offered to the network. To compute the number of transponders to install in every optical node we assume that the maximum of traffic doubles the mean. Then, the higher amount of connections having a given node as source or destination in the same time period can be computed as:

$$maxPaths^k = \left\lceil \sum_{\forall j \in S} 2 \cdot I_j^k \right\rceil \tag{6.16}$$

On the other hand, the cost of a link e (C_e) includes: firstly, the cost of using a pair of optical fibers, which is proportional to the cost per km, C_{FOKm}, and to the length of the link, $L(e)$. It is worth noting that we consider that the optical cables are already deployed so the total deployment cost of an optical cable is allocated among the different networks using some fibers from it; secondly, the cost of the optical amplifiers and dispersion compensators, each with a cost C_{OA}, which number depends on the length of the link and can be computed as floor($L(e)/AS$), where AS is the amplifier span length.

Finally, we can accurately estimate the CAPEX to deploy an optical network using the partitioning scheme k as:

$$\begin{aligned} CAPEX^k &= \sum_{\forall n \in N} \left(C_{BASE} + \delta_n^k \cdot C_{Trunk} + maxPaths^k \cdot C_{Transponder} \right) \\ &+ \sum_{\forall e \in E(k)} \left(L(e) \cdot C_{FOKm} + \left\lfloor \frac{L(e)}{AS} \right\rfloor \cdot C_{OA} \right) \end{aligned} \tag{6.17}$$

Regarding operational costs, several studies can be found in the literature providing models to compute OPEX only partially. Authors in [Ve06] present an activity based approach to quantify the cost part of the operational processes, those related with repair and provisioning. Non event-driven processes, such as preventive maintenance, or other related with the technology used or the amount of served traffic, such as power consumption, are, however, omitted. A specific ILP model to design the network minimizing the energy consumption is presented in [Sh09]. Finally the authors in [Ma08] quantify the impact of the protection schemes and the network component's availability on the OPEX.

Nevertheless, the OPEX is somehow related with the network's dimension, i.e. number and complexity of the nodes, total length of the links, etc., and then somehow related with CAPEX. Therefore and without loss of generality, in this work we consider that OPEX is proportional to CAPEX, i.e., OPEX=η*CAPEX, where η is in the range [0, 1]. In addition, we assume that revenues and OPEX remain invariable during the considered time period.

Regarding traffic, we assume that the network must guarantee, as a result of some market research, a certain amount of SP traffic. Likewise, owing to its reduced price, we assume that the connectivity market demands a large amount of BE traffic.

From equation (2.20) it is clear that projects' value can be improved by increasing revenues or, alternatively, reducing costs. We propose the OVALO problem to find the network design associated with a partitioning scheme, which maximizes NPV.

Then, the OVALO problem can be formulated as follows:

Given:

a) the physical topology of a network represented by a graph $G(N, E, WL)$,

b) a set S of classes of service to be provided,

c) the network operator's pricing structure, specified by a fixed fee C_j charged to the customers per time unit of class of service j,

d) the minimum SP intensity required I_{SP}^{min} and the blocking probability threshold Pb_j^{max} allowed for every class of service j.

e) a set K of wavelength partitioning schemes, index k. In this work we assume K={sh-WS, diff-WS}.

f) the network cost model,

g) the period of time Y where the study applies (e.g. 10 years) and the discount rate r.

Output

a) a wavelength partitioning scheme k,

b) the set of links $E(k)$ in the network designed for the partitioning scheme k ensuring that the resulting topology is planar and, at least, 2-connected,

c) the traffic intensities I_{SP}^{max} and I_{BE}^{max} for the given classes of service unleashing Pb_j^{max} thresholds.

Objective: Maximize the net present value for the designed network where the revenues come from serving traffic belonging to the defined classes. Thus, the OVALO objective function can be expressed as:

$$\text{(OVALO)} \quad \underset{\forall k \in K}{Maximize} \quad NPV^k \tag{6.18}$$

The next section presents models to solve the OVALO problem. Being its objective nonlinear, an iterative method that, at each iteration, solves a linearized version of the problem is proposed.

6.2.2 OVALO ILP model and iterative method

The mathematical formulation of the OVALO problem derives from the formulation presented for the NORMA++ problem. Additionally to the notation previously defined, the model for the OVALO problem defines δmin as the minimal nodal degree.

Using that notation, introducing the revenues and the intensity models to the NPV expression in eq.(2.20), and adapting it to be used as the objective function of OVALO (i.e., removing constants, grouping terms, etc.), we can write that for a given partitioning scheme k:

$$\text{maximize} \quad NPV^k \equiv \varepsilon_1^k \cdot \sum_{\forall e \in E} C_e \cdot \zeta_e + \varepsilon_2^k \cdot \left(\sum_{\forall d \in D} \sum_{\forall e \in E} \varpi_e^d \right)^{-\gamma(k,BE)} \tag{6.19}$$

where:

$$\varepsilon_1^k = -1 - \eta \cdot \left(\sum_{\forall t \in Y} \frac{1}{(1+r)^t} \right) \tag{6.20}$$

$$\begin{aligned} \varepsilon_2^k = \; & 10^{\alpha(k,BE)} \cdot |E|^{\beta(k,BE)} \cdot |D|^{\gamma(k,BE)} \cdot \left[\left(\sum_{\forall t \in Y} \frac{1}{(1+r)^t} \right) \cdot \right. \\ & \left. \cdot \left(|N| \cdot \rho_{BE}^k \cdot (1 - Pb_{BE}) \cdot \Delta t \cdot C_{BE} - 2\eta \cdot C_{transp} \right) - 2C_{transp} \right] \end{aligned} \tag{6.21}$$

In view of equation (6.19), we are facing to a non-linear problem. However, using mathematical regression techniques in the meaningful range of h values, we found a model to linearize the nonlinear part of equation (6.19):

$$\left(\sum_{\forall d \in D} \sum_{\forall e \in E} \varpi_e^d \right)^{-\gamma(k,BE)} \approx \varepsilon_3^k \cdot \sum_{\forall d \in D} \sum_{\forall e \in E} \varpi_e^d \tag{6.22}$$

with:

$$\varepsilon_3^k = -|D|^{\gamma(k,BE)-1} \cdot \tau^k \cdot \left(\frac{2 \cdot |E|}{|N|^2} \right)^{2\gamma(k,BE)-1} \tag{6.23}$$

where $\tau^{diffWS} = 1.724$, and $\tau^{shWS} = 2.933$.

An important conclusion from equations (6.21) and (6.23) is that the objective to maximize is a function of $-|E|^{\gamma(k,BE)}$ and, as a consequence, the number of links needs to be minimized since $\gamma(k,BE)$ is defined as strictly positive. In this regard, we propose an iterative method where at each iteration the problem is solved for a fixed number of links a. If the problem is feasible then a is decremented and a new problem is solved. On the contrary, if the problem is infeasible, the last feasible solution must be the optimal solution. Table 6-2 shows the OVALO iterative method to obtain the optimal solution for a given partitioning scheme.

As shown in the algorithm, the number of iterations, and thus the time complexity, of the algorithm depends on selecting the initial value of a as closer as possible to the optimal one. To this end, we propose to compute a^{ini} by solving the simultaneous equations composed by equation (5.9) together with the equation (3.1) to compute the average length of the shortest paths in a mesh network.

Finally, the OVALO ILP model for a fixed number of links can be formulated as follows:

$$\text{(OVALO) maximize} \quad \varepsilon_1^k \cdot \sum_{\forall e \in E} C_e \cdot \zeta_e + \varepsilon_2^k \cdot \varepsilon_3^k \cdot \sum_{\forall d \in D} \sum_{\forall e \in E} \varpi_e^d \tag{6.24}$$

subject to:

Constraints (6.5) to (6.15)

$$\sum_{\forall e \in E} \omega_e^d \leq \sum_{\forall e \in E} \kappa_e^d \quad \forall d \in D \tag{6.25}$$

$$\sum_{\forall d \in D} \sum_{\forall e \in E} \omega_e^d \leq |D| \cdot hmax \tag{6.26}$$

$$\sum_{\forall e \in \omega(n)} \zeta_e \geq \delta_{\min} \quad \forall n \in N \tag{6.27}$$

Constraints (6.5)-(6.15) are defined in the previous subchapter. Constraint (6.25) forces the primary route to be the shortest route. Constraint (6.26) ensures that the required traffic intensity for the SP traffic, I_{SP}^{min}, can be provided. From equation (5.9) we can convert a I_{SP}^{min} threshold into a h^{max} value which can be use in a linear constraint. It is worth noting that, traffic is not actually routed since it is assumed

dynamic. Instead, eq. (5.9) is used to ensure that enough resources are placed in the network such that the required traffic intensity can be provided. Finally constraint (6.27) guarantees that the degree of every node is higher than the minimum required nodal degree.

Table 6-2: OVALO Iterative Method

```
Procedure
Input: G(N, E, WL), X, {Le}, I_SP^min, Costs and prices
       structures, δ_min, δ_max, α(k,j), β(k,j), γ(k,j), ε(k,j).
Output: E(k), NPV
begin
   Compute Ce for each link
   Compute D
   Compute h^max
   Set initial point for a = a_ini
   BestSolution.NPV = -Infinite
   BestSolution.E(k) = Φ
   BestSolution.a = 0
   dir = -1
   while true do
     Solve OVALO ILP model with a links
     if feasible solution found then
       Compute NPV
       if NPV <= BestSolution.NPV then
         break
       BestSolution.E(k) = {e∈E, ζe=1}
       BestSolution.NPV = NPV
       BestSolution.a = a
     else
       if BestSolution.a>0 then
         break
       dir = +1
     a = a + dir
end
```

6.2.3 Illustrative numerical results

The OVALO iterative method and model were implemented in iLog-OPL and solved by the CPLEX v.12.0 solver on 2.4 GHz Quad-Core machines with 8 GB RAM. For evaluation, we used the DT series and the NSFNET series (see Appendix A).

Aiming at obtaining realistic CAPEX and revenues values, we have adapted equipment costs from [Ve06], the price of connectivity services from [Xi09], and the price ratio C_{SP}:C_{BE} equal to 5:1 as concluded previously. Finally, we consider an amortizable period Y=10 years and a discount rate r=5%.

Before comparing results in terms of NPV, let us firstly to analyze the CAPEX and revenues values obtained after solving OVALO. To this end, Fig. 6-5 plots CAPEX as a function of I_{SP}^{min}. It is worth noticing that the higher the required intensity the larger the amount of network equipment is needed to satisfy the required SP

traffic, which is clearly appreciated for both network topologies. Although the CAPEX values are very close for low I_{SP} intensities, for medium and high loads, networks for the sh-WS scheme are slightly cheaper (9% in the best case) that those for the diff-WS one. An interesting remark regarding the results for the NSFNET series is that the higher intensity with a feasible network solution is I_{SP}^{min}=1.5 in contrast to 4.5 for the DT series. This is a result of the highest nodal degree for any feasible network topology: for the NSFNET series is 3.3 whereas for the DT series is 4.28.

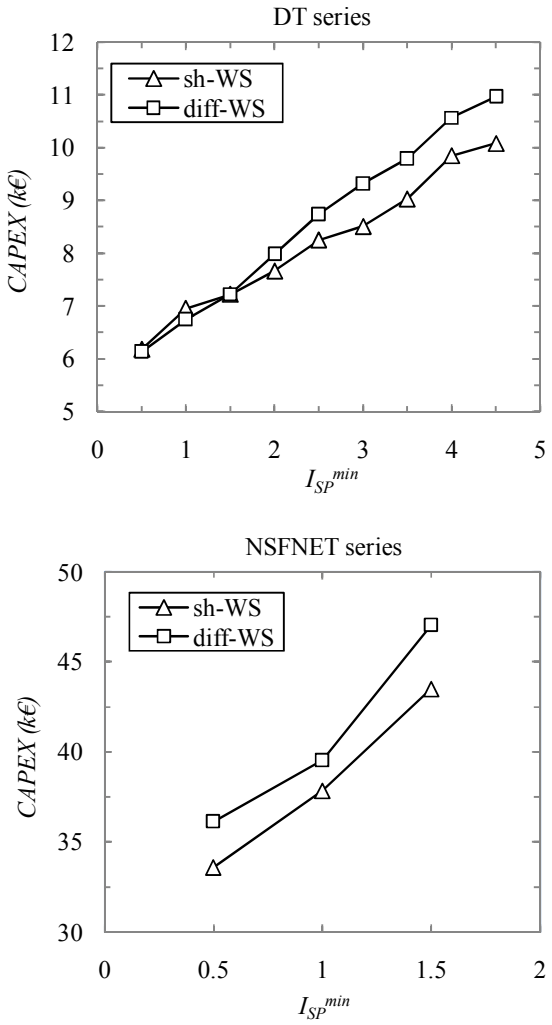

Fig. 6-5 CAPEX against SP intensity

We performed a similar study to compare revenues. Fig. 6-6 plots the values obtained for different I_{SP}^{min} values. In this case, diff-WS provides higher revenues than sh-WS for both series of topologies (up to 43% additional revenues). Note that revenues are computed from I_{SP}^{min} and I_{BE}^{max}, therefore, since I_{SP}^{min} is the same for both partitioning schemes, the difference lies in the amount of extra-traffic that can be supported in both partitioning schemes. In this regard, Fig. 6-6 also shows

the I_{BE}^{max} traffic that can be carried over the obtained network. As can be observed, diff-WS allows carrying several times more I_{BE}^{max} than sh-WS (up to 24 times for DT series and 38 for NSFNET series).

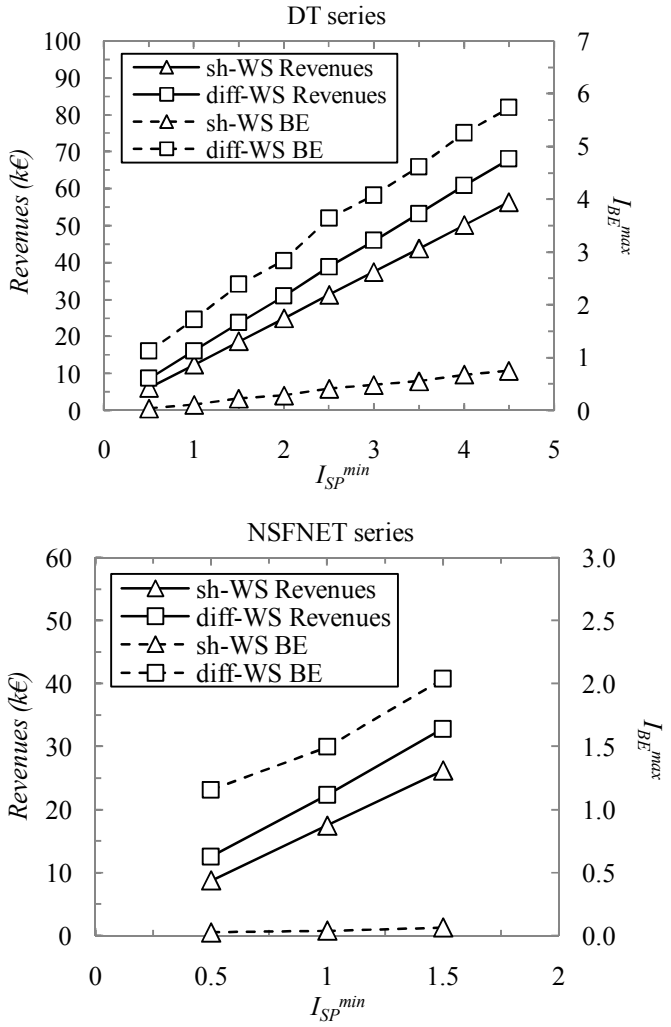

Fig. 6-6 Revenues against SP intensity

As a conclusion of Fig. 6-5 and Fig. 6-6, the diff-WS scheme provides higher revenues that sh-WS but at the cost of more expensive networks. Therefore, it is useful to use NPV to compare between them. Fig. 6-7 plots the NPV values obtained for both partitioning schemes. As shown, diff-WS provides higher NPV values than sh-WS. In fact, the on average increment is closer to 30% for DT series and 60% for NSFNET series. Moreover, it is worth noting the strong linear correlation between NPV and I_{SP}^{min}, in line with the trends observed in Fig. 6-5 and Fig. 6-6 for CAPEX and revenues, respectively.

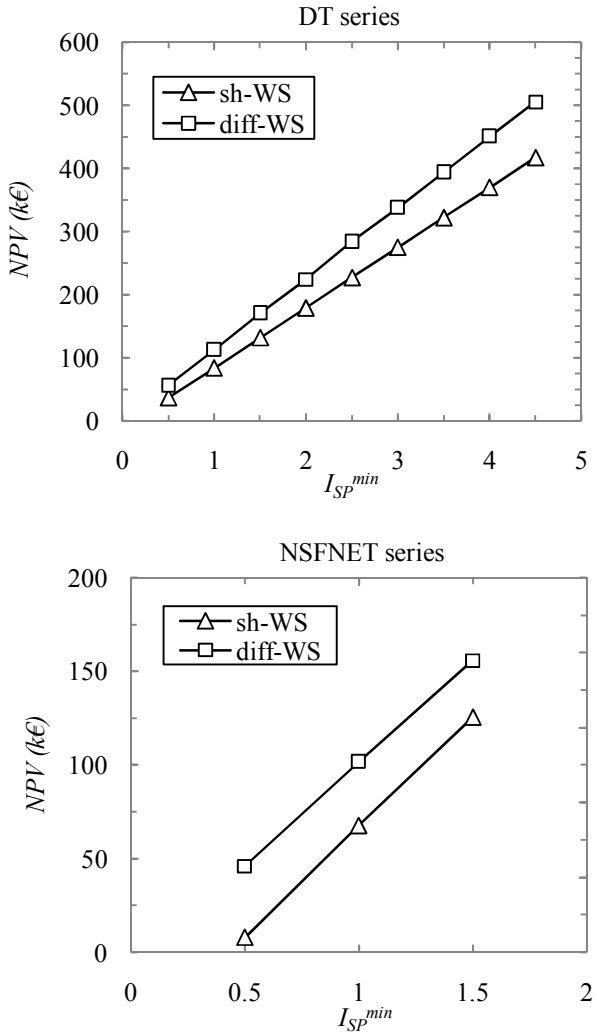

Fig. 6-7 NPV against SP intensity

Recall that OVALO looks for networks ensuring a given SP intensity I_{SP}^{min}. However, the resultant networks will be able to supporting higher intensity (I_{SP}^{max}) if required, without increasing CAPEX. Then, a sensitivity analysis in terms of NPV can be done, where the revenues increase as result of providing I_{SP}^{max}.

Table 6-3 shows, for each I_{SP}^{min} reference value, both the I_{SP}^{max} values and the NPV increment (*incNPV*) that would be obtained provided I_{SP}^{max} was served. The NPV gain using diff-WS instead of sh-WS (ΔNPV) is also detailed for I_{SP}^{min} and I_{SP}^{max}. Note that NPV could increase up to 38% if SP traffic increases to I_{SP}^{max}. Although this increase would be slightly higher when sh-WS is applied than when diff-WS is applied, the latter partitioning scheme would still remain providing the highest NPV values (23% of NPV gain).

Table 6-3: NPV sensitivity analysis

	sh-WS		diff-WS		ΔNPV (I_{SP}^{min})	ΔNPV (I_{SP}^{max})
I_{SP}^{min}	I_{SP}^{max}	$incNPV$	I_{SP}^{max}	$incNPV$		
0.5	0.73	37.46%	0.80	33.20%	53.02%	43.26%
1.0	1.25	21.77%	1.27	18.19%	35.19%	29.27%
1.5	1.86	25.53%	1.80	13.96%	29.46%	19.87%
2.0	2.21	9.96%	2.17	6.45%	25.28%	20.58%
2.5	2.80	11.11%	2.85	10.28%	25.14%	23.97%
3.0	3.19	6.08%	3.24	6.16%	22.95%	23.06%
3.5	3.73	6.20%	3.72	4.95%	22.23%	20.62%
4.0	4.65	14.19%	4.31	6.03%	21.88%	11.29%
4.5	5.09	11.65%	4.76	4.59%	21.06%	12.11%
				Average	28.34%	23.02%

6.3 Summary

In this chapter two network planning problems for maximizing network operator utility functions were introduced.

First, the NORMA++ problem was presented as an extension of the NORMA problem presented in Chapter 5. The objective of such a problem is the design of the optical network that maximizes network operator revenues from serving as much differentiated traffic as possible, while meeting certain GoS requirements.

The considered wavelength partitioning schemes were compared solving the NORMA++ problem for three backbone optical network series. The sh-WS scheme was proved to support slightly more SP traffic intensity than diff-WS when applied to moderately and highly meshed networks, whereas diff-WS allows much more BE traffic than sh-WS. This fact leads diff-WS to provide the highest revenues even in highly meshed network topologies.

In light of the extensive evaluation, we are able to conclude that diff-WS maximizes the revenues from operating a large range of different backbone networks. Specifically, the obtained revenues increase as the mean nodal degree in the network gets lower.

Second and aiming at maximizing not only revenues but also the value of the designed network, the economic impact of deploying and operating optical networks was studied from the investment project perspective. In order to consider revenues and costs in the same model, the OVALO problem was defined as the problem of

designing an optical network maximizing the expected NPV. Given a required SP intensity, OVALO finds the topology and the partitioning scheme that maximizes the NPV. Being NPV a non-linear function, linear programming techniques cannot be applied to obtain optimal solutions. Aiming at obtaining exact solutions, an iterative method based on an ILP was proposed, where a linear approximation of NPV was used as the objective function. After solving the problem for different number of network links, the solution with the highest NPV is returned as the optimal one.

The OVALO problem was solved for two well-known topologies enlarged with additional optical connectivity. From the results, we observed that NPV is maximized when diff-WS is applied. Although networks were slightly cheaper in terms of CAPEX under the sh-WS scheme, higher revenues coming from serving more BE traffic were expected for diff-WS. Moreover, the required I_{SP}^{min} could be increased to a maximum value I_{SP}^{max} without increasing network costs. In that case, NPV could be increased up to 38% under the deployed infrastructure.

From the OVALO performance analysis, we are able to conclude that diff-WS maximizes NPV from operating different backbone networks within the range of real topologies.

Chapter 7

Survivable IP/MPLS-over-DWDM network optimization

Previous chapters presented optimization problems to maximize some utility function from operating an optical network. Those problems considered a single layer architecture, where each demand is served using one lightpath. As introduced in Chapter 2, this architecture leads to a non-optimal use of the network capacity since the bandwidth requested by clients is usually much lower than the lightpath's capacity.

In this chapter, we face the problem of designing a multilayer optical network. More specifically, we study the survivable IP/MPLS-over-WSON multilayer network problem as a CAPEX minimization problem. Although some works propose similar approaches than the one proposed in this chapter as detailed in Chapter 3, to the best of our knowledge none of them studies the problem of hierarchical grooming together with survivability against IP/MPLS node, OE port, and optical link failures in IP/MPLS-over-WSON multilayer networks.

Two network approaches providing survivability against failures are compared: the classical *overlay* approach where two redundant IP/MPLS networks are deployed, and the new *joint* multilayer approach which provides the requested survivability through an orchestrated interlayer recovery scheme which minimizes the over-dimensioning of IP/MPLS nodes. Mathematical programming models are developed for both approaches.

Solving these models, however, becomes impractical for realistic networks. In view of this, evolutionary heuristics based on the BRKGA framework are also proposed. Exhaustive experiments on several reference network scenarios illustrate the effectiveness of the proposed approach in minimizing network CAPEX.

7.1 Survivable multilayer network design

Three types of nodes can be distinguished at the IP/MPLS packet layer: *metro* nodes performing client flow aggregation, *transit* nodes providing routing flexibility, and *interconnection* nodes supporting inter-operator connections. To minimize the number of ports, metro-to-metro connections are avoided being every metro node connected to one or more OXCs. Moreover, while it is typical that a transit node is collocated with an OXC, metro nodes are usually closer to clients, and thus, it is likely that some ad-hoc connectivity needs to be used to connect metro to OXCs. The IP/MPLS network must provide transport service to all demands, even in the event of any single failure. Specifically, we consider optical link cuts and IP/MPLS node and OE port failures. Fig. 7-1 illustrates the basic hierarchical IP/MPLS-over-WSON architecture considered in this chapter.

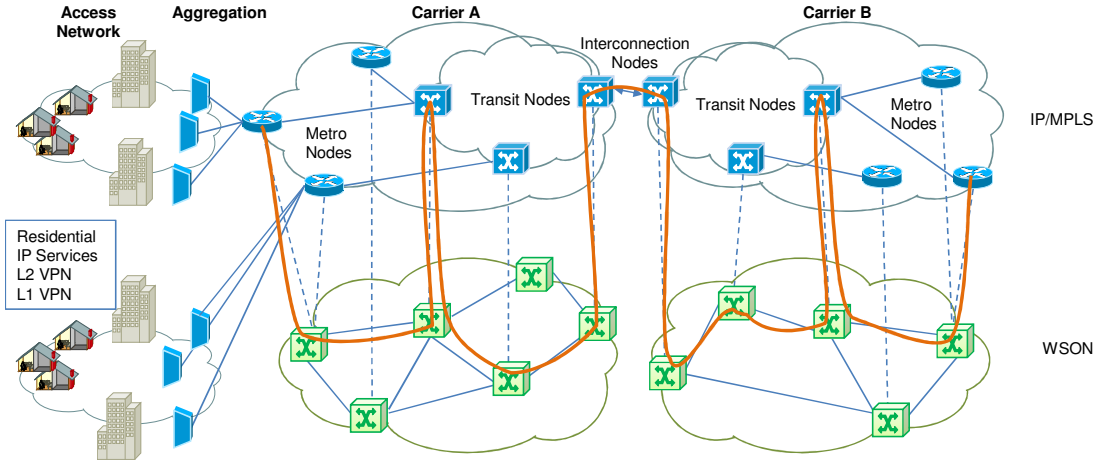

Fig. 7-1 Hierarchical IP/MPLS-over-WSON network

From the IP/MPLS network perspective, network planning could be faced keeping the layer independency following an overlay approach. In this case, recovery mechanisms are kept within each layer and hence no interlayer recovery mechanisms are required. For this reason, IP/MPLS node and virtual link redundancy must be foreseen at the IP/MPLS layer to prevent outages. As an example, Fig. 7-2a illustrates a design for an IP/MPLS network with redundancy against failures, where transit nodes are duplicated creating two parallel topologies. Note that in Fig. 7-2a transit node T1' is the redundant node of T1. If an optical link fails (O1-O4 in Fig. 7-2b), the affected MPLS LSP between metro nodes M2 and M3 is restored using connectivity capacity in the redundant topology. Obviously this scheme, although providing optimal network dimensioning for both layer networks separately, is far from achieving an optimal overall cost reduction.

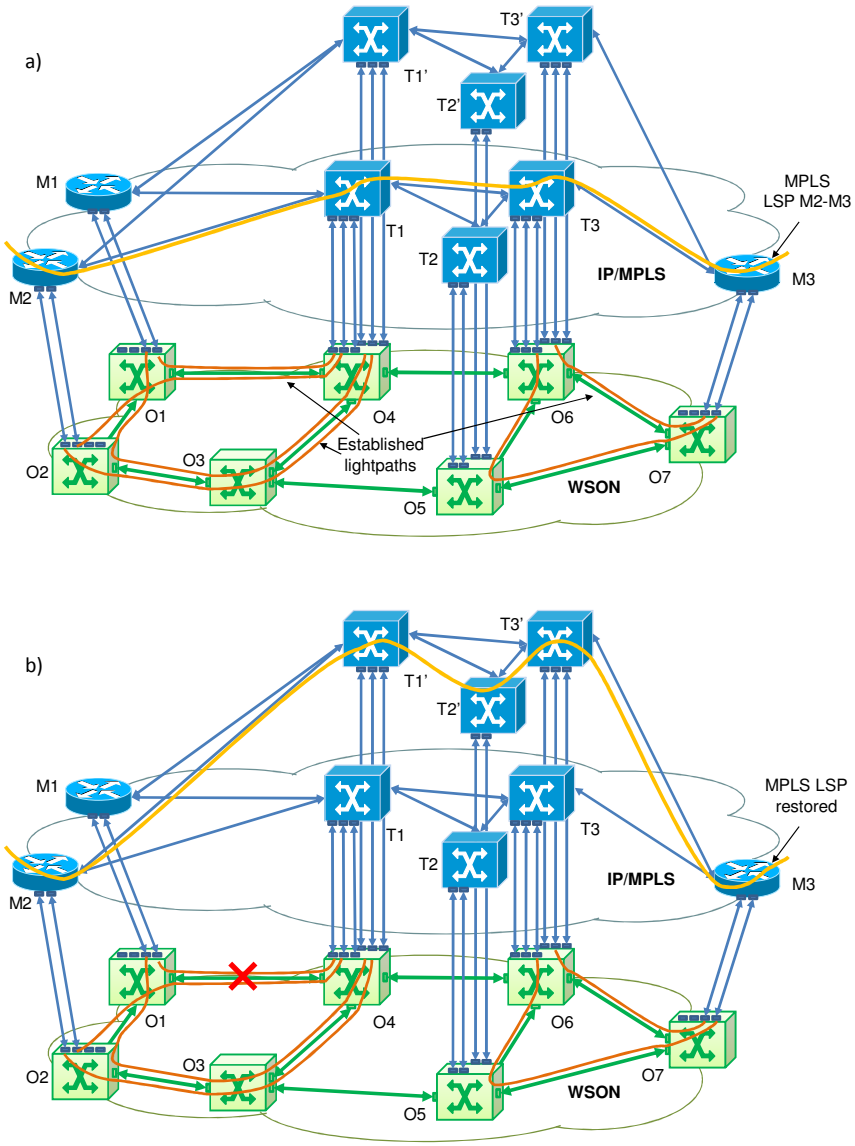

Fig. 7-2 The overlay network approach

On the contrary, specifically-designed restoration mechanisms which are able to trigger coordinated actions across the two layers can be applied to avoid IP/ MPLS node duplication. For example, those defined in [Ch03] for symmetrical multilayer networks. Fig. 7-3 depicts an example of our joint approach designed for non-symmetrical environments that illustrates how node and link redundancy can be avoided. Fig. 7-3a shows a multilayer network where each IP/MPLS metro node is connected to a transit node through virtual links creating a virtual topology. Each virtual link is supported by a lightpath routed through the minimum path cost over

the WSON network. In the example, metro nodes M1 and M2 are connected to transit node T1 and metro node M3 to transit node T3 through only one lightpath.

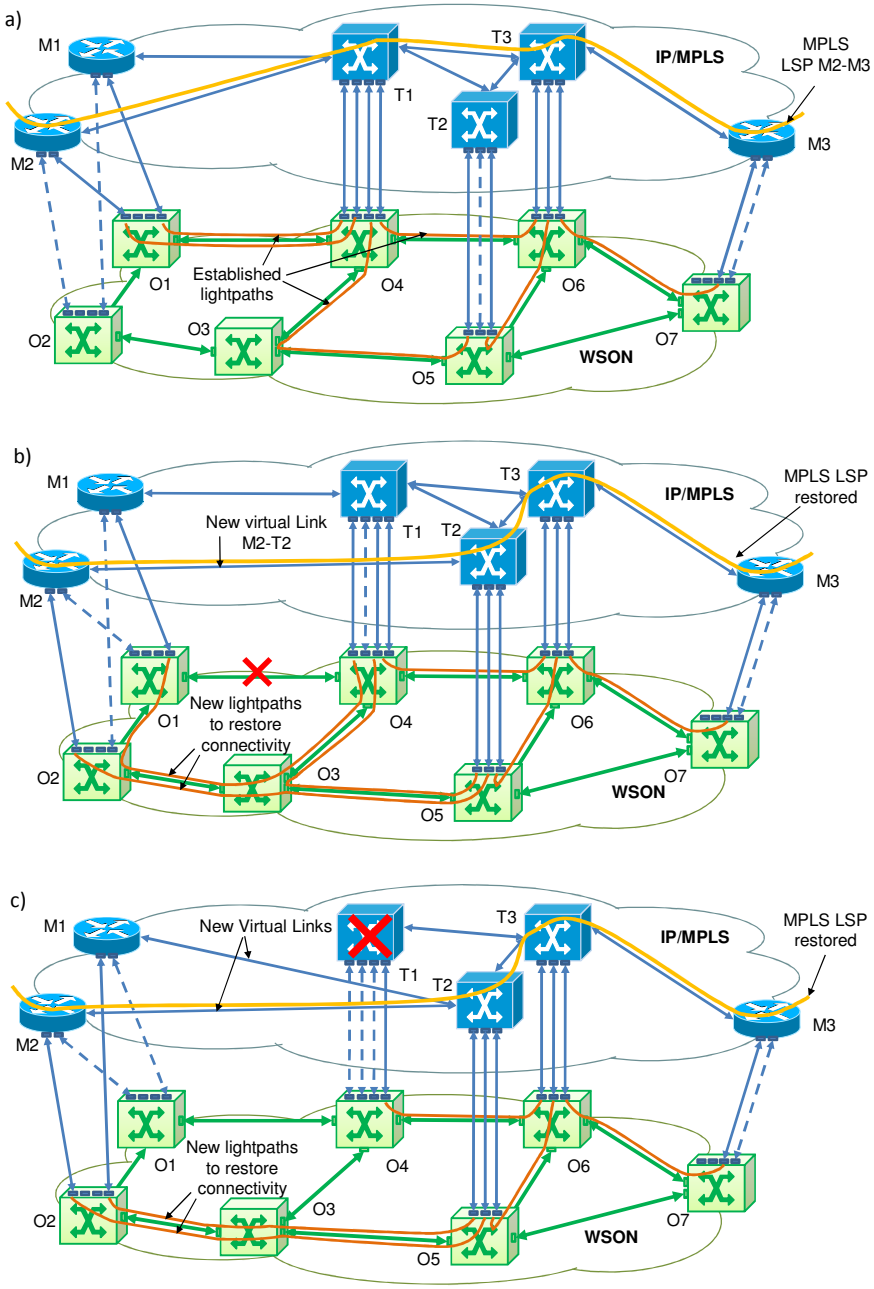

Fig. 7-3 The joint network approach

Note that in order to guarantee failure recovery, extra-capacity has been added in every node (dotted lines in Fig. 7-3).

When an optical link fails, the multilayer network applies joint recovery schemes to restore the affected traffic. For instance, when optical link O1-O4 fails (Fig. 7-3b),

recovery actions are taken to restore metro-to-transit connectivity. If a lightpath can be restored within the optical layer, the connectivity at the IP/MPLS remains unaltered (virtual link M1-T1 is restored through lightpath O1-O2-O3-O4). On the contrary, a new lightpath needs to be established to connect the IP/MPLS metro node to a different transit node, thus restoring the metro-to-transit connectivity (virtual link M2-T2 through new lightpath O2-O3-O5). Once the connectivity is restored, MPLS LSPs can be eventually rerouted over the reconfigured virtual topology.

In the event of an OE port failure, spare OE ports are added. Then, the affected lightpath can be torn down and set-up again on a different OE port. Finally, when an IP/MPLS node fails (Fig. 7-3c), new lightpaths are established between every metro node connected to the failed node to a different transit node, so as to restore the metro-to-transit connectivity, thus creating new virtual links. In the example, virtual links M1-T2 and M2-T2 are created. Once the connectivity is restored, the affected MPLS LSPs are rerouted.

Additionally, the introduction of WSON allows to perform optical by-passing, i.e. highly loaded metro-to-metro and metro-to-interconnection connectivity is performed directly at the optical layer without intermediate IP/MPLS routing. The gains are multi-fold: the number of OE interfaces as well as the switching capacity of the IP/MPLS nodes is kept to the absolute minimum and, hence, power consumption is kept on low/moderate levels. Although optical by-passing in general can reduce network costs, its use has been restricted to just highly loaded virtual links to avoid MAC address table explosion [Ch04].

The next section is first devoted to formally stating the SIMULTANEO problem, and second to present ILP-based models for both the joint and the overlay approaches.

7.2 The SIMULTANEO problem

7.2.1 Problem Statement

The problem can be formally stated as follows:

Given:

- An optical network, represented by a graph $G_O(N, Lo)$, being N the set of OXCs and Lo the set of fiber links connecting two OXCs,
- A set WL of available wavelengths in each link in Lo,
- The virtual network represented by a graph $G_V(V, E)$, being V the set of IP/MPLS nodes and E the set of virtual links defining the connectivity among IP/MPLS nodes,

- A set L_R containing the fiber links connecting an IP/MPLS node to an OXC,
- A set D of IP/MPLS demands to be transported,
- Equipment cost, specified by a fixed cost for every type of IP/MPLS node and OE port,
- Cost per km of using the already deployed fiber, depending on the lightpath recovery type (e.g. unprotected, restorable, etc.).

Output:

- The configuration of every IP/MPLS node in terms of switching capacity and number and bit-rate of OE ports,
- The set of OE ports in every OXC,
- The set of used virtual links, including its route over the WSON,
- The route of every demand over the virtual topology.

Objective: Minimize the expected CAPEX for the network designed for the given set of demands.

As previously discussed, the problem can be faced using two different network planning approaches. For each approach, an ILP-based model is provided next.

7.2.2 ILP model for the joint approach

The model for the joint approach optimizes both the IP/MPLS and WSON layers simultaneously by adding extra-capacity to overcome any single failure. It combines node-link and arc-path formulations respectively for IP/MPLS grooming, routing, and network planning, and WSON routing given a set of pre-computed optical routes. IP/MPLS demands are routed through a virtual topology, where each virtual link is divided in several channels. Each channel aggregates a number of IP/MPLS demands and is transported over a single lightpath in the WSON. For each channel carrying demands, four OE ports of the same bit-rate must be equipped (two at the end IP/MPLS nodes and two in the associated OXCs).

As aforementioned, in this work we consider IP/MPLS node, OE port, and fiber link failures. IP/MPLS nodes and fiber link are part of the invariants of the problem i.e. they are known beforehand, and so the set of failures that may affect them. In contrast, the number and location of OE ports are part of the outputs of the problem, and thus failures affecting them are unknown before the optimization. Owing to this fact, port failures may require the use of non-linear constraints given the quadratic form of the resulting constraints. To avoid such non-linearity, we have attached a pre-defined set of slots to each IP/MPLS node where each slot could contain one OE port. In this way, failures are related to slots instead to OE ports, and hence known in advance. Note that a failure in a non-equipped slot has null effect over the optimal solution.

For each failure, one single-failure scenario is defined by characterizing the set of resources (IP/MPLS nodes, slots, virtual links, and WSON links) that can be used to re-route the affected traffic when the failure occurs. Channel-to-slots and channel-to-lightpath assignments are determined for each failure scenario. Although these assignments strongly increase the size of the problem, they provide flexibility to overcome any failure. It is worth mentioning that network dimensioning ensures that every demand is successfully transported under any single failure scenario.

The following sets and parameters have been defined:

Optical Topology:

N	Set of OXCs.
L	Set of fiber links, index l. $L=L_O \cup L_R$
L_O	Subset of L connecting two OXCs.
L_R	Subset of L connecting an IP/MPLS node to an OXC.
W_l	Number of wavelengths of fiber link $l \in L_O$
len_l	Length of fiber link $l \in L$ in kilometers.
K	Set of WSON routes, index k.
$path_l^k$	Equal to 1 if route k contains fiber link l, 0 otherwise.

Virtual Topology:

V	Set of IP/MPLS nodes, index v.
V_M	Subset of V containing the metro nodes.
V_T	Subset of V containing the transit nodes.
V_I	Subset of V containing the interconnection nodes.
V_V	Subset of V containing the virtual nodes.
$S(v)$	Set of slots in node v, index s.
E	Set of virtual links, index e.
E_1	Subset of E containing metro-to-transit and transit-to-transit virtual links.
E_2	Subset of E containing metro-to-metro virtual links.
E_3	Subset of E containing transit-to-interconnection and interconnection-to-virtual virtual links.
E_4	Subset of E containing metro-to-interconnection virtual links.
E_5	Subset of E_3 containing interconnection-to-virtual virtual

links.

$E_x(v)$ Subset of virtual links belonging to subset E_x incidents to node v, for x = 1…5.

$I(e)$ Set of end nodes of virtual link e, index v.

$C(e)$ Set of channels of virtual link e, index c.

$K(e)$ Subset of K containing the WSON routes connecting both ends of virtual link e.

Demands:

D Set of IP/MPLS demands, index d.

D_1 Subset of D with low and moderate data-rate demands.

D_2 Subset of D with high data-rate demands, susceptible of optical by-passing.

$SD(d)$ Set of source and destination nodes of demand d.

b_d Bandwidth of demand d in Gbps.

h_d Equal to 1 if demand d belongs to subset D_2, 0 otherwise.

out_d Equal to 1 if an end node of demand d belongs to V_V, 0 otherwise.

Failures:

F Set of failure scenarios, index f. Scenario 0 represents the scenario without failure.

$wfail^{fk}$ Equal to 1 if WSON route k is available under failure scenario f, 0 otherwise.

$mfail^{fvs}$ Equal to 1 if slot s of node v is available under failure scenario f.

Equipments, costs and others:

PT Set of port bit-rates, index i.

pk_i Capacity of a port of bit-rate I in Gbps.

opc_i Cost of one port of bit-rate I in an OXC.

mpc_i Cost of one port of bit-rate I in an IP/MPLS node.

RT Set of node classes, index j. Each class defined by a switching capacity and a number of slots.

rk_j Switching capacity of a node class j in Gbps.

rpk_j Number of slots available in a node class j.

rc_j Cost of one node of class j.

c_{rest} Cost per kilometer of restorable lightpath.

M A large positive constant.

The decision variables are:

ω^f_{dec} Binary. Equal to 1 when demand d is routed through channel c of virtual link e, under failure scenario f. 0 otherwise.

Γ^f_d Binary. Equal to 1 if the route of demand d under failure scenario f must be the same than that in the non-failure scenario. 0 otherwise.

Φ^{fk}_{ec} Binary. Equal to 1 if channel c of virtual link e is assigned to WSON route k, under failure scenario f. 0 otherwise.

Ψ^{fvs}_{ec} Binary. Equal to 1 if channel c of virtual link e is assigned to slot s of node v, under failure scenario f. 0 otherwise.

P_i^{vs} Binary. Equal to 1 if slot s of node v is equipped with a port of bit-rate i. 0 otherwise.

Π_j^v Binary. Equal to 1 if node v is equipped with a node of class j. 0 otherwise.

T^{fvs} Positive integer with the total amount of traffic (in Gbps) in slot s of node v under failure scenario f.

Then, network CAPEX can be computed as the sum of the following expressions:

$$COST^{Joint}_{Equipment} = \sum_{v \in V \setminus V_V} \left(\sum_{s \in S(v)} \sum_{i \in PT} (mpc_i + opc_i) \cdot \rho_i^{vs} + \sum_{j \in RT} rc_j \cdot \pi_j^v \right) \quad (7.1)$$

$$COST^{Joint}_{Lightpaths} = C_{rest} \cdot \sum_{e \in E} \sum_{c \in C(e)} \sum_{k \in K(e)} \varphi_{ec}^{0k} \cdot \sum_{l \in L} len_l \cdot p_l^k \quad (7.2)$$

where equation (7.1) computes the cost of IP/MPLS nodes and OE ports and equation (7.2) the cost of the lightpaths.

Finally, the ILP for the joint approach is as follows:

SIMULTANEO – Joint

$$Minimize \quad CAPEX^{Joint} = COST^{Joint}_{Equipment} + COST^{Joint}_{Lightpaths} \quad (7.3)$$

subject to:

$$\sum_{e \in E_1(v)} \sum_{c \in C(e)} \omega^f_{dec} + h_d \cdot \sum_{e \in E_2(v)} \sum_{c \in C(e)} \omega^f_{dec} = 1 \quad \forall d \in D, f \in F, v \in SD(d) \cap \overline{V_V} \quad (7.4)$$

$$\sum_{e\in E_1(v)\cup E_3(v)}\sum_{c\in C(e)}\omega_{dec}^{f}+h_d\cdot\sum_{e\in E_4(v)}\sum_{c\in C(e)}\omega_{dec}^{f}=1\quad\forall d\in D,f\in F,v\in SD(d)\cap V_V \tag{7.5}$$

$$\sum_{e\in E_1(v)}\sum_{c\in C(e)}\omega_{dec}^{f}+out_d\cdot\sum_{e\in E_3(v)}\sum_{c\in C(e)}\omega_{dec}^{f}\le 2 \quad \forall d\in D,f\in F,v\in\overline{SD(d)}\cap\left(V_T\cup V_I\right) \tag{7.6}$$

$$\sum_{e\in E_1(v)}\sum_{c\in C(e)}\omega_{dec}^{f}+out_d\cdot\sum_{e\in E_3(v)}\sum_{c\in C(e)}\omega_{dec}^{f}\le 0 \quad \forall d\in D,f\in F,v\in\overline{SD(d)}\cap\left(V_M\cup V_V\right) \tag{7.7}$$

$$\sum_{\substack{e'\in E_1(v)\\ e\neq e'}}\sum_{c'\in C(e')}\omega_{de'c'}^{f}+out_d\cdot\sum_{\substack{e''\in E_3(v)\\ e\neq e''}}\sum_{c''\in C(e'')}\omega_{de''c''}^{f}\ge\sum_{c\in C(e)}\omega_{dec}^{f} \quad \forall d\in D,v\in\overline{SD(d)}\cap\left(V_T\cup V_I\right),e\in E_1\cup E_3,f\in F \tag{7.8}$$

$$\sum_{d\in D}\omega_{dec}^{f}\le M\cdot\sum_{k\in K(e)}wfail^{fk}\cdot\varphi_{ec}^{fk}\quad\forall f\in F,e\in E,c\in C(e) \tag{7.9}$$

$$\sum_{k\in K(e)}\varphi_{ec}^{fk}\le 1\quad\forall f\in F,e\in E,c\in C(e) \tag{7.10}$$

$$\sum_{e\in E}\sum_{c\in C(e)}\sum_{k\in K(e)}path_l^{k}\cdot\varphi_{ec}^{fk}\le w_l\quad\forall f\in F,l\in L_O \tag{7.11}$$

$$\sum_{d\in D}\omega_{dec}^{f}\le M\cdot\sum_{s\in S(v)}mfail^{fvs}\cdot\psi_{ec}^{fvs}\quad\forall f\in F,e\in E,c\in C(e),v\in I(e) \tag{7.12}$$

$$\sum_{s\in S(v)}\psi_{ec}^{fvs}\le 1\quad\forall f\in F,e\in E,c\in C(e),v\in I(e) \tag{7.13}$$

$$\sum_{e\in E(v)}\sum_{c\in C(e)}\psi_{ec}^{fvs}\le 1\quad\forall f\in F,v\in V,s\in S \tag{7.14}$$

$$\sum_{d\in D}b_d\cdot\omega_{dec}^{f}-M\cdot\left(1-\psi_{ec}^{fvs}\right)\le\tau^{fvs} \quad \forall v\in V\setminus V_V,s\in S(v),e\in E(v),c\in C(e),f\in F \tag{7.15}$$

$$\tau^{fvs}\le\sum_{i\in PT}pk_i\cdot\rho_i^{vs}\quad\forall v\in V\setminus V_V,s\in S(v),f\in F \tag{7.16}$$

$$\sum_{i\in PT}\rho_i^{vs}\le 1\quad\forall v\in V\setminus V_V,s\in S(v) \tag{7.17}$$

$$\sum_{s\in S(v)}\tau^{fvs}\le\sum_{j\in RT}rk_j\cdot\pi_j^{v}\quad\forall v\in V\setminus V_V,f\in F \tag{7.18}$$

$$\sum_{s\in S(v)}\sum_{i\in PT}\rho_i^{vs}\le\sum_{j\in RT}rpk_j\cdot\pi_j^{v}\quad\forall v\in V\setminus V_V,f\in F \tag{7.19}$$

$$\sum_{j \in RT} \pi_j^v \leq 1 \quad \forall v \in V \setminus V_V \tag{7.20}$$

$$\sum_{v \in I(e)} \sum_{s \in S(v)} \left(1 - mfail^{fvs}\right) \cdot \psi_{ec}^{0vs} + M \cdot \left(1 - \omega_{dec}^{f}\right) \geq \gamma_d^f \quad \forall d \in D, f \in F - \{0\}, e \in E, c \in C(e) \tag{7.21}$$

$$\sum_{c \in C(e)} \omega_{dec}^{0} - \sum_{c \in C(e)} \omega_{dec}^{f} \leq \left(1 - \gamma_d^f\right) \quad \forall d \in D, f \in F, e \in E \tag{7.22}$$

$$\sum_{c \in C(e)} \omega_{dec}^{0} - \sum_{c \in C(e)} \omega_{dec}^{f} \geq \left(\gamma_d^f - 1\right) \quad \forall d \in D, f \in F, e \in E \tag{7.23}$$

$$\gamma_d^f, \omega_{dec}^f, \varphi_{ec}^{fk}, \psi_{ec}^{fvs}, \rho_i^{vs}, \pi_j^v \in \{0,1\}, \tau^{fvs} \in \mathrm{Z}^+ \tag{7.24}$$

The objective function (7.3) minimizes the network CAPEX. Constraints (7.4)–(7.8) deal with routing and aggregating demands over the virtual topology. Constraint (7.4) and (7.5) ensure that demands not belonging and belonging to V_V, respectively are routed under any failure scenario. In these constraints, demands in D_2 can use optical by-passes, directly connecting metro-to-metro or metro-to-interconnection nodes. Constraint (7.6) avoids cycles and ensures that transit and interconnection nodes are used as intermediate nodes in the route of the demands. Contrarily, constraint (7.7) prevent from using metro and virtual nodes for routing demands. Finally, constraint (7.8) guarantees that a route over the virtual topology is computed for each demand.

Constraints (7.9)-(7.14) connect virtual and optical topologies together. More specifically, constraint (7.9) ensures that each channel transporting traffic in a virtual link is assigned to a WSON route. Under a specific failure scenario, every used channel must be associated to a failure-free optical route. The number of routes assigned to a channel is limited to 1, as defined in constraint (7.10). Additionally, constraint (7.11) makes sure that the WSON capacity is not exceeded. Constraint (7.12) guarantees that both ends of each used channel are assigned to some ports in the adjacent nodes. Constraint (7.13) makes sure that, at most, 1 slot is assigned to each end of a channel. Complementary, constraint (7.14) ensures that a slot is assigned to, at most, one channel.

Constraints (7.15)-(7.20) dimension the IP/MPLS network taking as inputs all possible assignments produced by constraints (7.9)-(7.14). The maximum amount of traffic routed through a slot is computed in constraint (7.15). Whilst constraint (7.16) provides the slot with enough bit-rate, constraint (7.17) ensures that only one port is equipped per slot. The needed switching capacity of each node is computed in constraint (7.18), whereas the needed capacity in number of ports is obtained by constraint (7.19). Then, the node class to be equipped in a node must ensure both switching capacity and number of ports constraints. Additionally, constraint (7.20) guarantees that only one router is installed in a node.

When a failure occurs, the non-affected IP/MPLS demands must remain in their current virtual route. In contrast, WSON route and/or OE port assignment changes are allowed. Constraint (7.21) fixes which demands must remain in their route under every failure scenario, and constraints (7.22) and (7.23) prevent that these IP/MPLS routes change.

Finally, eq. (7.24) defines the variables as binary or positive integer.

7.2.3 ILP-based algorithm for the overlay approach

The overlay approach is solved by means of two complementary ILPs: one for the IP/MPLS network and another for the WSON. First, the IP/MPLS network is planned by adding redundancy to OE ports and to transit and interconnection IP/MPLS nodes. One outcome of this optimization is the set of lightpaths to be established in the WSON. Second, for each optical demand, the second ILP finds a pair of link-disjoint routes over the WSON. In the case of a metro-to-transit optical demand, each route connects a metro node to one of the duplicated transit nodes. In the case of transit-to-transit and transit-to-interconnection, each route connects two nodes of the same duplicated transit sub-network, as depicted in Fig. 7-2.

In addition to the notation defined above, the following sets and parameters are defined:

P	Set of optical demands, index p.
$K(p)$	Set of WSON routes to support optical demand p.
$dist_e$	Distance in km of the shortest WSON route supporting virtual link e.
c_{unp}	Cost per kilometer of unprotected lightpath.

Moreover, the set of variables has been extended with:

δ_{eci}	Binary. Equal to 1 if a port of bit-rate I is installed in the end nodes of channel c of virtual link e.
$\kappa^{kq}{}_p$	Binary. Equal to 1 if lightpath q of optical demand p belongs to WSON route k, 0 otherwise. Two lightpaths per demand are needed (indexes 0 and 1).

Furthermore, eq. (7.1) and (7.2) are redefined to consider equipment duplication and unprotected lightpaths setup:

$$\begin{aligned} COST^{Overlay}_{Equipment} = \; & 4 \cdot \sum_{e \in E \setminus E_S} \sum_{c \in C(e)} \sum_{i \in PT} \left(mpc_i + opc_i \right) \cdot \delta_{eci} + \sum_{v \in V_M} \sum_{j \in RT} rc_j \cdot \pi_j^v \\ & + 2 \cdot \sum_{v \in V_T \cup V_I} \sum_{j \in RT} rc_j \cdot \pi_j^v \end{aligned} \tag{7.25}$$

$$COST^{Overlay}_{\text{Lightpaths}} = C_{unp} \cdot \sum_{p \in P} \sum_{k \in K} \left(\kappa_p^{k0} + \kappa_p^{k1} \right) \cdot \sum_{l \in L} len_l \cdot path_l^k \tag{7.26}$$

Then, we propose the following ILP formulation for the IP/MPLS network planning sub-problem:

Overlay IP/MPLS

$$Minimize \quad COST^{Overlay}_{Equipment} + C_{unp} \cdot \sum_{e \in E \setminus \mathrm{E}_5} \sum_{c \in C(e)} \sum_{i \in PT} dist_e \cdot \delta_{eci} \tag{7.27}$$

subject to:

Constraints (7.4) to (7.8), where F=Ø, and constraint (7.20).

$$\sum_{d \in D} B_d \cdot \omega_{dec} \le \sum_{i \in PT} pk_i \cdot \delta_{eci} \quad \forall e \in E \setminus E_5, c \in C(e) \tag{7.28}$$

$$\sum_{i \in PT} \delta_{eci} \le 1 \quad \forall e \in E \setminus E_5, c \in C(e) \tag{7.29}$$

$$\sum_{e \in E(v) \setminus \mathrm{E}_5} \sum_{d \in D} B_d \cdot \omega_{de} \le \sum_{j \in RT} rk_j \cdot \pi_j^v \quad \forall v \in V \setminus V_V \tag{7.30}$$

$$2 \cdot \sum_{e \in E(v) \setminus \mathrm{E}_5} \sum_{c \in C(e)} \delta_{eci} \le \sum_{j \in RT} rpk_j \cdot \pi_j^v \quad \forall v \in V_M \tag{7.31}$$

$$\sum_{e \in E(v) \setminus \mathrm{E}_5} \sum_{c \in C(e)} \delta_{eci} \le \sum_{j \in RT} rpk_j \cdot \pi_j^v \quad \forall v \in V_T \cup V_I \tag{7.32}$$

$$\delta_{eci} \in \{0,1\} \tag{7.33}$$

The cost function in (7.27) minimizes the cost of the IP/MPLS nodes and OE ports plus an approximation of the cost of the underlying lightpaths based on the shortest WSON routes for each used virtual link. As a consequence of OE ports and nodes duplication, no failure scenarios are considered in the overlay model. Then, constraints (7.4)-(7.8) are applied to the non-failure scenario for routing and aggregating demands. Note that the variable ω used for routing here becomes ω_{dec} instead of ω^f_{dec}. Constraint (7.28) deals with the dimensioning of OE ports. In contrast to the model proposed for the joint approach, here OE port dimensioning is performed in the virtual links without assigning channels to slots, thereby considerably reducing the problem size. Moreover, constraint (7.29) ensures that each used channel is equipped with only one couple of ports. Constraints (7.30)-(7.32) together with constraint (7.20) are responsible for dimensioning the nodes. Constraint (7.30) gets the minimum switching capacity for metro, transit and interconnection nodes. The minimum number of ports is computed in constraints (7.31) and (7.32) for metro and for transit and interconnection nodes, respectively. Note that ports are duplicated in metro nodes. Finally, eq. (7.33) defines the new variable as binary.

The optical demands routing sub-problem can be formulated as follows:

Overlay WSON

$$Minimize \quad COST_{Lightpaths}^{Overlay} \tag{7.34}$$

subject to:

$$\sum_{k \in K(p)} \kappa_p^{kq} = 1 \quad \forall p \in P, q \in \{0,1\} \tag{7.35}$$

$$path_l^k \cdot \left(\kappa_p^{k0} + \kappa_p^{k1}\right) \leq 1 \quad \forall p \in P, k \in K(p), l \in L_o \tag{7.36}$$

$$\sum_{p \in P} \sum_{k \in K(p)} path_l^k \cdot \left(\kappa_p^{k0} + \kappa_p^{k1}\right) \leq w_l \quad \forall l \in L_o \tag{7.37}$$

$$\kappa_p^{kq} \in \{0,1\} \tag{7.38}$$

The objective function (7.34) minimizes the total unprotected lightpath cost. Constraint (7.35) ensures that a couple of lightpaths is found for each optical demand, whereas constraint (7.36) makes sure that the lightpaths are link disjoint. Constraint (7.37) guarantees that the capacity of each link is not exceeded. Finally, constraint (7.38) defines the new variable as binary.

Table 7-1 shows the algorithm used to solve the SIMULTANEO problem with the overlay approach.

Table 7-1: Overlay Approach Algorithm

```
Procedure
begin
   Solve the Overlay IP/MPLS sub-problem
   P=Ø.
   For each e in E, c in C(e) and I in PT do
      if nodes in I(e) are not in V_v then
         if δ_eci = 1 then
            P=P∪{optical demand between nodes in I(e)}
   Solve the Overlay WSON sub-problem for the set P
   CAPEX^overlay = COST_Equipment^overlay + COST_Lightpaths^overlay
end
```

7.2.4 Complexity analysis

The SIMULTANEO problem can be considered NP-hard since simpler multilayer network planning problems without survivability have been proved to be *NP-hard* (e.g. [Zh10]). Regarding its size, Table 7-2 contains expressions to estimate the number of variables and constraints for the models presented above. Additionally, it provides numerical values for the networks presented in results subchapter.

Although the overlay algorithm can be solved for small instances, the ILP for the joint approach is impractical even in very small networks as a consequence of the large number of failure scenarios to be considered. Moreover, the large size of both

ILPs prevents the application of commercial solvers, such as CPLEX [CPLEX], to real backbone multilayer networks similar to those described in results subchapter. Aiming at providing near-optimal solutions with an acceptable computational effort, in the next section heuristic methods to solve the SIMULTANEO problem are presented.

Table 7-2: Size of the Models for both Approaches

Approach	Variables	Constraints
Joint	$\|F\| \cdot \|E\| \cdot \|C\| \cdot (\|D\| + \|K\|)$ (10^{10})	$\|F\| \cdot \|E\| \cdot \|D\| \cdot \|C\|$ (10^{9})
Overlay	$\|D\| \cdot \|E\| + \|K\| \cdot \|P\|$ (10^{4})	$\|D\| \cdot \|V\| \cdot \|E\| + \|P\| \cdot \|K\| \cdot \|L\|$ (10^{5})

7.3 Algorithms to solve SIMULTANEO

This section provides algorithms to solve SIMULTANEO for both joint and overlay architectures. Among different meta-heuristics, we chose the recently proposed BRKGA which, as introduced in Chapter 2, provides good quality solutions for network design problems. Since the BRKGA general framework has been previously presented, here we present the problem-dependent parts, i.e. the chromosome internal structure and the decoder.

Since the SIMULTANEO problem primarily consists in routing a set of demands over a virtual topology, we need one gene for each virtual link and for each IP/MPLS node. These genes are used to compute the metric of each virtual link and each IP/MPLS node which is later used for routing demands, i.e. shortest paths are computed with respect to these metrics. Besides, since the order in which the demands are routed influences the goodness of the solution, additional genes are needed to specify the order in which the demands are routed. In this regard, we use one additional gene for each demand which is used to sort the set of demands. Therefore, given a virtual network represented by the graph $G(V,E)$, each individual is represented by an array of $|V| + |E| + |D|$ genes.

To decode chromosomes into feasible solutions, we have designed the algorithm presented in Table 7-3 for the joint approach. As shown, metrics of IP/MPLS nodes and virtual links are initialized using the assigned gene of the input chromosome, whereas the order in which each demand will be routed is given by the remaining genes. After initializing the elements, the network is dimensioned through routing the set of demands. A solution for the non-failure scenario is obtained at this step. From this basic solution, the set of single-failure scenarios is built. For each failure scenario, we remove the element in failure from the network and compute the list of affected IP/MPLS paths, being each path subsequently rerouted. If additional

OE ports need to be installed in the IP/MPLS nodes, the feasibility of the solution is checked to ensure that the capacity of the node, in terms of number of ports, is not exceeded.

Table 7-3: Decoder Algorithm for the Joint Approach

```
Procedure
Input: network, chromosome
Output: fitness_value
begin
   v = network.numMPLSNodes
   for i=0, i<v do
      distances=network.MPLSNode[i].getDistanceIncidentVEdges()
      network.MPLSNode[i].metric = chromosome[i]* distances
   e = network.numVEdges
   for i=0, i<e do
     network.Vedge[i].metric =
        chromosome[v+i]*network.Vedge[i].distance
   d = network.numDemands
   for i=0, i<d do
     network.Demand[i].order = chromosome[v+e+i]
   sort(network.Demand)
   routeDemands (network)
   for i=0, i<v do
     computeNodeCapacity(network.MPLSNode[i])
   for each failure scenario f do
     pathList = doFailure(f, network)
     if (pathList is empty) then
        recoverFromFailure(f, network)
        continue Loop
     reroute(network, pathList)
     for i=0, i<v do
        incNodeCapacity(network.MPLSNode[i])
     recoverFromFailure(f, network)
     for each path p in pathList do
        route(p, network)
   fitness_value= ComputeCost(network)
end
```

It is worth mentioning that in the case of fiber link or OE port failure, lightpath restoration is tried as a first option during the list of affected paths computation phase. If a lightpath can be restored using the predefined set of restoration routes, the associated virtual link, and thus, every MPLS LSP using it, is automatically restored. On the contrary, MPLS LSPs are rerouted over the resulting virtual topology, hence, possibly increasing both IP/MPLS nodes switching capacity and OE ports.

Demand routing is mainly performed over a virtual topology which is pre-computed beforehand over the given network topology. Virtual links are created between pairs of IP/MPLS nodes (connecting metro-to-transit, transit-to-transit, and transit-to-interconnection nodes) satisfying that their distance is lower than a given threshold. For each virtual link, a set of routes over the optical network are computed: the shortest one and a number of restoration routes, one route for each

optical link in the shortest route. Then, a failure in an optical link affecting a virtual link can be recovered at the optical layer by restoring the underlying lightpath.

A set of feasible routes is then pre-computed for each demand. Here, we use a *k*-shortest path algorithm to pre-compute distinct routes. Two subsets of routes are pre-computed, one over the virtual topology and another over the optical topology, thus enabling optical by-passing. During the decoder process, route metric re-computation is performed ensuring that the shortest route, in terms of the metric, is chosen at each step.

We performed several tests to tune the parameters used in the algorithm. Table 7-4 shows the final values. It is worth pointing out that, as a consequence of the size of the problems, the length of the chromosome was higher than 400 genes. By choosing the size of the population equal to the length of the chromosome, the decoder algorithm took more than 50ms to decode the solution from any chromosome, and consequently, more than 15 seconds to build one generation.

Table 7-4: BRKGA parameter values

length of the chromosome (n)	$\|V\|+\|E\|+\|D\|$
size of population (p)	$\min\{50,n\}$
size of elite population	$0.2*p$
size of mutant population	$0.2*p$
elite inheritance probability	0.7

This greatly worsened the convergence properties of the algorithm. Hence, we reduced the size of the population so as to bring convergence within acceptable values.

The heuristic for the overlay approach uses a similar algorithm for the decoder, where the overlay network is obtained from the non-failure scenario and applying IP/MPLS nodes and OE ports redundancy as explained above. Moreover, pairs of link-disjoint optical routes need to be pre-computed during the virtual topology definition.

Aiming at evaluating the quality of the heuristics, several optimal and heuristic solutions are compared in the next section. After validating the BRKGA algorithms, both multilayer architectures are evaluated from the heuristic results.

7.4 Illustrative numerical results

7.4.1 Heuristic validation

First, we compared the performance of the joint ILP model and the proposed heuristic using the CARISMA optical topology (see Appendix A). Over this optical network topology, we generated a virtual topology consisting of 4 metro and 3 transit nodes, 15 virtual links, and 5 demands. We defined 6 different runs with the same traffic configuration but with a different number of failure scenarios. To be precise, we consider scenarios containing between 0 to 11 failures (the total number of single failure scenarios is 40), and which involve ports, IP/MPLS nodes and optical links. Failures in runs from 1 to 5 did not impact on the resources used to convey the demands, and thus the optimal solution is exactly the same as the one obtained in run 1. In contrast, run 6 included a failure impacting some resource used by the demands.

The ILP model was solved using CPLEX 12.0. Both the model and the heuristics were run in 2.4 GHz Quad-Core machines with 8 GB RAM. Table 7-5 illustrates the results obtained using CPLEX (we limit the execution time to 12h) and the results from the heuristic.

Table 7-5: BRKGA vs CPLEX for the joint approach

Run	ILP					Heuristic		
	Vars	Consts	Best Node	Best Int.	Time (h:m:s)	Solution	GAP (%)	Time (s)
1	2,100	300	599.500	599.500	00:00:20	599.500	0.00	0.252
2	6,300	900	580.759	630.375	12:00:00	599.500	--	0.431
3	10,500	1,500	548.696	--	12:00:00	599.500	--	0.182
4	14,700	2,100	557.399	--	12:00:00	599.500	--	0.174
5	18,900	2,700	523.186	--	12:00:00	599.500	--	0.387
6	23,100	3,300	524.526	--	12:00:00	639.125	--	1.565

As shown, only the run 1 could be solved (with the time constraint) using the ILP model. In this case, the heuristic found also the optimal solution. As soon as failure scenarios were included, no solution was found using the ILP model, as a consequence of the time constraint. In fact, CPLEX found an integer solution only for run 2. In contrast, the heuristic algorithm found the optimal solution in every run from 2 to 5 (which is the same as in run 1 as stated above). Running times were also very short, just several hundreds of ms. Finally, we could not prove the optimality of the heuristic solution obtained in run 6 since no exact solution could be found.

Aiming at deeper studying the performance of the heuristic algorithm, we designed a second test using the overlay ILP models (which do not consider failures as a consequence of the network architecture). In this case, we used the TEL_21n_34e topology (see Appendix A) for the optical layer and designed a virtual topology consisting of 8 metro and 4 transit nodes, 22 virtual links, and 7 different runs with a number of demands ranging from 8 to 56.

Table 7-6 illustrates the results obtained by solving the ILP models and running the proposed heuristic. Solving times for the heuristic represent the average of 10 executions for every run.

As shown, the heuristic found the optimal solution in all the runs considered. Moreover, and in contrast to CPLEX, the heuristic was able to solve the problem optimally within no more than a few seconds in the worst case.

In light of these results, we can conclude that the proposed heuristic provides near-optimal or optimal solutions for both the joint and the overlay models.

Table 7-6: BRKGA vs CPLEX for the overlay approach

Run	ILP				Heuristic		
	Vars	Consts	Solution	time (h:m:s)	Solution	GAP (%)	time (s)
1	30,682	4,869	164	00:02:5.2	164	0	0.133
2	31,783	5,045	226	00:02:8.2	226	0	0.054
3	50,017	6,860	342	00:03:20.2	342	0	0.094
4	62,515	8,126	458	00:07:57.9	458	0	3.193
5	80,774	9,943	644	00:29:50.9	644	0	0.104
6	87,492	10,666	762	00:34:2.9	762	0	0.603
7	96,286	12,078	898	02:38:40.7	898	0	4.264

7.4.2 Architecture comparison

The performance of the joint approach has been compared to that of the overlay approach in terms of CAPEX. To this end, both approaches have been applied over three national optical network topologies with different IP/MPLS topologies on the top. More precisely, we have considered three optical network topologies: the TEL_21n_34e, the BT_20n_32e, and the DT_21n_31e topologies (see Appendix A). In this chapter, we refer these topologies simply as TEL, BT, and DT, respectively.

Aiming at applying the heuristic algorithms over a wide range of multilayer networks, on the top of the optical topologies, different IP/MPLS topologies with 40 metro nodes and different number of transit and interconnection nodes are

designed. Table 7-7 specifies the location of transit and interconnection nodes (identified by the associated OXC) of each multilayer network. Moreover, the spatial position of metro nodes is characterized by a uniform coverage degree based on the Kolmogorov-Smirnov goodness-of-fit test [Ro04]. A value close to 100% indicates metro nodes uniformly located around every OXC node, whereas a low value denotes the presence of areas with high density of metro nodes. Table 7-7 also contains the coverage degree of the three networks under study. Regarding traffic, we assume two types of demands: national where both metro end nodes belong to the network and interconnection where one of the end nodes is outside of the network. The considered traffic mix is also detailed in Table 7-7. As shown, three different multilayer network scenarios can be identified, from an unbalanced scenario where 70% of the total is interconnection traffic with only 3 interconnection nodes and several high density metro areas, to the well-balanced scenario with 50% of interconnection traffic, 5 interconnection nodes and near-uniformly metro areas.

Table 7-7: IP/MPLS topologies

Net-work	Transit	Interconn.	Metro Coverage degree	Traffic Mix (National/Interconnection)
TEL	3, 4, 9, 11, 14, 15, 19, 21	6, 8, 20	0.1%	30% / 70%
BT	1, 9, 10, 12, 14, 16, 20	7, 13, 15, 19	30%	40% / 60%
DT	3, 4, 5, 8, 9, 14, 19, 21	6, 7, 10, 13, 20	90%	50% / 50%

Each multilayer network has been planned for six gradually increasing traffic loads, starting from an initial load of 4 Gbps per metro node and with increments of 45% at each step (roughly representing a year-over-year traffic increase). Aiming at providing accuracy, each traffic load has been executed 10 times with randomly generated demands following the above characteristics.

To compute the network CAPEX, we consider an adaptation of the equipment costs proposed in [Hu08]. Table 7-8 provides the used costs in cost unit (c.u.) for IP/MPLS nodes and OE ports. However, to the best of our knowledge, no study provides cost of using an already deployed WSON infrastructure. In view of this, Fig. 7-4 plots the CAPEX savings obtained by implementing the joint approach for various costs of unprotected lightpaths C_{unp} ranging from 0 to 0.5 c.u.. Each point in Fig. 7-4 has been obtained after computing the solution for both approaches on a set of 10 randomly generated executions for each of the considered loads.

Table 7-8: Cost of IP/MPLS Nodes and OE Ports (c.u.)

	Class 1	Class 2	Class 3	Class 4	Class 5
Capacity (Gbps)	160	320	640	1280	2,560
Max. ports	4	8	16	32	64
Cost	3	4.5	6.5	22.5	50.19

	1Gbps	10Gbps	40Gbps	100Gbps
Port in IP/MPLS node	0.35	1.25	7.625	20.625

As shown, the joint approach provides CAPEX savings even when the costs of using the WSON infrastructure are not considered (i.e. C_{unp}= 0), meaning that the cost of the IP/MPLS layer is cheaper with the joint network approach. However, and for the sake of a fair comparison, we consider C_{unp}= 0.1 which provides similar prices for WSON and for OE ports when computing lightpaths costs. Regarding the cost of restorable lightpaths C_{rest}, values ranging from 1.33 to 2 with respect to the cost of unprotected lightpaths are considered in Fig. 7-4. As depicted, the unbiased C_{rest}/C_{unp} ratio of 1.5, in between of the unprotected and the 1+1 protected cost, provides CAPEX savings ranging from 13% to 24% when the joint network approach is implemented.

Aiming at performing an in-depth analysis of the networks structure provided by both approaches, a set of graphs with the switching capacity of the IP/MPLS nodes and the installed OE ports as a function of the network load are provided. Similar behavior can be observed in all networks under consideration and for each approach. Fig. 7-5(left) shows the switching capacity equipped for each type of node. Both approaches equip IP/MPLS metro nodes with the same capacity since it only depends on the incoming traffic. On the contrary, the capacity of transit and interconnection nodes is higher in the joint approach as a result of both the extra capacity and OE ports added to deal with failures. To illustrate this Table 7-9 shows the number and average bit-rate of the OE ports installed under the non-failure and failure scenario, for the networks obtained under both approaches.

Table 7-9: OE Ports Analysis

	Joint		Overlay	
	Num.	Average Bit-rate (Gbps)	Num.	Average Bit-rate (Gbps)
Non-failure	134	67.94	134	67.94
Recovery	194	42.41	134	67.94
TOTAL	328	52.84	268	67.94

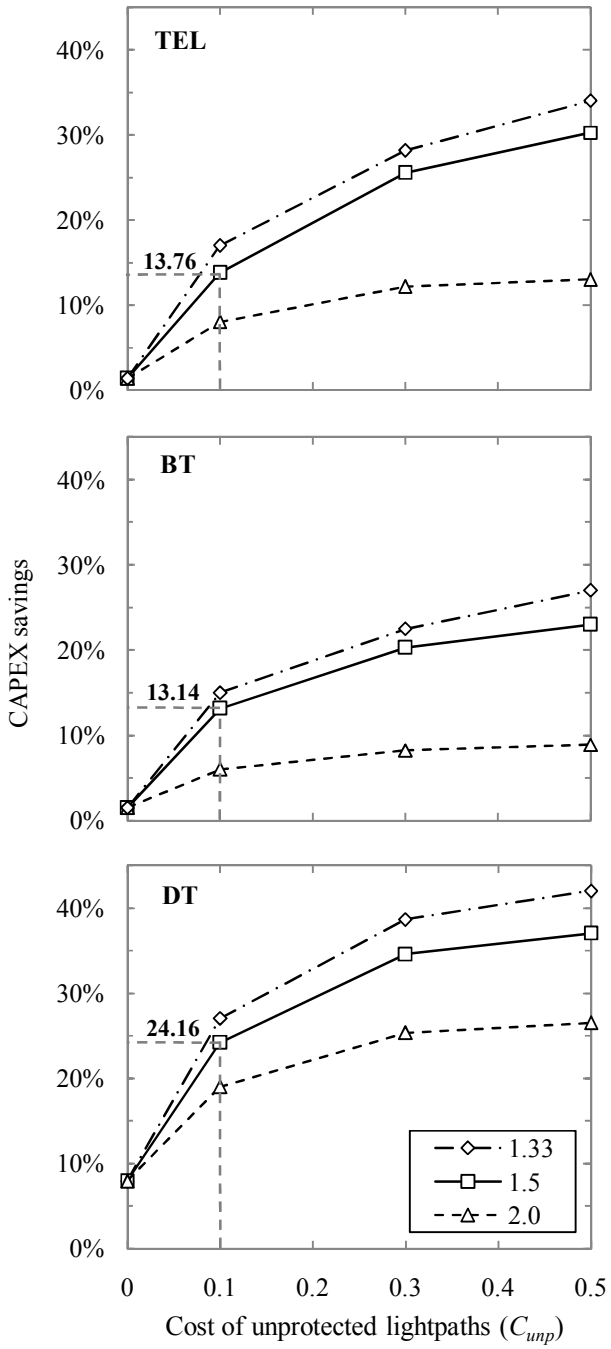

Fig. 7-4 On average CAPEX savings for several C_{rest}/C_{unp} ratios

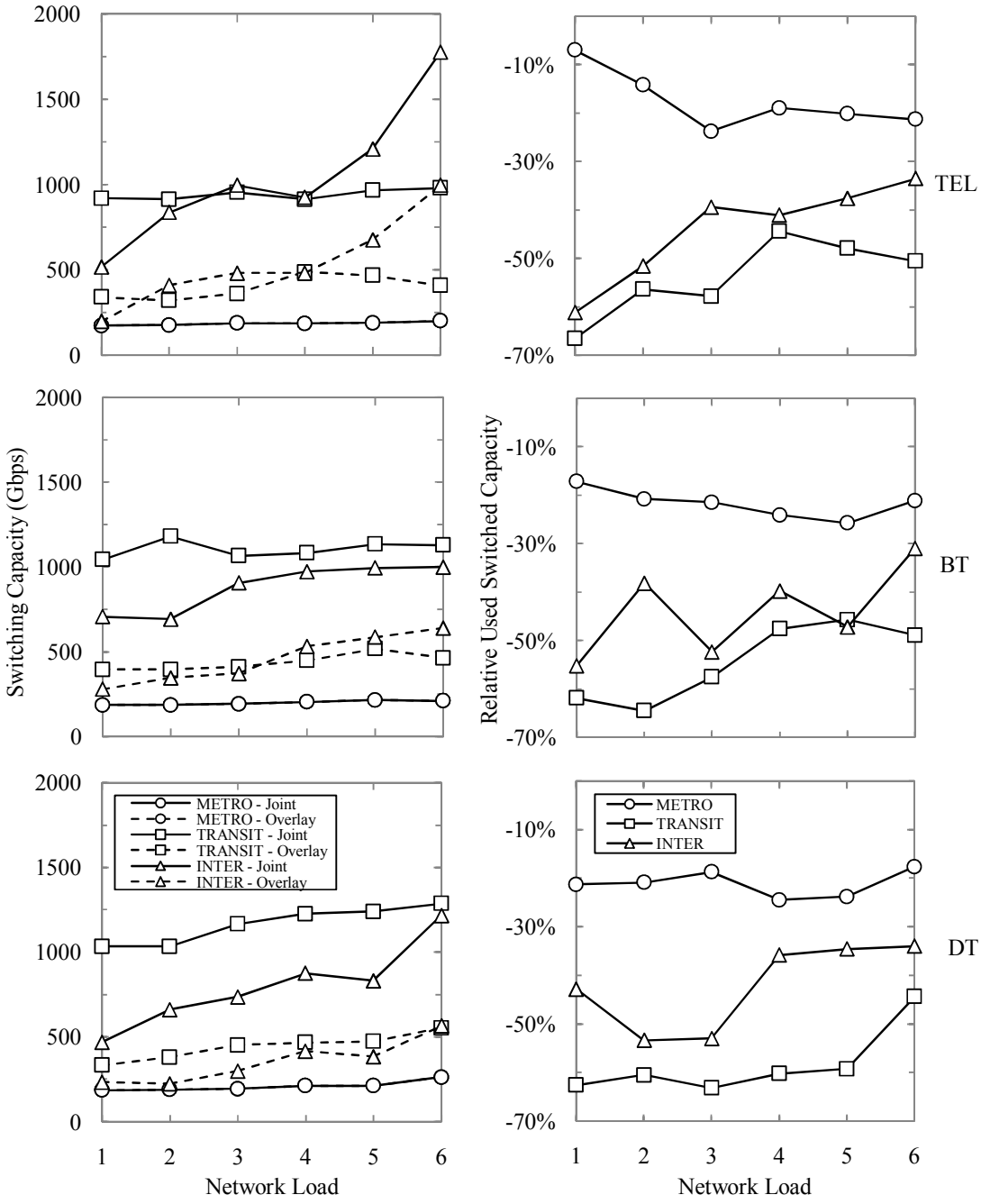

Fig. 7-5 Equipped (left) and used (right) switching capacity against network load

It is worth noting that, while both the number and the average bit-rate of OE ports is the same under the non-failure scenario, the joint approach needs more OE ports for recovery purposes. However, due to the recovery mechanism proposed (lightpath restoration first, connectivity recovery second, and LSP reroute third), the average bit-rate used for recovery in the joint approach is lower than in the overlay case, which simply duplicates OE ports. Note that when lightpaths can be recovered at the optical layer, virtual links are automatically restored avoiding

node over-dimensioning or the addition of extra OE ports. In case that only a subset of lightpaths can be restored after a failure, those using higher bit-rate (and more expensive) OE ports are restored first. The remaining lower rate lightpaths are then removed and connectivity recovery is performed, adding then extra capacity and OE ports.

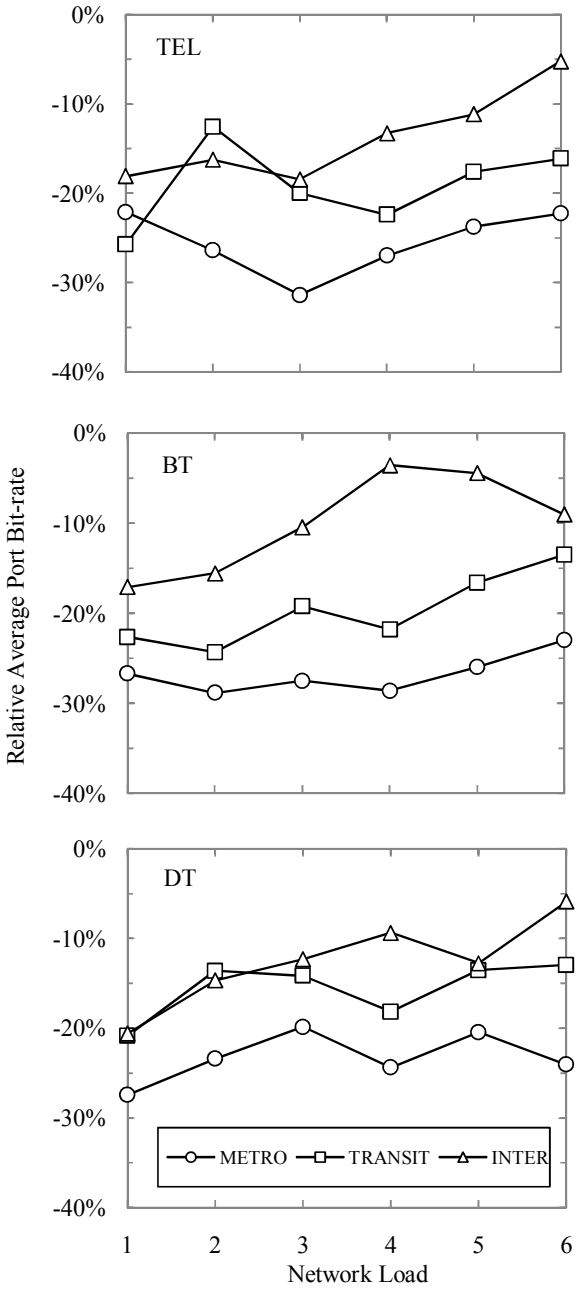

Fig. 7-6 Port bit-rate against network load

Supporting the previous statement, Fig. 7-5(right) shows the used switched capacity under the non-failure scenario in relative values. Nodes in the joint

approach have higher unused switching capacity than those in the overlay approach. Also as a consequence of the recovery mechanism proposed, the joint approach uses OE ports with lower average bit-rate than the overlay approach (Table 7-9 and Fig. 7-6).

Finally, Fig. 7-7 shows the evolution, in terms of relative gap to the best solution of the heuristic algorithm found in a 10h run, considering an intensity i=4, and for the three networks under consideration. In this figure, one can observe the amount of time that the BRKGA requires to reach convergence and thus the complexity of the problem for the joint approach. In this regard, a brief analysis of the proposed network instances identifies differences on the complexity of the problems. For instance, the size of virtual topology is 326, 361, and 408 virtual links for networks TEL, BT, and DT respectively. Thus, the mean number of feasible routes for a given demand significantly increases from TEL to DT networks which, as shown, affects the convergence time.

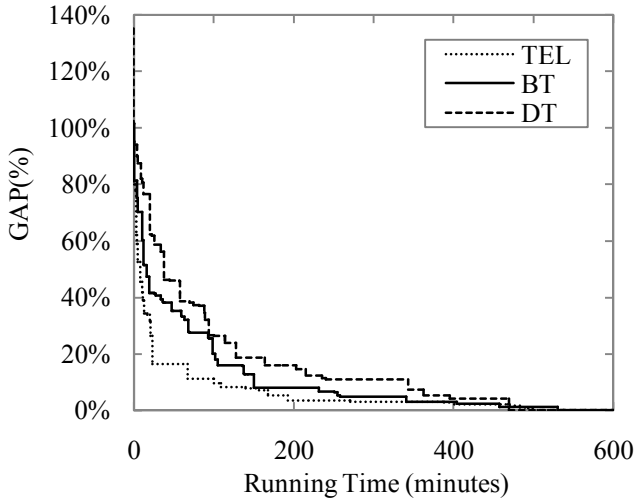

Fig. 7-7 Gap to the best solution against running time

7.5 Summary

This chapter addressed the design of survivable IP/MPLS-over-WSON multilayer networks against single IP/MPLS node, OE port, or fiber link failures. To this goal, two alternative approaches were compared with the objective of CAPEX minimization: the proposed joint approach consisting in over-dimensioning backbone IP/MPLS nodes and applying lightpath and connectivity recovery, and the conventional overlay approach consisting in duplicating backbone IP/MPLS nodes. ILP models for both approaches were presented and heuristic algorithms to

obtain near-optimal solutions were developed in view that the proposed ILP models become impractical if realistic problem instances are considered.

The performance of both approaches was extensively assessed considering three national optical network topologies with different IP/MPLS topologies on the top. From the results obtained, it can be concluded that the proposed joint approach leads to CAPEX savings as high as 24% in the DT network and 13% in the TEL and BT networks, when compared with the overlay approach. Analyzing the structure of the networks obtained under both approaches, the joint approach over-dimensions IP/MPLS nodes, not only to deal with failures, but also as a consequence of the extra OE ports required in each node for recovery purposes. However, the average bit-rate of extra OE ports in the joint approach is lower than those needed in the non-failure scenario as a result of the recovery strategy proposed.

As a final remark, it is worth pointing out that since the overlay approach duplicates both IP/MPLS transit and interconnection nodes and OE ports, the resulting networks require higher operational costs than those in the joint approach. Moreover, extra OE ports added for recovery purposes in the joint approach can remain switched-off while not used, thus leading to the additional benefit of energy savings.

Chapter 8

Re-optimization in dynamic multi-layer networks

In this chapter, we face the problem of the optimal use of optical resources in dynamic traffic scenarios. To this end, we design a centralized flow reallocation module for multilayer IP/MPLS-over-WSON optical networks. Here, every virtual link in the aggregation layer is dynamically created and needs two OE ports. OE ports are expensive resources and thus capital expenditures (CAPEX) can be reduced optimizing the necessary number of OE ports.

In static traffic scenarios, such as the considered in the previous chapter, the initial network planning phase can determine the number of OE ports in every node. Nevertheless, in dynamic traffic scenarios, client connection requests are routed using the set of currently available virtual links; when new virtual links are needed, new lightpaths are set-up at the optical layer. When virtual links do not transport any client LSP they are removed and the underlying lightpaths are torn-down, thus releasing the used OE ports. This dynamic process leads to a non-optimal use of resources.

In this chapter, we present the Optical Resources Optimization (ORO) problem, proposing an ILP model to solve it. Due to the complexity of the problem, the time needed to solve ORO (even in small networks) trend to be very long, and thus, that method may be not applicable to real-time problems. For this reason, we present several meta-heuristic algorithms to improve resources utilization. The performance of the algorithms is compared with the exact solution obtained by solving the ILP model. Finally, the performance of the best candidate heuristic is experimentally demonstrated in the CARISMA test-bed [Lu09].

8.1 Optical resources optimization problem

8.1.1 Motivation

As mentioned before, dynamic connection establishment along with a randomness of connection holding times, may lead to suboptimal resource allocation in the network at a certain time. For better understanding, consider the example depicted in Fig. 8-1(left). It might happen that, due to the previous resource state in the network, a lightpath going through A–E–F–G–D–C would have to be created to support a client LSP from node A to node C. Supposing that the flow requested ¼ of the total wavelength capacity, a virtual link from nodes A to C with ¾ unreserved bandwidth would be created (step 1). Imagine now that a client LSP request arrives from node A to node B, also requesting ¼ wavelength capacity. Provided that resources would be found on the direct link connecting both nodes, a direct lightpath would be set up, resulting as well in a virtual link from node A to C with ¾ unreserved bandwidth (step 2). Finally, a client LSP requesting ½ of the total capacity reaches node B with destination node C. As the total routing metric of reusing virtual links from B–A and A–C appears to be much higher than allocating a direct data link from B to C, a third lightpath is set up. This also triggers the establishment of a third virtual link with ½ unreserved bandwidth (step 3). Note that, if the client LSP request from A to C would have arrived now, rather than sometime before, this one would have reused the A–B and B–C virtual links.

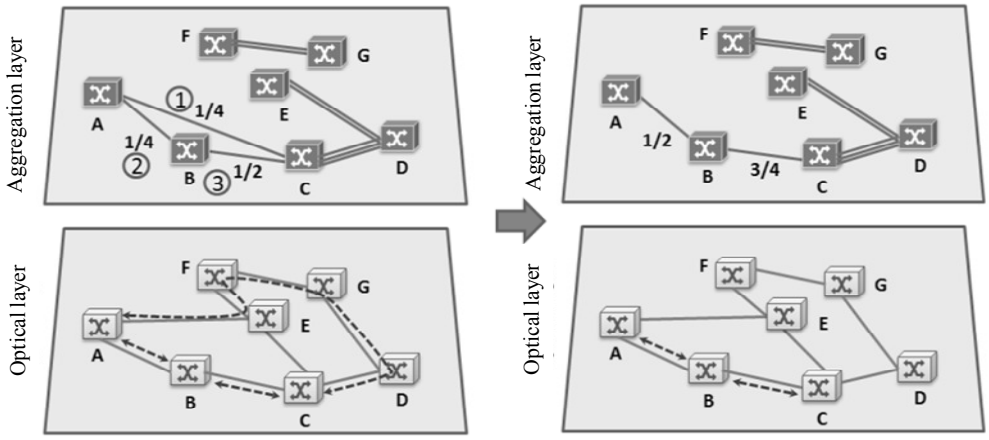

Fig. 8-1 Example of resource reallocation for optimization purposes in a two-layered network scenario.

This arouses concerns for deploying a centralized resource reallocation module in the network, which periodically checks the status of the already deployed virtual links and optimizes client LSP placement accordingly. If a resource reallocation would be triggered in the situation of Fig. 8-1 (left), this one could reallocate virtual

link A–C into virtual links A–B and B–C, which would result in resource savings of two OE ports and five optical data links as shown in Fig. 8-1 (right).

In the following sections, we address the reallocation process in a two-layered transport network. The main target is to minimize both the number of optical resources needed to carry the offered traffic to the network, as well as the number of hops of client LSPs. With such purposes in mind, we first define for the first time the ORO problem. Aiming at finding the optimal solution of the problem, we second introduce an ILP formulation. Finally, and motivated by the high complexity of the problem, we propose several GRASP-based meta-heuristics to obtain near-optimal solutions with low computational effort.

8.1.2 Problem statement

The ORO problem can be formally stated as follows:

Given

- The optical layer topology represented by the graph $G_O(N, L)$, where N represents the set of OXCs and L the set of fiber links,
- the length of each fiber link in L,
- the aggregation layer topology represented by the graph $G_C(V, E)$, where V represents the set of grooming-capable nodes and E represents the set of current virtual links,
- the capacity of each virtual link in E,
- the set D of established client-LSPs,
- the current route over the aggregation layer of each client-LSP in D,
- the source and destination nodes of each client-LSP,
- the bandwidth of each client-LSP.

Output:

- the set of released virtual links,
- the new route for each client-LSP whose current route uses, at least, one released virtual link.

Objective: Minimize the amount of OE ports of a certain aggregation layer topology, without affecting the service of any client LSP.

ORO releases as much optical resources as it can by releasing virtual links, so that the affected client-LSPs are re-routed using the minimum cost route, obtaining a most compacted network. In contrast to similar problems in the literature, our approach aims to reduce the needed optical resources without creating new lightpaths (i.e. avoiding traffic disruption). Hereafter a simpler and clearer

notation is used: the term *optical arcs* (or, simply, arcs) is used instead of virtual links and the term *paths* instead of client LSPs.

8.1.3 ILP formulation

We propose an arc-path based [Me07] ILP formulation for ORO. The following notations are used for sets and parameters:

- E: Set of optical arcs (indexed by e).
- C_e : Cost of optical arc e.
- M_e : Capacity of optical arc e.
- D: Set of paths (indexed by d).
- $R(d)$: Set of possible routes for path d (indexed by r).
- N_{dr} : Equal to 1 if path d was using route r before optimization.
- L_{dr}: Cost of route r for path d.
- Q^e_{dr}: Equal to 1 if route r of path d uses optical arc e.
- W_d : Bandwidth of path d

Additionally, the following notations are used for variables:

- ζ_e: Binary, equal to 1 if optical arc e is used after optimization (not removed). 0, otherwise.
- Δ_e: Positive integer with the used bandwidth in optical arc e
- η_{dr}: Binary, equal to 1 if path d uses route r after optimization
- ρ_d: Binary, equal to 1 if path d has been moved after optimization

Finally, the ILP formulation is as follows:

$$(ORO) \quad \min -\sum_{e\in E}(C_e\times(1-\zeta_e)) \quad + \quad \frac{\sum_{d\in D}\sum_{r\in R(d)}(L_{dr}\times\eta_{dr})}{\sum_{d\in D}\sum_{r\in R(d)}(L_{dr}\times N_{dr})} \quad + \quad \frac{\sum_{e\in E}\delta_e}{\sum_{e\in E}M_e} \tag{8.1}$$

subject to:

$$\sum_{r\in R(d)}\eta_{dr}=1, \quad \forall d\in D \tag{8.2}$$

$$\sum_{d\in D}\sum_{r\in R(d)}(W_d\times Q^e_{dr}\times\eta_{dr})\le\delta_e, \quad \forall e\in E \tag{8.3}$$

$$\zeta_e\le\delta_e\le(M_e\times\zeta_e), \quad \forall e\in E \tag{8.4}$$

$$\rho_d + \frac{\sum_{e \in E}\left(\zeta_e \times \sum_{r \in R(d)}(N_{dr} \times Q_{dr}^e)\right)}{\sum_{e \in E}\sum_{r \in R(d)}(N_{dr} \times Q_{dr}^e)} \geq 1, \quad \forall d \in D \tag{8.5}$$

$$\sum_{e \in E}\left((1-\zeta_e) \times \sum_{r \in R(d)}(N_{dr} \times Q_{dr}^e)\right) - \rho_d \geq 0, \quad \forall d \in D \tag{8.6}$$

$$\sum_{r \in R(d)}((1-N_{dr}) \times \eta_{dr}) = \rho_d, \quad \forall d \in D \tag{8.7}$$

$$\zeta_e, \eta_{dr}, \rho_d \in \{0,1\}, \ \delta_e \in Z \tag{8.8}$$

Constraint (8.2) ensures that every path is assigned to one and only one route. Constraints (8.3) and (8.4) guarantee a feasible path re-routing in terms of capacity of optical arcs kept in the solution. Constraint (8.5) makes sure that every path using an optical arc to be removed is re-routed. Conversely, constraint (8.6) ensures that paths supported on optical arcs kept in the solution are not re-routed. Constraint (8.7) provides the paths to be re-routed. Finally, constraint (8.8) defines variables as binary or integer. We assume that every optical arc supports at least one path. The objective function structure (8.1) and the cost values of arcs and paths ensure that the optimal solution releases as much OE ports as possible. For feasible solutions with the same number of released OE ports, the objective function selects the one with the minimum total path length. Finally and in the case of a double draw (number of OE ports and total path length), the solution containing the highest available optical capacity is selected.

Any method to solve ORO in real networks is conditioned by a very narrow time margin. Since ORO is designed to be applied in dynamic traffic environments, the time needed by getting the input data, solving the problem, and modifying the network according to the obtained solution should be very short (i.e. < 1 sec.). Thus, the execution time is the key factor for choosing the method. In this regard, solving ORO ILP by means of a linear solver engine like CPLEX could provide impractical long execution times, even in small networks. In fact, ORO can be defined as an NP-hard problem, since less complex network problems than ORO are already NP hard.

For this reason, several GRASP-based meta-heuristic are presented in the next section. The GRASP meta-heuristic framework provides a good tradeoff between solution quality and execution time. Although the aim of the method is to obtain the best possible solution, the optimal one is not required for real networks. This is because in dynamic traffic scenarios an optimal solution in a certain time moment becomes sub-optimal when first changes appear (i.e: new connection set-up and tear-downs).

8.1.4 GRASP-based meta-heuristic

In this section, several GRASP based meta-heuristics are presented for solving ORO. More specifically, the *constructive phase*, the *local search* algorithms and the stop criteria are detailed.

Let us define a solution of the ORO problem as a set of arcs to remove and a set of paths to re-route. Thus, we define two different RCLs: firstly, the *RCLarc* contains the list of arcs sorted in ascending order as a function of its used bandwidth. Its size is determined by the α_{arc} parameter. More formally, *RCLarc* can be defined from the notation above:

$$CL_{arc} = E \tag{8.9}$$

$$GCF_{arc}(e) = \sum_{d \in D} \sum_{r \in R(d)} W_{dr} \cdot Q_{dr}^{e} \tag{8.10}$$

Secondly, for every path, the *RCLpath* contains the list of feasible routes that do not contain a given arc. The *RCLpath* is sorted in ascending order by optical resources cost. The random degree of route selection is determined by α_{path}.

$$CL_{path}(d,e) = \left\{ r \in R(d) \mid Q_{dr}^{e} = 0 \right\} \tag{8.11}$$

$$GCF_{path}(d,r) = L_{dr} \tag{8.12}$$

Table 8-1 shows the *constructive phase* adapted for solving the ORO problem. The algorithm for rerouting the paths affected by an arc release is detailed in Table 8-2.

Table 8-1: ORO GRASP constructive phase

```
Input: Network graph, α_arc, and α_path
Output: List of optical arcs to remove, paths to move with
its new route and the cost of the solution
begin
  Build arc candidate list (CL_arc)
  while CL_arc ≠ ∅ do
    Build RCL_arc from CL_arc with α_arc.
    Get a random arc I from RCL_arc
    Remove I from CL_arc.
    If re-route (arc I, network graph) then
      Add I to the solution.
      Add every moved path to the solution.
      If there is any path in its original route then
        Remove that path from the solution.
    Compute solution cost.
End
```

Regarding solution improvement, Table 8-3 illustrates the local search algorithm, consisting on single arc exchanges between used and removed sets. Given an initial solution where the topology $G_C(V, E)$ has been reduced to $G^*_C(V, E^*)$, all the possible exchanges between one arc in E^* and one arc in $E \setminus E^*$ are attempted.

Table 8-2: Re-route algorithm

```
Input: Arc I to re-route, network graph
Output: Successful or failed re-route
begin
  Create an empty path listL.
  Remove arc I from the graph.
  For every path j using the optical arc I do
    Get a copy of the current route of the path j.
    Tear it down the path j.
    Build CL_path for pathj.
    If no route found then
      Restore the original route of the path j and set it up.
      Add the optical arc I to the graph.
      For every path k in the list L do
        Tear down the path k.
        Establish the path k in its original route.
      Return (failed to re-route).
    Build RCL_path from CL_path with α_path.
    Get a route r from the RCL_pathof path j.
    Remove r from CL_path.
    Establish the path jfor the selected route r.
    Add the path j to the list L.
  Mark every path in the list L as moved.
  Return (success)
end
```

Table 8-3: ORO GRASP Local Search

```
Input: Initial solution, list of removed arcs
Output: Final solution, list of removed arcs
begin
    Compute costBest= cost of Initial solution.
    Initialize improve="true".
    While improve="true" do
      improve="false"
      for each arc a in Initial solution do
        for each arc bin list of removed arcs do
           aux solution := Initial solution
           Change a by b in aux solution.
           Re-route connections affected by the change in aux
                solution
           if aux solution is feasible then
                Compute costAux = cost of aux solution
                if costAux<costBest then
                    costBest := costAux.
                    Initial solution := aux solution.
                    Remove b from list of removed arcs.
                    Add a tolist of removed arcs.
                    Improve="true".
                    Break for
        if improve=="true" then
           break for
    Final solution = Initial solution.
End
```

When one exchange provides a feasible solution with lower cost than the initial one, the initial solution is updated. The algorithm stops when any change improves the best founded solution.

Finally, we define a double stop criterion. First, the heuristic finishes when a maximum number of iterations without improving the best founded solution is attained. Note that this stop criterion may lead into execution times higher than the desired time threshold. For this reason, the second stop criterion is a maximum execution time.

Four different versions can be obtained by setting different values to these α parameters. The basic one has no randomness (both parameters fixed at 0) and we called it as the *GREEDY* version. In the *ARC GRASP* heuristic only α_{arc} has non-zero values. In the *PATH GRASP* heuristic the random selection is given by the α_{path} parameter. Finally, the *ARC-PATH GRASP* version combines both parameters. Table 8-4 illustrates the configuration of α parameters to define each heuristic.

Table 8-4: α configuration for each heuristic

	$\alpha_{arc} = 0$	$\alpha_{arc} > 0$
$\alpha_{path} = 0$	*GREEDY*	*ARC GRASP*
$\alpha_{path} > 0$	*PATH GRASP*	*ARC-PATH GRASP*

In the following section, the performance of the heuristics is evaluated for a real backbone topology. After comparing the results in terms of quality of the solution (comparing heuristic and exact solutions) and execution time, the one with the best trade-off between both factors will be implemented in the NMS of a real test-bed.

8.2 Illustrative numerical results

8.2.1 ILP model performance evaluation

We have tested the proposed model generating several instances with different traffic intensity over the EON_16n_23a depicted in Appendix A. For these tests we assume that every bidirectional optical link is equipped with 8 wavelengths. These instances have been solved on a 3GHz CPU computer with 1GB RAM memory, using CPLEX v.11.0 [CPLEX] as solver. The obtained results are shown in Fig. 8-2, where each point collects the average value obtained from a number of simulations ensuring statistical accuracy. For each network load (normalized to the total network capacity), the amount of released OE ports (in percentage) and the execution time is drawn.

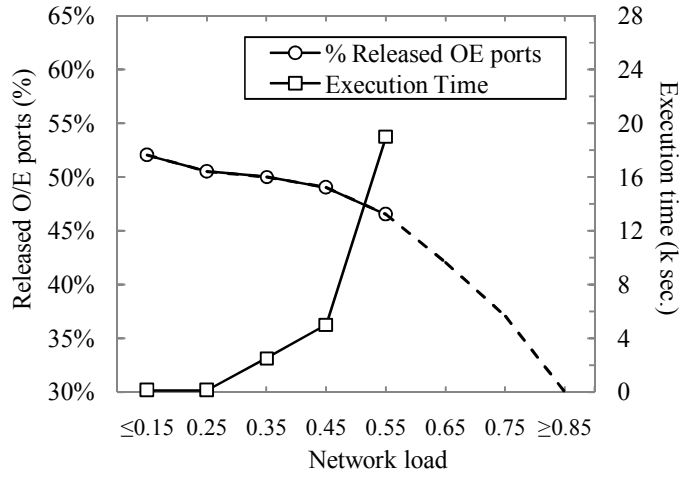

Fig. 8-2 Released OE ports and execution time against network load

As shown, the ORO formulation allows reducing the use of OE ports in about 50%. Nonetheless, each execution takes several hours for moderate traffic intensity scenarios. For network loads higher than 60%, the size of the problems is too large and CPLEX runs out memory without giving, in many cases, any solution.

Fig. 8-3 shows the relation between network load and problem sizes (in terms of number of binary variables). It is clear that network load and the number of variables of the ORO formulation present a closed correlation. Highly loaded instances could not be solved because of the large amount of variables. Moreover, the logarithm of the execution time increases linearly, which means that execution time increases exponentially when the problem size increases. Therefore, even solving the ORO formulation in more powerful computational environments, executions times would not be within an acceptable and practical range.

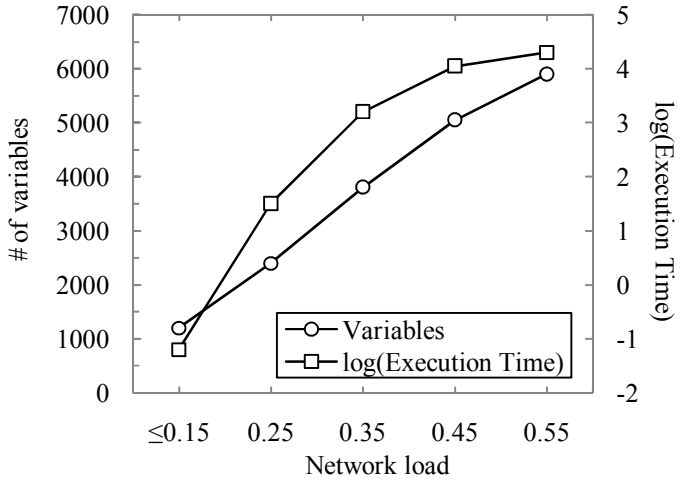

Fig. 8-3 Problem size and execution time against network load

Therefore, we can conclude that although the presented ILP formulation gives a significant reduction of used OE ports, solving times are unacceptable for real scenarios. For this reason, in the next section we propose alternative heuristic methods which provide near-optimal solutions but within limited times.

8.2.2 Heuristic performance evaluation

Fig. 8-4 and Fig. 8-5 show a performance comparison of the previously presented GRASP heuristics. For each heuristic, we have determined the best values for the tunable parameters (α_{arc}, α_{path}, and stop iterations), by performing several executions of the heuristics. The figures show the best results reached for each heuristic version.

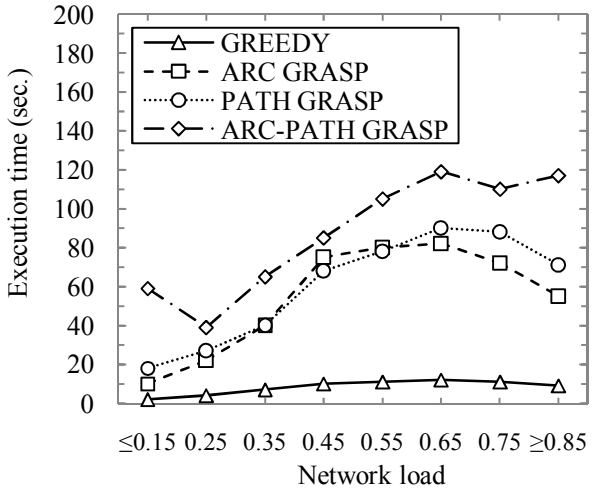

Fig. 8-4 Execution time against network load

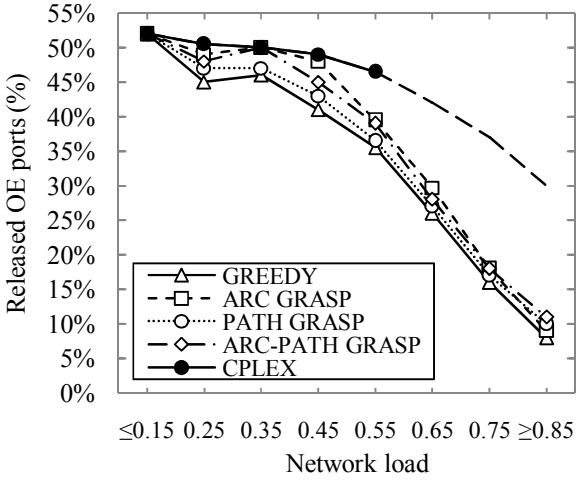

Fig. 8-5 Released OE ports against network load

Execution times for the heuristics increase linearly with the problem size, and it is higher in randomized versions. The number of released OE ports is higher in randomized versions that in the basic *GREEDY* one. In case of medium-loaded networks, the *ARC GRASP* gives the better values for the objective function. In highly-loaded networks, all the heuristics give similar results. The distance between the heuristics and the exact solution increases with the problem size and it could be very significant in highly-loaded networks. Nevertheless, after an ORO application in a dynamic traffic scenario, the optimal solution lasts until any change on the network (setup or teardown of paths) is done. For this reason, reaching the optimal solution is not strictly needed.

The analysis of results over simulated instances allows us choosing *ARC GRASP* as the most suitable optimization method for solving ORO problem. The quality of the solutions is near the exact references in comparable instances. Running time is acceptable in every case and it can be adjusted by setting different values on the stop criterion. Tuning this parameter, we obtain a simply way to balance the quality of the solutions and the execution times. Moreover, this algorithm does not need distinct routes pre-computation, since every affected path is always re-routed through the available shortest path. This condition is a key factor for choosing this heuristic instead of any of the rest of randomized versions.

8.2.3 CARISMA test-bed Performance

The *ARC GRASP* meta-heuristic has been implemented in the CARISMA NMS, and several sets of tests have been carried out over the test-bed. The CARISMA test-bed (see Appendix A) has been configured with 8 wavelengths per link. The performance of the *ARC GRASP* meta-heuristic has been tested with different traffic loads.

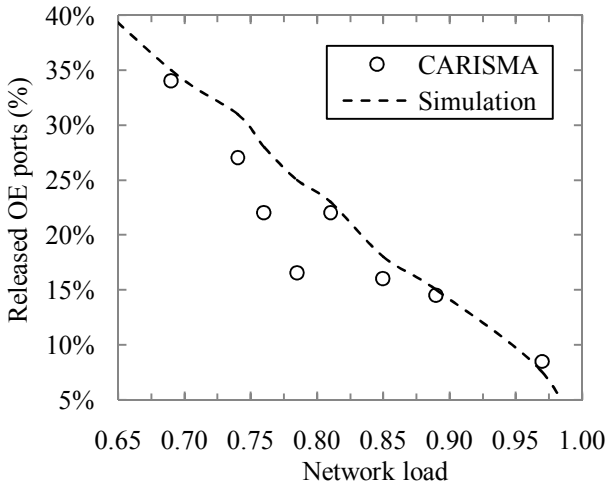

Fig. 8-6 Released OE ports in the CARISMA test-bed network

Fig. 8-6 shows the obtained experimental results in comparison with the obtained over simulated topologies depicted in Fig. 8-5. The number of released OE ports is similar in both simulated and experimental cases. This fact validates the simulated scenarios as good instances for testing optimization methods. Moreover, execution times in the CARISMA NMS have been within one second in all cases (between 200 and 700 ms).

Finally, the effect of applying ORO over the blocking probability is evaluated. Fig. 8-7 depicts the blocking probability against network load in CARISMA network when ORO is executed periodically. This curve is compared with the obtained when the re-optimization module is not active.

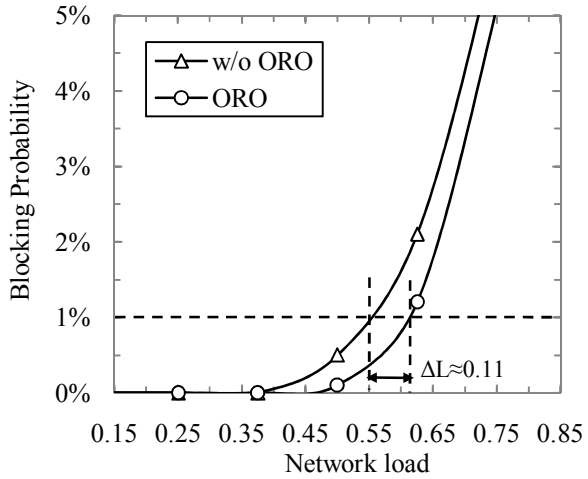

Fig. 8-7 Blocking probability in the CARISMA test-bed network

For a reference blocking probability (i.e.: 1%), the offered traffic load is an 11% higher using ORO. Note that ORO not only allows reducing network CAPEX, but also provides a better use of the network capacity in dynamic traffic environments. This fact provides a better blocking probability performance and the possibility to support more traffic without violating some blocking probability threshold.

8.3 Summary

In this chapter, the optical resources optimization problem has been introduced as an adaptive mechanism for OE ports use reduction in IP/MPLS-over-WSON multilayer networks. An integer linear programming formulation has been presented for describing the problem.

In the proposed examples, the exact solution reduces the needed OE ports up to 50%. Executions using CPLEX toke several hours for real traffic instances. These

long execution times make the exact solution to be not suitable to be implemented in real networks.

As an alternative, four heuristic algorithms have been developed and compared. The proposed greedy randomized heuristics give values for total reduction of optical cost near exact values. In contrast, execution times for the different heuristics are in the order of few seconds, which is much shorter than the exact method.

The *ARC GRASP* meta-heuristic has been chosen to be implemented in a real network management system, because of its good combination of solution quality and execution times. Moreover, this heuristic does not need route pre-computation.

The application of the *ARC GRASP* meta-heuristic in real traffic scenarios over the CARISMA test-bed network gave significant OE ports reduction, obtaining execution times under one second. With these results, the proposed heuristic has been proved to be a good method to optimize resources in optical networks.

Chapter 9

GMPLS control plane network design with resilience guarantees

Previous chapters are devoted to the data plane (i.e: design of optical and/or aggregation layer). In this chapter we face for the first time the design of the control plane in GMPLS-enabled networks regardless of the data plane topology. More specifically, we define the problem of obtaining the optimal GMPLS control plane topology, minimizing the network CAPEX while matching specific resilience requirements.

First, we provide analytical formulae to quantify the resilience of generic meshed control plane topologies. These expressions provide a valid method to estimate the resilience of a control plane from its number of links. Notwithstanding, a certain target resilience value could be obtained from different topologies with different costs.

Second and aiming to find the optimal control plane topology that ensures a certain resilience level, the ARCO problem is formulated as a mathematical combinatorial model. Since this model is unpractical to solve, a constructive iterative linear method is also presented. This model, however, does not scale properly for large backbone networks. In view of this, a GRASP-based meta-heuristic is defined with the aim to obtain good-quality solutions with low computational effort.

Finally, the benefits of ARCO are illustrated in terms of CAPEX minimization. The negligible effect of control plane reduction over data plane performance is also highlighted. Moreover, a comparison between optimal and heuristic results is presented in terms of objective function and computational time.

9.1 Resilience in GMPLS-based control plane

As introduced in Chapter 3, authors in [Pe07] introduced the new parameter P_d to quantify the resilience of the GMPLS control plane. This P_d stands for the

probability that any connection request or tear-down is dropped along the failure recovery time Δt. Equation (9.1) reproduces the analytical P_d expression:

$$P_d = 1 - e^{-\lambda \Delta t (1+P_L)} \sum_{k=0}^{C} \binom{C}{k} \left[\left(e^{\mu \Delta t} - 1 \right) (1 - P_L) \right]^k \tag{9.1}$$

where $C=ceil(\lambda/\mu)$ identifies the number of active connections in the network at the failure time. Note that the mathematical analysis behind P_d is valid to any network scenario, as it basically depends on the traffic characteristics. The parameter that captures the network topology under study and the traffic distribution over it is P_L, which stores the probability that a connection request or tear-down is signaled on a certain control plane link. While this P_L was particularized for symmetrical ring topologies in [Pe07], our work targets at a general P_L expression to allow P_d computation in asymmetrical meshed control planes.

9.2 Resilience quantification in a mesh control plane

9.2.1 Analytical model

Let $G_{DP}(N_{DP},E_{DP})$ and $G_{CP}(N_{CP}, E_{CP})$ identify the data and control plane graphs of a GMPLS-enabled transport network, respectively. For the ongoing model we assume that G_{DP} is bi-connected and planar. In fact, G_{DP} topology can be seen as a set of interconnected sub-rings, which for highly meshed networks can be as small as triangles. We also assume G_{CP} bi-connected, providing survivability to the control plane. Particularly, we restrict the control plane topology to be a subset (or the complete set) of the data plane one. More formally, we restrict G_{CP} to be a spanning subgraph of G_{DP}, being G_{DP} and G_{CP} related as:

$$N_{DP} \equiv N_{CP} \equiv N \tag{9.2}$$

$$E_{CP} \subseteq E_{DP} \tag{9.3}$$

In this scenario, we define a minimal bi-connected covering topology over G_{DP} (e.g. a Hamiltonian cycle or a minimum n-tree), so that $E^{it}{}_{DP}$ identifies the link subset in this minimal topology and $E^{ot}{}_{DP}$ the subset containing the rest of the data plane links. Hence, $E_{DP} = E^{it}{}_{DP} + E^{ot}{}_{DP}$. In what follows, this additional relation between G_{DP} and G_{CP} is imposed:

$$E_{CP} \supseteq E_{DP}^{it} \tag{9.4}$$

A *minimal* control plane topology ($E_{CP} = E^{it}{}_{DP}$) is defined. On this basis, any intermediate topology (hereafter, *partially meshed*) is created by adding links to the *minimal* topology, finally getting the *symmetrical* topology ($E_{CP} = E_{DP}$). From the assumptions above, G_{CP} consists at least on one ring (Fig. 9-1). Every link in

E^{ot}_{DP} added to E_{CP} creates a new sub-ring, either by sub-ring partitioning (splitting an existing sub-ring in two) or sub-tree closing (adding a new sub-ring external to the minimal topology). In any case, two data plane adjacent nodes will belong to the same sub-ring at the control plane.

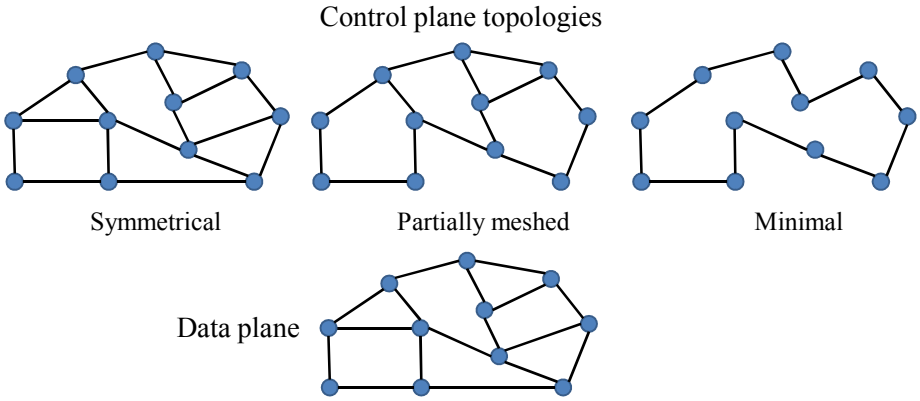

Fig. 9-1 A data plane topology (bottom) and three different control plane topologies

Let us define h_{DP} as the average hop length of the data paths. In a similar way, h_{CP} defines the average hop length of the control paths. As the RSVP-TE messages forwarded on the control plane should visit (i.e., configure) the same node sequence comprised in the computed data plane route, h_{CP} becomes a function of G_{CP} and G_{DP}.

At this point, we can define $P_L = D_L/D_T$, that is, the ratio between the amount of demands supported in the failed link L (D_L) with respect to the total number of demands (D_T). This finally leads to:

$$P_L = \frac{C \cdot h_{CP} / |E_{CP}|}{C} = \frac{h_{CP}}{|E_{CP}|} \tag{9.5}$$

As shown, P_L directly depends on the average hop length of control plane paths. As mentioned above, end-to-end RSVP-TE messages are processed hop-by-hop at every node in the route of the Label Switched Path (LSP) being signaled/torn-down. As a consequence of equation (9.4), adjacent nodes in the data plane may be not adjacent in the control plane. Thus, h_{CP} is proportional to h_{DP}, and can be expressed as

$$h_{CP} = \tau \cdot h_{DP} \tag{9.6}$$

where the parameter τ adjusts the distance (the number of hops) in the control plane between two adjacent nodes in the data plane.

Without loss of generality, we consider that every demand is routed through the shortest path. Besides, we assume the traffic uniformly distributed in the network. Then, the average length of the shortest paths in a mesh network can be approximated by [Ko04], where δ_{DP} is the average nodal degree in the data plane:

$$h_{DP} \approx \sqrt{\frac{|N|-2}{\delta_{DP}-1}} \tag{9.7}$$

To calculate τ we compute the distance at the control plane of all adjacent node pairs at the data plane. Being also adjacent at the control plane their distance equals to 1. Otherwise, their distance in the control plane $h_{CP}(i)$ is computed. Finally, it can be expressed as:

$$\begin{aligned}\tau &= \left(\sum_{\forall i \in E_{CP}} 1 + \sum_{\forall i \in E_{DP} \not\subset E_{CP}} h_{CP}(i)\right) \cdot \frac{1}{|E_{DP}|} = \frac{|E_{CP}|}{|E_{DP}|} + \frac{|E_{DP}|-|E_{CP}|}{|E_{CP}|} \cdot \frac{\sum_{\forall i \in E_{DP} \not\subset E_{CP}} h_{CP}(i)}{|E_{DP}|-|E_{CP}|} \\ &= \alpha + (1-\alpha)\cdot\kappa\end{aligned} \tag{9.8}$$

where α is the proportion of links at the control plane to those at the data plane, and κ represents the average distance of non adjacent nodes at the control plane.

We have focused on a *minimal* G_{CP} topology consisting in a Hamiltonian cycle, where the average lengths of E^{it}_{DP} and E^{ot}_{DP} links are similar. There, we have concluded (after several tests) that κ can be accurately estimated as $\sqrt{|N|}$. In a more general case, every sub-ring in the control plane acts as a cycle covering a subset of nodes of G_{DP}. Based on the previous results, we approximate $\kappa \approx \sqrt{V_{CP}}$, where V_{CP} is the mean number of nodes in a sub-ring.

As mentioned before, every pair of adjacent nodes at the data plane belongs to the same sub-ring at the control plane. Let R_{CP} denote the number of sub-rings at the control plane, and T_{CP} the sum of nodes in every individual sub-ring. Thus, V_{CP} satisfies:

$$V_{CP} = \left\lceil \frac{T_{CP}}{R_{CP}} \right\rceil \tag{9.9}$$

where:

$$T_{CP} \approx \left|E^{it}_{DP}\right| + 2\cdot\left|E^{ot}_{DP}\right| = 2\cdot|E_{CP}| - 2\cdot\left|E^{it}_{DP}\right| \tag{9.10}$$

$$R_{CP} = |E_{CP}| - |N| + 1 \tag{9.11}$$

Note that equation (9.10) gives an exact T_{CP} value when all sub-rings have been created by sub-ring partitioning. In any other case, however, it still represents a valid approximation, since sub-ring partitioning is much more frequent than sub-tree closing.

Finally, combining equations (9.5)-(9.9), P_L can be stated as:

$$P_L \cong \left[\alpha + (1-\alpha)\cdot\sqrt{V_{CP}}\right] \cdot \sqrt{\frac{|N|-2}{\delta_{DP}-1}} \cdot \frac{1}{|E_{CP}|} \tag{9.12}$$

9.2.2 Model validation

The obtained P_d model has been validated over different networks with different average node degrees. To this end, we consider the quite sparse NSFNET_28n_37e topology, the moderately meshed DT_14n_23e topology, and the highly meshed EONTT_28n_61e (see Appendix A). In this chapter we refer these topologies as NSFNET, DT, and EON, respectively. Besides, for each topology, we define four different control plane alternatives: the *symmetrical* topology, a *minimal* topology, and two *partially meshed* topologies in between. Table 9-1 reviews the number of links of each control plane topology under evaluation, for the *symmetrical*, *partially meshed* 1, *partially meshed* 2, and *minimal* topologies, respectively.

The performance of the model has been validated by simulation results. For them, enough wavelengths per link to guarantee that all requests are routed through the shortest path (accomplishing the wavelength continuity constraint) are assumed.

In such scenarios, uniformly distributed connection requests arrive at each node following a Poisson process, and connection holding times are exponentially distributed. The model and the simulation results for P_d as a function of Δt are plotted in Fig. 9-2. Each simulation is conducted in order to reach steady state results within a 95% confidence interval.

Table 9-1: Control plane topology parameters

	$\lvert E_{CP} \rvert$
DT	23 – 20 – 17 – 14
NSFNET	37 – 34 – 31 – 29
EON	61 – 41 – 34 – 28

As seen, the P_d model and the simulation results are really close in every experimented topology. Aiming to measure the discrepancy between the obtained P_d values and the expected ones, we have computed the Chi-square goodness of fit test in each scenario. To this goal, we compare the number of affected connections obtained by simulation with respect to the expected value of this variable (i.e., multiplying the P_d analytical value by the number of total simulated connections). In all cases, the null hypothesis can be clearly accepted (the difference between simulation and analytical results is zero), which highlights the accuracy of the model.

Motivated by the necessity of quality of resilience parameters, P_d could be proposed to quantify the maximum recovery time to meet certain control plane resilience requirements (i.e., a certain P_d value). In particular, the *minimal* topology requires very restrictive Δt values (Fig. 9-2). Since multiple demands are supported on each control link, the performance degradation caused by control link failures is very

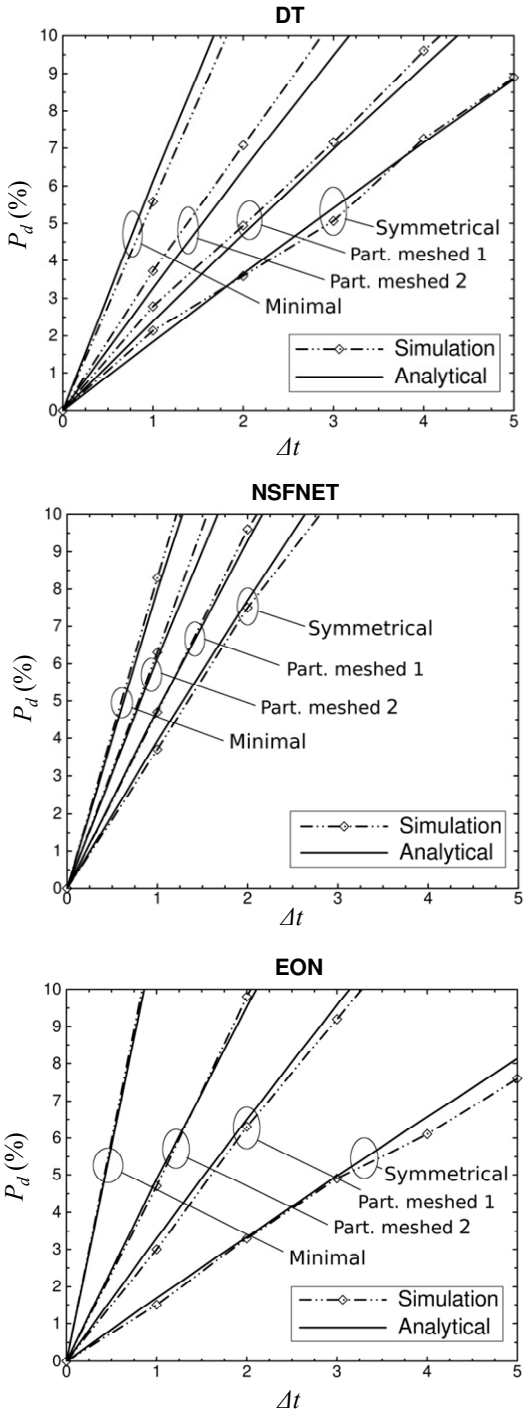

Fig. 9-2 P_d model against simulation results for evaluated topologies.

High. For instance, aiming at a P_d= 5% objective in the EON, Δt< 500 ms must be assured. However, by increasing the connectivity at the control plane, P_d steadily decreases. In the *symmetrical* topology, as only one demand is supported on each control link, $\Delta t \approx$ 3 s already fits P_d= 5%. Between both extremes we have the

partially meshed topologies, which target at a trade-off between resilience and required resources.

Experimental results allow validating the P_d model for real backbone topologies. Thus, network operators could benefit from the proposed model to quantify the number of control plane links needed to fit certain P_d requirements (i.e., a maximum P_d value), given a Δt achievable by their control plane recovery mechanisms (e.g., IP layer re-routing, dedicated link protection,...).

This model, however, provides the on-average number of control plane links to fit some target P_d requirements. For control plane topologies with the same number of links, P_d could widely range. To illustrate this, Fig. 9-3 shows the P_d value for the best and the worst founded control plane topology over NSFNET given a number of control plane links. As shown, the optimal control plane topologies allow a P_d reduction of more than 50% with respect to the worst control plane topology.

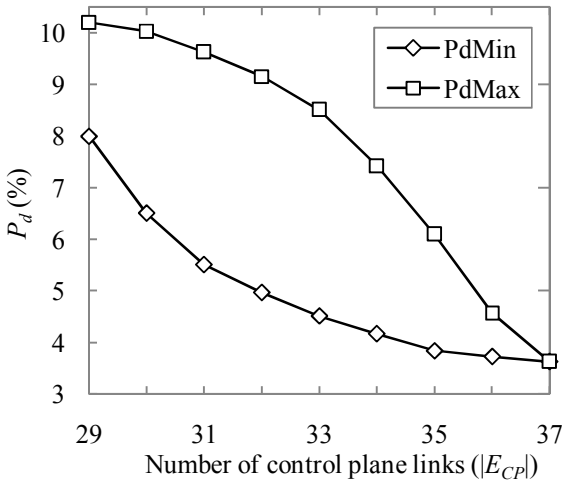

Fig. 9-3 Minimum and maximum P_d against the number of control plane links.

Aiming at finding the optimal control plane topology, an optimization method using these resilience requirements values as input data is presented in the next section.

9.3 Resilience-aware GMPLS control plane network optimization problem (ARCO)

9.3.1 Problem definition

In this section, we introduce the problem of designing, for a given data plane topology, the optimal control plane topology that fits the requested resilience requirements (quantified by a requested P_d and Δt values). Besides, this service

condition must be guaranteed for a given range of traffic intensities. Hereafter, we refer to this problem as ARCO.

The problem can be formally stated as follows:

Given:

- a data plane topology G_{DP},
- a set of traffic intensities, represented by a set of arrival rates Λ and a service rate μ,
- a set of resilience requirements defined by: a P_d threshold (P_d^{max}) and a maximum failure recovery time (Δt),

Output:

- a control plane topology G_{CP},

Objective: Minimize the number of control plane links, fitting the requested resilience requirements for all traffic intensities.

For the definition of ARCO, we initially present a non-linear combinatorial model that chooses the optimal control plane topology from $\Gamma(G_{DP})$, that is, the set of pre-computed candidate control plane topologies over G_{DP}. Every candidate topology must follow equations (9.2)-(9.4), so that the *minimal*, the *symmetrical* and a large number of *partially-meshed* topologies are included in $\Gamma(G_{DP})$. Then, for each control plane topology g in $\Gamma(G_{DP})$, we compute P_L^g and its cost a^g (i.e., the number of arcs).

The combinatorial model for the ARCO problem (ARCO-CNL) uses the following sets and parameters:

G_{DP}	Data plane graph
$\Gamma(G_{DP})$	Set of candidate control plane topologies built over the data plane topology G_{DP}, index g
a^g	Cost of the candidate topology g
P_L^g	P_L of the candidate topology g
Λ	Set of arrival rates
μ	Average service rate
Δt	Failure recovery time
P_d^{max}	Maximum allowed P_d

Additionally, the variable γ^g is defined, which equals 1 if and only if the control plane topology g is optimal. Using this notation, we can formulate ARCO-CNL as:

$$(\text{ARCO-CNL})\ \text{Minimize}\ \left|E_{CP}\right| = \sum_{\forall g \in \Gamma(G_{DP})} a^g \cdot \gamma^g \tag{9.13}$$

subject to:

$$\sum_{\forall g \in \Gamma(G_{DP})} \gamma^g = 1 \tag{9.14}$$

$$P_d\left(\lambda_i, \mu, \Delta t, P_L^g\right) \cdot \gamma^g \le P_d^{\max} \quad \forall g \in \Gamma(G_{DP}), \lambda_i \in \Lambda \tag{9.15}$$

$$\gamma^g \in \{0,1\}, \quad \forall g \in \Gamma(G_{DP}) \tag{9.16}$$

Constraint (9.14) ensures that only one control plane topology is chosen. Constraint (9.15) guarantees that $P_d{}^g$ is lower than $P_d{}^{max}$ for all the traffic intensities under consideration. Finally, constraint (9.16) defines γ^g as binary.

The number of variables and constraints in ARCO-CNL is proportional to the summation of the number of $|E^{ot}{}_{DP}|$-element subsets of an ($|E_{DP}|$-$|E^{it}{}_{DP}|$)-element set, from the *minimal* to the *symmetrical* topology. Thus,

$$\left|\Gamma(G_{DP})\right| \approx \sum_{\left|E_{DP}^{ot}\right|=0}^{\left|E_{DP}\right|-\left|E_{DP}^{it}\right|} \binom{\left|E_{DP}\right| - \left|E_{DP}^{it}\right|}{\left|E_{DP}^{ot}\right|} = 2^{\left|E_{DP}\right|-\left|E_{DP}^{it}\right|} \tag{9.17}$$

Considering that the whole $\Gamma(G_{DP})$ set has to be explored to find the optimal solution, the ARCO-CNL problem can be classified as NP-Complete. Furthermore, its formulation requires a pre-computation of the set of candidate topologies, as well as the calculation of their respective $P_L{}^g$ and a^g values.

Table 9-2 shows a procedure to obtain this input data for ARCO-CNL. The complexity of a single iteration in this pre-processing algorithm is given by the complexity to compute all shortest paths between each pair ofadjacent nodes in the data plane over the candidate control plane topology *g*. This can be approximated to $|E_{DP}|$ times the complexity of the Dijkstra shortest-path algorithm that, from [Bh99], equals $O(|E_{DP}|*\log|N|)$. Hence, the resulting pre-processing algorithm complexity raises to $O(|E_{DP}|^2*\log|N|*2\text{^}(|E_{DP}|-|N|))$.

Table 9-2: Pre-processing algorithm for ARCO

```
Input: G_DP, D_T
Output: set Γ(G_DP), set of P_L, set of a.
begin
   Initialize Γ(G_DP) = ∅
   while more candidate control plane topologies can be found do
      Find new control plane topology g
      a^g=number of links of topology g
      Compute h_CP of traffic demand D_T over topology g
      P_L^g= h_CP/a^g
      Update setΓ(G_DP), set of P_L, and set of a
end
```

Note that the complexity of the proposed combinatorial model (i.e., pre-processing plus mathematical programming) clearly leads to unacceptable solving times. Indeed, this model was only intended to be an initial formulation of ARCO.

In the following section, we present an improved constructive method that builds itself feasible topologies from a pre-computed set of routes given G_{DP}.

9.3.2 ARCO iterative linear method

As mentioned above, the parameter τ adjusts the distance in the control plane between those adjacent nodes in the data plane (i.e., the number of hops). In other words, τ represents the average number of control plane hops between a pair of data plane adjacent nodes. Equation (9.18) presents an alternative expression to evaluate τ, where the number of hops in the control plane $h_{CP}(i)$ for a given data plane link are weighted by the number of demands supported on this link $D_{DP}(i)$:

$$\tau = \frac{\sum_{i \in E_{DP}} h_{CP}(i) \cdot |D_{DP}(i)|}{\sum_{i \in E_{DP}} |D_{DP}(i)|} \tag{9.18}$$

Note that P_L depends on the traffic distribution, as it is proportional to h_{DP}. In this work, we assume a uniform traffic distribution. In such a case, having enough data plane resources (e.g., wavelengths), every demand is routed through its shortest path. Hence, h_{DP} (and also P_L) can be computed irrespective of the offered load. Proposition 1 relates P_d values for different traffic intensities.

Proposition 1: Given a set of constant (and strictly positive) parameters (μ, Δt, and P_L) and two arrival rates λ_1 and λ_2, it is accomplished that:

$$P_d^1(\lambda_1, \mu, \Delta t, P_L) > P_d^2(\lambda_2, \mu, \Delta t, P_L) \quad \forall \lambda_1 > \lambda_2 \tag{9.19}$$

Proof: The partial derivate of P_d with respect to λ (equation 9.19) is strictly positive

$$\frac{\partial P_d}{\partial \lambda} = f(\mu, \Delta t, P_L) \cdot e^{-\lambda \Delta t (1+P_L)} > 0 \tag{9.20}$$

Here, f is a strictly positive function that depends only on μ, Δt, and P_L. As the exponential function is an increasing continuous function, the partial derivate is positive in the whole λ domain. Therefore, P_d is continuous and increasing with λ. □

Proposition 1, jointly with the assumption of independence between P_L and the traffic parameters, allows us to obtain the optimal control plane topology by solving the ARCO-CNL problem only for the highest traffic intensity. In order to reduce the number of variables in our problem even more, we also define a constructive method for ARCO, different than the combinatorial approach previously proposed.

With such purposes in mind, we could have introduced a model that minimizes the number of control plane links. Then, a constraint ensuring $P_d \leq P_d^{max}$ would have had to be included, turning the model into non-linear. This would have prevented

the use of efficient linear solvers, raising the ARCO execution times eventually. In contrast, a linear ARCO model is attempted in this section. We denote it as ARCO-IL. In order to define this model, the following mathematical propositions that relate P_d, P_L and E_{CP} have to be introduced.

Proposition 2: Given a set of constant parameters (λ, μ, and Δt) and two different values of P_L (P_L^1 and P_L^2), all strictly positive, it is accomplished that

$$P_d^1\left(\lambda,\mu,\Delta t,P_L^1\right) < P_d^2\left(\lambda,\mu,\Delta t,P_L^2\right) \quad \forall\, P_L^1 < P_L^2 \tag{9.21}$$

Proof: Using the same argument as in Proposition 1, the partial derivate of P_d with respect to P_L is

$$\frac{\partial P_d}{\partial P_L} = \left(1-P_d\right)\cdot\left(\lambda\Delta t + C\cdot\frac{e^{\mu\Delta t}-1}{1+\left(e^{\mu\Delta t}-1\right)\cdot\left(1-P_L\right)}\right) \tag{9.22}$$

Since P_L is a value comprised between (0,1], and the other parameters are strictly positive, the derivate is strictly positive unless P_d equals 1. This happens when the connection inter-arrival time is lower than the control failure recovery time (i.e., $\lambda^*\Delta t > 1$), which is far from the usual traffic dynamics in circuit-switched networks. As will be discussed in the results section, few seconds can be expected to recover the control plane in GMPLS-controlled transport networks. These times are much lower values than the expected minutes or hours' inter-arrival times to make circuit-switching efficient. Therefore, we can consider $P_d<1$ in all cases, being an increasing continuous function with respect to P_L. □

Proposition 2 allows to ensure that a control plane topology minimizing P_d for a given set of feasible control plane topologies and a set of traffic parameters also minimizes P_L.

Proposition 3: Let G^1_{CP} and G^2_{CP} be two different control plane topologies over the same data plane topology G_{DP} that satisfy

$$\left|E^1_{CP}\right| > \left|E^2_{CP}\right| \tag{9.23}$$

Furthermore, let P_L^1 and P_L^2 be the P_L values for these topologies, respectively. If both G^1_{CP} and G^2_{CP} are optimal graphs with respect to P_d, it is accomplished that

$$P_L^1 < P_L^2 \tag{9.24}$$

Proof: From equations (9.18) and (9.23), the summation of $h_{CP}(i)$ is lower in G^1_{CP} than in G^2_{CP}, since both are optimal graphs with respect to P_d. Then, since $\tau^1 < \tau^2$, we have that

$$P_L^1 = \frac{\tau^1\cdot h_{DP}}{\left|E^1_{CP}\right|} < \frac{\tau^2\cdot h_{DP}}{\left|E^2_{CP}\right|} = P_L^2 \tag{9.25}$$

□

From Proposition 3, we can conclude that the removal of one arc from the control plane topology results in a new control plane topology with higher P_L. In addition, we can state that given $|E_{CP}|$, we can minimize P_L by minimizing τ alternatively.

With propositions 2 and 3 in hand, we are finally able to propose ARCO-IL. Using integer linear programming, this model minimizes P_L by minimizing τ, instead of minimizing P_d directly. The integer linear model generates the optimal control plane topology with respect to P_L for a given $|E_{CP}|$. The value of P_d is computed based on the obtained P_L, ensuring that it is lower than the threshold value. This must be repeated iteratively, modifying $|E_{CP}|$.

For the ongoing formulation, a set of routes over the *symmetrical* topology are pre-computed for every data plane link. Next, a subset of these routes is chosen to provide control plane connectivity to every data plane link. Finally, a subset of E_{DP} is added to E_{CP} to make these routes feasible.

In addition to the notation previously defined, the following sets and parameters are used for ARCO-IL:

E_{DP}	Set of links in the data plane
E_{CP}	Set of links in the control plane
$R(i)$	Set of control plane routes for data plane link i. A control plane route is a path between the end nodes of a data plane link over the symmetrical topology.
Q_{ijk}	Equal to 1 if the control plane route j for data plane link I uses control plane link k, 0 otherwise
C_{ij}	Cost (in number of hops) of control plane route j for data plane link i.
D_T	Set of connections offered to the network
$D_{DP}(i)$	Set of connections supported on data plane link i.
ρ	Predefined number of control plane links
M	A large positive constant

Additionally, the following variables are used:

ζ_k	Binary, equal to 1 if link k is created in the control plane, 0 otherwise.
Ω_{ij}	Primary route. Binary, equal to 1 if data plane link i is assigned to the control plane route j, 0 otherwise.
K_{ij}	Back up route. Binary, equal to 1 if data plane link i is assigned to the control plane route j, 0 otherwise.

Using this notation, we can redefine the parameter τ as:

$$\tau = \frac{\sum_{\forall i \in E_{DP}} \left(|D_{DP}(i)| \cdot \sum_{\forall j \in R(i)} (C_{ij} \cdot \omega_{ij}) \right)}{\sum_{\forall i \in E_{DP}} |D_{DP}(i)|} \tag{9.26}$$

As a result, the integer linear programming model for ARCO-IL becomes:

$$\text{(ARCO - IL) Minimize } \tau \tag{9.27}$$

subject to

$$\sum_{\forall j \in R(i)} \omega_{ij} = 1 \quad \forall i \in E_{DP} \tag{9.28}$$

$$\sum_{\forall j \in R(i)} \kappa_{ij} = 1 \quad \forall i \in E_{DP} \tag{9.29}$$

$$\sum_{\forall j \in R(i)} Q_{ijk} \cdot (\omega_{ij} + \kappa_{ij}) \leq 1 \quad \forall i,k \in E_{DP} \tag{9.30}$$

$$\left(\sum_{\forall k \in E_{DP}} \zeta_k \cdot Q_{ijk} \right) - C_{ij} + M \cdot (1 - \omega_{ij} - \kappa_{ij}) \geq 0 \quad \forall i \in E_{DP}, j \in R(i) \tag{9.31}$$

$$\sum_{\forall k \in E_{DP}} \zeta_k = \rho \tag{9.32}$$

$$\zeta_k, \omega_{ij}, \kappa_{ij} \in \{0,1\} \quad \forall i,k \in E_{DP}, j \in R(i) \tag{9.33}$$

Fixing the number of control plane links and based on equations (9.5) and (9.6), the objective function (9.27) minimizes τ using the definition provided in equation (9.26).

Constraints (9.28), (9.29) and (9.30) ensure the two-connectivity at control plane. Constraint (9.28) guarantees that every data plane link has one primary control plane route, whereas constraint (9.29) guarantees one back up route. Constraint (9.30) ensures that both control plane routes are link-disjoint. Constraint (9.31) makes sure that all control plane routes only use active control plane links. Note that no additional constraint to ensure that every primary control plane route is the shortest possible one is necessary, as the length of the route is already minimized in the objective function. This allows reducing the size of the problem eventually. Constraint (9.32) ensures that the number of control plane links is equal to the specified number. Finally, constraint (9.33) defines the variables as binary.

After each ARCO-IL execution, the resulting P_d value in the obtained control plane topology is calculated using the formula in equation (9.1). Depending on the relation between this result and the maximum P_d permitted, a new iteration can be

executed by modifying the number of control plane links. The algorithm ends either when the optimal solution is found or the *minimal* or the *symmetrical* topology is reached. Table 9-3 shows the details of the ARCO-IL method. The number of iterations needed to find the optimal solution strongly depends on the quality of the number of control plane links initially provided. Departing from the P_d analytical model presented and using statistical inference techniques over the observed values, we have obtained a two-step procedure to predict the number of control plane links from P_d and a certain set of traffic and data plane characteristics.

Table 9-3: ARCO-IL method

```
Input: G_DP, D_T, set Λ, μ, Δt, P_d^max
Output: G_CP
begin
  Let ρ as the fixed number of control plane links
  Compute H_DP of traffic demand D_T over the G_DPtopology
  for every link I in E_DP do
     Compute D_i from D_T
     R(i) = compute all routes between link I end nodes inG_DP
  Compute Q and C from R
  λ:=max(Λ)
  Set initial point for ρ:= ρ^ini
  Setρ_ant:=ρ
  while no Optimal G_CP founded do
     Solve ARCO-IL ILP model
     Evaluate P_d of obtained solution
     if P_d≤ P_d^max and ρ_ant<ρ then
        Optimal G_CP founded
     else if P_d ≤ P_d^max and ρ_ant ≥ ρ then
        Actualize incumbent G_CP
        ρ_ant:=ρ
        ρ:=ρ−1
        if ρ<|E^it_DP| then break
     else if P_d>P_d^max and ρ_ant>ρ then
        Optimal G_CP founded
     else if P_d>P_d^max and ρ_ant ≤ ρthen
        Actualize incumbent G_CP
        ρ_ant:=ρ
        ρ:=ρ+1
        if ρ>|E_DP| then break
end
```

Firstly, we have approximated the inverse of equation (9.1) as follows, which allows us obtaining P_L from P_d:

$$P_L \cong \left(\frac{1}{2 \cdot \lambda \cdot \Delta t \cdot |N|} + \frac{1}{10} \right) \cdot P_d \tag{9.34}$$

Secondly, we have obtained an expression to estimate the number of links in the control plane given the objective P_L value and the number of nodes and links in the data plane. We denote δ_{DP} to the average nodal degree in the data plane.

$$\rho^{ini} = \left\lceil \left(\frac{5}{4} \cdot |E_{DP}| \right) \cdot (1 - P_L)^{\left[\left(\frac{|N|}{25} + 2 \right) \cdot \delta_{DP} + \frac{|N|}{5} \right]} + |N| \right\rceil \quad (9.35)$$

The obtained ρ^{ini} value estimates the number of links in the optimal control plane topology and can be used as the initial point for the ARCO-IL method.

The complexity of the ARCO-IL pre-computing algorithm can be derived from the complexity to obtain all routes in the control plane for each pair of data plane adjacent nodes. Let us define *Rmax* as the maximum number of feasible control plane routes between a pair of data plane adjacent nodes. Then, the algorithm's complexity becomes $O(Rmax^*|E_{DP}|^*\log|N|)$. As can be seen, the number of control plane routes influences the size and the execution time of ARCO-IL. Note that all control plane routes for each pair of data plane adjacent nodes need to be computed to ensure two-connectivity of the control plane.

Analyzing the size of the ARCO-IL model, the number of variables and constraints can be approximated by $2^*|E_{DP}|^*Rmax$ and $|E_{DP}|^*(|E_{DP}|+Rmax)$, respectively. Then, as the ARCO constructive method is iterative, its total execution time is given by K times the solving time of one integer linear model.

Note that the worst performance appears when ρ^{ini} is the maximum number of control plane links (i.e.,$|E_{DP}|$), but the optimal topology requests the minimum number of links (i.e. $|E^{it}_{DP}|$). In this case, $|E_{DP}|-|E^{it}_{DP}|$ iterations are required. Contrarily, the best performance is achieved if ρ^{ini} equals the number of control plane links in the optimal topology. In this case, only two iterations are needed, namely, a first one to obtain the optimal topology and a second one to verify the optimality. Being the optimal solution coincident with the *symmetrical* or the *minimal* topology, the final optimality verification might not be needed if ρ^{ini} predicts it. In the section results, we evaluate the average number of ARCO-IL iterations in different networks, validating the performance of the proposed method as well as the accuracy of ρ^{ini}.

Although ARCO-IL provides a valid method to solve the unpractical ARCO-CNL, the expected ARCO-IL execution time increases exponentially with the size of the problem. In the next section, a heuristic based on the GRASP procedure (Chapter 2) is presented with the aim to obtain good feasible solutions in practical execution times.

9.3.3 GRASP-based heuristic

This section provides the details of the *constructive phase* (Table 9-4) and the *local search* (Table 9-5) algorithms for solving the ARCO problem.

Table 9-4 shows the details of the *constructive phase*. Since the *symmetrical* topology is the one with lowest P_d, the *constructive phase* starts from this topology and iteratively removes one link at each step. The reduction concludes when the

minimal topology is reached or when the P_d^{max} threshold cannot be ensured. The selection of the link is based on its associated greedy cost (*GrC*). Being l a link of the control plane topology G_{CP}, $GrC(l)$ is defined as the resultant h_{CP} associated to the topology where the set of links is E_{CP}-{l}. Thus, the lower $GrC(l)$ the lower increase of P_L causes the candidate link l and, consequently, of P_d. At each *constructive phase* step, the candidate list (*CL*) is built adding every link which elimination results into a two-connected topology.

Table 9-4: ARCO Constructive phase

```
Input: G_DP, λ, μ, Δt, P_d^max, α.
Output: G_CP^ITE
begin
     Initialize G_CP:=G_DP.
     Initialize G_CP^ITE:=∅.
     Compute P_d of G_CP from equation (9.1).
     while P_d≤ P_d^max do
        G_CP^ITE=G_CP.
        For each link in G_CP do
           twoCon:="false".
           If G_CP-{l}is two-connected then
           twoCon:="true".
           Add l to the CL.
        If twoCon =="true" then
           Build RCL.
           Choose randomly l_sel from RCL.
           Update G_CP:=G_CP-{l_sel}.
           Compute P_d of G_CP from equation (9.1).
        else break for.
End
```

Table 9-5: ARCO Local search

```
Input: G_CP^INC, G_DP
Output: G_CP^OPT
begin
     Initialize G_CP^OPT:= G_CP^INC.
     Compute P_d^OPT of G_CP^OPT.
     Initialize G_CP^AUX= ∅.
     Initialize improve="true".
     While improve="true" do
        improve="false"
        for each link a in G_CP^OPT do
           for each link b in G_DP\G_CP^OPT do
           G_CP^AUX= G_CP^OPT-a+b.
           if G_CP^AUX is two-connected then
              Compute P_d^AUX of G_CP^AUX
              if P_d^AUX< P_d^OPT then
                 G_CP^OPT= G_CP^AUX.
                 P_d^OPT=P_d^AUX.
                 improve="true".
                 Break for
        if improve=="true" then
           break for
end
```

Aiming at reducing the P_d of a feasible solution, the *local search* algorithm (illustrated in Table 9-5) explores the neighborhood of the current solution looking for feasible interchanges between one link in the solution (in E_{CP}) and one link not in the solution (in $E_{DP} \setminus E_{CP}$). When an interchange reduces the current P_d, the solution is modified. In that case, the *local search* algorithm continues exploring the new neighborhood. On the contrary, when the neighborhood is completely explored without any improvement, it finishes. Since the complexity of the *local search* algorithm is high and its execution provides a fine improve of a feasible solution, the local search phase is applied only once, i.e.: when the stop criterion is met, with the aim to refine the best solution.

Finally, a maximum number of iterations without improving the best incumbent solution is fixed as stop criterion. Note that if a solution with the same number of links and lower P_D than the incumbent one is founded, the incumbent solution is not updated and, thus, the counter of iterations without improving is not restarted.

9.4 Illustrative numerical results

The performance of the proposed ARCO methods has been validated over the DT and NSFNET data plane topologies defined in the previous section and the EONLT_37n_57e (see Appendix A), hereafter refered as EON.

As obtained in [Pe07], P_d depends highly on the connection inter-arrival time (iat=1/λ) rather than on the connection holding time (ht=1/μ) for a given offered load. Taking this into account, in the experiments that follow we set the maximum offered load that can be offered to the network without violating the Pb<1% requirement. In such a high load scenario, we quantify the benefits of using ARCO for different iat (and consequently ht) values. Note, however, that the λ/μ quotient (i.e., the offered load) is kept constant in the graphs. Besides, for better illustration, the inter-arrival times in the considered scenarios have been normalized to the value such that the optimal control plane topology is equal to the *symmetrical* topology under the most stringent resilience requirements.

Regarding resilience requirements, we have considered two alternative sets of P_d and Δt values, namely, *RRq1* and *RRq2*, which would illustrate two different network situations. *RRq1* identifies the situation where $P_d \leq 5\%$ must be assured having a recovery mechanism able to restore the control plane in $\Delta t \leq 1.5$ s. Alternatively, *RRq2* depicts a different scenario where $P_d \leq 10\%$ must be satisfied, but having a slower control plane recovery mechanism able to restore a control plane failure in $\Delta t \leq 3.5$ s.

Without going into the details of the recovery mechanisms, the $\Delta t \leq 1.5$ s in *RRq1* could be achieved with control plane link failure detection based on LMP (failure detection time < 450 ms [Lg05]) and pre-computed backup control channels (e.g., using hop-by-hop explicit IP routing or MPLS tunneling). For the $\Delta t \leq 3.5$ s in

RRq2, LMP-based control plane link failure detection and standard IP layer re-routing might be enough. Here we would assume that the IP forwarding in the network can converge dynamically in approximately 3s from the failure detection.

9.4.1 ARCO-IL performance

Table 9-6 shows the complexity of ARCO-CNL and ARCO-IL in terms of the mathematical programming problem size. As seen, the number of topologies in ARCO-CNL grows exponentially, as predicted in equation (9.17). Due to the size of the mathematical programming problem and the complexity of the pre-processing algorithm, ARCO-CNL leads to intractable problems, even for relatively small instances. Furthermore, its non-linear nature increases its overall complexity even more.

Table 9-6: Size of ARCO-CNL and ARCO-IL

	ARCO-CNL		ARCO-IL		
	Vars.	Cons.	Vars.	Cons.	ΣR(i)
DT	2^9	2^9 |Λ|	2,503	1,816	1,240
NSFNET	2^8	2^8 |Λ|	3,675	3,263	1,819
EON	2^{18}	2^{18} |Λ|	591,151	298,911	295,547

Even though the dimensions of ARCO-CNL and ARCO-IL are not strictly related, the number of constraints can be reduced by a $|\Lambda|$ factor (the number of traffic intensities), as a consequence of proposition 1. The size of an ARCO-IL instance directly depends on the characteristics of the network topology under evaluation. While the size becomes small and similar for both DT and NSFNET networks, it is a hundred times larger for the EON, which is translated into more complex instances and slower convergence times. Recall that ARCO-IL needs to pre-compute the set of control plane routes for every data plane link ($R(i)$). The total number of pre-computed routes is presented in the last column of Table 9-6, which increase in a similar way as the number of variables and constraints in the different topologies.

Concerning the number of iterations in ARCO-IL, we discussed that it depends on the quality of the initial point (ρ^{ini}). Interestingly, we found that ARCO-IL did not require more than three iterations in any experiment conducted on the DT, NSFNET or EON networks, proving the high precision of the expressions in equation (9.34) and (9.35).

The ARCO-IL method was implemented in iLog-OPL and solved by the CPLEX v.11.0 optimizer [CPLEX] on a 2.4 GHz Quad-Core machine with 8 GB RAM memory. Fig. 9-4 shows the obtained execution times for ARCO-IL as a function of the inter-arrival time to the test topologies.

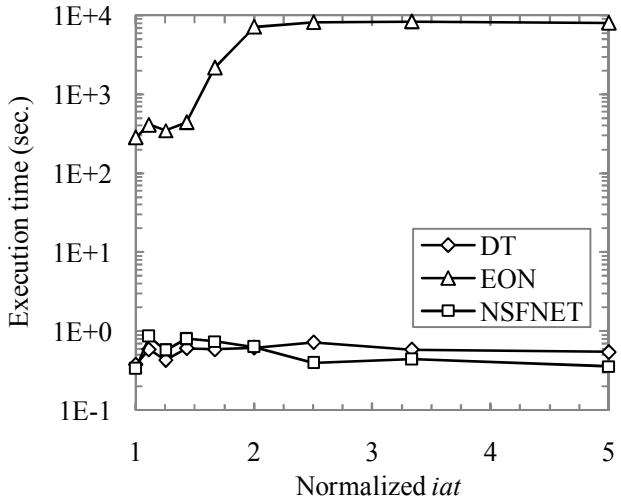

Fig. 9-4 ARCO-IL execution time as a function of the inter-arrival time.

From the obtained results, the execution times are in line with the size of the ARCO-IL instances. As seen, sub-second execution times are achieved in the DT and NSFNET topologies, whereas tens of minutes to several hours are required in the EON. Specifically, large execution time differences are observed in the EON between short and long inter-arrival times, where the feasible solutions are relatively reduced or numerous, respectively.

Fig. 9-5 shows the number of links in the optimal control plane topology as a function of the normalized *iat* in the DT, NSFNET, and EON topologies. Note that the y-axis of the graphs comprises the number of control plane links from the *minimal* to the *symmetrical* topology in each case. Moreover, each graph contains two separated plots, one for *RRq1* and another for *RRq2*. Looking at the results, the optimal control plane topology tends to be the *symmetrical* one for short inter-arrival times. Conversely, when the *iat* increases, the number of control plane links decreases, finally reaching the *minimal* topology.

Aiming to evaluate the actual cost reduction achieved by means of ARCO-IL, we have highlighted in Fig. 9-5 two particular ht values, ht = 30 min and ht = 60 min. As shown, the minimal control plane topology could be almost reached in the DT, NSFNET and EON networks for ht = 60 mins. This enables a reduction of 8, 8, and 18 control plane links, respectively. For ht = 30 min, since the connection *iat* is reduced, a quite lower reduction is achieved, enabling 6, 7 and 15 control plane links to be removed from the *symmetrical* topology for the most stringent requirements, respectively. Note that such savings are obtained in practical core network scenarios under high traffic loads, which makes them especially interesting.

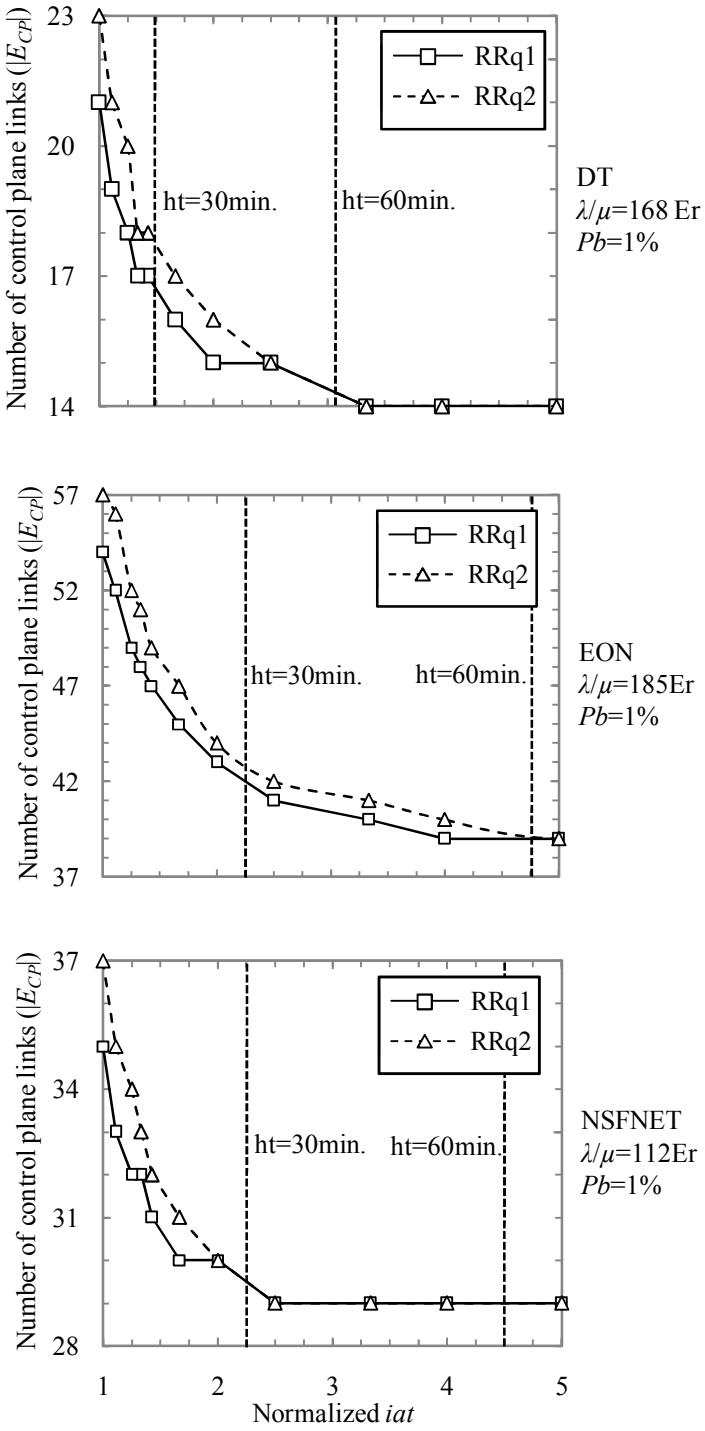

Fig. 9-5 Number of links in the optimal solution against *iat*.

As mentioned in the introduction, link reduction in the control plane may affect connection establishment and restoration times, since signaling messages must travel longer distances. In order to better assess the outcome of ARCO-IL, we have

quantified such increments using the equation proposed in [Ve10] for intra-domain restoration, which has been adapted to fit single domain scenarios. The obtained results in the DT, NSFNET and EON networks are depicted in Table 9-7, where the optimal partially-meshed topology resulting from ARCO-IL for *ht* = 30min is compared to the *symmetrical* and *minimal* topologies. As seen, the *symmetrical* topology provides the minimum restoration times as no link reduction is done.

Average restoration times under 50ms can be obtained only for the DT network as a consequence of the shorter link lengths; in contrast longer restoration times can be expected for the NSFNET and EON networks. The restoration times achieved in the partially-meshed topology, and even in the *minimal* topology, are still very reasonable, around 100 ms in the worst case. Note that restoration times under 50ms can be still obtained for the DT network over the *minimal* topology.

Table 9-7: Restoration Times

	Symmetrical	Partially meshed	Minimal
DT	35.33 ms	39.27 ms	40.32 ms
NSFNET	78.31 ms	94.39 ms	102.96 ms
EON	64.25 ms	75.74 ms	93.26 ms

Fig. 9-6 compares the expected P_d values by ARCO-IL to the ones obtained by simulation in the DT, NSFNET and EON networks for four different normalized *iat* values. Each graph contains two plots, one for each set of resilience requirements. As seen, the results validate the assumptions done and the model defined in this work, since most of the obtained values by ARCO-IL lie within the 95% confidence interval of the simulation results. Specifically, the ARCO-IL method chooses these topologies with expected P_d value as close as possible and below the threshold value. For large *iat* values, the optimal solution is limited by the set of constraints over the characteristics of the feasible topologies (basically the two-connected requirement), and the *minimal* topology is chosen. On the contrary, if no optimal solution is found, ARCO-IL selects the *symmetrical* topology as the best solution, although the P_d requirement cannot be satisfied. In particular, having a P_d value significantly below the threshold, a post-processing method can be additionally applied to relax the resilience requirements, as it will be presented later.

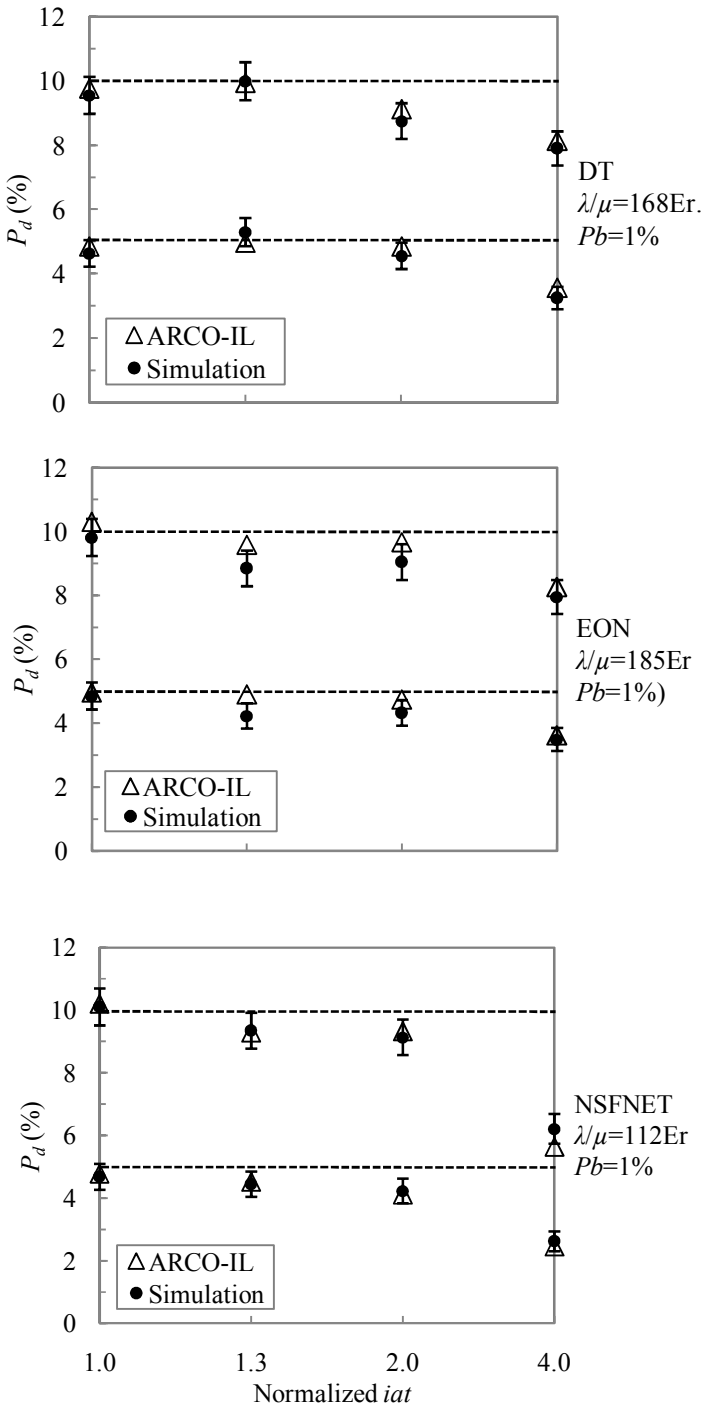

Fig. 9-6 P_d as a function of the *iat*

From the results in Fig. 9-6, a similar cost reduction is achieved no matter if *RRq1* or *RRq2* requirements are matched. However, extra links are needed in the optimal control plane topology to satisfy *RRq2*, even permitting a higher P_d value. Fig. 9-7

shows the explanation to this fact in the NSFNET topology. Remember that *RRq1* and *RRq2* have been defined as a tuple of P_d and Δt values.Therefore, providing the control plane recovery mechanism a specific Δt value, we can create more or less stringent requirements by modifying P_d accordingly, which finally results into different optimal control plane topologies. However, as P_d and Δt are related by equation (9.1), the final requested resilience to the network cannot be appreciated by comparing P_d and Δt independently. This has been illustrated in Fig. 9-7. Although *RRq1* seems to be more restrictive than *RRq2* when comparing the allowed P_d and Δt values independently, more links in the optimal control plane topology are needed for *RRq2*, as the overall requested resilience is higher in this case.

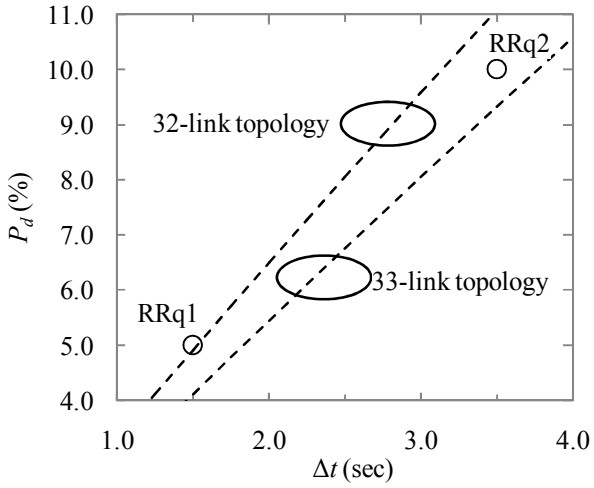

Fig. 9-7 P_d against Δt for two control plane networks over the NSFNET topology.

Finally, Fig. 9-8 addresses a sensitivity analysis of P_d against Δt in an optimal control plane topology. For this purpose, we have focused on the NSFNET topology with a normalized *iat* equal to 2.5. Assuming that the resilience requirements in *RRq2* have to be matched, ARCO-IL comes up with the depicted optimal control plane topology, where 8 control plane links are saved compared to the *symmetrical* one (dotted lines in the figure). This optimal control plane topology leads to $P_d \approx$ 8.5% for Δt = 3.5 s. Nevertheless, Δt can still be increased to 4.12 s before reaching the P_d=10% threshold, as observed in Fig. 9-8. This new Δt value may allow the deployment of simpler control plane recovery mechanisms, yielding reduced network costs while still matching the required control plane resilience.

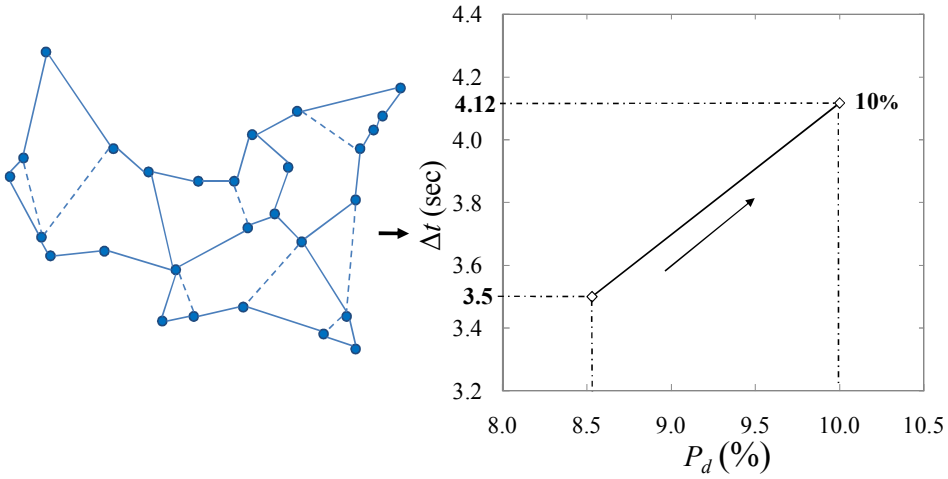

Fig. 9-8. Example of sensibility analysis (Δt against P_d) for the depicted topology.

9.4.2 Meta-heuristic results

The results of the GRASP-based heuristics were compared with the optimal solutions obtained with ARCO-IL. The heuristic has been implemented in Matlab and 2.4 GHz Quad-Core machines with 8 Gb RAM were used to run a wide execution set.

Aiming at determining the best value of α, we solved each instance 100 times with a low value of *itemax* given by the number of links of the data plane. Fig. 9-9 shows the average gap obtained for each α.

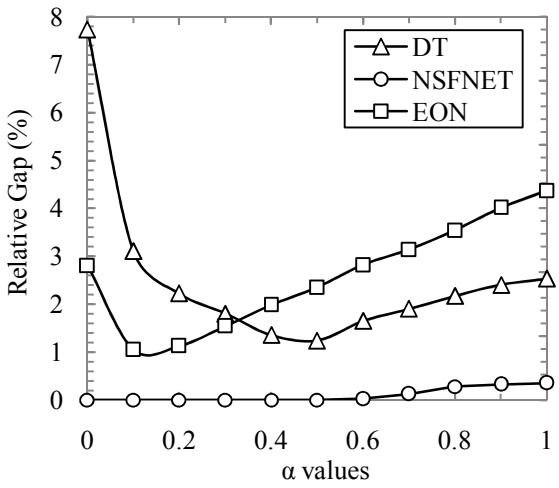

Fig. 9-9 Relative gap against α values, with *maxite*=|E_{DP}|

As illustrated, the best performance is obtained with α = 0.5 for the DT, α = 0 for the NSFNET. And α = 0.1 for the EON topologies respectively. In general, a low degree of randomness (i.e.: $\alpha \leq 0.3$) provides the best performance for large

networks. In fact, when the network has very low average nodal degree, the heuristic without randomized selection in the *constructive phase* provides the best performance (as observed in NSFNET). However, it is necessary to increase α when the size of the network is reduced (e.g.: DT topology), in order to allow enough amount of links in the *RCL*. The previous experiment has been repeated for different *itemax* values fixing α to the best configuration. Fig. 9-10 shows the average gap of the best 95% of repetitions for each tested *itemax*. Note that for *itemax* equal to 100 for the DT, 1 for the NSFNET, and 520 for the EON topologies respectively, the gap is equal to 0. Then, we conclude that our GRASP heuristic provides the optimal solution in every case.

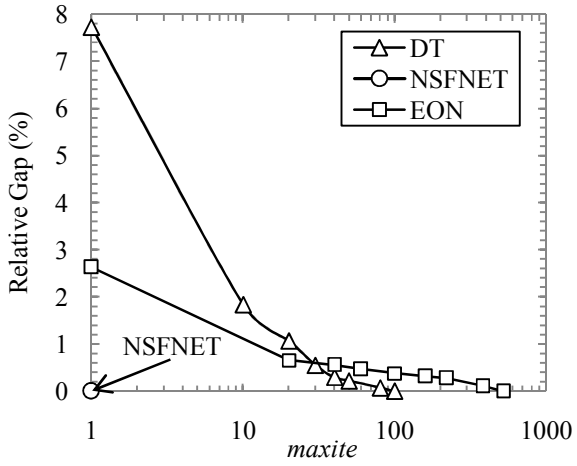

Fig. 9-10 Relative gap against *maxite* values, with optimal α values.

Fig. 9-11 shows the running times needed to reach the optimal solution and compares them with the obtained using CPLEX.

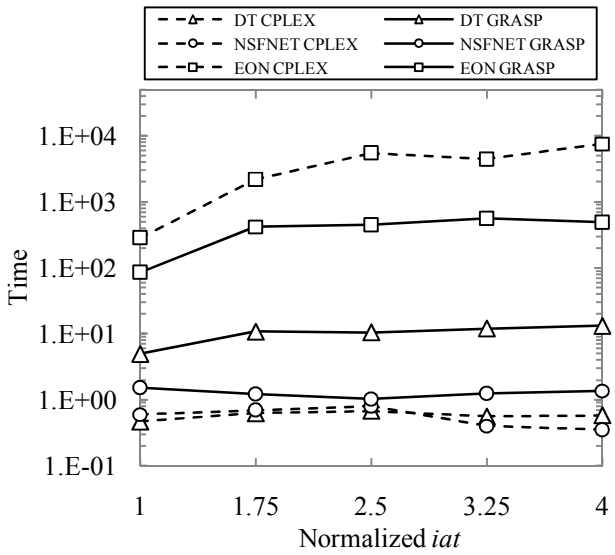

Fig. 9-11 Comparison between CPLEX and GRASP in terms of running time.

As illustrated, the heuristic provides affordable and scalable computational times in contrast with the obtained solving the ILP model. In fact, the computational time of the heuristic presents a polynomial increase with respect to the network size, in contrast with the exponential increase of the ILP model.

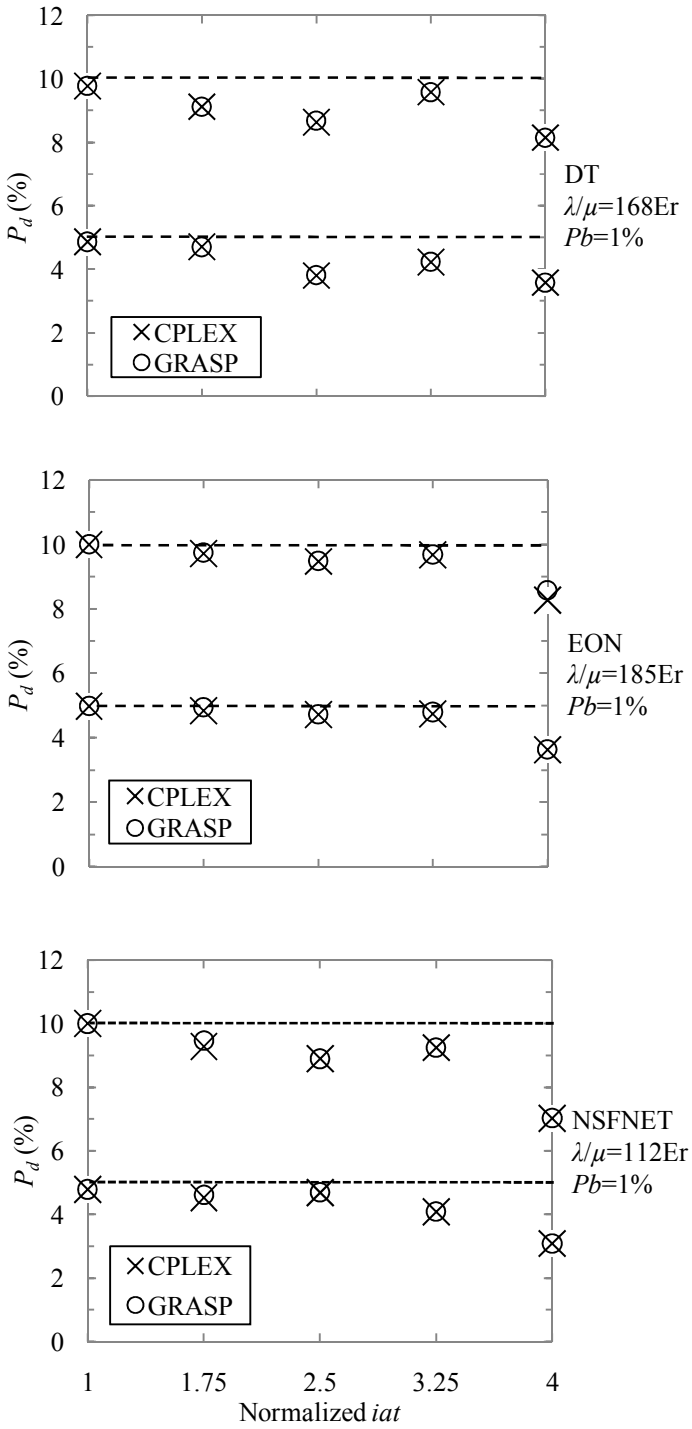

Fig. 9-12 Comparison between CPLEX and GRASP in terms of P_d minimization.

Finally, Fig. 9-12 shows the P_d values of each optimal topology, obtained solving ARCO-IL and with the heuristic. In just few cases the P_d value obtained with the heuristic is higher than the optimal value. Although the topologies contain the same number of links, this P_d difference entails that the topologies are slightly different. Nevertheless, the post-optimization process proposed in the previous section and illustrated in Fig. 9-8 can be also successfully applied as extension of the heuristic optimization.

9.5 Summary

This chapter addressed, for the first time, the design of the control plane topology in GMPLS-enabled transport networks. To this goal, two challenges were initially posed: firstly, the minimization of network CAPEX and OPEX derived from the provisioning, configuration and maintenance of control plane links; secondly, the fulfillment of the required control plane resilience to support future network services. Although a reduction of control plane links leads to lower network costs it increases however the amount of control information in the remaining control plane links, accentuating the negative effects of control plane link failures and leading to degraded network resilience performance. Therefore, control plane design methods that make a good trade-off between network cost and resilience are necessary.

Aiming to accurately compute the resilience in control plane mesh topologies, an analytical expression was proposed. From [Pe07], we extended the quantification of P_d for *asymmetrical out-of-band* mesh configurations. Experimental results validated the accuracy of the model for three reference backbone topologies.

Then, three models were proposed to solve the problem of obtaining the optimal GMPLS control plane topology given the data plane topology, a set of resilience requirements (quantified in terms of P_d and Δt) and the range of offered loads to the network. First of all, a non-linear combinatorial model of the problem (ARCO-CNL) was initially introduced. This model, however, offers a poor scalability as the network size grows up. Having this in mind, the problem was reformulated as a constructive linear model (ARCO-IL), providing optimal results with much lower execution times. Nevertheless, execution time increases exponentially with the problem size, since the problem is NP-hard. For these reason, we proposed a third method consisting of a GRASP-based meta-heuristic.

Into operation, ARCO-IL focuses on minimizing the average number of hops in the control plane for every data plane adjacent node pair, identified as τ. While P_d and P_L are non-linear functions, it was proved that τ becomes linear if the number of control plane links remains constant. In view of this, an iterative method was introduced in ARCO-IL, which modifies the number of control plane links per iteration. In order to provide an initial number of control plane links close to the

optimal one, that is, minimizing the number of iterations of the method, a two-step procedure that computes this value as a function of the objective P_d was also proposed.

The performance of ARCO-IL was extensively assessed over the three reference network topologies. From the obtained results, ARCO-IL leads to sub-second execution times in the DT and the NSFNET topologies. In the EON topology, however, even though the execution times increased significantly due to the huge network dimensions, they were still bearable. Aiming to quantify the actual cost savings achieved by applying ARCO-IL, the reduction in terms of control plane links in the optimal control plane topology against the *symmetrical* one was obtained for the DT, NSFNET and EON networks. From 6 to 15 control plane links can be reduced in high load scenarios (Pb=1%), while still meeting the required control plane resilience.

A side effect of reducing the number of control plane links can be an increment of the connection establishment times, which may be particularly critical if control-plane-driven restoration for data plane recovery is implemented. Nonetheless, we found that the restoration times over the optimal control plane topology were not highly increased compared to the *symmetrical* one, remaining below 100 ms in the three reference network topologies. As a final result, a sensitivity analysis was conducted on the optimal control plane topology provided by ARCO-IL to relax, if still possible, the control plane failure recovery time to be achieved by the control plane recovery mechanism without exceeding the specified resilience thresholds. In fact, more relaxed control plane recovery requirements opens the deployment of simpler and, thus, cheaper control plane recovery mechanisms, reducing in this way the network costs even more.

In order to obtain good-quality solutions in less computational time than ARCO-IL, we presented a GRASP-based meta-heuristic. After tuning some heuristic parameters, the best configuration has been used to solve a set of instances using two well-known backbone optical networks. The performance of the proposed heuristic has been compared with exact results obtained with ARCO-IL instances solved by CPLEX. Our heuristic algorithm provided the optimal solution for every instance and non-significant differences in terms of P_d were detected. Moreover, regarding computational time, our heuristic needed just some seconds to few minutes to provide the optimal solution, in contrast with the time, several orders of magnitude higher, needed by CPLEX.

In light of these results, we conclude that ARCO considerably reduces the CAPEX of the control plane, by reducing the number of links. The effect of this link reduction over the data plane recovery can be considered negligible. Moreover, we conclude that the proposed GRASP-based heuristic is the most efficient method to solve ARCO, providing an excellent trade-off between solution quality and computational effort.

Chapter 10

Closing discussion

10.1 Main contributions

This section summarizes the main contributions and conclusions of each of the goals developed in this thesis.

We started at the physical layer, where we provided a statistical methodology to compute the Q-factor for solving IA-RWA problems. More specifically, we provided two statistical models to compute the XPM variance that allow efficiently solving on-line and off-line IA-RWA problems. First, we presented an accurate polynomial model that can be used in on-line IA-RWA problems, providing negligible Q-factor computation times compared with the analitycal XPM procedure which needs even seconds for each Q-factor computation. Second, we presented a linear method that can be used in MILP formulations of off-line IA-RWA problems. Although the goodness-of-fit of this linear model is slightly lower than that of the polynomial one, the linear model is valid enough to estimate XPM values without significant error. Finally, we proved that both models provide accurate Q-factor values in real traffic scenarios.

Moving to the optical layer and aiming at improving the GoS of extra traffic in SPP environments, we presented a new wavelength partitioning scheme (*diff-sw*) that allows maximizing the amount of BE service provided (without affecting the GoS of the main SP service) with respect to the current scheme (*sh-sw*). To evaluate both schemes, we first defined several statistical models to estimate the amount of service (traffic intensity) that a network can support without violating a target GoS. Taking advantage of the intensity statistical models, we defined three different network planning problems to analyze the performance of the partitioning schemes: i) the NORMA problem, that returns the partitioning scheme which maximizes the expected revenues; ii) the NORMA++ problem that returns the 165ortioning scheme and the topology that maximizes the expected revenues; and iii) the OVALO problem that returns the partitioning scheme and the topology that

maximizes the expected NPV. Solving these problems for real backbone networks, we concluded that our proposed diff-WS maximizes both revenues and NPV.

In multilayer networks, we presented the SIMULTANEO problem as a hierarchical survivable IP/MPLS-over-WSON network planning problem. With this problem, we tackled the design of multilayer networks against single failures at the IP/MPLS layer (i.e.: IP/MPLS node and OE port), as well as single failures at WSON links. To efficiently solve SIMULTANEO, we proposed a new approach (*joint* approach) based on over-dimensioning IP/MPLS devices and lighpath connectivity and recovery. This approach differs from the conventional solution (*overlay* approach) which is based on duplicating backbone IP/MPLS nodes. After evaluating both approaches by means of ILP models and BRKGA-based heuristic algorithms, we concluded that our proposed joint approach leads to significant CAPEX savings (up to 24%) compared with the overlay approach. Moreover, OPEX and energy savings are also expected with the joint approach, since the number of IP/MPLS nodes and the number of switched-on O/E ports is lower with respect to the overlay approach.

In addition, we introduced the ORO problem as an adaptive mechanism to reduce the usage of O/E ports of IP/MPLS-over-WSON multilayer networks in dynamic scenarios. To solve ORO, an ILP formulation and several GRASP-based heuristics were developed and used to solve real-size instances generated by simulation. After validating the quality of the heuristics against the model, we concluded that the ORO problem allows reducing the usage of O/E ports in up to 50%. Finally, we chose the best heuristic algorithm in terms of complexity, computational time, and optimality gap and we implemented it in the NMS of the ASON/GMPLS CARISMA test-bed, obtaining the same performance that that anticipated by simulation results but with very reduced computational times.

Finally, we addressed the design of resilient control plane topologies in GMPLS-enabled transport networks. In a first stage and aiming at accurately quantifying the resilience in control plane mesh networks, we proposed a novel analitycal model to quantify the network variable P_d which was previously proposed for resilience quantification in ring networks. After validating the accuracy of the model with experimental results over real backbone topologies, we defined the ARCO problem to design the topology of the control plane. The ARCO problem aims to reduce the number of control plane links (i.e.: control plane CAPEX) without violating some given resilience requirements. To solve ARCO, we proposed an exact iterative linear method based on an ILP formulation which allows concluding, after an exhaustive performance evaluation, that a significant reduction in the number of control plane links can be performed for real backbone topologies and traffic scenarios. Nevertheless, since the scalability of this method is slightly poor for large networks, we proposed a GRASP-based meta-heuristic to solve ARCO. After comparing heuristic results against exact ones, we concluded that the heuristic provides optimal results with lower computational effort.

Therefore, the main goals of this thesis have been successfully achieved.

10.2 Publications

10.2.1 Journals

[CL12] **M. Ruiz**, L. Velasco, P. Monti, and L. Wosinska, "A Linearized Statistical XPM Model for Accurate Q-factor Computation", IEEE Communications Letters, 16, 1324-1327, 2012.

[JOCN12] L. Velasco, A. Jirattigalachote, **M. Ruiz**, P. Monti, L. Wosinska, and G. Junyent, "Statistical Approach for Fast Impairment-Aware Provisioning in Dynamic All-Optical Networks", IEEE/OSA Journal of Optical Communications and Networking (JOCN), 4, 2012.

[COR11] O. Pedrola, **M. Ruiz**, L. Velasco, D. Careglio, O.Gonzalez de Dios, and J. Comellas, "A GRASP with path-relinking heuristic for the survivable IP/MPLS-over-WSON multi-layer network optimization problem," Elsevier Computers & Operations Research (COR) (In press), 2011.

[JOCN11.1] **M. Ruiz**, O. Pedrola, L. Velasco, D. Careglio, J. Fernández-Palacios, and G. Junyent, "Survivable IP/MPLS-over-WSON Multilayer Network Optimization," IEEE/OSA Journal of Optical Communications and Networking (JOCN), 3, 629-640, 2011.

[JOCN11.2] L. Velasco, **M. Ruiz**, J. Perelló, S. Spadaro, and J. Comellas, "Service and Resource Differentiation in Shared-Path Protection Environments to Maximize Network Operator's Revenues", IEEE/OSA Journal of Optical Communications and Networking (JOCN), 3, 117-126, 2011.

[JLT11] **M. Ruiz**, J. Perelló, L. Velasco, S. Spadaro, J. Comellas, and G. Junyent, "GMPLS Control Plane Network Design with Resilience Guarantees", IEEE/OSA Journal of Lightwave Technology (JLT), 29, 37-47, 2011.

[JN10] F. Agraz, L. Velasco, J. Perelló, **M. Ruiz**, S. Spadaro, G. Junyent, and J. Comellas, "Deployment and Validation of GMPLS-Controlled Multi-layer Integrated Routing over the ASON/GMPLS CARISMA Test-bed", Journal of Networks, 5, 1321-1327, 2010.

[CL09] **M. Ruiz**, J. Perelló, L. Velasco, S. Spadaro, and J. Comellas, "An Analytical Model for GMPLS Control Plane Resilience Quantification", IEEE Communications Letters, 13, 977-979, 2009.

[JOCN09] F. Agraz, L. Velasco, J. Perelló, **M. Ruiz**, S. Spadaro, G. Junyent, and J. Comellas, "Design and Implementation of a GMPLS-Controlled Grooming-capable Optical Transport Network", IEEE/OSA Journal of Optical Communications and Networking

(JOCN), 1, A258-A269, 2009.

10.2.2 Conferences and workshops

[ICC12] C. Cavdar, **M. Ruiz**, P. Monti, L. Velasco, and L. Wosinska, "Design of Green Optical Networks with Signal Quality Guarantee", Accepted in IEEE International Conference on Communications (ICC), 2012.

[DRCN11] **M. Ruiz**, L. Velasco, J. Comellas, G. Junyent, "Optical Network Net Present Value Optimization in Shared Path Protection Environments", *Design of Reliable Communication Networks* (DRCN), 2011.

[ICTON11.1] L. Velasco, **M. Ruiz**, J. Comellas, G. Junyent, "NORMA: Network Operator Revenues Maximization", *International Conference on Transparent Optical Networks* (ICTON), 2011.

[ICTON11.2] **M. Ruiz**, L. Velasco, G. Junyent, J. Comellas, "A GRASP-based heuristic to design the GMPLS control plane network topology with resilience guarantees", *International Conference on Transparent Optical Networks* (ICTON), 2011.

[WGN10] C. Cid, **M. Ruiz**, L. Velasco, and G. Junyent, "Costs and Revenues Models for Optical Networks Architectures Comparison", *IX Workshop in G/MPLS Networks*, 2010.

[ICTON09] F. Agraz, L. Velasco, J. Perelló, **M. Ruiz**, S. Spadaro, G. Junyent, and J. Comellas, "An Experimental GMPLS-Controlled Network Test-bed Enabling Sub-Wavelength Connection Provisioning", *International Conference on Transparent Optical Networks* (ICTON), 2009.

[NOC09] **M. Ruiz**, L. Velasco, S. Spadaro, J. Comellas, and G. Junyent, "Resources optimization in GMPLS-based optical multilayer networks", *European Conference on Networks and Optical Communications* (NOC), 2009.

[JTID+09] **M. Ruiz**, L. Velasco, S. Spadaro, J. Comellas, and G. Junyent, "Optimización de Recursos en Redes de Transporte Ópticas Multicapa", *Jornadas Telecom I+D*, 2009.

10.2.3 Others

[UPC11] **M. Ruiz**, L. Velasco, P. Monti, and L. Wosinska, "Fast and

Accurate Statistical Q-factor computation for impairment-aware RWA problems", Universitat Politecnica de Catalunya (UPC), Tech. Rep. UPC-DAC-RR-CBA-2011-7, September 2011.

[UPC10] L. Velasco, **M. Ruiz**, and C. Cid, "Maximización del Valor Actual Neto en Redes Ópticas", Universitat Politècnica de Catalunya, ISBN 978-84-693-5523-7, 2010.

10.3 National and European research projects

Part of the material presented in this thesis has been developed within the framework of the following National and European research projects:

- STRONGEST: "Scalable, Tunable and Resilient Optical Networks Guaranteeing Extremely-high Speed Transport", FP7 n° 247674, 2010-2012.
- ENGINE: "Engineering Next Generation Optical Transport Networks", TEC2008-02634, 2009-2011.
- DICONET: "STREP – Dynamic Impairment Constraint Networking for Transparent Mesh Optical Networks", FP7 nº 216338, 2008-2010.
- BONE NoE: "Building the Future Optical Network in Europe: The e-Photon/One Network", FP7 nº 216338, 2008-2010.
- PAIS: "Plataforma Avanzada Integrada de Servicios", 2009-2010.

10.4 Topics for further research

10.4.1 Flexgrid optical network optimization problems

One of the main characteristics and, at the same time, limitation of DWDM optical networks is that they operate within a rigid frequency grid where each one of the wavelengths supports high-speed streams (up to 100 Gbps). As previously introduced, this lack of flexibility is overcome by means of a client aggregation layer that grooms low-speed traffic streams into lightpaths with the aim to provide high bandwidth usage.

With the future advent of flexible frecuency grid (*flexgrid*, [Li11]) networks, a high degree of flexibility will be introduced in the optical layer and, consequently, the spectral resources will be used more efficiently. Without entering into details, in a flexgrid optical network the optical frequency spectrum is divided into narrow frequency slices and each lightpath is determined by its routing path and a subset of these slices, depending on the requested bandwidth and some characteristics of

the transmitted signal. In this context the role played by the client aggregation layer should be redefined since the subjacent optical layer includes newer flexibility capabilities. Thus, new issues in the design of IP/MPLS-over-Flexgrid multilayer networks are opened for future research.

Moreover, this flexibility allows not only supporting lightpaths with heterogeneous allocated spectrum size but also opens the possibility to adapt the allocated spectrum to bandwidth fluctuations in time. For these reasons, the research in dynamic scenarios with bandwidth-variable demands will represent a hot topic in network design and management.

10.4.2 Decomposition methods for large-scale problems

In this thesis, optimization methods such as ILP-based iterative procedures and meta-heuristics to solve real-size instances have been proposed. Nevertheless, the increasing complexity of future network planning problems (with flexgrid networks, time-dependent demands) directs towards the development of more powerful optimization methods. Among those methods, decomposition and relaxation methods such as Lagrangian relaxation, Benders decomposition, or column generation [Ah93, De05] will be more important in future research to obtain meaningful solutions for real size scenarios. Although those procedures are general frameworks that can be applied to a great range of optimization problems, each specific application needs specific mathematical development and implementation, so that research opportunities are plentiful in this area.

Appendix A. **List of topologies used for evaluation**

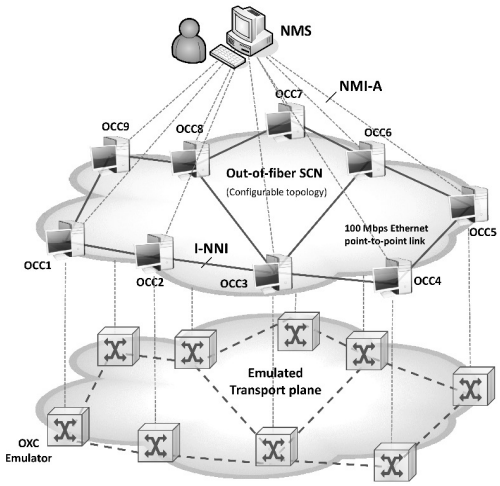

Fig. 1 CARISMA_9n_11e

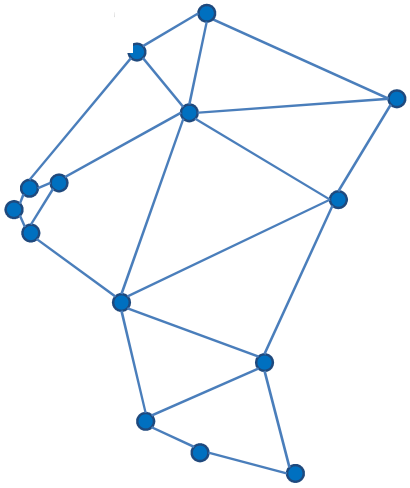

Fig. 2 DT_14n_23e

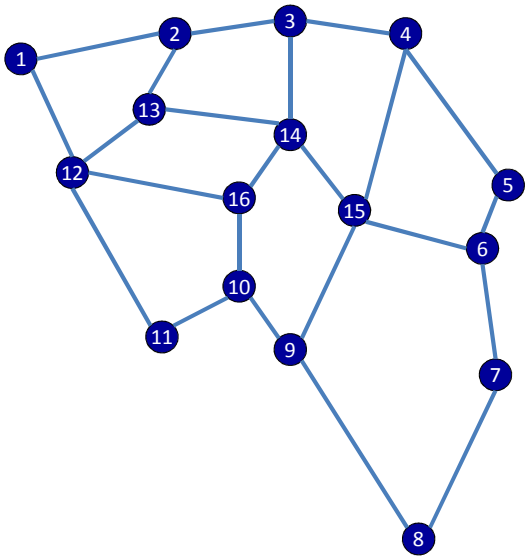

Fig. 3 EON_16n_23e

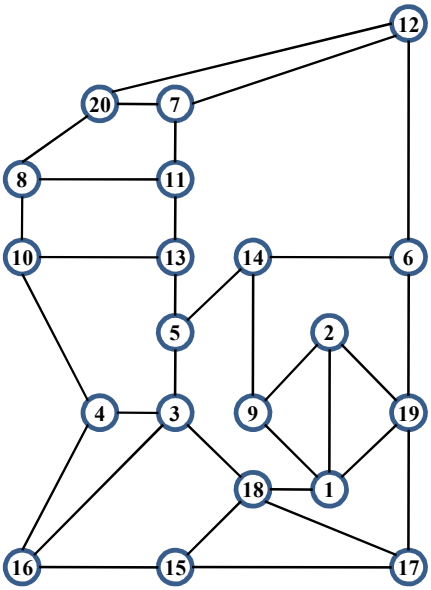

Fig. 4 BT_20n_32e

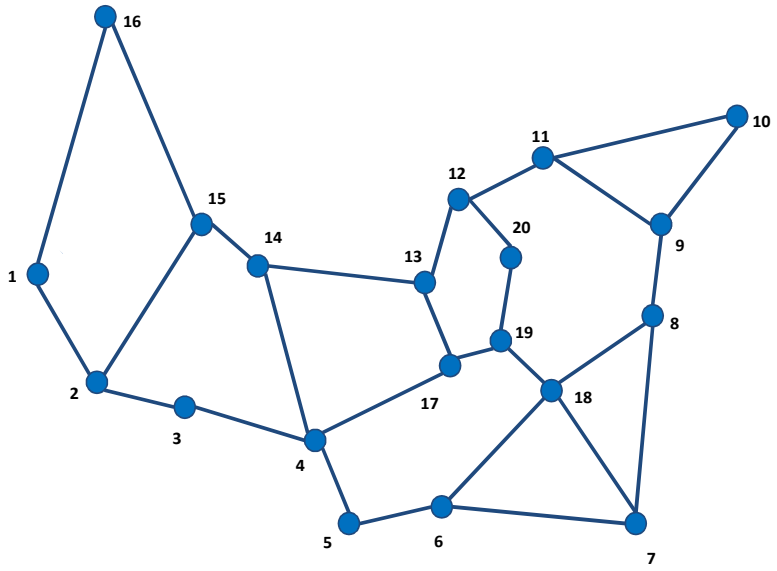

Fig. 5 NSFNET_20n_28e

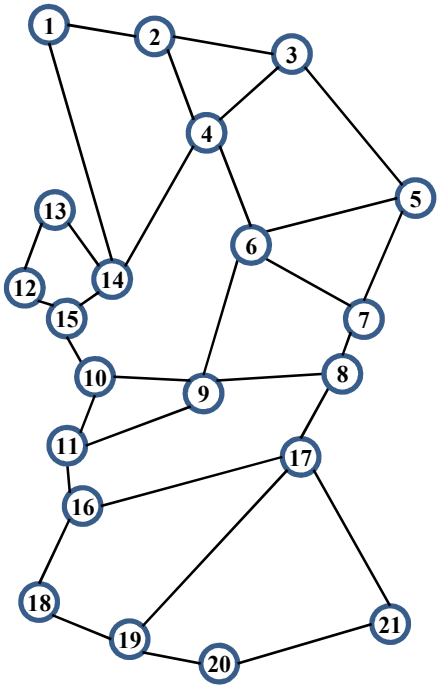

Fig. 6 DT_21n_31e

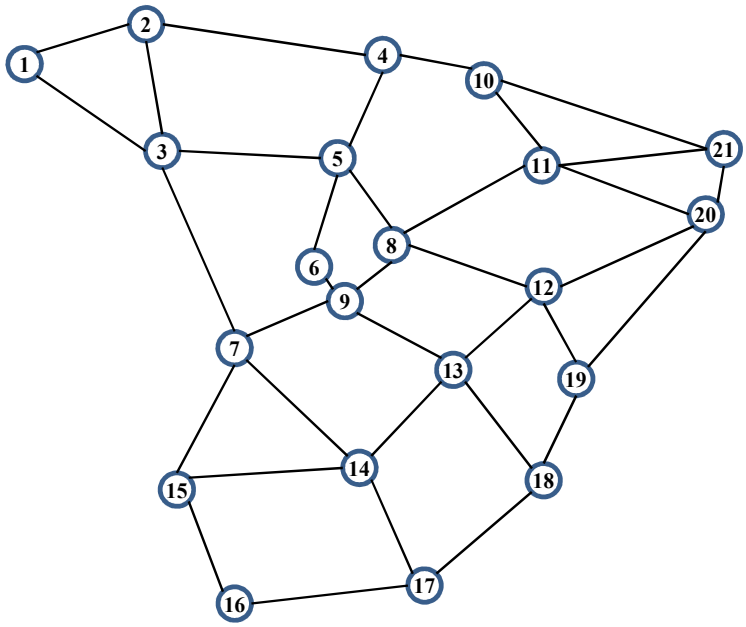

Fig. 7 TEL_21n_34e

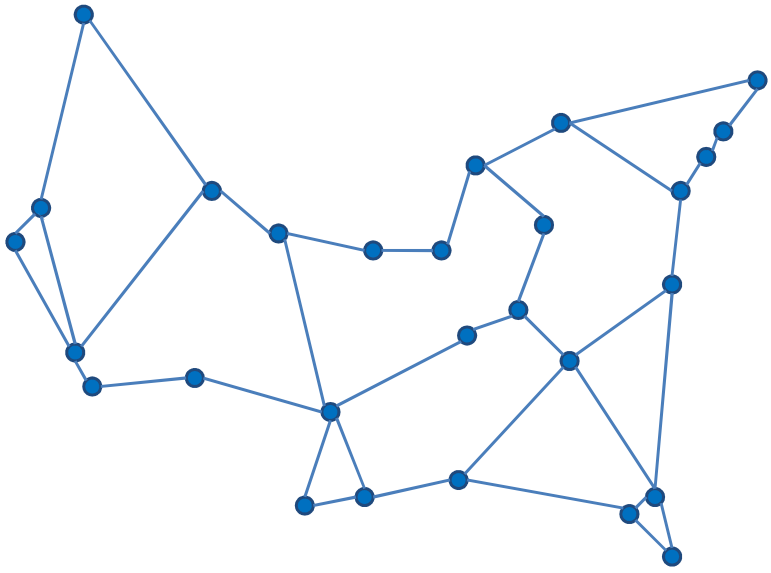

Fig. 8 NSFNET_28n_37e

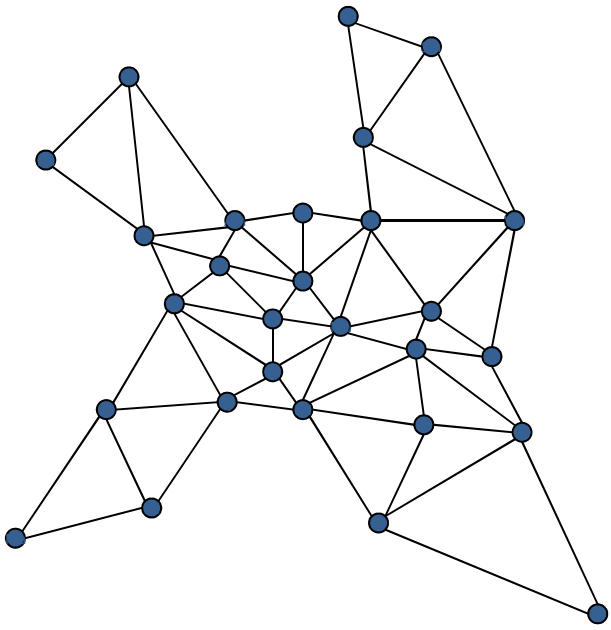

Fig. 9 EONTT_28n_61e

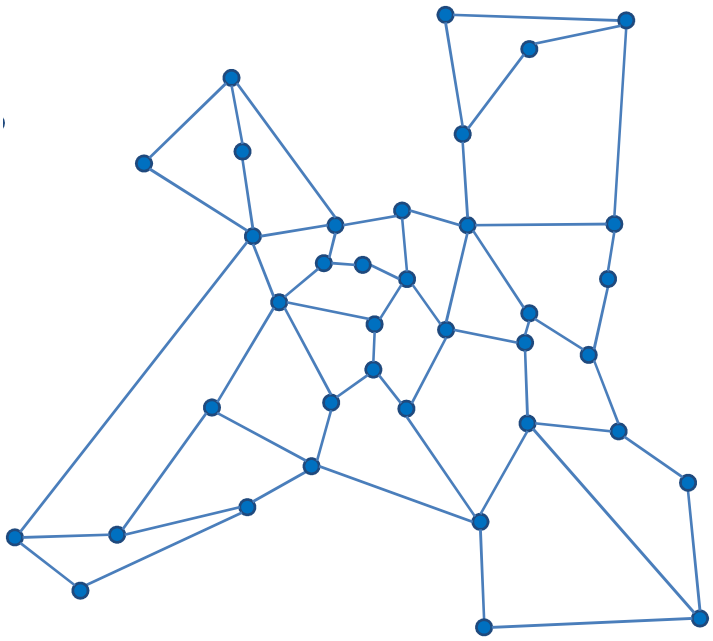

Fig. 10 EONLT_37n_57e

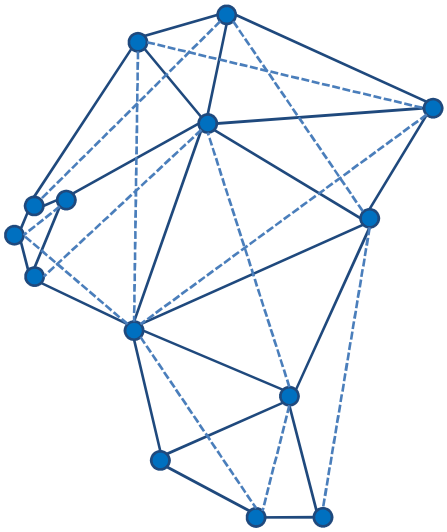

Fig. 11 DT SERIES

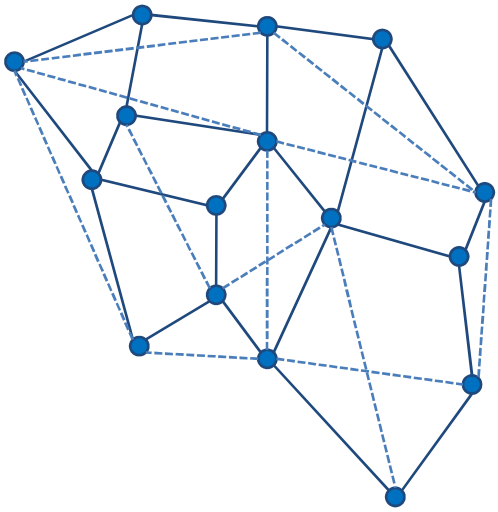

Fig. 12 EON SERIES

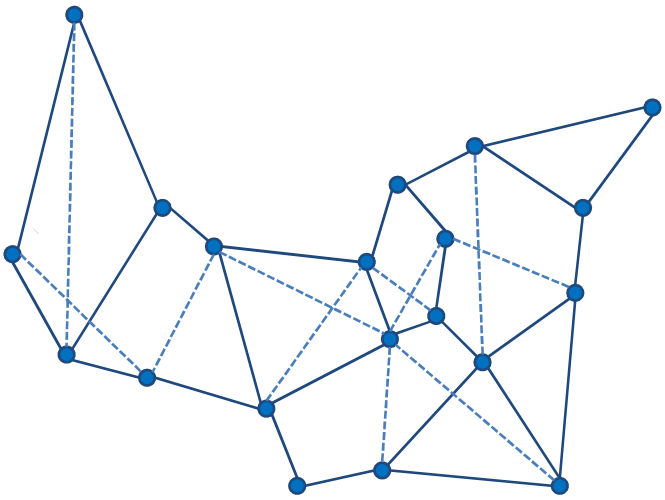

Fig. 13 NSFNET SERIES

List of Acronyms

AIC	Akaike Information Criterion
ARCO	Resilience-aware GMPLS control plane network optimization
ASE	Amplifier Spontaneous Emission
ASON	Automatically Switched Optical Network
BE	Best Effort
BRKGA	Biased Random Key Genetic Algorithm
BT	British Telecom
CAFES	Compute A Feasible Solution
CAPEX	CAPital Expenditures
CCABA	Centre de Comunicacions Avançades de Banda Ampla
	(Advanced Broadband Communications Center)
CD	Chromatic Dispersion
CWDM	Coarse Wavelength Division Multiplexing
diff-WS	Differentiated Wavelength Set
DPP	Dedicated-Path Protection
DT	Deutsche Telekom
DWDM	Dense Wavelength Division Multiplexing
EON	European Optical Network
FA	Forwarding Adjacencies
FCAPS	Failure management, Configuration management, Accounting, Performance management, and Security
FF	Flow Formulation
FSC	Fiber Switched Capable
FWM	Four-Wave Mixing

GA	Genetic Algorithm
Gbps	Gigabit per second
Ghz	Gigahertz
GLM	Generalized Linear Model
GMPLS	Generalized Multiprotocol Label Switching
GoS	Grade of Service
GRASP	Greedy Randomized Adaptative Search Procedure
GRWA	Grooming, Routing and Wavelength Assignment
GVD	Group Velocity Dispersion
HDTV	High Definition Television
ht	Holding Time
IA-RWA	Impairment-aware Routing and Wavelength Assignment
iat	Inter-Arrival Time
IEEE	Institute of Electrical and Electronics Engineers
IETF	Internet Engineering Task Force
ILP	Integer Linear Programming
IP	Internet Protocol
ITU-T	International Telecommunication Union–Telecommunication Standardization Sector
LM	Linear Model
LP	Linear Programming
LR	Lightpath Rerouting
LRRA	Lightpath Rerouting Algorithm
LSC	Lambda Switched Capable
LSP	Label Switched Path
MILP	Mixed Integer Linear Programming
MOLC	Minimum Overlap wavelength to LeastCongested wavelength
MP	Mathematical Programming
MPLS	Multiprotocol Label Switching
MSE	Mean Squared Error
MTV-WR	Move-To-Vacant Wavelength Retuning

NLP	Non-Linear Programming
NMS	Network Management System
NORMA	Network Operator Revenues Maximization
NPV	Net Present Value
NSFNET	National Society Foundation NETwork
O/E/O	Optical-to-electrical-to-optical
OE	Opto-electronic
OPEX	Oprational EXpenditures
ORO	Optical Resources Optimization
OSA	Optical Society of America
OTN	Optical Transport Network
OVALO	Optical etwork net present value optimization
OXC	Optical Cross-Connect
PLI	Physical Layer Impairments
PMD	Polarization Mode Dispersion
PSC	Packet Switched Capable
QoS	Quality of Service
RCL	Restricted Candidate List
RF	Route Formulation
RFC	Request For Comments
RFWA	Routing, Fiber, and Wavelength Assignment
RSVP-TE	Resource Reservation Protocol – Traffic Engineering
RWA	Routing and Wavelength Assignment
SDH	Synchronous Digital Hierarchy
SF	Source Formulation
sh-WS	Shared Wavelength Scheme
SIMULTANEO	Survivable IP/MPLS-over-DWDM network optimization
SLA	Service Level Agreement
SONET	Synchronous Optical Networking
SP	SPP-based Protected
SPM	Self-Phase Modulation

SPP	Shared-Path Protection
SPWRR	Shortest Path Wavelength ReRouting
STRONGEST	Scalable, Tunable and Resilient Optical NetworksGuaranteeing Extremely-high Speed Transport
TDMC	Time-Division Multiplexing Capable
UPC	Universitat Politècnica de Catalunya
	(Technical University of Catalonia)
VT	Virtual Topology
VTD	Virtual Topology Design
VTR	Virtual Topology Reconfiguration
VWP	Virtual Wavelength Path
WDM	Wavelength Division Multiplexing
WP	Wavelength Path
WSON	Wavelength-Switched Optical Networks
WSS	Wavelength Selective Switches
XPM	Chross-phase Modulation

References

[Ah93] R. K. Ahuja, T. L. Magnanti, and J. B. Orlin, *Network Flows: Theory, Algorithms and Applications*, Prentice Hall, 1993.

[Ak06] I. Akgun, F. Buzluca, "Virtual topology reconfiguration on optical WDM networks considering traffic grooming," Optical Switching and Networking, vol.3, pp.11–23, 2006.

[Al00] M. Ali, B. Ramamurthy, and J.S. Deogun, "Routing and wavelength assignment with power considerations in optical networks," Computer Networks, vol. 32, pp. 539-555, 2000.

[Al05] A.Alyatama, "Wavelength decomposition approach for computing blocking probabilities in WDM optical networks without wavelength conversions," Computer Networks, vol.49, pp. 727–742, 2005.

[Az09] S. Azodolmolky, M. Klinkowski, E. Marín, D. Careglio, J. Solé-Pareta, and I. Tomkos, "A Survey on Physical Layer Impairments Aware Routing and Wavelength Assignment Algorithms in Optical Networks," Computer Networks, vol. 53, pp. 926-944, 2009.

[Ba00] D. Banerjee and B. Mukherjee, "Wavelength-routed optical networks: Linear formulation, resource budgeting tradeoffs and a reconfiguration study," IEEE/ACM Transactions on Networking, pp. 598-607, Oct. 2000.

[Ba01] I. Baldine and G. N. Rouskas, "Traffic adaptive WDM networks: A study of reconfiguration issues," Journal of Lightwave Technology, vol. 19, pp. 433–455, Apr. 2001.

[Ba96.1] D. Banerjee and B. Mukherjee, "A practical approach for routing and wavelength assignment in large wavelength-routed optical networks," IEEE Journal on Selected Areas in Communications, pp. 903-908, Jun. 1996.

[Ba96.2] K. Bala, G. Ellinas, M. Post, S. Chien-Chung, J. Wei, and N. Antoniades, "Toward hitless reconfiguration in WDM optical networks for ATM transport," in Proc. IEEE GLOBECOM, 1996, pp. 316–320.

[Ba96.3] R. Barry and P. Humblet, "Models of Blocking Probability in All-Optical Networks with and Without Wavelength Changers," IEEE Journal on Selected Areas in Communications, vol. 14, no. 5, Jun.

1996.

[Be08] P. Belotti, A. Capone, G. Carello, and F. Malucelli, "Multi-layer MPLS network design: The impact of statistical multiplexing," Computer Networks, vol. 52, pp.1291-1307, 2008.

[Bh99] R. Bhandari, *Survivable Networks: Algorithms for Diverse Routing*, Kluwer Academic Publishers, 1999.

[Bi96] A. Birman, "Computing approximate blocking probabilities for a class of all optical networks," IEEE Journal on Selected Areas in Communications, vol.13, pp. 852–857, Jun. 1996.

[Bl03] C. Blum and A. Roli, "Metaheuristics in combinatorial optimization: Overview and conceptual comparison," ACM Computing Surveys, vol. 35, Issue 3, pp. 268-308, Sep. 2003.

[Ca07] D. R. Campelo, R. C. Almeida, and H. Waldman, "Analytical calculation of blocking probabilities in WDM rings with the first-fit algorithm," Photonic Network Communications, vol. 14, no. 2, pp. 177-181, July 2007.

[Ca98] B.V. Caenegem, W. V. Parys, F.D. Turck, and P.M. Deemester, "Dimensioning of survivable WDM networks," IEEE Journal on Selected Areas in Communications, pp. 1146-1157, Sep. 1998.

[Ca99] A. Cartaxo, "Cross-Phase Modulation in Intensity Modulation-Direct Detection WDM Systems with Multiple Optical Amplifiers and Dispersion Compensators," IEEE/OSA Journal of Lightwave Technology, vol.17, pp.178-190, 1999.

[Ch01] A. Chiu and J. Strand, "Joint IP/optical layer restoration after a router failure," in Proc. OFC 2001, Anaheim, CA, USA, Mar. 2001.

[Ch03] C. Chigan, G. W. Atkinson, and R. Nagarajan, "Cost effectiveness of joint multilayer protection in packet-over-optical networks," *IEEE/OSA* Journal of Lightwave Technology, vol. 21, pp. 2694-2704, Nov. 2003.

[Ch04] G. Chiruvolu, A. Ge, D. Elie-Dit-Cosaque, M. Ali, and J. Rouyer, "Issues and approaches on extending Ethernet beyond LANs," IEEE Communications Magazine, vol. 42, pp. 80-86, Mar. 2004.

[Ch07] X. Chu, T. Bu, and X. Li, "A study of lightpath rerouting schemes in wavelength-routed WDM networks," in Proc. IEEE Int. Conf. Communications, Glasgow, UK, 2007.

[Ch08] B. Chen, G. Rouskas, and R. Dutta, "On Hierarchical Traffic Grooming in WDM Networks," IEEE/ACM Transactions on Networking, 16, pp. 1226-1238, 2008.

[Ch10.1] B. Chen, G. Rouskas, and R. Dutta, "Clustering Methods for Hierarchical Traffic Grooming in Large-Scale Mesh WDM Networks," Journal of Optical Communications and Networking, vol. 2, pp. 502-514, 2010.

[Ch10.2] P. Cholda and A. Jajszczyk, "Recovery and its quality in multilayer networks," IEEE/OSA Journal of Lightwave Technology, vol. 28, pp. 372-389, Feb. 2010.

[Ch83] V. Chvatal, *Linear Programming*, Ed. Freeman, 1983.

[Ch92] I. Chamtlac, A. Ganz, and G. Karmi, "Lighpath communications: An approach to high-bandwidth optical WAN's," IEEE/ACM Transactions on Networking, vol. 40, no. 7, pp. 1172-1182, Jul. 1992.

[Ch97] R. Christensen, "Log-Linear Models and Logistic Regression", Springer Texts in Statistics, New York, 1997.

[CPLEX] IBM ILOG CPLEX, http://www-01.ibm.com/software/integration/optimization/cplex-optimizer/

[De05] G. Desaulniers, J. Desrosiers, and M. Solomon, *Column Generation*, Springer, 2005.

[Di07] D. Din, "A genetic algorithm for solving virtual topology configuration transition problem in WDM network," Computer Communications, vol. 30, issue 4, pp. 767-781, 2007.

[Fe95] T. Feo and M. Resende, "Greedy Randomized Adaptive Search Procedures," Journal of Global Optimization, Vol. 51, pp.109-133, Jun. 1995.

[Fo02] A. Forsgren, P. E. Gill, and M. H. Wright, "Interior Methods for Nonlinear Optimization," Society for Industrial and Applied Mathematics Review, vol. 44, no. 4, pp. 525–597, 2002.

[Fr73] L. Fratta, M. Gerla, and L. Kleinrock, "The Flow Deviation Method: An Approach to Store-and-forward Network Design," Networks vol. 3, pp 97-133, 1973.

[G.8080] ITU. Rec. G.8080/Y.1304: Architecture for the automatically switched optical network (ASON), International Telecommunication Union, ITU-T, November 2001.

[Ge03] A.Gençata and B. Mukherjee, "Virtual-Topology Adaptation for WDM Mesh Networks Under Dynamic Traffic," IEEE/ACM Transactions on Networking, vol. 11, no. 2, Apr. 2003.

[Gi83] A. Girard and S. Hurtubise, "Dynamic routing and call repacking in circuit-switched networks," IEEE Transactions on Communications, vol. 31, no. 12, pp.1290–1294, 1983.

[Gl03] F. Glover and F. Kochenberger, *Handbook of metaheuristics*, International Series in Operations Research & Management Science, Springer, 2003.

[Go10] J. Gonçalves and M. Resende, "Biased random-key genetic algorithms for combinatorial optimization," J. Heuristics, in press, on-line Aug. 2010.

[Gr01] A. Grosso, E. Leonardi, M. Mellia, and A. Nucci, "Logical Topologies

Design over WDM Wavelength Routed Networks Robust to Traffic Uncertainties," IEEE Communications Letters, vol.5, no.4, pp.172-174, Apr. 2001.

[Gr03] W. Grover, "Mesh-based Survivable Transport Networks: Options and Strategies for Optical, MPLS, SONET and ATM Networking," Prentice Hall, 2003.

[Gu04] G. Maier, A. Pattavina, L. Barbato, F. Cecini and Mario Martinelli, "Routing Algorithms in WDM Networks under Mixed Static and Dynamic Lambda-Traffic", Photonic Network Communications, vol. 8, no. 1, pp. 69-87, 2004.

[Gu06] L. Guo, J. Cao, H. Yu, L. Li, "Path-Based Routing Provisioning With Mixed Shared Protection in WDM Mesh Networks", IEEE Journal of Lightwave Technology, vol. 24, pp. 1129-1141, 2006.

[Gur] Gurobi Optimizer 4.5, http://www.gurobi.com

[Ha07] J. W. Hardin and J. M. Hilbe, *Generalized Linear Models and Extensions*, Stata Press, 2nd Edition, 2007.

[Ha94] F. Harary, *Graph Theory*, Reading, 1994.

[Hu04.1] J.Q. Hu and B. Leida, "Traffic Grooming, Routing, and Wavelength Assignment in Optical WDM Mesh Networks," in Proc. IEEE INFOCOM 2004.

[Hu04.2] S. Huang and R. Dutta. "Research problems in dynamic traffic grooming in optical networks," in Proc. Broadnets, 2004.

[Hu08] R. Huelsermann, M. Gunkel, C. Meusburger, and D. Schupke, "Cost modeling and evaluation of capital expenditures in optical multilayer networks," OSA Journal of Optical Networking, vol. 7, pp. 814-833, Sep. 2008.

[ITU05] Telecom Development Bureau, *Teletraffic Engineering Handbook*, ITU, 2005.

[Ja06] A. Jaekel, S. Bandyopadhyay, and Y. Aneja, "Logical Topology Design for WDM Networks Using Survivable Routing," in Proc. IEEE International Conference on Communications, pp.2471-2476, Jun. 2006.

[Ji10] A. Jirattigalachote, P. Monti, L. Wosinska, K. Katrinis, and A. Tzanakaki, "ICBR-Diff: an Impairment Constraint Based Routing Strategy with Quality of Signal Differentiation," Journal of Networks, vol. 5, pp. 1279-1289, 2010.

[Jj06] A. Jajszczyk and P. Rozycki, "Recovery of the Control Plane after Failures in ASON/GMPLS Networks," IEEE Network, vol. 20, no. 1, Jan. 2006.

[Ka05] S. Kaneda, T. Uyematsu, N. Nagatsu, and K. Sato, "Network design and cost optimization for label switched multilayer photonic IP networks," IEEE Journal on Selected Areas in Communications, vol.

23, no. 5, pp. 1612-1619, 2005.

[Kn07] A. Knippel and B. Lardeux, "The multi-layered network design problem," European Journal of Operational Research, vol. 183, no. 1, pp. 87–99, Nov. 2007.

[Ko04] S.K. Korotky, "Network global expectation model: a statistical formalism for quickly quantifying network needs and costs," IEEE/OSA Journal of Lightwave Technology, vol. 22, no. 3, Mar. 2004.

[Ko05] A. Kodian, W. Grover, "Multiple-Quality of Protection Classes Including Dual-Failure Survivable Services in p-Cycle Networks," In Proc. IEEE Broadnets 2005.

[Ko08] O. Komolafe, J. Sventek, "Impact of GMPLS Control Message Loss," IEEE/OSA Journal of Lightwave Technology, vol. 26, pp. 2029-2036, Jul. 2008.

[Kr01] R. Krishmaswamy and K. N. Sivarajan, "Algorithms for routing and wavelength assignment based on solution of LP-relaxation," IEEE Communications Letters, vol.5, no.10, pp.435-437, Oct. 2001.

[Ku05.1] E. Kubilinskas and M. Pioro, "Two layers design problems for the IP/MPLS over WDM networks," in Proc. Design of Reliable Communication Networks, Oct. 2005.

[Ku05.2] E. Kubilinskas and M. Pioro, "An IP/MPLS over WDM network design problem," in Proc. International Network Optimization Conference, Lisbon, Portugal, Mar. 2005.

[La05] J.-F. P. Labourdette, E. Bouillet, R. Ramamurthy, and A. Akyamaç, "Fast approximate dimensioning and performance analysis of mesh optical networks," IEEE Transactions on Networking, vol. 13, no. 4, pp. 906–917, Aug. 2005.

[La94] J.-F. P. Labourdette, G. W. Hart, and A. S. Acampora, "Branch-exchange sequences for reconfiguration of lightwave networks," IEEE Transactions on Communications, vol. 42, pp. 2822–2832, Oct. 1994.

[Le96] K. Lee and V.O.K. Li, "A wavelength rerouting algorithm in wide area all-optical networks," IEEE Journal of Lightwave Technology, vol. 14, no. 6, pp. 1218–1229, 1996.

[Le98] C.M. Lee, C.C. Hui, F. Tong, and P. Yum, "Network dimensioning in WDM based all optical networks", in Proc. IEEE GLOBECOM, 1998, vol.1, pp. 328-333.

[Lg05] J. Lang, "Link Management Protocol (LMP)," IETF RFC 4204, Oct. 2005.

[Li00] L. Li and A. K. Somani, "A New Analytical Model for Multifiber WDM Networks," IEEE Journal on Selected Areas in Communications, vol.18, no. 10, pp. 2138–2145, Oct. 2000.

[Li02] G. Li, J. Yates, D. Wang, and C.Kalmanek, "Control Plane design for reliable optical networks," IEEE Communications Magazine, vol. 40, February 2002.

[Li11] Y. Li, F. Zhang, and R. Casellas, "Flexible grid label format in wavelength switched optical network," IETF RFC Draft, Jul. 2011.

[Lu09] Luis Velasco, *Recovery mechanisms in ASON/GMPLS networks,* PhD thesis, Universitat Politecnica de Catalunya, May 2009.

[Ma08] C. Mas, O. Moe, and M. Jäger, "Impact of protection schemes and network component's availability on operational expenditures," J. Opt. Netw. 7, 142-150 2008.

[Ma09] K. Manousakis, K. Christodoulopoulos, and E. A. Varvarigos, "Impairment-Aware Offline RWA for Transparent Optical Networks," in Proc. of INFOCOM 2009, pp.1557-1565, 2009.

[Me07] D.Medhi and K. Ramasamy, *Network routing: algorithms, protocols, and architectures,* Elsevier, 2007.

[Mo04] D. Montgomery, *Design and Analysis of Experiments*, Wiley & Sons, 2004.

[Mo11] R.M. Morais, C. Pavan, A. N. Pinto, and C. Requejo, "Genetic Algorithm for the Topological Design of Survivable Optical Transport Networks," IEEE/OSA Journal of Optical Communications and Networking, vol.3, no.1, pp.17-26, Jan 2011.

[Mo99] G. Mohan and C.S.R. Murthy, "A time optimal wavelength rerouting algorithm for dynamic traffic in WDM networks," IEEE Journal of Lightwave Technology, vol. 17, no. 3, pp. 406-417, 1999.

[Mu08] R. Muñoz, R. Casellas, R. Martinez, "An Experimental Signalling Enhancement to Efficiently Encompass WCC and Backup Sharing in GMPLS-enabled Wavelength-Routed Networks," In Proc. IEEE ICC 2008.

[Mu96] B. Mukherjee, D. Banerjee, S. Ramamurthy, and A. Mukherjee, "Some principles for designing a wide-area WDM optical network," IEEE/ACM Transactions on Networking, vol. 4, pp. 684–696, Oct. 1996.

[Na00] A. Narula-Tam and E. Modiano, "Dynamic load balancing for WDM based packet networks," in Proc. IEEE INFOCOM, 2000, pp.1010–1019.

[OIF01] OIF. User Network Interface (UNI) 1.0 Signaling Specification, Optical Internet working Forum, OIF, October 2001.

[Or07] S. Orlowski, A. Koster, C. Raack, and R. Wessaly, "Two-layer network design by branch-and-cut featuring MIP-based heuristics," in Proc. International Network Optimization Conference, Spa, Belgium, Apr. 2007.

[Ou04.1] C. Ou, K. Zhu, H. Zang, J. Zhang, H. Zhu, L.H. Sahasrabuddhe, and B. Mukherjee, “Traffic grooming for survivable WDM networks – dedicated protection,” OSA Journal of Optical Networking, vol. 3, pp. 50–74, Jan. 2004.

[Ou04.2] C. Ou, J. Zhang, L. H. Sahasrabuddhe, and B. Mukherjee, “New and improved approaches for shared-path protection in WDM mesh networks,” IEEE/OSA Journal of Lightwave Technology, vol.22, pp. 1223-1232, 2004.

[Oz03] A.E. Ozdaglar and D.P. Bertsekas, "Routing and wavelength assignment in optical networks," IEEE/ACM Transactions on Networking, vol. 11, no.2, pp. 259- 272, Apr 2003.

[Pa03] S. Pachnicke and E. Voges, "Analytical assessment of the Q-factor due to cross-phase modulation (XPM) in multispan WDM transmission systems," in Proc. SPIE, 2003.

[Pa08] S. Pachnicke, T. Paschenda, and P. Krummrich, “Assessment of a constraint-based routing algorithm for translucent 10 Gbit/s DWDM networks considering fiber non-linearities,” OSA Journal of Optical Networking, vol. 7, pp. 365-377, 2008.

[Pa09] P. Pavon-Mariño, S. Azodolmolky, R. Aparicio-Pardo, B. Garcia-Manrubia, Y. Pointurier, M. Angelou, J. Sole-Pareta, J. Garcia-Haro, and I. Tomkos, "Offline Impairment Aware RWA Algorithms for Cross-Layer Planning of Optical Networks," IEEE/OSA Journal of Lightwave Technology, vol. 27, pp. 1763-1775, 2009.

[Pa10] C. Pavan, R. Morais, J. Ferreira, and A. Pinto, “Generating Realistic Optical Transport Network Topologies,”IEEE/OSA Journal of. Optical Communications and. Networking, vol 2, pp. 80-90, 2010.

[Pe07] J. Perelló, S. Spadaro, J. Comellas, and G. Junyent, “An Analytical Study of Control Plane Failures Impact on GMPLS Ring Optical Networks,” IEEE Communication Letters, vol. 11, no. 8, Aug. 2007.

[Pe09] Jordi Perelló, *Resource Management in GMPLS-Controlled Hybrid OBS/OCS Transport Networks*, PhD thesis, Universitat Politècnica de Catalunya, May 2009.

[Pi04] M. Pióro and D. Medhi, *Routing, Flow, and Capacity Design in Communication and Computer Networks*, Elsevier, 2004.

[Pi06] M. Pickavet, P. Demeester, D. Colle, D. Staessens, B. Puype, L. Depré, and I. Lievens, “Recovery in Multilayer Optical Networks”, IEEE/OSA Journal of Lightwave Technology, vol. 24, pp. 122-134, 2006.

[Po99] F. Poppe and P.M. Demeester, “Wavelength requirement of mesh-restorable multi-wavelength optical networks,” IEEE/ACM Transactions on Networking, vol.3, no.5, pp. 767-778, Oct. 1999.

[Qi10] Y. Qin, et al. "Demonstration of C/S based Hardware Accelerated

QoT Estimation Tool in Dynamic Impairment-Aware Optical Network," in Proc. European Conference on Optical Communication (ECOC), 2010.

[Qi11] Y. Qin, S. Azodolmolky, M. Gunkel, R. Nejabati, and D. Simeonidou, "Hardware Accelerated Impairment-Aware Control Plane for Future Optical Networks," IEEE Communication Letters, vol. 15, pp. 1004-1006, 2011.

[Ra00] B. Ramamurthy and A. Ramakrishnan, "Virtual topology reconfiguration of wavelength routed optical WDM networks," in Proc. IEEE GLOBECOM, 2000, pp. 1269–1275.

[Ra04] G. Raghukiran and S. Ramamurthy, "QoS Based Survivable Logical Topology Design in WDM Optical Networks," Photonic Network Communications, vol.7, no.2, pp. 193-206, 2004.

[Ra07] P. Rajalakshmi and A. Jhunjhunwala, "Wavelength reassignment algorithms for all-optical WDM backbone networks," Optical Switching and Networking, vol. 4, pp. 147–156, 2007.

[Ra87] P. Raghavan and C. D. Tompson, "Randomized rounding: A technique for provably good algorithms and algorithmic proofs," Combinatorica, vol. 7, no.4, pp.365–374, 1987.

[Ra95] R. Ramaswami and K.N. Sivarajan, "Routing and wavelength assignment in all-optical networks", IEEE/ACM Transactions on Networking, vol.3, no.5, pp. 489-500, Oct. 1995.

[Ra98] R. Ramaswami and K.N. Sivarajan, *Optical Networks: a practical perspective*, Morgan Kauffman Publishers, 1998.

[RFC3031] E. Rosen, A. Viswanathan, and R. Callon, "Multiprotocol Label Switching Architecture," IETF RFC 3031, Jan. 2001

[RFC3717] B. Rajagopalan, J. Luciani, and D. Awduche, "IP over Optical Networks: A Framework," IETF RFC 3717, Mar. 2004.

[RFC3945] E. Mannie, "Generalized Multi-Protocol Label Switching Architecture," IETF RFC 3945, Oct. 2004.

[Ro02] S. Ross, R. Westerfield, J. Jaffe, *Corporate Finance*, McGraw-Hill, 2002.

[Ro04] C.P. Robert and G. Casella, *Monte Carlo Statistical Methods*, 2nd ed., New York, NY, USA, Springer, 2004.

[Ro08] P. Roorda, B. Collings, "Evolution to Colorless and Directionless ROADM Architectures," National Fiber Optic Engineers Conference (NFOEC), 2008.

[Ro95] G. N. Rouskas and M. H. Ammar, "Dynamic reconfiguration in multihop WDM networks," Journal of High Speed Networks, vol. 4, no. 3, pp. 221–238, 1995.

[Sa02] M. Saad and Z. Luo "A Lagrangian decomposition approach for the

routing and wavelength assignment in multifiber WDM networks," in Proc. IEEE GLOBECOM, Taipei, Nov. 2002.

[Sa09] C.V. Saradhi and S. Subramaniam, "Physical Layer Impairment Aware," IEEE Communications surveys & Tutorials, vol. 11, no. 4, 2009.

[Sa11] N. Sambo, M. Secondini, F. Cugini, G. Bottari, P. Iovanna, F. Cavaliere, P. Castoldi, "Modeling and Distributed Provisioning in 10–40–100-Gb/s Multirate Wavelength Switched Optical Networks," IEEE/OSA Journal of Lightwave Technology, vol. 29, pp. 1248-1257, 2011.

[Sa99] D. Saha, M. D. Purkayastha, and B. Mukherjee, "An approach to wide area WDM optical network design using genetic algorithms," Computer Communications, vol. 22, pp. 156–172, 1999.

[Se09] S. Sebbah and B. Jaumard, "A Resilient Transparent Optical Network Design with a Pre-Configured Extended-Tree Scheme," in Proc. IEEE International Conference in Communications, 2009.

[Sh09] G. Shen and R. Tucker, "Energy-Minimized Design for IP Over WDM Networks," J. Opt. Commun. Netw. 1, 176-186, 2009.

[Sn80] G.W. Snedecor and W.G. Cochran, *Statistical Methods*, Iowa State University Press, 1980.

[Sr01] N. Sreenath, C. S. R. Murthy, B. H. Gurucharan, and G. Mohan, "A two-stage approach for virtual topology reconfiguration of WDM optical networks," Optical Networks Magazine, pp. 58–71, May 2001.

[Sr06] N. Sreenath and P. Ramaswamy, "Virtual Topology Reconfiguration for Link Failures in IP-over-WDM Networks," in Proc. ICNICONSMCL, 2006.

[Ta02] H. Takagi, Y. Zhang, X. Jia, and H. Takagi, "Virtual topology reconfiguration for wide-area WDM networks," in Proc. IEEE International Conference on Communications, 2002.

[Te99] S. Ten, K. Ennser, J. Grochocinski, S. Burtsev, and V. da Silva, "Comparison of four-wave mixing and cross phase modulation penalties in dense WDM systems," in Proc. OFC, 1999.

[To07] M. Tornatore, G. Maier, and A. Pattavina, "WDM Network Design by ILP Models Based on Flow Aggregation," IEEE/ACM Transactions on Networking, vol. 15, no. 3, pp. 709-720, Jun. 2007.

[Ve06] S. Verbrugge, D. Colle, M. Pickavet, and P. Demeester, "Methodology and input availability parameters for calculating OpEx and CapEx costs for realistic network scenarios," OSA Journal of Optical Networking, vol. 5, pp. 509-520, 2006.

[Ve07] S. Verbrugge, D. Colle, M. Pickavet, and P. Demeester, "Techno-economic evaluation of the island based introduction of optical cross connects in an IP-over-WDM network," Photonic Network

Communication, vol. 13, pp. 241–255, 2007.

[Ve08] L. Velasco, S. Spadaro, J. Comellas, G. Junyent, "Introducing OMS protection in GMPLS-based optical ring networks," Computers Networks, vol. 52, pp. 1975-1987, Jul. 2008.

[Ve09.1] L. Velasco, S. Spadaro, J. Comellas, and G. Junyent, "Shared-path protection with extra traffic in ASON/GMPLS ring networks," OSA Journal of Optical Networking, vol. 8, issue 2, pp. 130-145, 2009.

[Ve10] L. Velasco, F. Agraz, R. Martínez, R. Casellas, S. Spadaro, R. Muñoz, and G. Junyent, "GMPLS-based Multidomain Restoration: Analysis, Strategies, Policies and Experimental Assessment," IEEE/OSA Journal of Optical Communications and Networking, vol. 2, pp. 427-441, Jun. 2010.

[Wa10.1] A. Wason and R.S. Kaler, "Rerouting technique with dynamic traffic in WDM optical networks," Optical Fiber Technology, vol. 16, pp. 50–54, 2010.

[Wa10.2] A. Wason and R.S. Kaler, "Lightpath Rerouting Algorithm to enhance blocking performance in all-optical WDM network without wavelength conversion," Optical Fiber Technology vol. 16, pp. 146-150, 2010.

[Wa96] N. Wauters and P.M. Deemester, "Design of the optical path layer in multiwavelength cross-connected networks," IEEE Journal on Selected Areas in Communications, vol.14, pp. 881-891, Jun. 1996.

[Xi03] Y. Xi, G.N. Rouskas, and H.G. Perros, "On the Physical and Logical Topology Design of Large-Scale Optical Networks," IEEE Journal of Lightwave Technology, vol. 21, no. 4, pp. 904–915, Apr. 2003.

[Xi05] C. Xiaowen and J. Liu, "A new adaptive routing scheme in WDM mesh networks," in Proc. IEEE International Conference on Communications vol.3, pp. 1797–1801, 2005.

[Xi09] M. Xia, M. Tornatore, C. Martel, and B. Mukherjee, "Service-Centric Provisioning in WDM Backbone Networks for the Future Internet," IEEE Journal of Lightwave Technology, vol. 27, pp. 1856-1865, 2009.

[Xu00] S. Xu, L. Li, and S. Wang, "Dynamic routing and assignment of wavelength algorithms in multifiber wavelength division multiplexing networks," IEEE Journal on Selected Areas in Communications, vol. 18, pp. 2130–2137, Oct. 2000.

[Ya04] W. Yao and B. Ramamurthy, "Rerouting schemes for dynamic traffic grooming in optical WDM mesh networks," Proc. of IEEE GLOBECOM 2004, pp.1793–1797, 2004.

[Za02] H. Zang, J. Jue, L. Sahasrabuddhe, R. Ramamurthy, and B. Mukherjee, "Dynamic lightpath establishment in wavelength routed WDM networks," IEEE Communications Magazine, vol. 39, issue 9, pp. 100-108, Aug. 2002.

[Zh10] X. Zhang, F. Shen, L. Wang, S. Wang, L. Li, and H. Luo, "Two-layer mesh network optimization based on inter-layer decomposition," *Photon. Netw. Commun.*, in press, online Nov. 2010.